Small-molecule activation at gold: synthesis and reactivity of cyclometalated Au(III) complexes

Dissertation for the degree of Philosophiae Doctor

Marte Sofie Martinsen Holmsen

Department of Chemistry

Faculty of Mathematics and Natural Sciences

University of Oslo

2018

Acknowledgements

The work presented in this thesis was carried out at the Department of Chemistry, University of Oslo, starting from autumn 2013 until autumn 2018, under the supervision of Professor Mats Tilset, Dr. Richard H. Heyn (SINTEF), and Dr. Ainara Nova.

First, I would like to thank my great supervisors Mats, Rick, and Ainara. Thanks to all three of you for your great enthusiasm on gold chemistry, it has been fantastic to work together with you. Thank you Mats, for giving me the chance to work on this exciting project and for always having the door open for some golden discussions. Thank you Rick, for a lot of fruitful discussions and suggestions, and for your great help with writing manuscripts. Also, thanks to you and SINTEF for allowing me to use the facilities there. Ainara, thank you for great discussions on DFT calculations and mechanisms. When something new was discovered in the lab, you always quickly followed up with calculations and I think this close collaboration between experiment and theory has been a great advantage for this project.

I would like to acknowledge the Norwegian Research Council for financing my project (221801/F20). Thanks to the Department of Chemistry for financing my 4th year of the Ph.D. and thereby giving me the chance to do teaching, which I enjoyed a lot. Onwards, I would like to thank the Department of Chemistry and the FutureFeed project for each financing one and a half months extension of my Ph.D. project, which gave me valuable time towards the end of the project. COST (COST Action CM1205) is acknowledged for giving Dr. Eirin Langseth and me the chance to go to École Poloytechnique Fédérale de Lausanne (EPFL) for a two week research stay in February 2014.

I want to thank all past and present group members in the Tilset group and the Catalysis group. I would especially like to thank all past and present members of the gold team. A big thanks goes to Eirin Langseth. You gave me the best lab-introduction to the gold project one can dream of and I am very thankful for that. You have also been a great office and lab mate, and I enjoyed having you around. I would also like to thank Franziska Stefanie Ihlefeldt for great collaboration on the gold project, we had great fun in the lab. I would like to thank Dr. David Balcells for fruitful collaborations. Thanks to Knut Tormodssønn Hylland for always having time to answer various questions on organic chemistry, practical aspects in the lab, and literature related questions. Thanks to Sina Witzel and Inga Schmidtke for being great office mates during my last year of the Ph.D., after sitting some years alone in the office, I really enjoyed having some company again.

I would like to thank Knut Tormodssønn Hylland and Peter Molesworth for taking your time to read through my thesis. I appreciate your feedback a lot, and it has been very helpful during the writing

Abstract

The interest in organogold chemistry has increased rapidly during the last 20-30 years, and nowadays there are numerous research group across the world working with gold and its rich chemistry. Au(I) complexes have been more studied that Au(III) complexes, but lately, there has been an increased interest in Au(III) complexes and their reactivity as well. Gold is known for its ability to activate alkenes, alkynes, and other unsaturated species towards nucleophilic addition, and addition of nucleophiles to coordinated unsaturated species at gold are key steps in gold catalysis. In this thesis, the reactivity of Au(III) complex Au(OCOCF$_3$)$_2$(tpy) (**2**, tpy= 2-(*p*-tolyl)pyridine) towards a wide variety of small molecules was investigated. The nucleophilic addition of different oxygen-based nucleophiles to various alkenes at complex **2** furnishing β-functionalized Au(III) alkyl complexes is presented in Chapter 2. In Chapter 3, metallacycle construction at complex **2** was achieved upon reaction with ethylene, water, and acetonitrile. In Chapter 4, the catalytic transformation of acetylene into vinyl trifluoroacetate using complex **2** as a precatalyst is presented. The mechanism of the catalytic trifluoroacetoxylation was studied both experimentally and computationally. There are only a few examples of C(sp^3)-H activation at Au(III), whereas C(sp^2)-H activation is common at Au(III). In Chapter 5, the synthesis and characterization of a (*N,C,C*) Au(III) pincer complex *via* both C(sp^2)-H and C(sp^3)-H activation is presented. The (*N,C,C*) Au(III) pincer complex is found to outperform complex **2** as a catalyst for the acetylene trifluoroacetoxylation, because it is significantly more robust towards the conditions where catalysis takes place. Finally, in Chapter 6, the generation and characterization of Au(III) η^1 and η^3 allyl complexes is described. Transition metal η^3 allyl complexes have been thoroughly studied, but there are no well-characterized Au(III) η^3 allyl complexes reported in the literature.

Graphical abstract

Chapter 2: Nucleophilic addition to alkenes at Au(III)
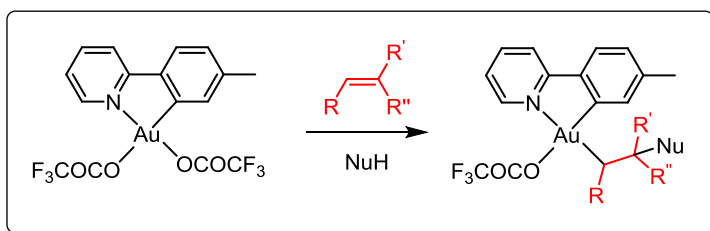
Chapter 3: Metallacycle formation at Au(III)
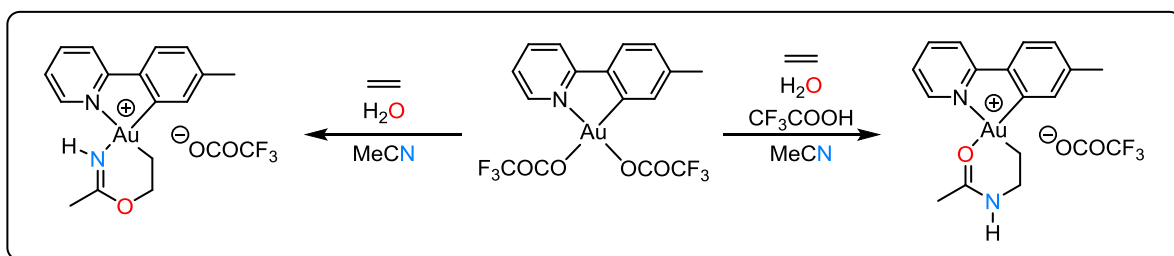
Chapter 4: Catalytic transformation of acetylene at Au(III)
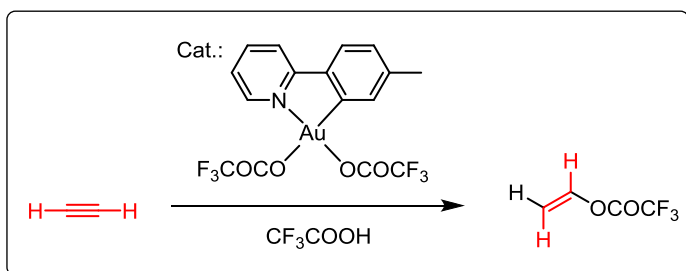
Chapter 5: C(sp^3)-H activation at Au(III): synthesis of a Au(III) (*N,C,C*) pincer complex
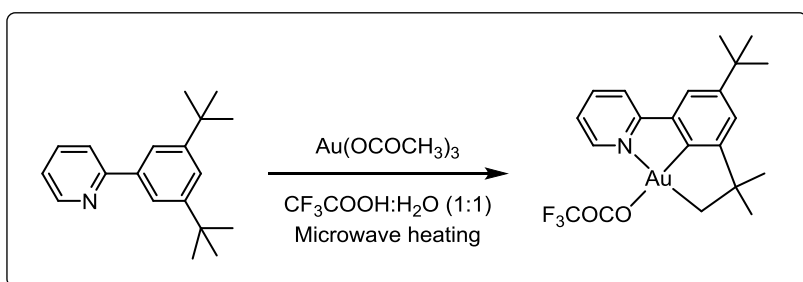
Chapter 6: Generation of Au(III) η^1 and η^3 allyl complexes

List of compounds

5a

5b

6a

6b

7

8

9

10

11

12

2-OCOCH₃

2-OMe

13

14

15

16

18

20

27

31b

X = unknown

31-H₂O

32

33
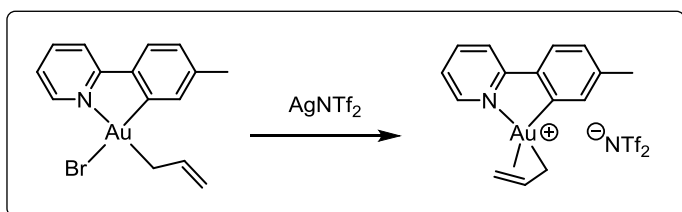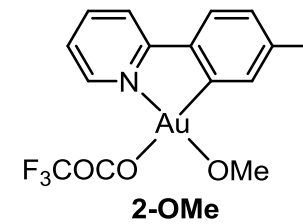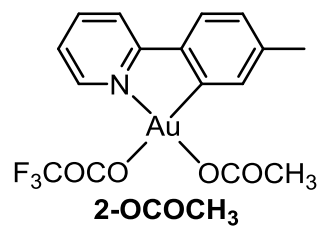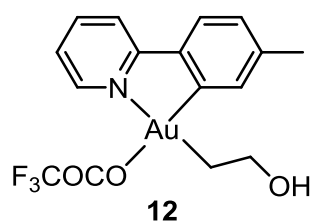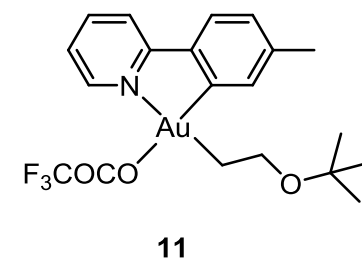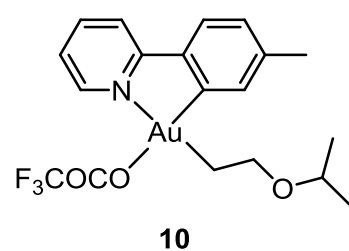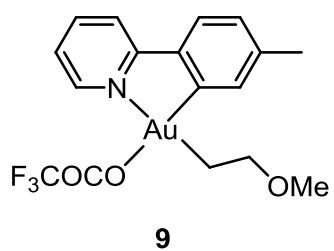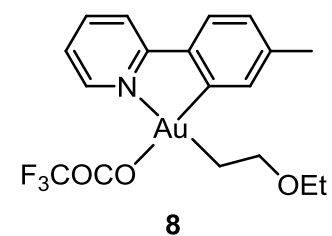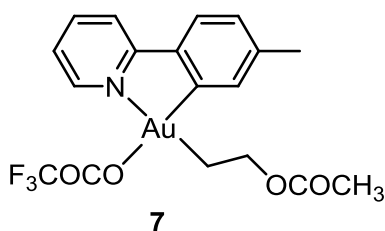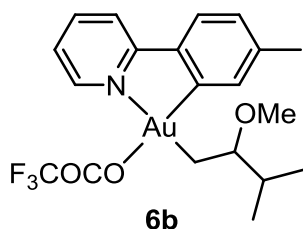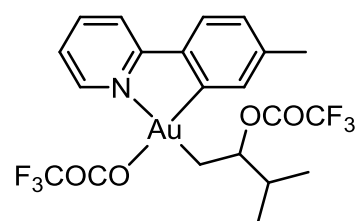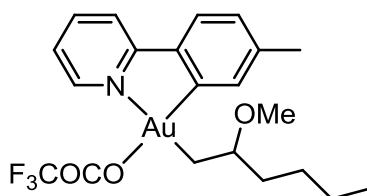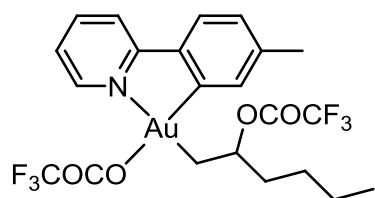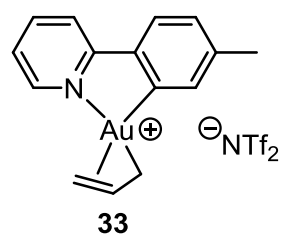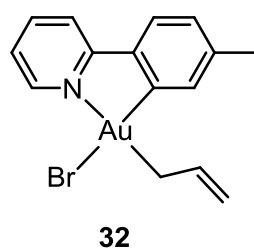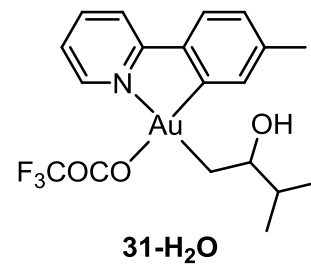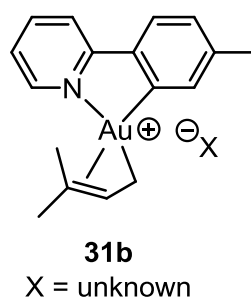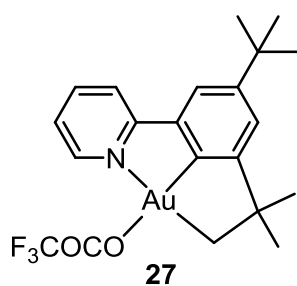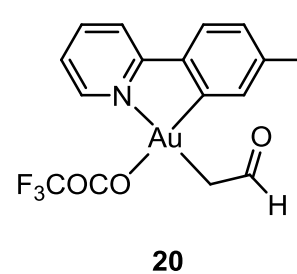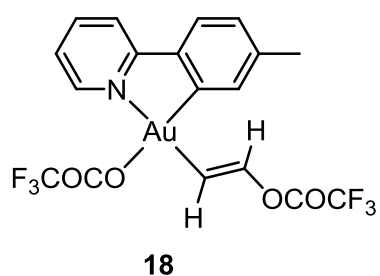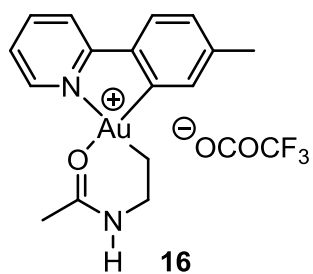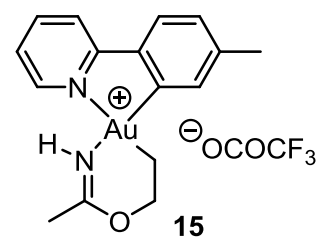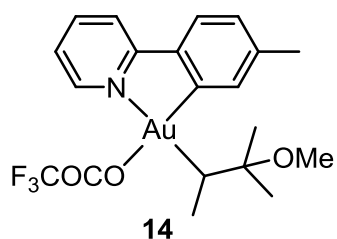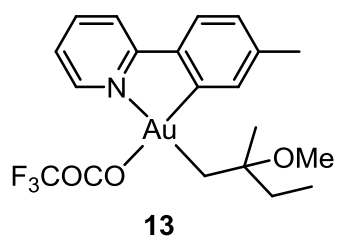
The list of compounds is included to aid the reader and is not intended as a full list of all compounds discussed in this thesis.

List of publications

Paper I

Markovnikov at Gold: Nucleophilic Addition to Alkenes at Au(III)

Marte Sofie Martinsen Holmsen, Franziska Stefanie Ihlefeldt, Sigurd Øien-Ødegaard, Eirin Langseth, Yannick Wencke, Richard H. Heyn, and Mats Tilset

Organometallics **2018**, *37*, 1937-1947

Paper II

Small-molecule Activation at Au(III): Metallacycle Construction from Ethylene, Water, and Acetonitrile

Marte Sofie Martinsen Holmsen, Ainara Nova, David Balcells, Eirin Langseth, Sigurd Øien-Ødegaard, Eline Aasen Tråseth, Richard H. Heyn, and Mats Tilset

Dalton Trans. **2016**, *45*, 14719-14724

Paper III

trans-Mutation at Gold(III): A Mechanistic Study of a Catalytic Acetylene Functionalization via a Double Insertion Pathway

Marte Sofie Martinsen Holmsen, Ainara Nova, David Balcells, Eirin Langseth, Sigurd Øien-Ødegaard, Richard H. Heyn, Mats Tilset, and Gábor Laurenczy.

ACS Catal. **2017**, *7*, 5023-5034

Paper IV

Synthesis of a (N,C,C) Au(III) Pincer Complex via C_{sp3}-H Bond Activation: Increasing Catalyst Robustness by Rational Catalyst Design

Marte Sofie Martinsen Holmsen, Ainara Nova, Knut Hylland, David S. Wragg, Sigurd Øien-Ødegaard, Richard H. Heyn, and Mats Tilset

Chem. Commun. **2018**, *54*, 11104-11107

List of contributors to the publications

Paper I

Marte Sofie Martinsen Holmsen: experimental work and writing of publication

Franziska Stefanie Ihlefeldt: experimental work

Sigurd Øien-Ødegaard: X-ray diffraction analyses

Eirin Langseth: experimental work

Yannick Wencke: experimental work

Richard H. Heyn: supervision and writing of publication

Mats Tilset: supervision and writing of publication

Paper II

Marte Sofie Martinsen Holmsen: experimental work and writing of publication

Ainara Nova: supervision, computational work, and writing of publication

David Balcells: computational work and writing of publication

Eirin Langseth: experimental work

Sigurd Øien-Ødegaard: X-ray diffraction analyses

Eline Aasen Tråseth: experimental work

Richard H. Heyn: supervision and writing of publication

Mats Tilset: supervision and writing of publication

Paper III

Marte Sofie Martinsen Holmsen: experimental work and writing of publication

Ainara Nova: supervision, computational work, and writing of publication

David Balcells: computational work and writing of publication

Eirin Langseth: experimental work

Sigurd Øien-Ødegaard: X-ray diffraction analyses

Richard H. Heyn: supervision and writing of publication

Mats Tilset: supervision and writing of publication

Gábor Laurenczy: initial experiments leading to the work in the paper was performed at Ecole Polytechnique Fédérale de Lausanne under the guidance of GL.

Paper IV

Marte Sofie Martinsen Holmsen: experimental work and writing of publication

Ainara Nova: supervision, computational work, and writing of publication

Knut Hylland: experimental work

Sigurd Øien-Ødegaard: X-ray diffraction analysis

David S. Wragg: X-ray diffraction analysis

Richard H. Heyn: supervision and writing of publication

Mats Tilset: supervision and writing of publication

List of conference contributions: oral presentations

Catalysis at gold(III): A mechanistic study of a catalytic acetylene functionalization
Marte Sofie Martinsen Holmsen, Ainara Nova, David Balcells, Richard H. Heyn, and Mats Tilset
33. Organisk Kjemisk Vintermøte
11.01-14.01, 2018, Skeikampen, Norway

Small molecule activation at Au(III) complexes
Marte Sofie Martinsen Holmsen, Franziska Stefanie Ihlefeldt, Eirin Langseth, Sigurd Øien-Ødegaard, and Mats Tilset
32. Organisk Kjemisk Vintermøte
12.01-15.01, 2017, Skeikampen, Norway

Au(III) complexes and their reactivity towards alkenes and alkynes
Marte Sofie Martinsen Holmsen, Franziska Stefanie Ihlefeldt, Ainara Nova, Yannick Wencke, Eirin Langseth, Sigurd Øien-Ødegaard, and Mats Tilset
6th EuCheMS Chemistry Congress, John Dalton 250th Anniversary Symposium
11.09-15.09, 2016, Seville, Spain

NMR and organometallic chemistry – some examples from Au(III) chemistry
Marte Sofie Martinsen Holmsen, Ainara Nova, Yannick Wencke, Eirin Langseth, Sigurd Øien-Ødegaard, and Mats Tilset
The 14th National MR Meeting – MR2016
16.06-17.06, 2016, Bergen, Norway

Au(III) complexes and their reactivity towards alkenes and alkynes
Marte Sofie Martinsen Holmsen, Franziska Stefanie Ihlefeldt, Ainara Nova, Yannick Wencke, Eirin Langseth, Sigurd Øien-Ødegaard, and Mats Tilset
4th Nordic Organometallic Symposium
30.03-31.03, 2016, Reykjavik, Iceland

Au(III) complexes and their reactivity towards alkenes and alkynes
Marte Sofie Martinsen Holmsen, Franziska Stefanie Ihlefeldt, Yannick Wencke, Eirin Langseth, Sigurd Øien-Ødegaard, and Mats Tilset
Gold 2015 - 7th International Gold Conference
26.07-29.07, 2015, Cardiff, Wales

Au(III) complexes and their reactivity towards alkenes and alkynes
Marte Sofie Martinsen Holmsen, Franziska Stefanie Ihlefeldt, Yannick Wencke, Eirin Langseth, Sigurd Øien-Ødegaard, and Mats Tilset
3rd Annual Meeting of COST Action CM1205 – CARISMA
18.03-20.03, 2015, Tarragona, Spain

List of conference contributions: poster presentations

Au(III) complexes and their reactivity towards alkenes and alkynes
Marte Sofie Martinsen Holmsen, Franziska Stefanie Ihlefeldt, Yannick Wencke, Eirin Langseth, Sigurd Øien-Ødegaard, and Mats Tilset
Swedish NMR Centre 25 Year Anniversary
12.10-13.10, 2016, Gothenburg, Sweden

Au(III) complexes and their reactivity towards alkenes and alkynes
Marte Sofie Martinsen Holmsen, Franziska Stefanie Ihlefeldt, Yannick Wencke, Eirin Langseth, Sigurd Øien-Ødegaard, and Mats Tilset
31. Organisk Kjemisk Vintermøte
07.01-10.01, 2016, Skeikampen, Norway

Au(III) complexes and their reactivity towards alkenes and alkynes
Marte Sofie Martinsen Holmsen, Franziska Stefanie Ihlefeldt, Yannick Wencke, Eirin Langseth, Sigurd Øien-Ødegaard, and Mats Tilset
3rd Annual Meeting of COST Action CM1205 – CARISMA
18.03-20.03, 2015, Tarragona, Spain

Au(III) complexes and their reactivity towards alkenes
Marte Sofie Martinsen Holmsen, Franziska Stefanie Ihlefeldt, Yannick Wencke, Eirin Langseth, Sigurd Øien-Ødegaard, and Mats Tilset
3rd Nordic Meeting on Organometallic Chemistry
11.03-12.03, 2015, Lund, Sweden

Insertions of unsaturated molecules into Au-O bonds
Marte Sofie Martinsen Holmsen, Franziska Stefanie Ihlefeldt, Yannick Wencke, Eirin Langseth, Sigurd Øien-Ødegaard, and Mats Tilset
30. Organisk Kjemisk Vintermøte
08.01-11.01, 2015, Skeikampen, Norway

Abbreviations

Ar	aryl
BAr^{F}	tetrakis[3,5-bis(trifluoromethyl)phenyl]borate
bipy	2,2'-bipyridine
bnpy	2-benzylpyridine
br	broad (NMR)
Bu	butyl
cif	crystallographic information file
cod	1,5-cyclooctadiene
COSY	correlation spectroscopy (NMR)
δ	chemical shift in ppm (NMR)
d	day(s), doublet (NMR)
d1	relaxation delay (NMR)
DFT	density functional theory
EDG	electron donating group
equiv	equivalent(s)
ESI	electronic supporting information
ESI-MS	electrospray ionization mass spectrometry
Et	ethyl
EWG	electron withdrawing group
G	Gibbs free energy
h	hour
HMBC	heteronuclear multiplebond–correlation spectroscopy (NMR)
HOESY	heteronuclear Overhauser effect spectroscopy (NMR)
(HR)MS	(high resolution) mass spectrometry
HSQC	heteronuclear single–quantum correlation (NMR)
i	*iso*
ISTD	internal standard
J	coupling constant (NMR)
L	neutral 2 electron donor ligand
M	metal, molar
m	multiplet (NMR)
m	*meta*
Me	methyl
MW	microwave
m/z	mass-to-charge ratio (MS)
n	normal
η	hapticity
NMR	nuclear magnetic resonance
NOE	nuclear Overhauser effect (NMR)
NOESY	nuclear Overhauser effect spectroscopy (NMR)
ns	number of scans (NMR)
Nu	nucleophile
o	*ortho*
OLED	organic light-emitting diodes
ORTEP	Oak Ridge thermal ellipsoid plot
p	*para*
Ph	phenyl
ppm	parts per million (NMR)

ppy	2-phenylpyridine
Pr	propyl
q	quartet (NMR)
rel	relative
R	an organic group
rt	room temperature
s	singlet (NMR)
T	temperature
t	*tertiary*
t	triplet (NMR)
Tf	trifluoromethylsulfonyl (SO_2CF_3)
THF	tetrahydrofuran
TON	turnover number ($n_{product}/n_{catalyst}$)
tpy	2-(*p*-tolyl)pyridine
TS	transition state
Ts	*p*-toluenesulfonyl ($SO_2C_6H_4CH_3$)
X	anionic one electron donor ligand
XRD	X-ray diffraction analysis
Å	Ångström (10^{-10} m)
⋯	denotes a non-covalent interaction (*e.g.* hydrogen bonding)
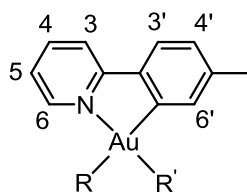
Figure 1. Numbering scheme used for reporting the NMR data. All chemical shifts are reported in CD_2Cl_2 unless otherwise noted.

Table of Contents

xx

Chapter 1 – Introduction

1.1 General introduction

1.1.1 Gold

When we are young we meet gold in fairytales and comic books. Many of us may remember Scrooge McDuck diving in his gold coins, or what about the tales of the pirates roaming the seas for gold? Gold (Au) belongs to group 11 in the periodic table and has atomic number 79. Gold is often referred to as one of the "coinage metals" or one of the "precious metals". Gold has a melting point of 1065 °C and a boiling point of 2807 °C.[1] The nice and shiny yellow colour of metallic gold is due to the relativistic effect, without the relativistic effect gold would look like silver.[1, 2] Gold has a very high reduction potential (E^o = +1.68 V) and is therefore often found in nature in its elemental form, for example as gold nuggets.[3] Mankind has been hunting gold for ages and tons of gold are mined every year. Up to 2012 a total of 161 000 tons of gold had been mined; combining all these tons of gold would give a 20 m sided cube of gold.[2] Gold has accompanied mankind throughout the history and is found in many historical artifacts, one of the most famous being the tomb of Tutankhamun in Egypt which contained the largest discovered collection of gold and jewelry, including a gold coffin.[2] Gold has been used to create coloured glass (for example "gold ruby" and "purple of Cassius") by creating small, nano-sized gold particles, and some of these techniques are still in use today.[2] Nowadays, we meet gold in everyday life, for example through jewelry (if we can afford it) and most of us probably also have gold in our mobile phone and other electronic devices at home. Metallic gold is not toxic and it has its own E-number (E175) which makes it allowed as a food additive in the European Union.[2] Gold is also used in dental care and medicine, one example being the use of auranofin (sold as Ridaura) as an anti-rheumatic drug (Figure 2).[4, 5] There are also several Au(I) and Au(III) complexes that can act as antitumor agents and some examples are given in Figure 2.[4-6]
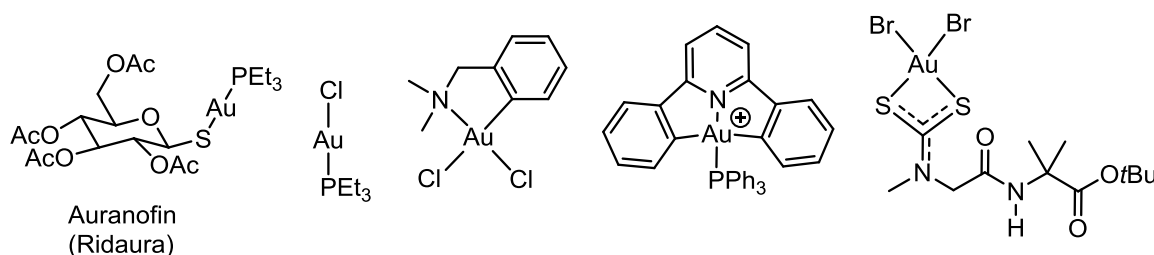
Figure 2 Au(I) and Au(III) complexes showing antitumor properties (and also antirheumatic properties for Auranofin).[4-6]

Many gold complexes show luminescence[7-9] and the synthesis of luminescent gold complexes have gained a lot of attention due to their potential use in light-emitting devices, for example in organic light-emitting diodes (OLEDs).[7, 10] Some examples of luminescent Au(I) and Au(III) complexes are given in Figure 3.[10-13]
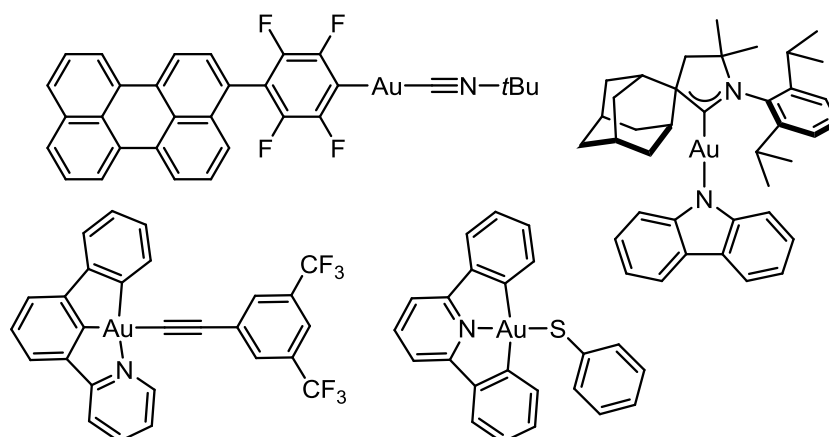
Figure 3. Some examples of luminescent Au(I) and Au(III) complexes.[10-13]

1.1.2 Au(I) and Au(III)

The oxidation states +1 and +3 are by far the most common for organometallic complexes of gold. For Au(I) d^{10} 14 electron complexes with linear two-coordinate geometry is preferred (Figure 4). For Au(III) d^8 16 electron complexes with square planar four-coordinate geometry is preferred (Figure 4).[1, 14] There are a few examples of gold in the oxidation state +2 reported in the literature and with very electropositive metals gold in the oxidation state −1 can be found.[1, 15-17] There are also some rare reports of gold in the oxidation states +4 and +5.[1, 15-17] Very recently the possibility for gold in the oxidation state +6 was predicted by advanced computational methods.[18]

$$L-Au-X$$
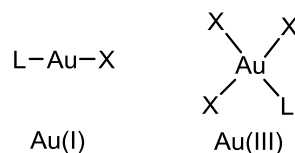
Au(I)   Au(III)

Figure 4. Preferred coordination geometries of Au(I) and Au(III), where X is an anionic 1 electron donor and L is a neutral 2 electron donor.[1, 14]

In the field of organogold chemistry, Au(I) complexes have been much more widely investigated than Au(III) complexes. But lately, the interest in Au(III) complexes has rapidly increased as well. In this thesis, the main focus will be on gold in the oxidation state +3, and only a brief introduction to gold in the oxidation state +1 will be given.

1.2 Gold catalysis

1.2.1 General introduction

Gold was for a long time believed to be unreactive, probably due to the inertness of metallic gold. Elemental gold can only be transformed in a few ways, for example by dissolving it in aqua regia (HCl:HNO$_3$, 3:1 (v:v)) forming HAuCl$_4$, by dissolving it in cyanide under oxidizing conditions forming $^-$Au(CN)$_2$, or by treating it with halogens such as Cl$_2$ forming AuCl$_3$.[1, 19, 20] Aqua regia and its ability to dissolve gold was discovered as early as the 8th century by alchemist Jabir Ibn Hayyan (730-813 AD),

while the cyanidation process was not discovered before the modern era, in 1887.[20] Due to the inertness of metallic gold, there has been a lack of studies on gold, and gold was for a long time believed to be catalytically dead. However, this turned out not to be true, and the last 20-30 years the interest in gold and its exciting chemistry has exploded. Nowadays there are numerous research groups across the world working with gold and its rich chemistry; gold catalysis has become a hot topic![i]

A great advantage of gold catalysis is that it is often compatible with mild conditions and ambient conditions can often be applied. Furthermore, gold complexes are usually less sensitive towards oxygen and water compared to many other transition metal complexes, which is of a great advantage for the chemist executing the catalysis. In addition, studies have shown that gold complexes are also often more active than other transition metals catalyzing the same reactions.[21] Gold is known for its ability to activate unsaturated species, such as alkenes and alkynes, towards nucleophilic attack, and nucleophilic addition to coordinated unsaturated species at gold are key steps in gold catalysis (Scheme 1).[21-30] First, a coordination of the alkene or alkyne to gold occurs (step a), followed by a nucleophilic addition to form a gold alkyl or vinyl species (step b), and then a protolytic cleavage might occur to release the product (step c). Alkynes are the most common substrates for these reactions.[21]
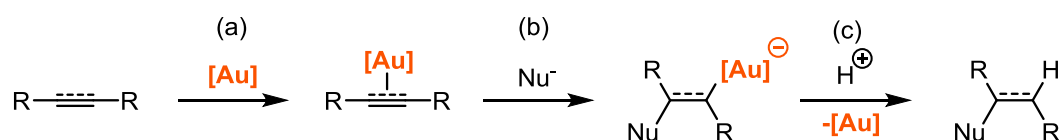
Scheme 1. Proposed general scheme for the activation of alkenes and alkynes toward nucleophilic attack at Au.[21]

Gold catalysis is not only limited to activation of unsaturated molecules towards nucleophilic addition and during the years of the work described in this thesis the field of Au chemistry has evolved dramatically. Many of the elementary organometallic reactions have now been demonstrated for gold and direct evidence for elementary organometallic steps such as reductive elimination, oxidative addition, transmetalation and migratory insertion have been reported.[31] Recently, evidence for β-hydride elimination from Au(III) complexes and agostic interactions at Au(III) centers were also reported.[32, 33] As the focus of this thesis is mainly on alkene and alkyne activation, these reactions will not be discussed in detail here.

1.2.2 Isolated putative intermediates in Au(I) and Au(III) catalysis

Gold π complexes of alkenes and alkynes, together with gold vinyl complexes, are all invoked as putative intermediates in gold catalysis (Scheme 1).[22, 24, 34] For gold in the oxidation state +1, the

---

[i] Searching for "gold + catalysis" on SciFinder (19.10.2018) gave 37000 hits.

3

nucleophilic addition to alkenes and alkynes have been widely investigated and all the Au(I) intermediates proposed for the mechanism of the reaction in Scheme 1 were isolated and characterized early compared to similar isolated Au(III) analogues. The first report of gold alkene complexes arrived in 1964, reported by Chalk. These complexes were generated by mixing AuCl and AuCl₃ with 1,5-cyclooctadiene (cod) and were characterized by IR spectroscopy and elemental analysis.[35] The first reports of structurally characterized Au(I) alkene[36] and Au(I) alkyne[37] complexes were reported in 1987 and 1995, respectively. Following these, several Au(I) alkene and alkyne π complexes have been reported.[22, 24] However, for gold in the oxidation state +3 less research has been performed, probably due to the fact that less methods have been developed for the synthesis of Au(III) complexes, and it was just recently that the first well characterized Au(III) alkene[38, 39] and alkyne[40] complexes were reported. The two first reports on Au(III) alkene complexes arrived almost at the same time. First, in 2013, Bochmann and co-workers reported (*C,N,C*) Au(III) pincer alkene complexes with ethylene, cyclopentene, and norbornene coordinated at Au(III) (Scheme 2, top).[39] These complexes were isolated and characterized by NMR. Shortly after, our group reported the first structurally characterized Au(III) alkene complex, [Au(cod)Me₂]⁺[BArᶠ]⁻ (Scheme 2, bottom; BArᶠ = tetrakis[3,5-bis(trifluoromethyl)phenyl]borate).[38] Later, Bourissou and co-workers reported (*P,C*) cyclometalated Au(III) norbornene[41] and arene complexes.[42] Very recently, Bochmann and co-workers reported (*C,C*) Au(III) π complexes of 1,5-cyclooctadiene and norbornene, which were thermally stable under ambient conditions.[43]
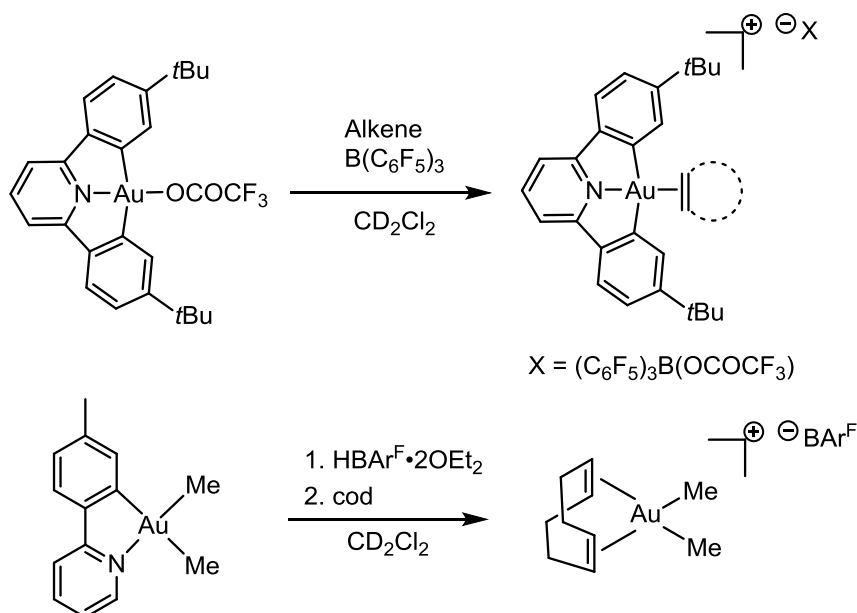
Scheme 2. The first reported Au(III) alkene complexes.[38, 39] In (a), alkene = ethylene, cyclopentene, and norbornene.

The first report of Au(III) alkyne complexes did not arrive until 2017. In the paper by Bochmann and co-workers three different types of Au(III) alkyne complexes are reported (Figure 5).[40] One set of

4

(*C,N,C*) pincer complexes with the alkyne bonded *trans* to pyridine-*N* (**A**), one set of (*N,C*) arylpyridine complexes where the alkyne is bound *trans* to aryl-*C* (**B**), and one tetrameric complex (**C**) containing three Au atoms and one Ag atom with the alkyne bound *trans* to the aryl-*C* of the Au moiety. **A** and **B** were characterized by NMR, and **C** was characterized by X-ray diffraction analysis.
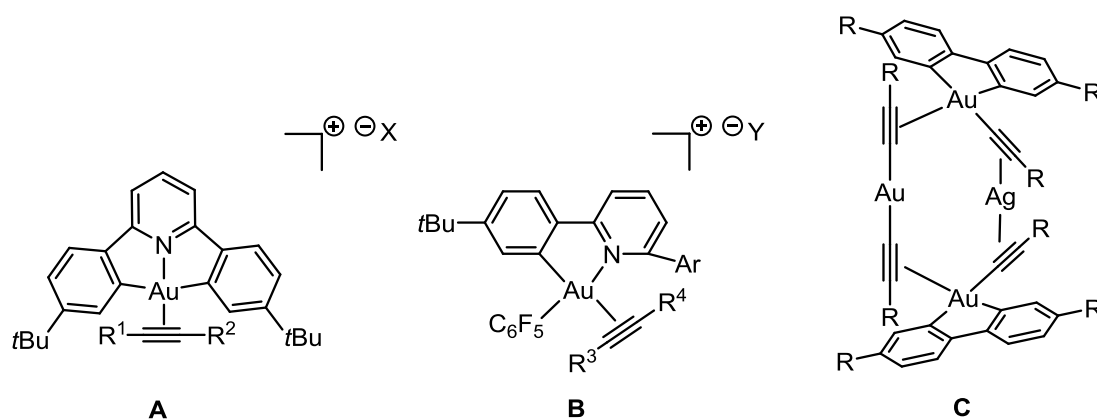
Figure 5. Au(III) alkyne complexes.[40] In **A** R^1 = *t*Bu, R^2 = Me or R^1 = R^2 = adamantyl, X = $(C_6F_5)_3B(OCOCF_3)$. In **B** R^3 = *t*Bu, R^4 = Me, or R^3 = R^4 = Et, Y = $H_2N(B(C_6F_5)_3)_2$. In **C** R = *t*Bu.

Au(III) vinyl complexes, which may result from nucleophilic addition to alkynes at Au(III), are more common than their Au(III) alkyne "cousins". However, there are still rather few reports on Au(III) vinyl complexes.[44-47] In the case of Au(I), there are several examples of vinyl complexes reported in the literature and these will not be discussed here.[24] Ahn and co-workers reported the Au(III) mono- and divinyl complexes, **A-D** in Scheme 3, which were isolated from reactions between *N*-(propargyl) benzamides and AuCl$_3$ and characterized by NMR, **A** and **C**-**D** were also characterized crystallographically.[44]
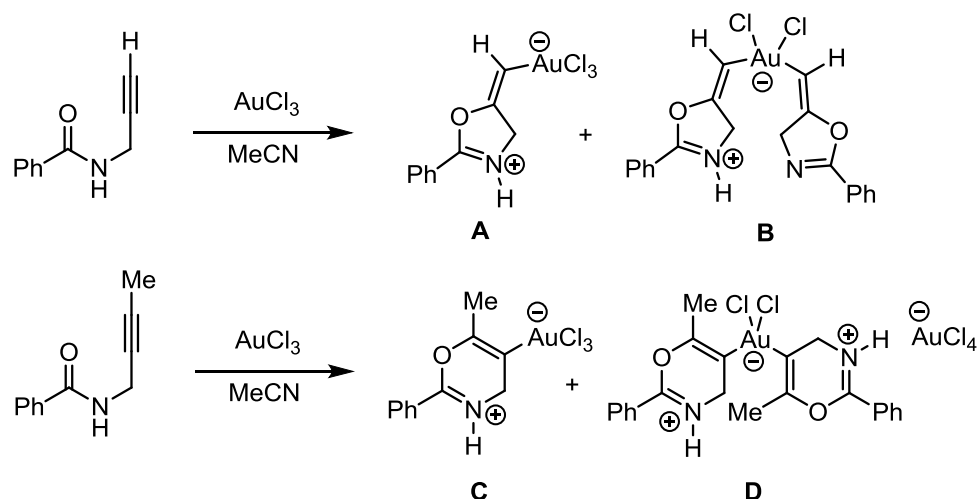
Scheme 3. Au(III) vinyl complexes prepared by reacting AuCl$_3$ with *N*-(propargyl) benzamides.[44]

More recently, Bochmann and co-workers reported alkyne hydrometallation with Au(III) hydrides, leading to Au(III) vinyl complexes (Figure 6, left).[46] Following this, Nevado and co-workers reported

the reaction of a Au(III) formate (Figure 7, top left, *vide infra*) with di-*tert*-butyl acetylenedicarboxylate yielding a Au(III) vinyl complex (Figure 6, right).[48]
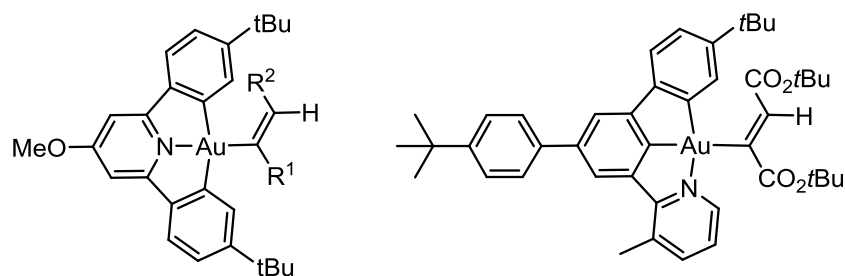
Figure 6. Au(III) vinyl complexes reported by Nevado[48] and Bochmann.[46] R^1,R^2 = H, alkyl, aryl, silyl.

As mentioned previously, gold catalysis is not limited to activation of unsaturated molecules towards nucleophilic addition, even though this is the main focus in this thesis. Other important classes of Au(III) complexes have recently been discovered, including the following types of complexes: Au(III) hydride[47], Au(III) fluoride,[12] Au(III) carbene,[49] Au(III) formate,[48] Au(III)CO,[50] and Au(III)CO$_2$[50] (Figure 7).
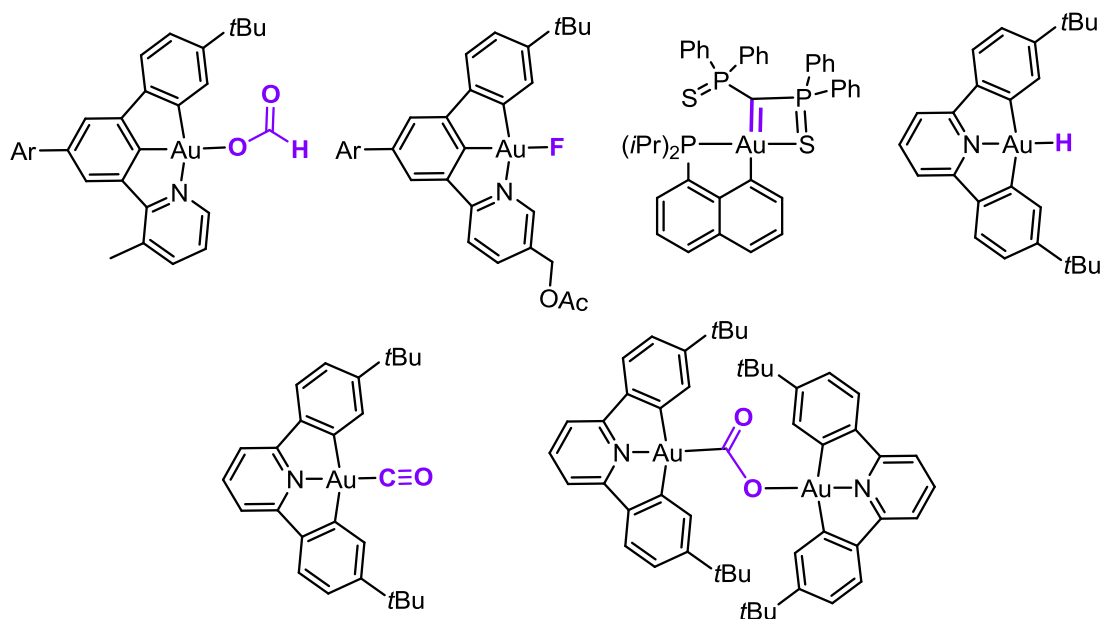
Figure 7. New classes of Au(III) complexes recently discovered.[12, 47-50]

1.2.3 Heterogeneous gold catalysis

Heterogeneous gold catalysis is an important part of gold catalysis. However, since the work described in this thesis mainly covers molecular complexes and homogeneous catalysis, the topic of heterogeneous catalysis will only be discussed briefly, including only a few selected examples of heterogeneous gold catalysis. However, it is important to know a bit about heterogeneous gold catalysis when working with homogenous gold catalysis. Heterogeneous catalysis can occur as a background reaction when performing catalysis with molecular complexes in solution, either due to

trace impurities present or due to decomposition of the molecular complexes into for example Au particles. This issue will be further addressed in Chapter 4, Section 4.2.5.

One of the oldest gold catalyzed reactions reported is the hydrogenation of alkenes.[27] Pioneering studies in the field of activation of hydrogen at Au was performed by Bone and Wheeler in 1906 followed by the work of Couper and Eley in 1950.[27] Following these studies, several examples of Au catalyzed alkene and alkyne hydrogenation have been reported.[27] One example is the work of Bond and co-workers (Scheme 4) from 1973 where they report the hydrogenation of 1-pentene, 1,3-butadiene, and 2-butyne.[51] In the case of 1-pentene only one product, pentane, is obtained. Whereas, with 1,3-butadiene and 2-butyne a mixture of the three products; 1-butene, *trans*-2-butene, and *cis*-2-butene were obtained. Starting with 1,3-butadiene led to the formation of 1-butene as the major product and starting with 2-butyne led to *cis*-2-butene as the major product.[51]
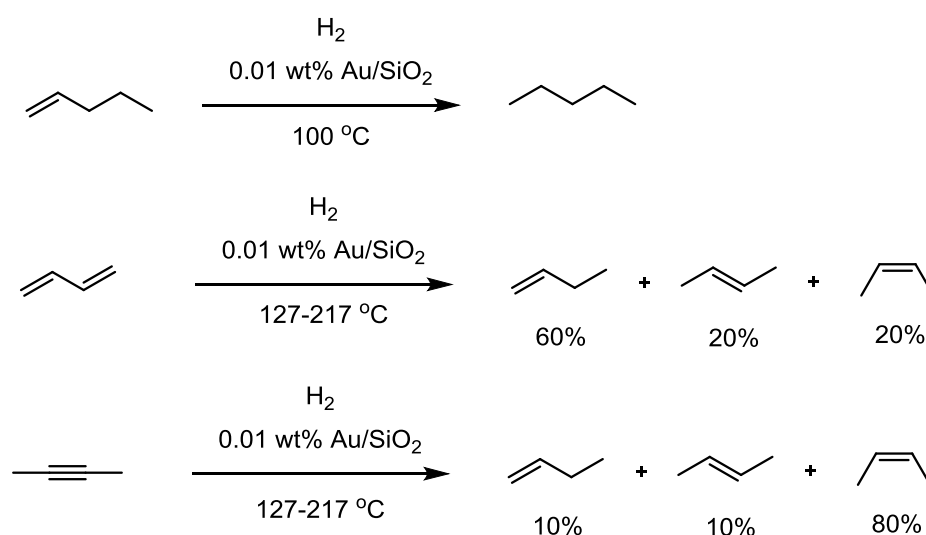
Scheme 4. Au catalyzed hydrogenation of 1-pentene, 1,3-butadiene, and 2-butyne.[51]

Another important example from heterogeneous gold catalysis is the acetylene hydrochlorination reaction. Hydrochlorination of acetylene is an important route for the production of vinyl chloride, which is an important monomer in the polymer industry for making polyvinyl chloride (PVC).[52] Traditionally, the acetylene hydrochlorination has been performed using a mercuric chloride catalyst supported on carbon (Scheme 5, top).[52] However, it is desirable to avoid the use of mercury due to its toxicity.[3, 53, 54] Furthermore, there have been other problems with the mercury catalyst such as loss of mercury and short lifetime of the catalyst.[52] In 1985, Hutchings predicted that Au(III) would be an ideal catalyst for the acetylene hydrochlorination due to its high standard reduction potential.[55] In 2008, a mechanistic study of the acetylene hydrochlorination over a Au/C catalyst was reported (Scheme 5, top).[56] During these mechanistic studies, 1-hexyne was investigated in addition to acetylene. It was found that upon reacting 1-hexyne with deuterated hydrochloric acid (DCl) the

Markovnikov product was obtained by *anti* addition of DCl to 1-hexyne (Scheme 5, bottom).[52, 56] In 2015, 30 years after the initial discovery, a commercial process utilizing a supported Au/C catalyst prepared by Hutchings and co-workers was developed and is now operating at a pilot plant in China.[52] Furthermore, a dedicated catalyst manufacturing plant for the supported Au catalyst has been built.[52]
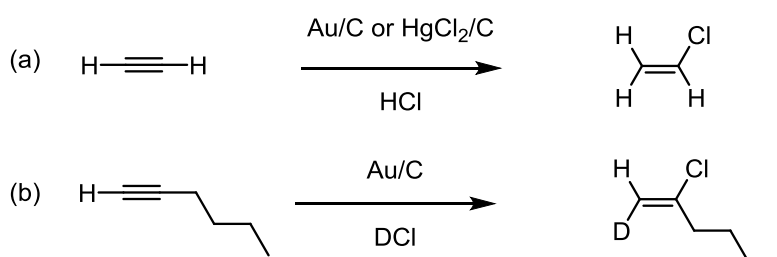
Scheme 5. (a): Acetylene hydrochlorination with either supported Au(III) or Hg(II).[52, 54, 56] (b): Reaction of 1-hexyne with DCl yielding the Markovnikov product *via anti* addition.[52, 56]

CO oxidation is also a popular topic within heterogeneous gold catalysis.[57] In 1980, Haruta and co-workers discovered the oxidation of CO to CO_2 over supported Au nanocrystals at temperatures far below 0 °C[58] and thereby outperforming the other catalyst alternatives present at that time.[57]

1.2.4 Homogenous gold(I) catalysis

Au(I) catalysis has become a very popular topic within catalysis and organic chemistry.[21, 59] Au(I) complexes are more frequently used than Au(III) complexes in gold catalysis, probably due to the fact that the synthesis of Au(I) complexes has been more explored than that of Au(III). Furthermore, there is quite a good selection of Au(I) catalysts available from commercial sources, [ii] making them more available to researchers which do not specialize in organogold chemistry. The typical Au(I) catalyst (LAuX, Figure 8) usually bears a *N*-heterocyclic carbene ligand or a phosphine ligand (L) and a chloride ligand (X).[60] These catalysts are usually activated *in situ via* abstraction of the chloride by a silver salt (typically: $AgSbF_6$, $AgNTf_2$, $AgBF_4$, etc.; Tf = SO_2CF_3) forming the cationic complex $[LAu]^+ X^-$.[26, 60-62] Due to the *in situ* activation step, the "silver effect" in gold catalysis has recently been investigated and it has been found that, in a few cases, silver is not completely innocent; it can participate in the catalysis.[61]
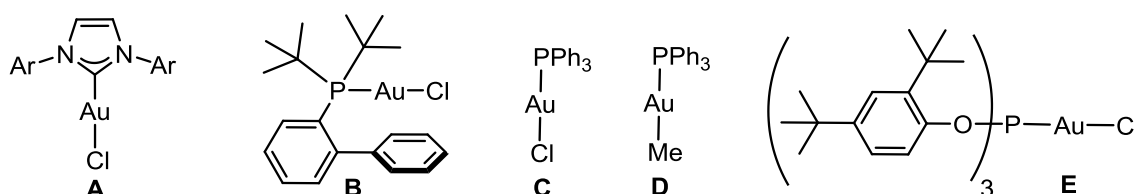
Figure 8. Some common Au(I) precatalysts (before activation by abstraction of the halide with a silver salt) often encountered in literature.[21, 60] Ph₃PAuMe is usually activated by reacting it with $MeSO_3H$.

[ii] Some examples of Au(I) complexes available from Sigma Aldrich/Merck per. 17.09.2018 include Ph₃PAuCl, IPrAuCl (complex **A**, Figure 8, with Ar = 2,6-diisopropylphenyl), and JohnPhosAuCl (Complex **B**, Figure 8).

The first example of homogenous Au(I) catalysis did not appear until 1998 where addition of alcohols to alkynes was reported (one example is given in Scheme 6).[63] In this work by Teles and co-workers, the putative active Au(I) catalyst is generated *in situ* by reacting Ph₃PAuMe with methanesulfonic acid.[63] After this discovery, the interest in homogenous Au(I) catalysis has exploded and there are several publications on Au(I) catalysis in the literature.[21, 25-27, 60, 64] One example of the use of Au(I) catalysis in total synthesis is given in Scheme 7 where the use of Ph₃PAuCl (activated with AgOTf) in the synthesis of the hexacyclic core of Communesin B was demonstrated.[65]
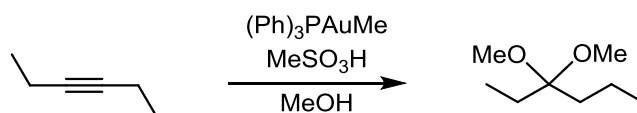
Scheme 6. Au(I) catalyzed addition of MeOH to 3-hexyne.[63]
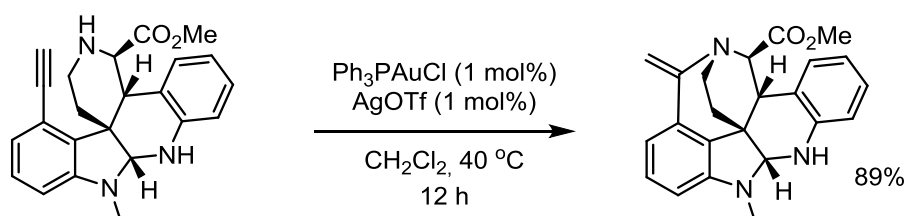
Scheme 7. Use of Au(I) catalysis in the total synthesis of the Communesin B hexacyclic core.[65]

1.2.5 Homogenous gold(III) catalysis

One of the first examples of homogenous gold(III) catalysis was reported in 1976 by Thomas and co-workers where they investigate the reactivity of mono- and disubstituted alkynes towards HAuCl₄ in a methanol and water mixture at elevated temperatures (Scheme 8).[21], [66] In these experiments they obtained the corresponding ketones as the major products (**A**, when R^2 = H and $R^1 \neq$ H) by Markovnikov addition of water to the triple bond. When internal alkenes (R^1, $R^2 \neq$ H) were used, **B** was obtained as well. Small amounts of **C** and **D** were also obtained in these experiments.
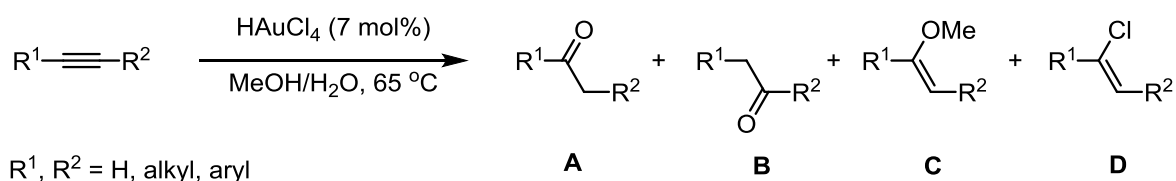
Scheme 8. Reactivity of alkynes towards HAuCl₄ in a MeOH and H₂O mixture.[21, 66]

Gold catalyzed synthesis of heterocycles has gained a lot of attention the recent years.[67] Some examples of heterocycles easily accessed by gold catalysis are furans, pyridines, and pyrroles.[67] The first generation of gold catalyzed synthesis of heterocycles was initiated by the work of Utimoto and co-workers.[67] In their work, they report the Au(III) catalyzed synthesis of tetrahydropyridines and one example is given in Scheme 9.[68]
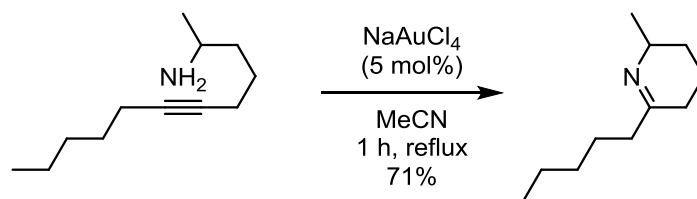
Scheme 9. Au(III) catalyzed synthesis of a tetrahydropyridine.[67, 68]

Three examples of Au(III) catalyzed furan syntheses are given in Scheme 10 where (*Z*)-3-ethynylallyl alcohols, an allenyl ketone, and a propargyl ketone are cyclized to furnish furanes with various substitution patterns, utilizing low catalyst loadings of $AuCl_3$.[69, 70]
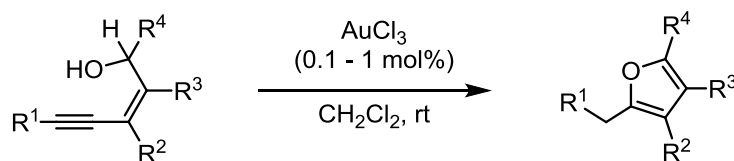
R^1, R^2, R^3, R^4 = alkyl, aryl, etc.
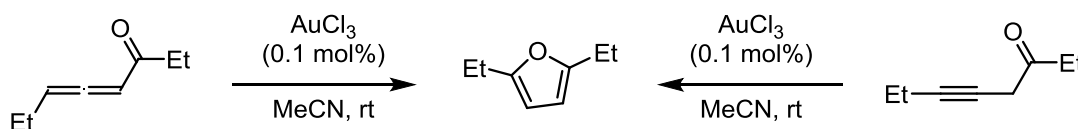
Scheme 10. Au(III) catalyzed synthesis of furans.[69, 70]

A vast majority of the catalysis with Au(III) is performed by using simple Au(III) salts such as $AuCl_3$, $HAuCl_4$, $KAuCl_4$, $NaAuCl_4$ etc.[71] This is also the case for the examples shown in Scheme 8, Scheme 9, and Scheme 10. Hashmi and co-workers demonstrated the importance of tuning the ligands in gold catalysis in their phenol synthesis (Scheme 11). Whereas the tested Au(I) complexes did not give the desired reactivity, $AuCl_3$ could do the job with more simple substrates (R = Ts; Ts = 4-$CH_3C_6H_4SO_2$), but when moving to more complicated substrates, a more sophisticated pre-catalyst, such as the Au(III) complex shown in Scheme 11 with a chelating (*N,O*) pyridine type ligand, was needed in order to achieve full conversion into the desired product.[72] Furthermore, when performing the reaction shown in Scheme 11, an induction period was observed experimentally. When repeating the catalysis one more time with the "pre-used catalyst" this induction period disappears. This may indicate that the true catalyst is not the Au(III) complex shown in Scheme 11, but is actually another complex which is generated *in situ*.[72] When working with catalysis, it is important bear in mind that the complex one weighs out and puts into the flask in the lab is not always the active catalyst. Chelated Au(III) (*N,O*) complexes such as the one showed in Scheme 11 have gained a lot of attention and have been used as catalysts for a wide variety of transformations since the first generation of these complexes were synthesized in 1992 by Parish and co-workers.[7, 73]
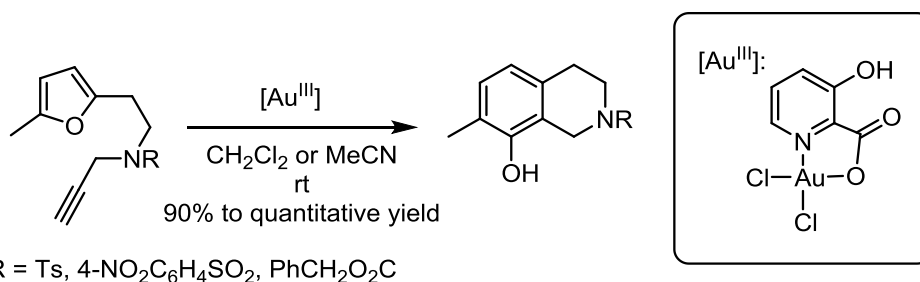
Scheme 11. Au(III) catalyzed phenol synthesis.[72] The reaction with R = Ts (Ts = SO₂C₆H₄Me) could also be performed with [Au^{III}] = AuCl₃ and AuCl₃(pyridine), and other related chelated complexes based on pyridine-2-carboxylates.

Au(III) arylpyridines have also been used in gold catalysis. One example being the work of Urriolabeitia, Contel, and co-workers where they report a Au(III) catalyzed addition of 2-methylfuran to methyl vinyl ketone (Scheme 12).[74] In this reaction, AuCl₂(ppy) (ppy = 2-phenylpyridine) could be used as a pre-catalyst in combination with AgOTf. The ppy-ligand in AuCl₂(ppy) resembles the ligand used in the complexes prepared in this thesis bearing the closely related 2-(p-tolyl)pyridine ligand (tpyH). Au(III) iminophosphorane complexes and other related complexes could also be used as pre-catalysts in the reaction in Scheme 12.
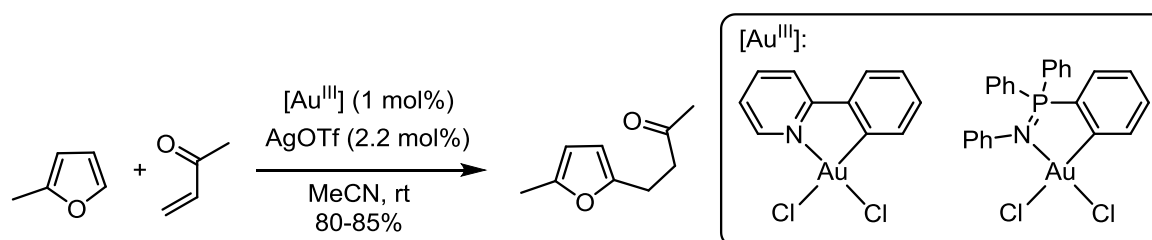
Scheme 12. Au(III) catalyzed addition of 2-methylfuran to methyl vinyl ketone.[74]

Furthermore, Strand and co-workers reported that AuCl₂(bnpy) (bnpy = 2-benzylpyridine) could catalyze the three component synthesis of substituted oxazoles (Scheme 13).[75]
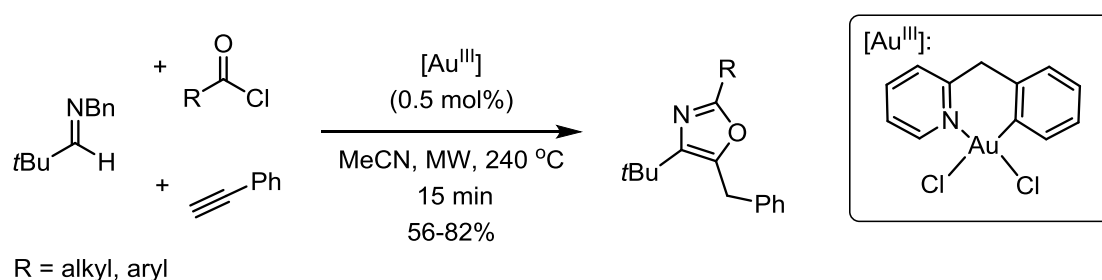
Scheme 13. Au(III) catalyzed three component synthesis of substituted oxazoles.[75]

1.3 Synthesis of cyclometalated Au(III) complexes

Cyclometalation is an intramolecular process where a C-R bond (R = C, O, Si or H, where R = H is by far the most common) in a ligand is activated forming a M-C bond (Scheme 14).[76, 77] The reaction usually consists of two consecutive steps: first ligand coordination *via* a heteroatom donor group (for example N, O, P, S, Se, and As) and then subsequent C-R (usually C-H) activation.[77] A large majority of the

cyclometalated Au(III) complexes are (*N,C*) complexes containing pyridine-*N* as the donor atom,[7, 78] this is also the case for the complexes prepared in this thesis, and therefore the main focus will be on (*C,N*) cyclometalated complexes. Au(III) complexes bearing tridentate pincer ligands are also a popular type of cyclometalated complexes and will be further discussed in Chapter 5.
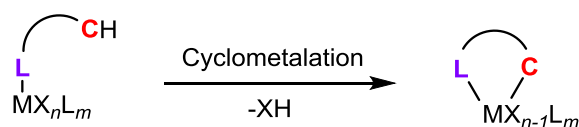
Scheme 14. General representation of cyclometalation where **L** represents the donor group and R = H.[76, 77]

Cyclometalated Au(III) complexes have gained a lot of popularity due to the increased stabilization of the Au(III) center towards reductive elimination to Au(I).[7, 78] Upon cyclometalation with gold (cycloauration), a five membered ring chelate is usually formed, but there are also several examples of six-membered ring chelates.[78] Most of the examples involves activation of a C(sp^2)-H bond, but there are also a few examples of C(sp^3)-H activation, this will be further discussed in Chapter 5.[7, 78] Some examples of cyclometalated Au(III) complexes are given in Figure 9.
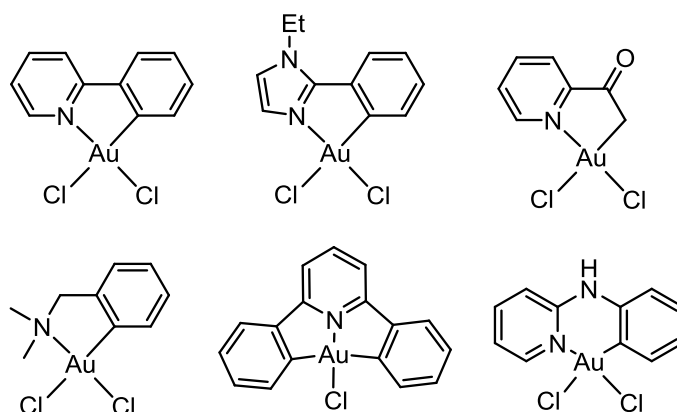
Figure 9. Some examples of cyclometalated Au(III) complexes.[13, 79-83]

There are three main strategies for synthesizing cylcometalated Au(III) complexes reported in the literature:[7, 78]

(a) By transmetalation from the corresponding organomercury precursor.

(b) By heteroatom coordination (*e.g.* coordination of Ar-*N*) followed by Ag(I) promoted halogen abstraction to give cyclometalation.

(c) By direct coordination of heteroatom (*e.g.* coordination of Ar-*N*) followed by strong heating or microwave conditions to furnish the cyclometalation.

Traditionally, transmetalation from organomercury compounds has been the main strategy for preparing cyclometalated Au(III) complexes and a wide variety of complexes can be prepared by this

method.[78] Two examples of preparation of cyclometalated Au(III) complexes *via* transmetalation from organomercury compounds are shown in Scheme 15.[13, 84] However, as many organomercury compounds are highly toxic it is desirable to avoid using the mercury strategy.[3, 53, 54]
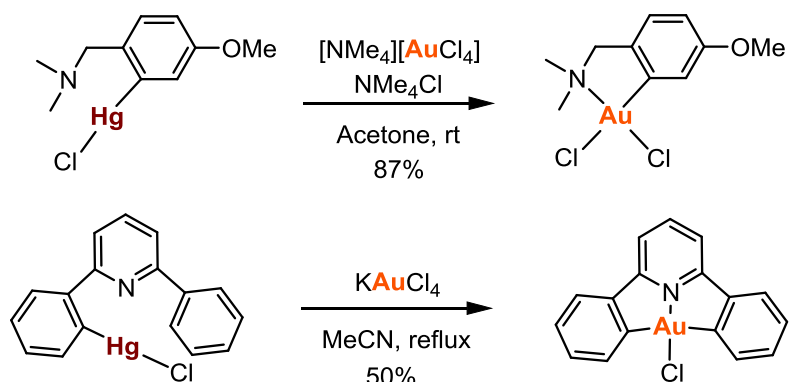
Scheme 15. Two examples of synthesis of cyclometalated Au(III) complexes *via* transmetalation from organomercury complexes (method a).[13, 84]

Although reported in the literature,[7, 78] the Ag(I) assisted method for the synthesis of cyclometalated Au(III) complexes (method b) has been used to a lesser extent than the organomercury method (method a), one example is given in Scheme 16.[85] One major advantage of method b is that the use of toxic organomercury compounds is avoided.
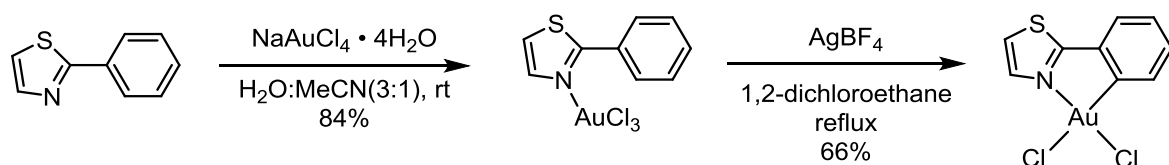
Scheme 16. Ag(I) assisted synthesis of a cyclometalated Au(III) complex (method b).[85]

Pioneering work in the field of cyclometalated Au(III) complexes was performed by Constable and Leese in 1989. They investigated the reactivity of HAuCl$_4$ and NaAuCl$_4$ towards 2-phenylpyridine (ppyH) furnishing the ppy-*N* bonded AuCl$_3$(ppyH) which upon heating in MeCN underwent cyclometalation to form AuCl$_2$(ppy) (Scheme 17).[79] This thermal method (method c) is mercury-free, which is a great advantage avoiding toxic organomercury compounds. It is also beneficial to avoid the use of stoichiometric amounts of silver salts.
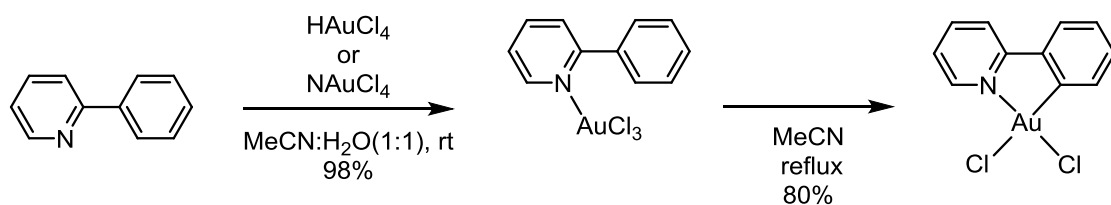
Scheme 17. Synthesis of AuCl$_3$(ppy) (ppy = 2-phenylpyridine) and AuCl$_2$(ppy) reported by Constable and Leese (method c).[79]

There has however been reported in the literature that the mercury-free method in Scheme 17 gives variable results. For example, Eisenberg and co-workers report quantitative recovery of AuCl$_3$(ppyH) when attempting to synthesize AuCl$_2$(ppy), and from thermogravimetric studies, they found that the cyclometalation occurred between 150-220 °C,[86] which is significantly higher than the MeCN reflux temperature utilized by Constable and Leese for the synthesis of AuCl$_2$(ppy).[79] Following the work by Constable and Leese, Henderson and co-workers reported the synthesis of AuCl$_2$(tpy) (**1**) by utilizing the same synthetic strategy as was used for AuCl$_2$(ppy).[87] However, the synthesis gave a rather low yield of **1**. These findings exemplify the need to develop a robust, mercury free, synthetic protocol for the preparation of this type of Au(III) complexes. In 2011 our group reported a microwave assisted synthesis furnishing AuCl$_2$(ppy) in good yields (83%) in a one pot reaction starting from 2-phenylpyridine and HAuCl$_4$, which is heated at 160 °C in water in a closed microwave vessel for 1 hour (Scheme 18).[88] AuCl$_2$(ppy) could also be synthesized by microwave heating of AuCl$_3$(ppyH) in water. In the same paper, the microwave assisted synthesis of the six membered chelate AuCl$_2$(bnpy) and the five membered ring chelate **1** by microwave heating of aqueous mixtures of HAuCl$_4$ and bnpyH or tpyH, respectively, were reported (Scheme 18).[88]
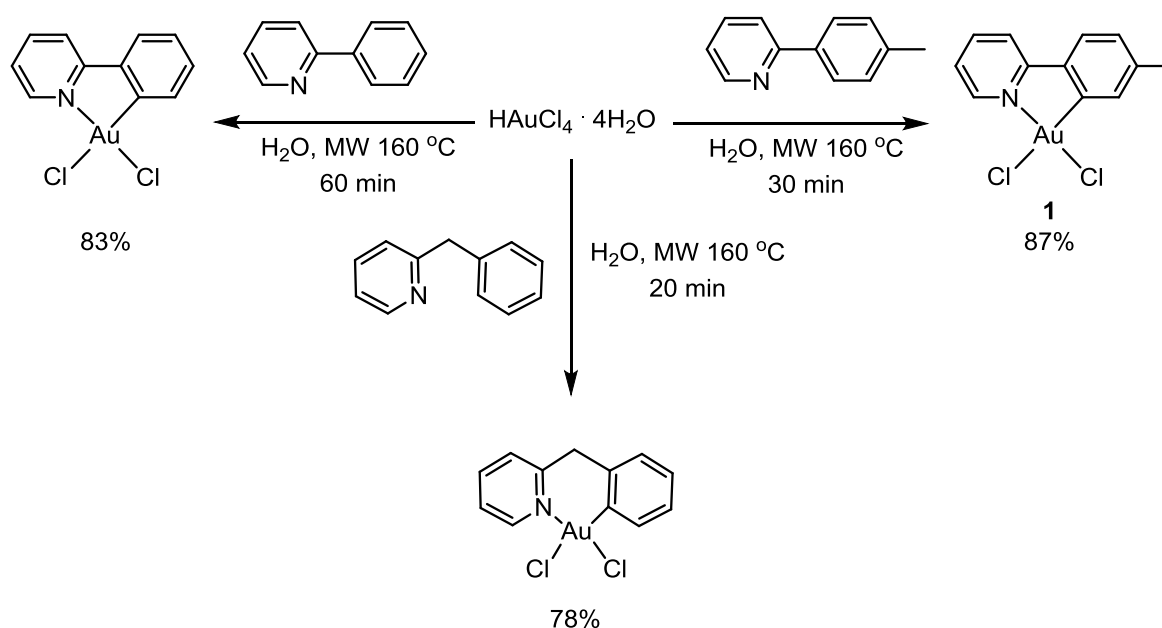
Scheme 18. Microwave assisted synthesis of AuCl$_2$(ppy), AuCl$_2$(tpy) (**1**), and AuCl$_2$(bnpy).[88]

1.3.1 Bis(trifluororacetate) Au(III) complexes

Acetates and trifluoroacetates are becoming popular ligands in Au(III) complexes. The lability of acetate and trifluoroacetate ligands renders complexes with such ligands more reactive than their corresponding chloro counterparts.[7] In 2012, our group reported the successful microwave assisted synthesis of Au(OCOCF$_3$)$_2$(tpy) (**2**) bearing two trifluoroacetate ligands.[89] Complex **2** was obtained in high yield by microwave heating of a mixture of tpyH and Au(OCOCH$_3$)$_3$ in a 1:1 mixture of CF$_3$COOH

and H$_2$O (Scheme 19). Complex **2** has shown a lot of interesting reactivity[89, 90] and will be a key complex in the research presented in this thesis.
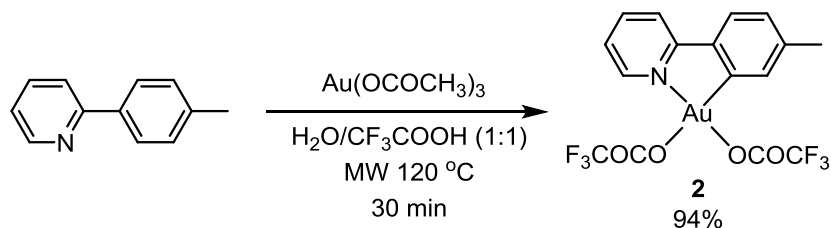
Scheme 19. Microwave assisted synthesis of Au(OCOCF$_3$)$_2$(tpy) (**2**).[89]

Very recently, Bourissou and co-workers reported the catalytic hydroarylation of alkynes using (*P,C*) cylcometalated Au(III) complexes bearing two trifluoroacetate ligands and one example is given in Scheme 20.[91] Interestingly, complex **2** together with two other related (*N,C*) cyclometalated Au(III) bis(trifluoroacetate) complexes were investigated in the reaction in Scheme 20 and it was found that the (*P,C*) system was superior over the (*N,C*) system (complex **2** gave only traces of product after prolonged reaction time and increased catalyst loadings, 24 h and 10 mol%, respectively).[91]
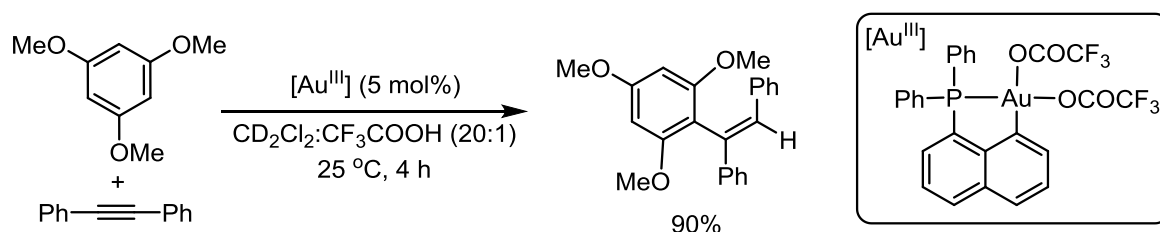
Scheme 20. One example of catalytic hydroarylation of alkynes using a (*P,C*) cyclometalated Au(III) bis(trifluoroacetate) complex.[91]

Complex **2** could be mono- or dialkylated by the use of Grignard reagents and organolithium reagents, respectively (Scheme 21).[89, 92, 93] The alkylations were also investigated for the corresponding AuCl$_2$(tpy) (**1**) complex and the dialkylation using organolithium reagents could be performed with prolonged reaction times. However, for the monoalkylation of complex **1** utilizing Grignard reagents a mixture of products were obtained.[89]

R = Ph, Me, CH$_2$SiMe$_3$, CCPh, *p*-tolyl

R = Me, Et, Ph, CHCH$_2$, CCH
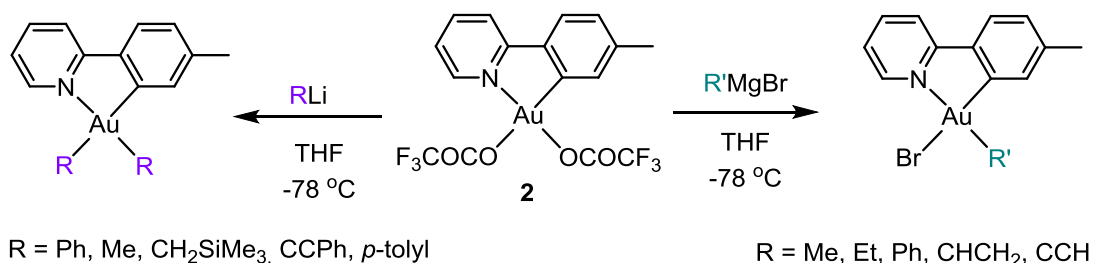
Scheme 21. Mono- and dialkylation of complex **2** using organolithium reagents and Grignard reagents.[89, 92, 93]

Several other cyclometalated Au(III) complexes with two trifluoroacetate ligands have been synthesized in the Tilset research group (Figure 10), but none of these have been published yet.

Complexes **2-Me₂**,[94] **2-OMe**,[95] and **2-COOH**,[96] and **2-COOEt**[96] have been prepared by present or previous group members. Complexes **2-CF₃**, **2-F₂**, and **2-CF₃Pyr** have been prepared by the author in collaboration with M.Sc. Knut Hylland, the synthesis and characterization of these complexes are not presented in this thesis.[97]
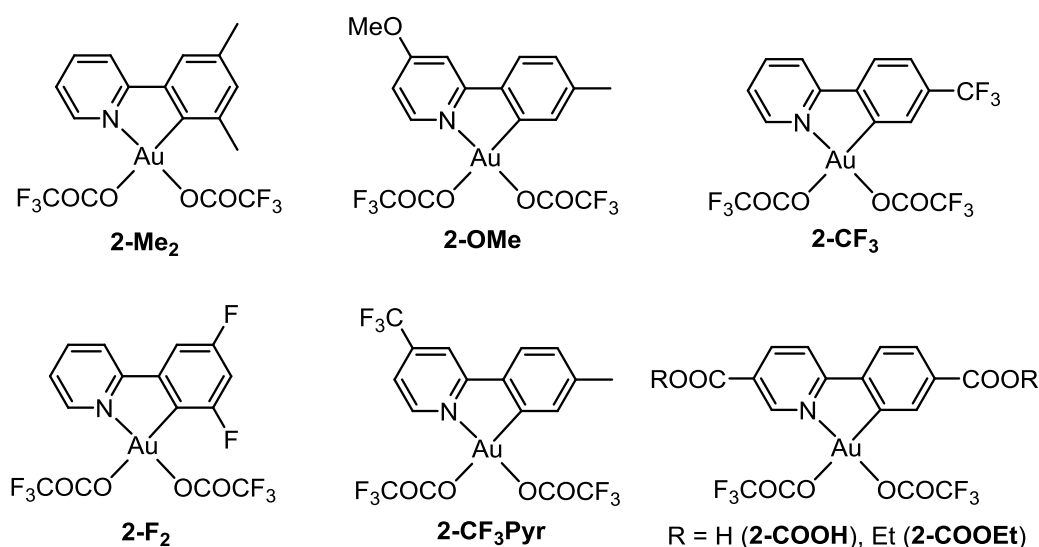
Figure 10. Other cyclometalated Au(III) bis(trifluoroacetate) complexes than **2** prepared in the Tilset group.[94-96]

1.4 Ethylene functionalization at Au(III)

There are only a few examples of ethylene functionalization at Au(III) in the literature and a brief summary is given in this section. Atwood and co-workers reported that ethylene could be stoichiometrically functionalized at [Au(bipy)Cl₂]⁺ (bipy = 2,2'-bipyridine) to furnish Au(III) hydroxyalkyl complexes that were observed in solution by ¹H NMR but not isolated (Scheme 22, top).[98] Furthermore, Bochmann and co-workers reported that ethylene undergoes a slow formal insertion into the Au-OCOCF₃ bond in a diarylpyridine (*C,N,C*) pincer complex (Scheme 22, bottom).[39] Bourissou and co-workers recently reported coordination-insertion reactions of norbornene[41, 42, 99] and ethylene,[32, 42] the latter followed by *β*-hydride elimination, into Au-C(*sp³*) and Au-C(*sp²*) bonds in (*P,C*) cyclometalated Au(III) alkyl and aryl complexes (one example is given in Scheme 23, top). Very recently, Bourissou and co-workers investigated the reactivity of a cationic (*N,C*) cyclometalated Au(III) complex towards ethylene. In this case a double insertion of ethylene into the Au-C(*sp²*) bond *trans* to aryl-*N* occurred, but no *β*-hydride elimination nor any rearrangement of the linear (CH₂)₄Ph chain were observed (see Scheme 23, bottom).[100] It is suggested that the absence of *β*-hydride elimination is due to the thermodynamically unfavored arrangement with a hydride *trans* to the high *trans* influence aryl-*C*.[100] Russell, Bower, and co-workers reported an oxidative 1,2-difunctionalization of ethylene *via* gold catalysis where one of the proposed key steps involves addition of an alcohol to ethylene at Au(III) (Scheme 24).[101]

16
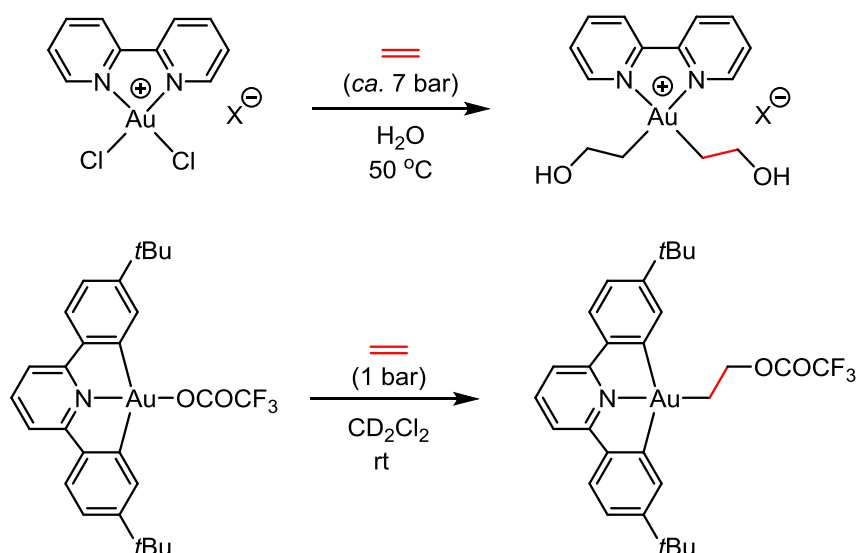
Scheme 22. Ethylene functionalization at AuCl$_2$(bipy)$^+$ X$^-$ (bipy = 2,2'-bipyridine, X = Cl or PF$_6$)[98] and a Au(III) (C,N,C) pincer complex.[39]

(a) *Insertion, β-H elimination, re-insertion*
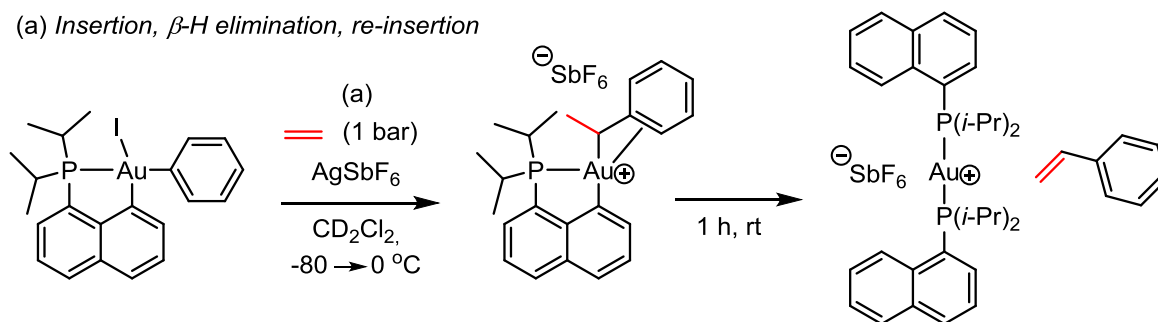
(b) *Double insertion*
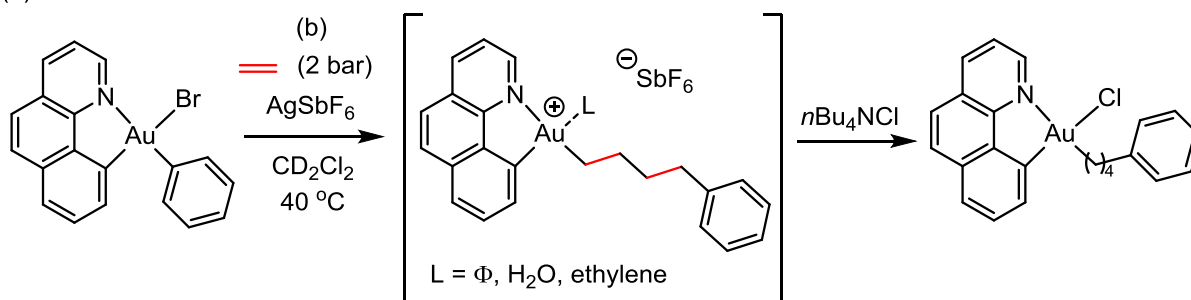
Scheme 23. Insertion of ethylene into Au-C(sp^2) and Au-C(sp^3) bonds in cationic Au(III) (P,C) and (N,C) cyclometalated complexes.[42, 100] In the (P,C) system, the insertion is followed by β-H elimination and re-insertion into the Au-H bond.[42] In the (N,C) system a double insertion occurred and no β-H elimination followed.[100]
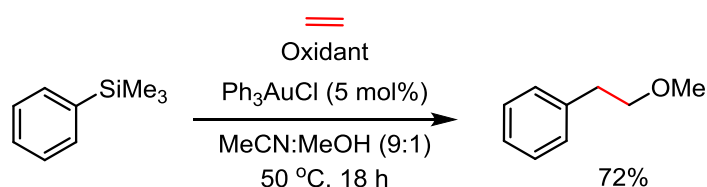
Scheme 24. Au catalyzed oxidative 1,2-difunctionalization of ethylene.[101]

The Tilset research group reported the formal insertion of ethylene into the Au-O bond *trans* to tpy-*N* in complex **2** furnishing complex **3** (Scheme 25).[90] The formal insertion is a two-step process where

first a ligand exchange of the $OCOCF_3$ ligand *trans* to tpy-*N* in complex **2** with ethylene occurs *via* associative substitution. Following this, an intermolecular (*anti*) nucleophilic addition of $^-OCOCF_3$ to ethylene furnish complex **3**.[90] In contrast to the formal insertion process, the coordination-insertion processes reported by Bourissou and co-workers discussed previously is a one-step concerted process.[31, 32, 41, 42, 99, 100]
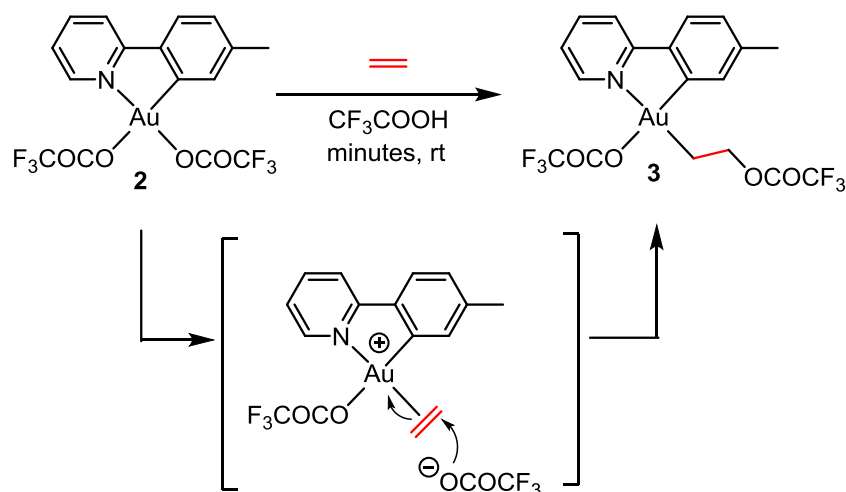
Scheme 25. Formal insertion of ethylene into the Au-O bond *trans* to tpy-*N* in complex **2** furnishing complex **3**.[90]

It could be shown experimentally that the nucleophilic addition of $^-OCOCF_3$ to ethylene was reversible.[90] Upon treating **3-d_4** with non-labelled ethylene, formation of **3** occurred, indicating that the nucleophilic addition is reversible under these conditions (Scheme 26).
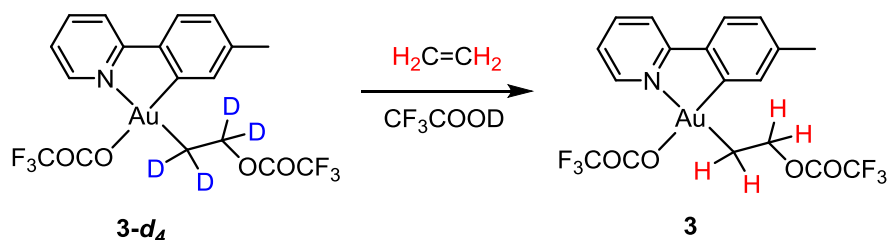
Scheme 26. Treating **3-d_4** with unlabeled ethylene led to the formation of **3**, indicating that the nucleophilic addition is reversible under these conditions.[90]

According to DFT calculations, the nucleophilic addition step is preferred both kinetically and thermodynamically *trans* to tpy-*N* over *trans* to tpy-*C*, which is in agreement with the experimental findings where complex **3** was observed as the only product of the reaction and no insertion *trans* to tpy-*C* occurred.[90] It was also possible to perform a nucleophilic addition of CF_3CH_2OH to ethylene at complex **2** furnishing complex **4**, and it was found that complexes **3** and **4** could be interconverted by appropriate solvent choice (Scheme 27), further indicating that the nucleophilic addition is reversible.[90] The reaction of ethylene and **2** in CF_3COOH comes to a stop after one ethylene insertion. Several attempts at achieving a catalytic process for this reaction was performed, including addition

of the stronger triflic acid (TfOH) and increasing both the ethylene pressure and the temperature (50 °C and 60 bar of ethylene), but none of these attempts led to catalysis.[90]
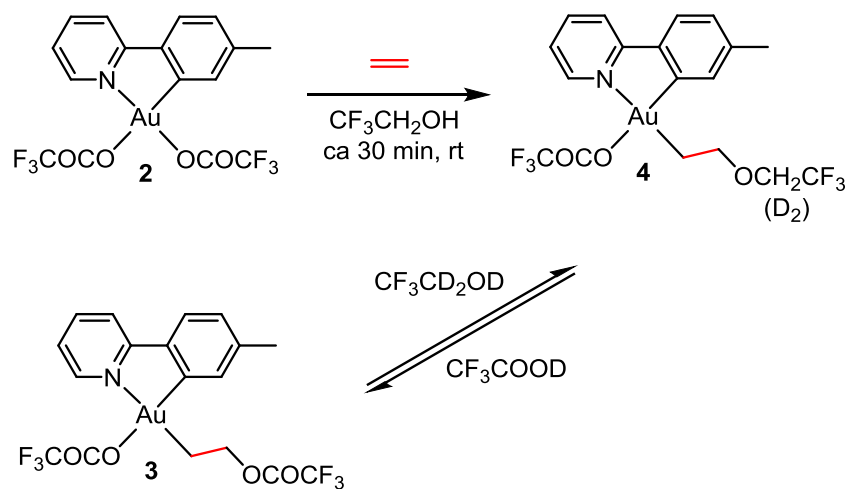
Scheme 27. Nucleophilic addition of CF_3CH_2OH to ethylene at **2** furnishing **4** and interconversion of **3** and **4**.[90]

The reactivity of Au(III) complex **2** towards ethylene depicted in Scheme 25 and Scheme 27 lays the foundation for the chemistry presenter in Chapter 2, Chapter 3, and Chapter 4.

Chapter 2 – Nucleophilic addition to alkenes at Au(III)

2.1 General introduction and scope of the chapter

The work presented In this chapter will focus on the nucleophilic addition of several different nucleophiles to a wide variety of alkenes at Au(III) complex **2** furnishing Au(III) complexes with C(sp^3) bonded ligands (Scheme 28). Most of the work presented in this chapter is covered in Paper I.

R, R', R" = H, alkyl or aryl

NuH = CF_3COOH, CH_3COOH, MeOH, EtOH, *i*-PrOH, *t*-BuOH, H_2O
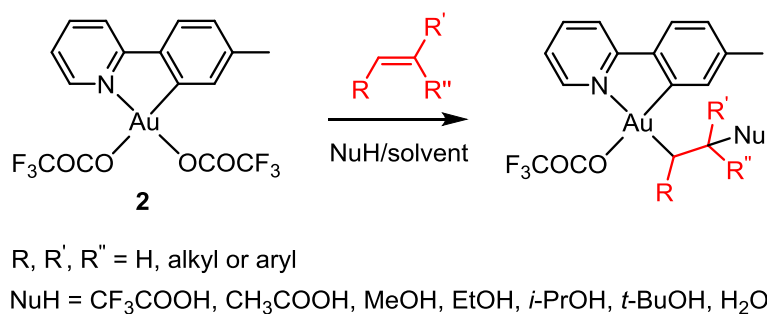
Scheme 28. Reactivity of **2** towards a range of alkenes and nucleophiles furnishing β-functionalized Au(III) alkyl complexes.

As mentioned in Chapter 1, gold is known for its ability to activate alkenes, alkynes and other unsaturated species towards nucleophilic addition, which is often the key step in gold catalysis.[21-30] Functionalization of alkynes and alkenes under mild conditions is of great interest, since cheap and readily available hydrocarbon building blocks then can be converted into more complex and useful compounds.[21, 23, 25, 67] The most studied substrates in these types of reactions are alkynes, but a lot of studies have been performed on alkenes and other unsaturated compounds as well. While the main focus has been on Au-mediated functionalization of unsaturated molecules towards more complex organic structures, there has been less work done on the more simple precursors such as ethylene and other small alkenes. Furthermore, more work has been performed on Au(I) than on Au(III) and consequently, there are only a few examples of Au(III) mediated functionalization of the important and readily available building block ethylene (see section 1.4, Chapter 1).[39, 42, 90, 98, 100, 101]

The work presented in this chapter builds on previous work performed in the Tilset research group, where the experimental work was performed by Dr. Eirin Langseth and M.Sc. Eline Aasen Tråseth and computational work was performed by Dr. Ainara Nova.[90] This work was described in Chapter 1 and a short reminder is given in Scheme 29, where the formal insertion of ethylene into the Au-O bond *trans* to tpy-*N* furnishing complex **3** is depicted. When the reaction in Scheme 29 was performed in CF_3CH_2OH, complex **4** was obtained instead. Following this, we were interested in learning more about the scope and regiochemistry of the reaction depicted in Scheme 29. Therefore, a wide variety of alkenes with different substitution patterns and different nucleophiles were investigated in this reaction (Scheme 28).
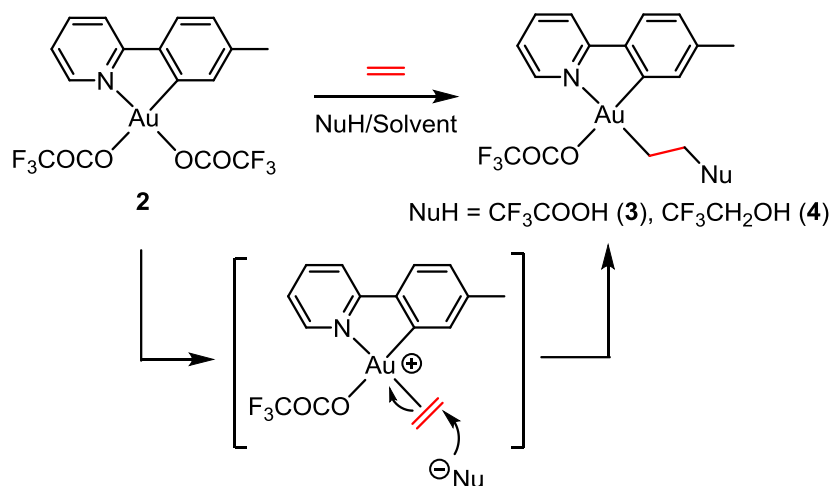
Scheme 29. Previously reported formal insertion of ethylene into the Au-O bond *trans* to tpy-*N* in complex **2**, furnishing complex **3**. If the reaction is performed in CF₃CH₂OH, complex **4** is formed instead.[90]

Several students in the Tilset research group were involved in the project described in this chapter and the main focus will be given on the author's contribution to the project. One of the other main contributors to this work was M.Sc. Franziska Stefanie Ihlefeld who worked on this project during her master degree studies.[102] Her work focused on reactions with various internal alkenes, dienes, and styrene and some highlights will be presented at the end of this chapter. M.Sc. Yannick Wencke worked on the reactions with 1-hexene described in Section 2.2 and 2.4 together with the author of this thesis. M.Sc. Erlend Solbakken Aunan worked on a related project as a part of his bachelor project and he has contributed to the work described in this chapter by growing crystals for single crystal X-ray diffraction analysis of complex **6a**.

2.2 Substituted alkenes with ⁻OCOCF₃ as nucleophile

2.2.1 1-Hexene

In the reaction of **2** with 1-hexene, there are two potential positions for the nucleophilic addition of ⁻OCOCF₃ to occur, either at the internal position of the double bond (C^b, in a Markovnikov manner), furnishing complex **5a**, or at the terminal position of the double bond (C^a), furnishing complex **5a'** (Scheme 30). When monitoring the reaction of complex **2** with 1-hexene in CF₃COOD by ¹H NMR, a clean transformation of **2** into **5a** (*vide infra*) was observed within minutes (Figure 11). However, complex **5a** was rather unstable, and after 3 hours *ca.* 40 % of **5a** had decomposed, and after 20 hours only traces of **5a** were left and the solution contained tpyD₂⁺ and several other decomposition products. Since complex **5a** decomposes upon removal of the solvent, it could not be isolated. Complex **5a** could however be generated and characterized in a mixture of CD₂Cl₂ and CF₃COOH (*ca.* 2 vol % CF₃COOH in CD₂Cl₂) by standard NMR techniques. In the ¹H NMR spectrum of **5a** some characteristic resonances are observed; at δ 5.40 a resonance with a complicated splitting pattern is found. This resonance originates from H^b (see labelling, Scheme 30) and indicates the formation of **5a**

and not **5a'** (in **5a'** H^b would be expected at a lower ppm value). Furthermore, at δ 2.42 and δ 2.46-2.50 the resonances of the two diastereotopic protons (H^a, the latter overlapping with tpy-*CH$_3$*) are observed ($^2J_{HH}$ = 10.4 Hz), again indicating the formation of **5a** and not **5a'**, since in **5a'** these would be expected at significantly higher ppm values. H^c is observed at δ 1.94, the overlapping resonances of H^d and H^e are found at δ 1.20-1.50, and a triplet belonging to the methyl group at the end of the alkyl chain is observed at δ 0.91. The characteristic shift of the resonance of H$^{6'}$ (see labelling, Figure 1) to a higher ppm value which was observed previously when going from **2** to **3** and **4**,[90] is also observed for complex **5a** (Δδ(H$^{6'}$) = 0.73). In the ^{19}F NMR spectrum of **5a**, two resonances corresponding to the two OCOCF$_3$ groups are observed at δ −77.1 and δ −78.0, similar to those observed for the previously reported complex **3**.[90] A ^{19}F-^{1}H HOESY experiment established that the resonance at δ −77.1 arises from the OCOCF$_3$ ligand *trans* to tpy-*C*. In agreement with the previously reported reaction of **2** with ethylene in CF$_3$COOD,[90] the insertion occurred in the position *trans* to tpy-*N*, as could be seen from a ^{1}H-^{1}H NOESY experiment where a NOE was observed between H^a and H$^{6'}$ and between H^b and H$^{6'}$. Selected key ^{1}H and ^{19}F NMR chemical shifts for complex **5a** and the other related complexes presented in this chapter (*vide infra*) are summarized in Table 1 (page 33) to aid the reader in the following NMR discussions.
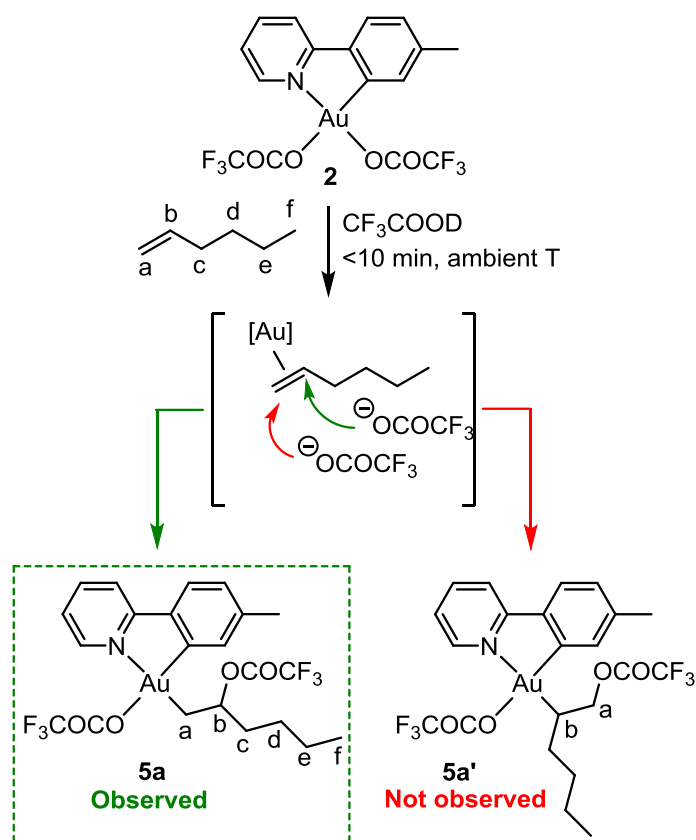
Scheme 30. Nucleophilic addition of $^-$OCOCF$_3$ to 1-hexene at **2** furnishing complex **5a**. Complex **5a'** was not observed. The atoms in the former 1-hexene unit are here labelled a-f to simplify the NMR discussions. [Au] = [Au(OCOCF$_3$)(tpy)]$^+$.
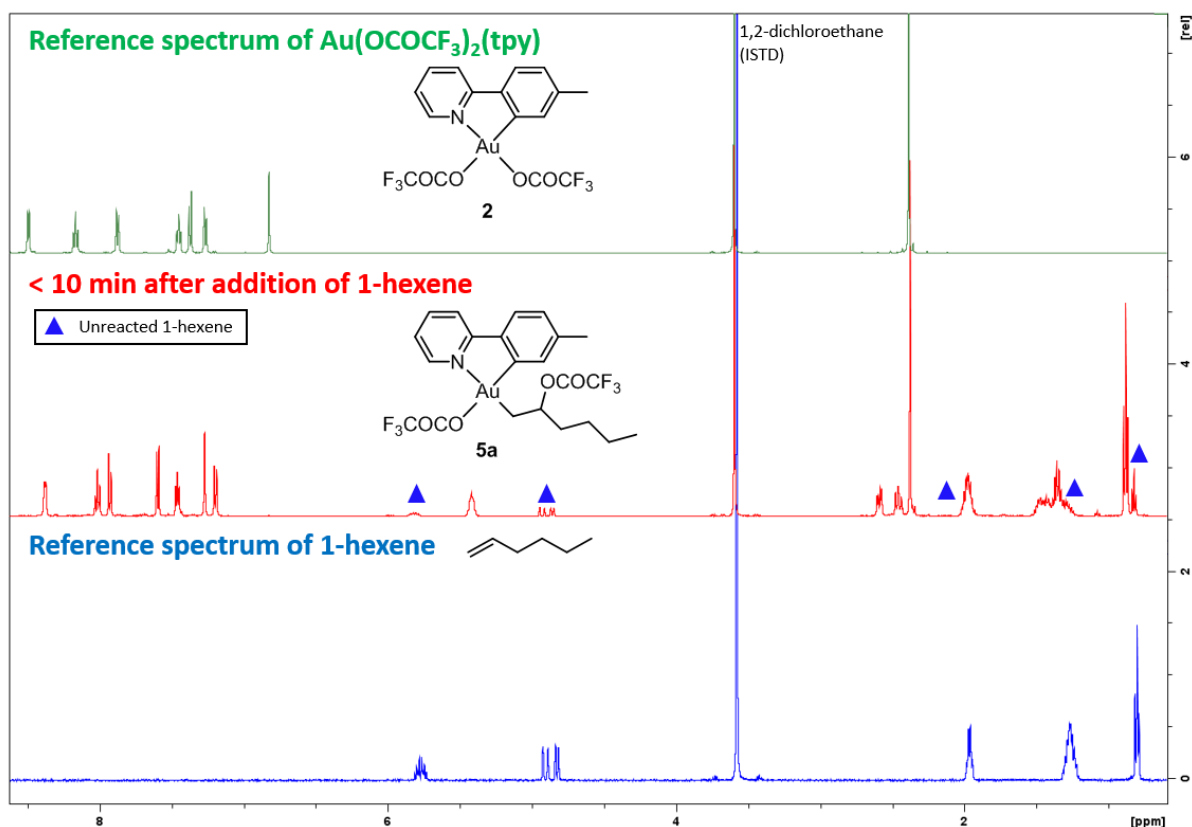
Figure 11. Stacked ^{1}H NMR (500 MHz, CF$_3$COOD) spectra showing the reaction of complex **2** with 1-hexene. Top: Reference spectrum of **2**, Middle: Spectrum acquired <10 minutes after mixing **2** with 1-hexene, showing a clean transformation of **2** into **5a**. Bottom: Reference spectrum of 1-hexene.

2.2.2 3-Methyl-1-butene

Nucleophilic addition to the more sterically crowded alkene 3-methyl-1-butene could also be achieved (Scheme 31). Upon reacting complex **2** with 3-methyl-1-butene in CH$_2$Cl$_2$, complex **6a** was obtained. The reaction with 3-methyl-1-butene had to be performed in CH$_2$Cl$_2$ instead of CF$_3$COOH due to the instability of the alkene in acidic media. Complex **6a** was significantly more stable than **5a** and was readily isolated in 60-77% yield. Complex **6a** was characterized by NMR, MS, X-ray diffraction analysis (as a CHCl$_3$ solvate, *vide infra*),[iii] and elemental analysis. As in the reaction with 1-hexene, nucleophilic addition occurred at the internal position of the alkene, in a Markovnikov manner. In the ^{1}H NMR spectrum of **6a**, H^b (see labelling, Scheme 31) is found at δ 5.31, comparable to that of **5a** (δ(H^b) = 5.40). The two diastereotopic protons (H^a) are found at δ 2.60 and δ 2.32 ($^2J_{HH}$ = 10.7 Hz), which is also similar to that of **5a**. H^c is found at δ 2.21 and the two diastereotopic methyl groups (CH$_3^d$ and CH$_3^e$) are found at δ 1.07 and δ 1.05 as two doublets. Two resonances are observed at δ −77.0 and δ −77.9 in the ^{19}F NMR spectrum of **6a**, similar to those of **5a**, corresponding to the two OCOCF$_3$ groups. A ^{19}F-^{1}H HOESY experiment show that the resonance δ −77.0 arises from the OCOCF$_3$ *trans* to

---

[iii] The crystal of **6a** used for the single crystal X-ray diffraction analysis was grown by M.Sc. Erlend Solbakken Aunan as a part of his bachelor thesis where he worked on synthesis and characterization of Au(III) complexes.[106]

24

tpy-*C*. Furthermore, two pairs of quartets corresponding to the two carbons in the OCOCF$_3$ groups are found in the ^{13}C NMR spectrum of **6a** at δ 161.3, 157.6, 118.2, and 115.0 with $^2J_{19F-13C}$ = 37.3 and 41.6 Hz and $^1J_{19F-13C}$ = 290.1, and 286.4 Hz, respectively. As was also observed for complex **5a**, a NOESY experiment established that the reaction had occurred in the position *trans* to tpy-*N*; a NOE was observed between H^a and H$^{6'}$ and between H^b and H$^{6'}$.
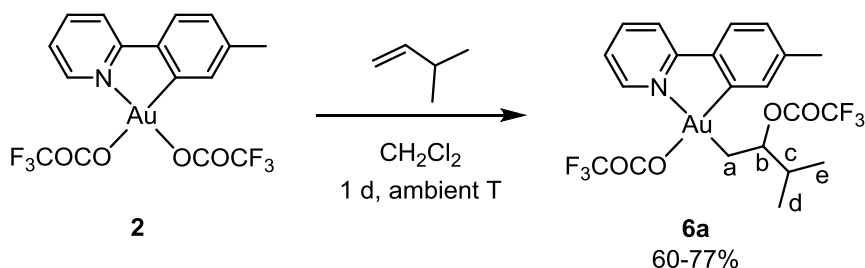
Scheme 31. Formal insertion of 3-methyl-1-butene into the Au-O bond *trans* to tpy-*N* in complex **2** furnishing complex **6a**. The atoms in the former 3-methyl-1-butene unit are here labelled a-e to simplify the NMR discussions.

The disubstituted and trisubstituted alkenes 2-methyl-1-butene and 2-methyl-2-butene were also investigated under the same reaction conditions as **5a**, but no insertion products could be isolated.

2.3 Ethylene with other nucleophiles

2.3.1 Acetic acid, methanol, and ethanol

The formal insertions with $^-$OCOCF$_3$ as a nucleophile showed a limited scope and gave products of variable stability. Therefore, other nucleophiles were investigated to extend the scope of the reaction. Initially, acetic acid and ethanol were investigated in the ethylene reaction (Scheme 32), since they are closely related to the previously investigated trifluoroacetic acid and trifluoroethanol. It was found that upon bubbling ethylene through a mixture of **2** in either CH$_3$COOH or EtOH for two minutes, followed by stirring at ambient temperature, the corresponding acetate and ethoxy products **7** (84-90% yield) and **8** (55-74% yield), respectively, could be obtained (Scheme 32). The reaction in CH$_3$COOH was rather slow, and 12 days were needed to achieve full conversion of **2** into product. The reaction in EtOH was faster, but in this case side product formation complicated the reaction. Small amounts (<15 %) of a side product, which later was found to be Au(OCOCF$_3$)(CH$_2$CH$_2$OH)(tpy) (**12**, *vide infra*), were formed along with **8**. Complex **12** will be further discussed in Section 2.3.2. Methanol was also investigated as a nucleophile in the ethylene reaction. Upon bubbling ethylene through a mixture of **2** in MeOH for two minutes, followed by stirring at ambient temperature for 1 day, complex **9** could easily be obtained in 72-74% yield (Scheme 32).[iv]

[iv] The reaction between **2** and ethylene in MeOH has previously been performed by Dr. Eirin Langseth but the product of the reaction was not characterized (See Dr. Eirin Langseth's Ph.D thesis for further details).[92]

Complexes **7** and **9** were characterized by NMR, MS, X-ray diffraction analysis (*vide infra*), and elemental analysis. Complex **8** was characterized by NMR and MS. All the complexes **7**-**9** exhibit the characteristic resonance for the CH_2CH_2 unit originating from ethylene in the ^{1}H NMR spectrum (at δ 4.42 and δ 2.38 for **7**, at δ 3.74 and δ 2.40 for **8**, and at δ 3.68 and δ 2.39 for **9**). In the ^{1}H NMR spectrum of **7**, the resonance corresponding to the acetate group is found at δ 2.04. For **8**, the resonances corresponding to the ethoxy group are found as a quartet at δ 3.55 and as a triplet at δ 1.19. The resonance corresponding to the methoxy group in **9** is found at δ 3.38. In all the complexes **7**-**9**, a NOE is observed between the CH_2CH_2 protons and H$^{6'}$, indicating that the reactions have occurred in the position *trans* to tpy-*N*. When investigating the complexes by ^{19}F NMR, it turned out that the OCOCF$_3$ ligand *trans* to tpy-*C* had remained in all the complexes. No exchange of the OCOCF$_3$ ligand with either OCOCH$_3$, OEt, or OMe was observed. For all three complexes **7**-**9**, one single resonance is observed in the ^{19}F NMR spectrum at δ −77.0, corresponding to the OCOCF$_3$ ligand *trans* to tpy-*C*. Furthermore, in the ^{13}C NMR spectrum of **7**-**9**, two quartets corresponding to the two carbons in the OCOCF$_3$ ligand are found.
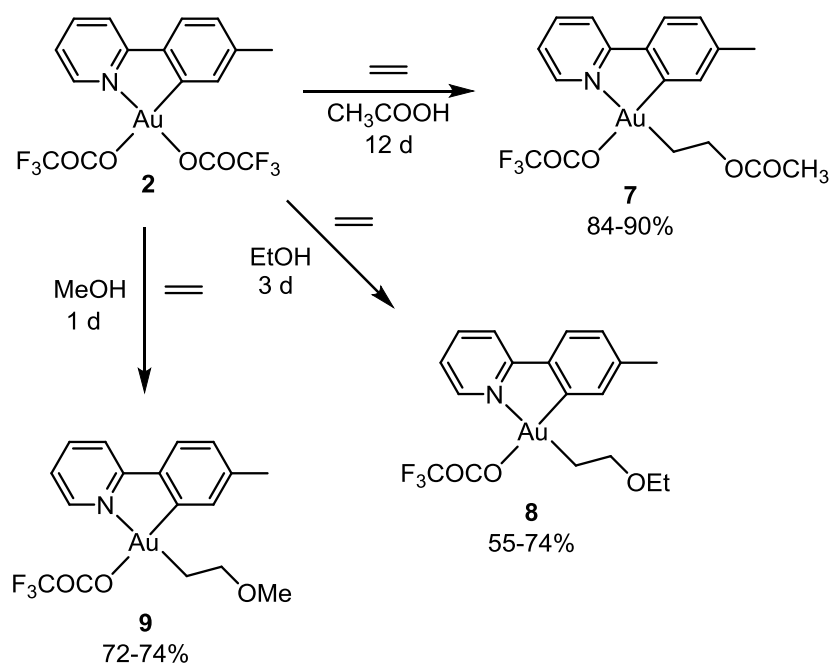
Scheme 32. Au(III) mediated nucleophilic addition of CH$_3$COOH, EtOH, and MeOH to ethylene at complex **2**, furnishing complexes **7**, **8**, and **9**. All the reactions depicted in this scheme are performed at ambient temperature.

2.3.2 *i*-Propanol and *t*-butanol

The more sterically crowded nucleophiles *i*-PrOH and *t*-BuOH were also investigated in the reaction with ethylene and complex **2** (Scheme 33). In the reactions depicted in Scheme 33, competition from the nucleophilic addition of $^-$OCOCF$_3$ (which has to dissociate from **2**) to ethylene was observed, leading to formation of **3**[90] as well as the desired products **10** and **11**. Furthermore, another side product (**12**, which was also formed in small amounts in the reaction with **2**, ethylene and EtOH in

Scheme 32) was formed in the reactions depicted in Scheme 33. Complex **12** is believed to originate from the addition of water to ethylene at **2** (*vide infra*). Despite repeated efforts to exclude water from the reactions furnishing complexes **8**, **10**, and **11**, complex **12** was always formed. Therefore, complexes **10** and **11** were characterized by NMR and MS in a mixture with **3** and **12**. In the ^{1}H NMR spectra of **10** and **11**, the resonances of the CH_2CH_2 unit are found at δ 3.74 and δ 2.37 for **10** and at δ 3.70 and δ 2.32 for **11**. Furthermore, in complex **10**, the characteristic resonances of the *i*-Pr group are observed in the ^{1}H NMR spectrum; at δ 1.16 and δ 3.68 the resonances of the methyl groups and the CH group are observed, respectively. For complex **11**, the characteristic *t*-Bu resonance is observed at δ 1.21 in the ^{1}H NMR spectrum. A NOE is observed between the CH_2CH_2 unit and H$^{6'}$ for both complexes, again indicating that the reactions have occurred in the position *trans* to tpy-*N*, in agreement with previous findings. In the ^{19}F NMR spectrum of complexes **10** and **11**, one single resonance is observed at δ −77.0 corresponding to the OCOCF$_3$ ligand *trans* to tpy-*C*, in agreement with that observed for complexes **7**-**9**.
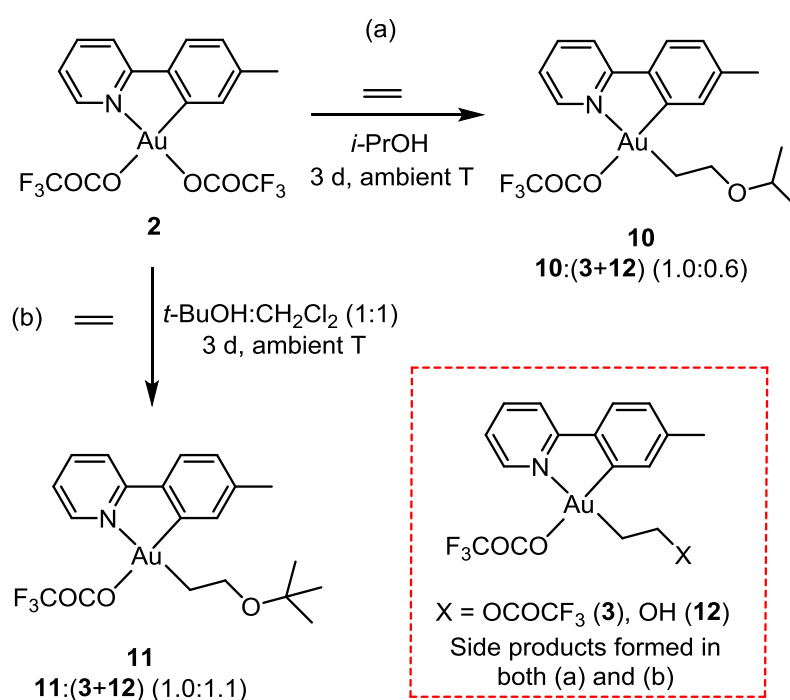
Scheme 33. Au(III) mediated nucleophilic addition of *i*-PrOH and *t*-BuOH to ethylene at complex **2**, furnishing complexes **10** and **11**. Complexes **3** and **12** were formed as side products in both reactions.

As mentioned previously, complex **12** was formed as a side product in the synthesis of complexes **8**, **10**, and **11** (Scheme 32 and Scheme 33). Therefore, it was desired to isolate and characterize complex **12**. It was found that complex **12** could be formed either by reacting complex **2** with ethylene in the presence of water, or by treating complex **3** with water (Scheme 34). Unfortunately, full conversion of **2** or **3** into **12** could not be achieved, and **12** was always formed in a mixture with **3**. However, it was found that **12** could be isolated in a low yield (27%, Scheme 34) through crystallization from wet CH$_2$Cl$_2$

and pentane.[v] Complex **12** was characterized by NMR and MS. In the ^{1}H NMR spectrum of **12**, the characteristic resonances of the protons in the CH_2Cl_2 unit are found at δ 3.87 and δ 2.48. Furthermore, at δ 2.76, a broadened resonance corresponding to the hydroxyl group is observed. In the ^{19}F NMR spectrum of **12**, one resonance at δ −77.1 is found, and in the ^{13}C NMR spectrum of **12** one pair of quartets are observed corresponding to the $OCOCF_3$ ligand *trans* to tpy-*C*, in agreement with previous findings. Finally, in a NOESY experiment, a NOE correlation between the protons in the CH_2Cl_2 unit and $H^{6'}$ is found, indicating that the reaction has occurred in the position *trans* to tpy-*N*. The presence of **12** in the reaction mixtures obtained when preparing **8**, **10**, and **11** were confirmed by spiking the reaction mixtures with pure **12** in a ^{1}H NMR experiment.
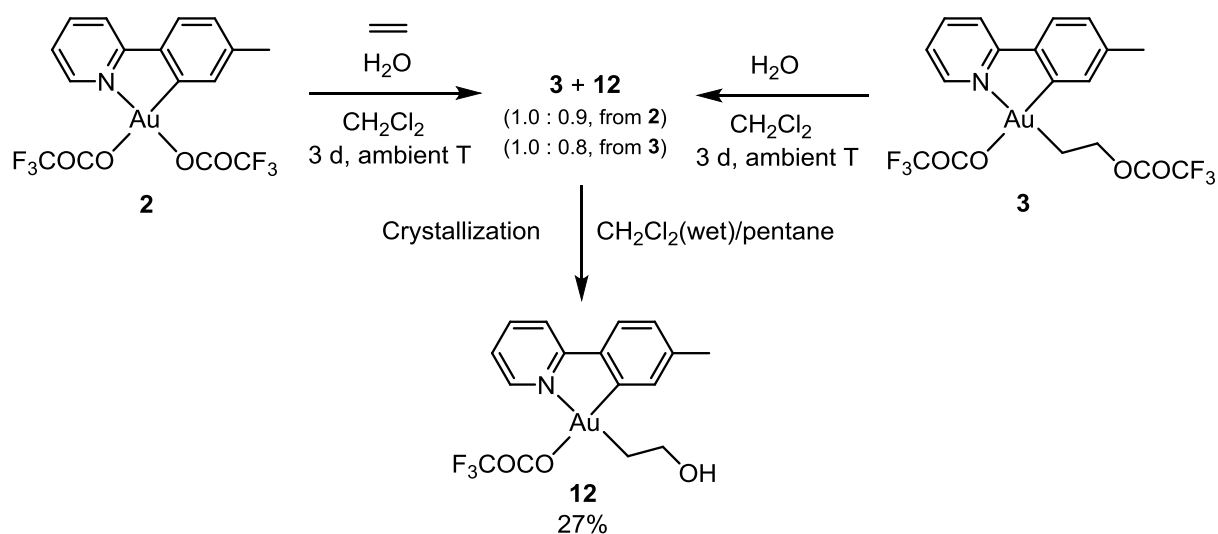
Scheme 34. Synthesis of Au(III) complex **12**. The use of wet CH_2Cl_2 (CH_2Cl_2 saturated with water) was necessary to crystallize out clean **12**.

Interestingly, in all complexes **7**-**12**, the $OCOCF_3$ ligand *trans* to tpy-*C* remains in place, even in the presence of a large excess of other possible ligands which could have coordinated instead of $OCOCF_3$. This strong preference for $OCOCF_3$ *trans* to tpy-*C* was further demonstrated in two experiments. First, upon heating **2** in CH_3COOH at reflux for 7 days, a close to selective exchange[vi] of the $OCOCF_3$ ligand *trans* to tpy-*N* with $OCOCH_3$ furnishing **2-OCOCH₃** (Scheme 35, left) occurred. As was observed previously, the $OCOCF_3$ ligand *trans* to tpy-*C* remained in place. In the ^{1}H NMR spectrum of **2-OCOCH₃**, the characteristic resonance of the $OCOCH_3$ ligand is found at δ 2.22 and in a NOESY experiment a NOE correlation between the $OCOCH_3$ ligand and $H^{6'}$ is observed, indicating that the reaction occurred in the position *trans* to tpy-*N*. In the ^{19}F NMR spectrum of **2-OCOCH₃**, one single resonance is observed

---

[v] The reaction between **2**, ethylene, and water has also been investigated by Dr. Eirin Langseth, but the product of the reaction was not characterized (See Dr. Eirin Langseth's Ph.D thesis for further details).[92]

[vi] **2-OCOCH₃** was formed as the main product (>80%) together with small amounts of unreacted **2**. Small amounts (ca 5 %) of Au(OCOCH₃)₂(tpy) was also formed. Au(OCOCH₃)₂(tpy) has been isolated and characterized (see Section 2.10).

at δ –77.0 and one pair of quartets are observed in the ^{13}C NMR spectrum corresponding the OCOCF$_3$ ligand *trans* to tpy-*C*. The same selectivity was also observed when reacting complex **2** with MeOH where the OCOCF$_3$ ligand *trans* to tpy-*N* is exchanged with OMe (Scheme 35, right) to give **2-OMe**. This experiment was first performed as a NMR experiment in CD$_3$OD and the conversion of **2** into **2-OMe-*d₃*** was monitored by ^1H NMR (See ESI, Paper I). Significant amounts of **2-OMe-*d₃*** was formed immediately after mixing, and after 3 days an approximately 1:1 mixture of **2:2-OMe-*d₃*** was obtained. After 32 days, almost full conversion into **2-OMe-*d₃*** was achieved. However, some decomposition had occurred at this point as well. Based on the results from the NMR experiment, the synthesis of **2-OMe** was designed, and upon stirring **2** in MeOH for 28 days at ambient temperature **2-OMe** could be obtained in a good yield (80%). Complex **2-OMe** was characterized by NMR and MS. Complex **2-OMe** is unstable in CD$_2$Cl$_2$ (probably due to dissociation of OMe), which is usually the NMR solvent of choice for the type of Au(III) complexes described herein. Complex **2-OMe** was instead characterized in CD$_3$OD. As expected, an exchange of the OMe ligand with OCD$_3$ was observed in CD$_3$OD. Luckily, **2-OMe** had a long enough lifetime in CD$_2$Cl$_2$ to achieve a ^1H NMR spectrum where the OMe resonance is present at δ 3.68 and a NOESY experiment on a partially decomposed sample of **2-OMe** in CD$_2$Cl$_2$ showed a NOE between the OMe and H$^{6'}$, indicating that the reaction had occurred *trans* to tpy-*N*.
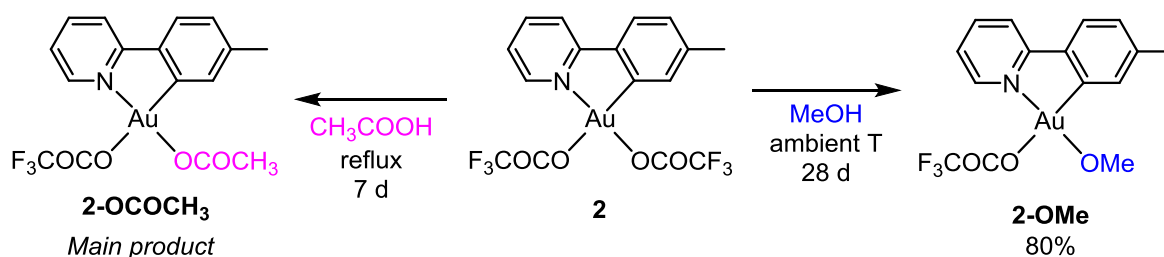
Scheme 35. Reactivity of complex **2** towards CH$_3$COOH and MeOH furnishing **2-OCOCH$_3$** (as the main product in a mixture with **2** and Au(OCOCH$_3$)$_2$(tpy)) and **2-OMe**.

This selective (or nearly selective) formation of **2-OCOCH$_3$** and **2-OMe** from complex **2** and CH$_3$COOH or MeOH depicted in Scheme 35, together with the observations for complexes **7–12**, shows that even though the site *trans* to tpy-*C* is kinetically more accessible than the site *trans* to tpy-*N*,[90] the thermodynamic preference of a low *trans* influence ligand (*i.e.* OCOCF$_3$ instead of OCOCH$_3$ or other possible ligands) controls the observed product selectivity.

2.4 1-Hexene with methanol as nucleophile

Since the use of methanol as a nucleophile was promising and since **5a** was not stable enough to be isolated, the reaction of **2** and 1-hexene was repeated in MeOH. Upon stirring a mixture of **2** and 1-hexene in MeOH for 1 day, the stable product **5b** could be obtained in good yields (80-83%, Scheme 36). Complex **5b** was characterized by NMR, MS, X-ray diffraction analysis (*vide infra*), and elemental analysis. The ^1H NMR spectrum of **5b** is rather similar to that of **5a**, but there are some characteristic

differences. H^b (see labelling, Scheme 36) is found at δ 3.52 whereas in **5a**, it was found at δ 5.40, due to the more electron withdrawing OCOCF$_3$ group (compared to OMe in **5b**) bonded to the same carbon as H^b in **5a**. In complex **5b**, the resonance of the OMe group is found at δ 3.39, similarly to that of the OMe group of **9** at δ 3.38. The two diastereotopic H^a are found at δ 2.44-2.47 (overlaps with tpy-CH_3) and δ 2.36 ($^2J_{HH}$ = 9.9 Hz). H^c is found at δ 1.69, H^d and H^e are found as overlapping signals at δ 1.29-1.50, and finally the methyl group (CH$_3$^{f}) at the end of the hexyl chain is found at δ 0.91. One single resonance is observed in the ^{19}F NMR spectrum of **5b** at δ −77.1, and two quartets are observed in the ^{13}C NMR of **5a**, corresponding to the OCOCF$_3$ ligand *trans* to tpy-*C*. In a NOESY experiment, a NOE is observed between H^a and H$^{6'}$, and between H^b and H$^{6'}$ indicating that the reaction has occurred in the position *trans* to tpy-*N* in agreement with previous findings.
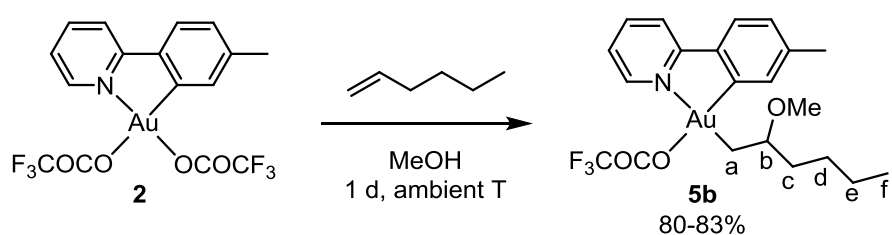
Scheme 36. Au(III) mediated nucleophilic addition of MeOH to 1-hexene at **2** furnishing **5b**. The atoms in the former 1-hexene unit are here labelled a-f to simplify the NMR discussions.

It was desirable to gain more insight into the increased stability of complex **5b** compared to complex **5a**. As mentioned in Chapter 1, the nucleophilic addition of $^-$OCOCF$_3$ to ethylene at **2** is reversible.[90] Since $^-$OMe is a poorer leaving group than $^-$OCOCF$_3$, it may slow down the reverse reaction, and thus stabilize the product. Indeed, upon treating **9-d_4** with unlabeled ethylene, no formation of the corresponding unlabeled **9** was observed, indicating that the nucleophilic addition is irreversible under the reaction conditions depicted in Scheme 37.
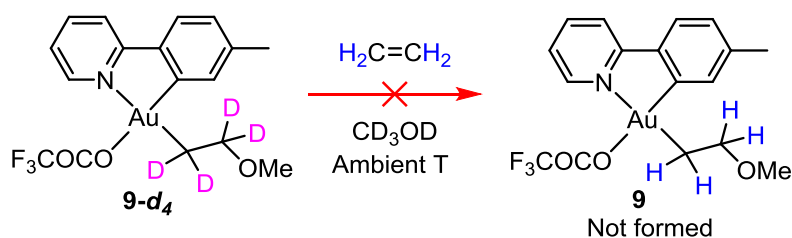
Scheme 37. Treating **9-d_4** with unlabeled ethylene did not lead to the formation of **9**.

2.5 Substituted butenes with methanol as nucleophile

Four butenes with different degrees of substitution were investigated. It turned out to be possible to perform a nucleophilic addition of MeOH to the monosubstituted alkene 3-methyl-1-butene, the disubstituted alkene 2-methyl-1-butene, and even the trisubstituted alkene 2-methyl-2-butene furnishing complexes **6b**, **13**, and **14**, respectively (Scheme 38). However, the yields decrease with

increasing alkene substitution. The tetrasubstituted alkene 2,3-dimethyl-2-butene (not shown in Scheme 38) did not react under these conditions. In the reactions depicted in Scheme 38, the increased stability of the products obtained from nucleophilic addition of MeOH compared to that of nucleophilic addition of $^-$OCOCF$_3$ was demonstrated: The reactions with 2-methyl-1-butene and 2-methyl-2-butene with $^-$OCOCF$_3$ as nucleophile did not lead to any isolation of insertion products, while MeOH gave products which could be isolated.
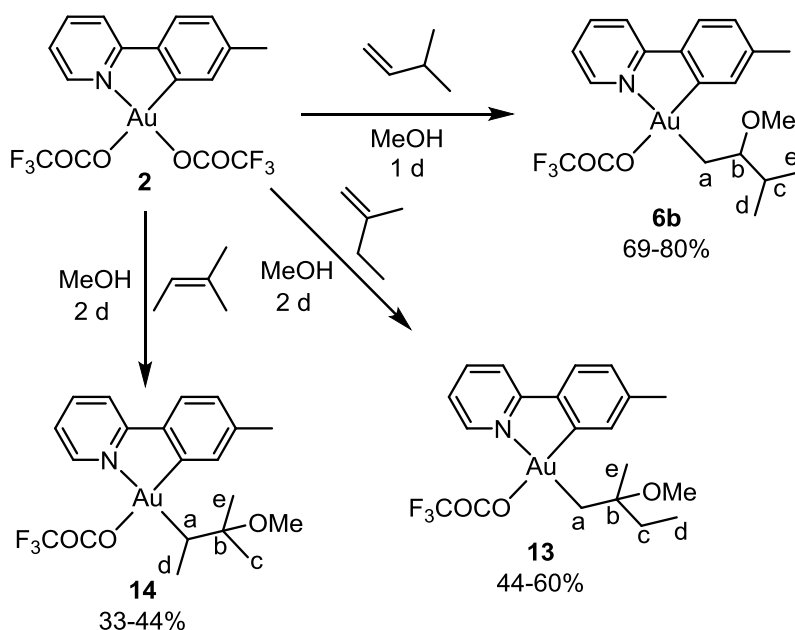
Scheme 38. Au(III) mediated nucleophilic addition of MeOH to a series of mono-, di-, and tri-substituted butenes at **2** furnishing **6b**, **13**, and **14**. All the reactions were performed at ambient temperature. The atoms in the former butene units are here labeled a-e to simplify the NMR discussions.

In all three complexes **6b**, **13**, and **14** the nucleophilic addition occurred at the most substituted site of the double bond, in agreement with previous findings. Complex **6b** was characterized by NMR, MS, X-ray diffraction analysis (*vide infra*), and elemental analysis. The ^{1}H NMR spectrum of complex **6b** resembles that of complex **6a**, but there are some characteristic differences; the most prominent change being the change in chemical shift of H^b (see labeling, Scheme 38) from δ 5.31 in **6a** to δ 3.35 in **6b**, due to the more electron withdrawing OCOCF$_3$ substituent in **6a**, similar to that observed for **5b** (δ 3.52) and OCH$_2$ in **9** (δ 3.68). The OMe group is found at δ 3.40, similar to that observed for **9** and **5a**. The two diastereotopic H^a are found at δ 2.43-2.46 (overlaps with tpy-CH$_3$) and δ 2.30 ($^2J_{HH}$ = 10.0 Hz), H^c is found at δ 2.01, and the two diastereotopic methyl groups are found as two overlapping doublets at δ 0.98-1.00. In a NOESY experiment, a NOE correlation between H^a and H$^{6'}$, and H^b and H$^{6'}$ is observed, indicating that the reaction has occurred in the position *trans* to tpy-*N*.

For the synthesis of complexes **13** and **14** a prolonged reaction time was needed compared to that of complex **6b**, and the complexes were obtained in moderate to low yields. Complexes **13** and **14** were

characterized by NMR, MS, and elemental analysis. Complex **14** was also characterized by X-ray diffraction analysis. In the ^{1}H NMR spectrum of complex **13** the OMe resonance is found at δ 3.19, which is slightly lower than that of **5b**, **6b**, and **9**. The two diastereotopic H^a are found at δ 2.59 and δ 2.53 ($^2J_{HH}$ = 10.3 Hz), CH$_3^e$ is found at δ 1.33, the two diastereotopic H^c are at δ 1.75 and δ 1.70, and finally, at δ 0.95, CH$_3^d$ is found as an apparent triplet. In a NOESY experiment, a NOE correlation is observed between H^a and H$^{6'}$, and CH$_3^e$ and H$^{6'}$, indicating that the reaction has occurred in the position *trans* to tpy-*N*. In the ^{1}H NMR spectrum of **14**, H^a is found as a quartet at δ 2.91, which is a slightly larger ppm value than that observed for H^a in **6b** and **13**. The three methyl groups, CH$_3^c$, CH$_3^d$, and CH$_3^e$ are found as overlapping resonances at δ 1.28-1.36. The OMe resonance is found at δ 3.21, similar to that of **13**. In agreement with previous findings, a NOESY experiment established that the reaction has occurred *trans* to tpy-*N*. For all the complexes **6b**, **13**, and **14** one single resonance corresponding to the OCOCF$_3$ ligand *trans* to tpy-*C* is found in the ^{19}F NMR spectra at δ −77.0, δ −77.1, and δ −77.3, respectively. In the ^{13}C NMR spectra of the three complexes, one pair of quartets are observed, also corresponding to the OCOCF$_3$ ligand.

As mentioned above, the yields for complexes **13** and **14** are significantly lower than that of the other related complexes described herein. When investigating the reaction mixtures obtained from the synthesis of **13** and **14** by ^{1}H NMR before work up, large amounts of what is probably a decomposition product was observed. In the work up of **13** and **14** a mixture of the decomposition product and variable small amounts of **13** or **14** is precipitated out of the solution, and the remaining solution contains clean **13** or **14**. Small amounts of clean decomposition product could be isolated from the workup of **14** and this material was subjected to NMR analysis. Based on the NMR analysis, the decomposition product is now tentatively assigned to be [Au(tpy)$_2$]$^+$[OCOCF$_3$]$^-$ (Scheme 39). The mechanism of formation of [Au(tpy)$_2$]$^+$[OCOCF$_3$]$^-$ has not been investigated, and further characterization is needed in order to confidently assign the structure of this complex. Previously, a co-worker obtained the crystal structure of [Au(tpy)$_2$]$^+$[OCOCF$_3$]$^-$ in an attempt to grow crystals of an unstable Au(III) complex.[103]
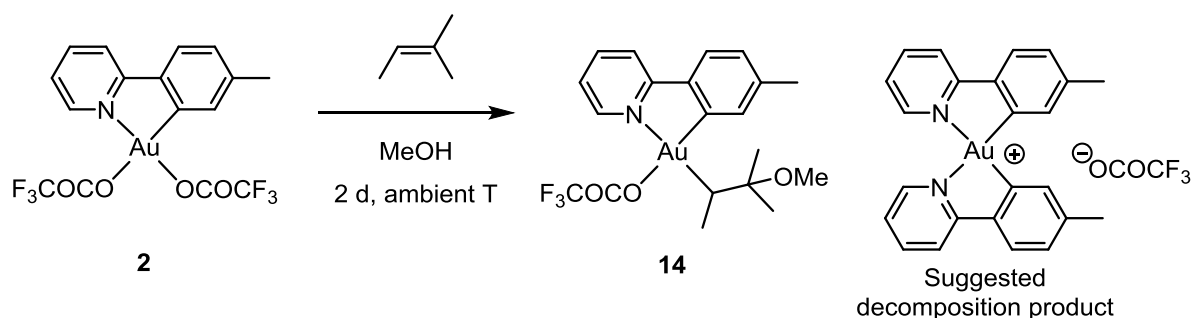
Scheme 39. Formation of the decomposition product tentatively assigned as [Au(tpy)$_2$]$^+$[OCOCF$_3$]$^-$ during the synthesis of **14**.

Table 1. Key [1]H (500, 600, or 800 MHz) and ^{19}F (188 MHz) NMR chemical shifts for complexes **5a**, **5b**, **6a**, **6b**, and **7-14** in CD_2Cl_2. In **5a**, *ca.* 2 vol% of CF_3COOH was added to the NMR sample used.

	H^a/AuCH$_2$	H^b/CH$_2$Nu	Nu	OCOCF$_3$ *trans* to C
5a	δ 2.46-2.50, δ 2.42	δ 5.40	δ −78.0 (OCOCF$_3$)	δ −77.1
5b	δ 2.44-2.47, δ 2.36	δ 3.52	δ 3.39 (OMe)	δ −77.1
6a	δ 2.60, δ 2.32	δ 5.31	δ −77.9 (OCOCF$_3$)	δ −77.0
6b	δ 2.43-2.46, δ 2.30	δ 3.35	δ 3.40 (OMe)	δ −77.0
7	δ 2.38	δ 4.42	δ 2.04 (OCOCH$_3$)	δ −77.0
8	δ 2.40	δ 3.74	δ 3.55, δ 1.19 (OEt)	δ −77.0
9	δ 2.39	δ 3.68	δ 3.38 (OMe)	δ −77.0
10	δ 2.37	δ 3.74	δ 3.68, δ 1.16 (O*i*-Pr)	δ −77.0
11	δ 2.32	δ 3.70	δ 1.21 (O*t*-Bu)	δ −77.0
12	δ 2.48	δ 3.87	δ 2.76 (OH)	δ −77.1
13	δ 2.59, δ 2.53	-	δ 3.19 (OMe)	δ −77.1
14	δ 2.91	-	δ 3.21 (OMe)	δ −77.3

2.6. Crystallographic structure determination

Complexes **5b**, **6a** (as the CHCl$_3$ solvate), **6b**, **7**, **9**, and **14** have been structurally characterized and their ORTEP plots are given in Figure 12 and selected metrical parameters are given in Table 2. The crystallographic structure determinations were performed by Dr. Sigurd Øien-Ødegaard. The asymmetric unit in **7** consists of two complexes and the metrical parameters for both complexes are given. All the complexes exhibit the nearly square planar geometry which is commonly observed for Au(III) complexes. The structures are in agreement with the NMR observations; the reactions have occurred in the position *trans* to tpy-*N* and the OCOCF$_3$ ligand *trans* to tpy-*C* remains in place in all complexes. As can be seen from the molecular structures of **5b**, **6a**, **6b**, and **14**, the nucleophilic additions have occurred at the most substituted site of the double bond, in a Markovnikov manner. The N1-Au1-C1 chelate angle slightly deviates from the idealized 90° in all the complexes, ranging from 81.6(3)° (in **5b**) to 81.1(3)° (in one of the complexes is the asymmetric unit of **7**), in agreement with that observed in the related complexes **2**, **3**, and **4**.[89, 90] The Au1-N1, Au1-C1, and Au-O1 ligand distances are comparable to those reported for related complexes.[89, 90] The shortest Au1-C2 bond distances is that of **9** (2.012(15) Å) followed by **7** and **5b** (2.023(8) and 2.025(9) Å, respectively). The longest Au1-C2 bond distance is observed for **14** (2.080(4) Å). Complexes **6a**, **6b**, and one of the complexes in the asymmetric unit of **7** have Au1-C2 distances of 2.045(5), 2.055(9), and 2.043(7) Å, respectively, which is similar to, or slightly longer, than that observed in the related complexes **3** and **4** (2.042(3) and 2.040(4) Å, respectively).[90]
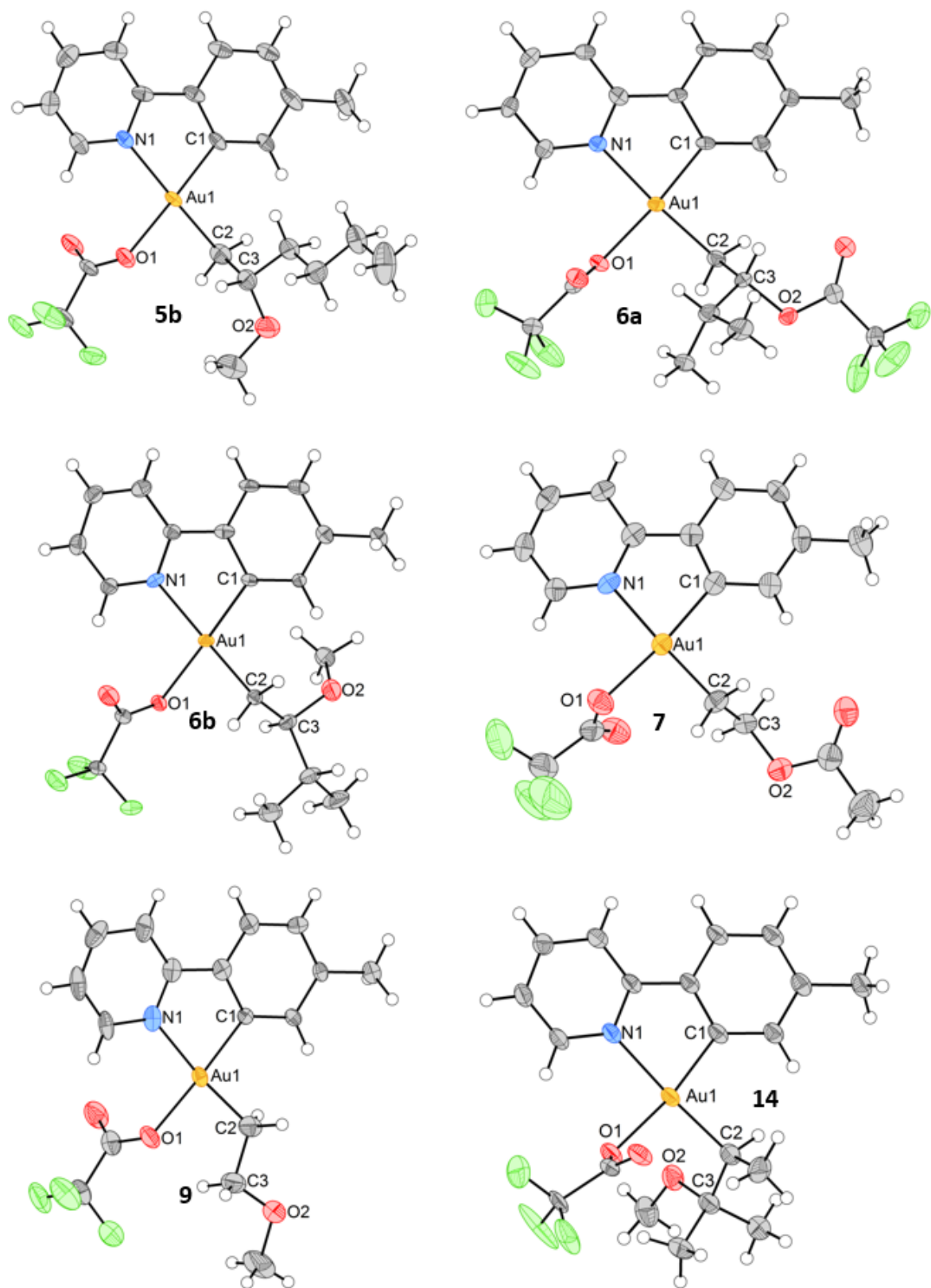
Figure 12. ORTEP plots of complexes **5b**, **6a**, **6b**, **7**, **9**, and **14** with 50 % ellipsoids. For **6a**, $CHCl_3$ was removed for clarity. In complex **14**, the $OCOCF_3$ ligand is disordered (See ESI, Paper I). The crystallographic structure determinations were performed by Dr. Sigurd Øien-Ødegaard.

Table 2. Selected bond lengths [Å] and angles [º] for complexes **5b**, **6a**, **6b**, **7**, **9**, and **14**. The crystallographic structure determinations were performed by Sigurd Øien-Ødegaard.

	5b	6a	6b	7	9	14
Au1-N1	2.117(7)	2.110(5)	2.108(8)	2.104(6), 2.094(6)	2.089(11)	2.137(3)
Au1-C1	1.999(8)	2.013(5)	1.998(9)	2.002(7), 2.014(7)	2.018(10)	2.012(3)
Au1-O1	2.109(6)	2.114(3)	2.115(7)	2.087(6), 2.101(5)	2.102(9)	2.111(2)
Au1-C2	2.025(9)	2.045(5)	2.055(9)	2.043(7), 2.023(8)	2.012(15)	2.080(4)
C2-C3	1.517(13)	1.512(7)	1.526(13)	1.521(11), 1.522(10)	1.522(17)	1.549(5)
C3-O2	1.426(13)	1.503(6)	1.433(13)	1.463(9), 1.447(9)	1.41(2)	1.439(5)
O1-Au1-N1	96.0(3)	93.88(15)	96.4(3)	93.3(2), 92.1(2)	95.1(4)	89.62(10)
N1-Au1-C1	81.6(3)	81.57(19)	81.5(4)	81.3(3), 81.1(3)	81.5(4)	81.38(12)
C1-Au1-C2	96.6(4)	94.9(2)	96.2(4)	96.1(3), 95.7(3)	92.0(5)	93.79(14)
C2-Au1-O1	85.8(3)	89.55(18)	86.0(3)	89.4(3), 91.0(3)	91.5(5)	95.31(12)
C1-Au1-O1	177.1(3)	174.82(18)	177.5(4)	174.2(3), 173.1(3)	176.4(5)	170.81(12)
N1-Au1-C2	177.9(3)	176.02(18)	175.3(3)	177.2(3), 176.3(3)	173.3(5)	173.84(12)

2.7 Alkenes and dienes investigated by other group members

As mentioned previously, M.Sc. Franziska Stefanie Ihlefeldt worked on the project described in this chapter during her master degree studies. The main focus of her work was to study the reactivity of complex **2** towards various internal alkenes, dienes, and styrene. Some of her findings are shown in Scheme 40, but for a full description of her work the reader is recommended to read her master thesis.[102] During her work, she found that it was possible to perform a nucleophilic addition of MeOH to styrene to furnish complex **B** (Scheme 40, right). Furthermore, when performing the reaction of **2** with the 2,3-disubstituted alkene *trans*-2-hexene in MeOH a 1:1 mixture of the two isomers **C** and **D** was obtained (Scheme 40, bottom), originating from nucleophilic addition on either one or the other side of the double bond. These two isomers could be separated by crystallization followed by separation of crystals under a microscope (see ESI, Paper III). Single crystal X-ray diffraction analysis and NMR characterization were performed using these crystals. From the molecular structures of **C** and **D**, it was also possible to distinguish whether the nucleophilic addition occurred in a *syn* or *anti* fashion. One pair of diastereomers would form upon *anti* addition (*R,S* and *S,R*) and another pair would form upon *syn* addition (*S,S* and *R,R*). From the molecular structures of **C** and **D** it is clear that the nucleophilic addition of MeOH to *trans*-2-hexene occurred in an *anti* fashion (See Paper I for more details), which is in agreement with the findings for the analogous reaction with ethylene in CF_3COOH.[90] M.Sc. Ihlefeld also investigated the nucleophilic addition of $^-OCOCF_3$ to dienes. It proved possible to perform a nucleophilic addition of $^-OCOCF_3$ to 1,4-pentadiene furnishing complex **A** (Scheme 40, top). In this case only one of the double bonds reacted to furnish **A**, while the other double bond remained intact. Following this, 1,5-hexadiene was investigated to find out if it would react analogously to that of 1,4-pentadiene. Upon reacting **2** with 1,5-hexadiene in CF_3COOH a clean transformation into one product occurred, but a complex related to that of **A** was not formed; instead cyclization occurred to form a six-membered ring and the complex was carefully characterized as complex **E** (Scheme 40, left). The mechanism of the formation of **E** has not been investigated, but one hypothesis is shown in Scheme 40 (see inset, upper left corner) where first the $OCOCF_3$ ligand *trans* to tpy-*N* is substituted by one of the double bonds in 1,5-hexadiene, followed by a cyclization and concomitant addition of $^-OCOCF_3$ to furnish **E**. It is worth noticing that in the cyclization step, the double bond that is not coordinated to Au adds to the double bond at Au in a non-Markovnikov manner, in contrast to all the other nucleophilic additions discussed in this chapter. The reasons for this selectivity has not yet been studied, but it might be attributed to the driving force of forming a six-membered ring. Complexes **A** and **E** could not be isolated since they decompose upon removal of solvent, whereas complexes **B**, **C** and **D** were stable and could be isolated.
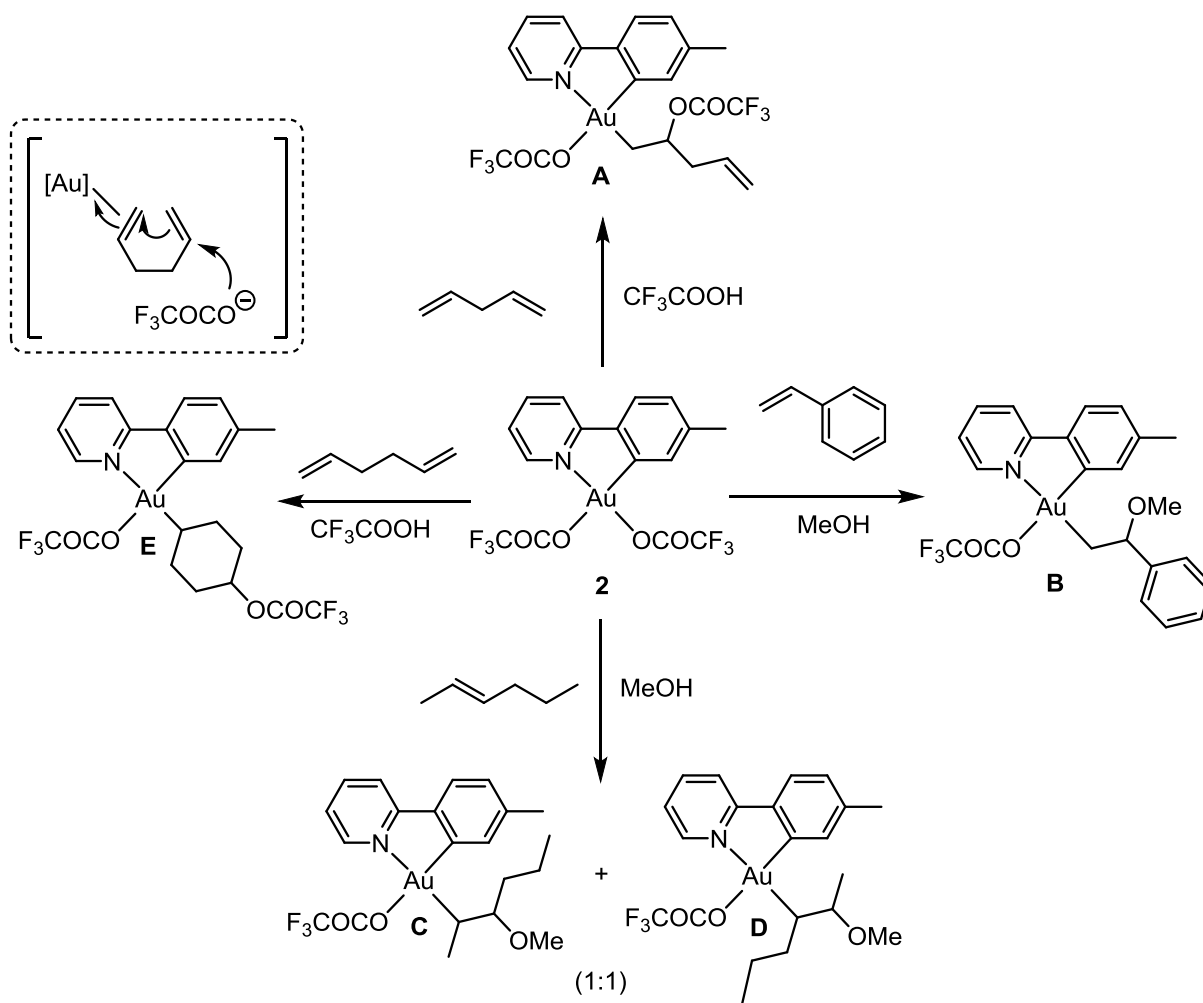
Scheme 40. Some examples of other alkenes and dienes investigated by co-worker M.Sc. Franziska Stefanie Ihlefeldt.[102] [Au] = [Au(OCOCF₃)(tpy)]⁺.

2.8 Relevance for catalysis

Going from a stoichiometric functionalization to a catalytic process for reactions discussed in this chapter would lead to very useful methods for producing ethers and esters from cheap and readily available building blocks under mild reaction conditions. Unfortunately, the reactions described in this chapter come to a stop after the first alkene functionalization *trans* to tpy-*N* and no catalytic process could be achieved. Experiments where CF₃COOH was added to a mixture of insertion product, excess of alkene, and solvent/nucleophile did not lead to any catalysis and the complexes remained stable in solution over time (See ESI, Paper I for details). For example, treatment of **9-*d₃*** (generated *in situ* from **2** and ethylene in CD₃OD) with CF₃COOH in the presence of excess ethylene did not yield the expected ether product which would be formed upon protolytic cleavage of the Au-C bond *trans* to tpy-*N*, even upon heating at elevated temperatures (50-60 °C, Scheme 41). Furthermore, addition of CF₃COOH to the more sterically crowded complex **14** in CD₃OD with excess 2-methy-2-butene did also not lead to the expected protodeauration product; but in this case decomposition into unknown products occurred. When adding CF₃COOH to a solution of **14** in CD₂Cl₂, formation of **2** occurred, which indicates

the release of the alkyl group *trans* to tpy-*N*. However, from this experiment it cannot be determined whether this is due to protolytic cleavage of the Au-C bond *trans* to tpy-*N* or *via* other mechanisms such as protonation of the methoxy group, and further experiments will have to be carried out to gain insight into this. In addition to the experiments described herein, Dr. Eirin Langseth made attempts to achieve a catalytic process for the formal insertion of ethylene into the Au-O bond *trans* to tpy-*N* in **2** furnishing **3**.[90, 92] Treating complex **3** with triflic acid (TfOH) did not lead to any protolytic cleavage of the Au-C(sp^3) bond. Also, pressurizing a solution of complex **3** in CF_3COOD with 60 bar of ethylene did not lead to any catalysis, even after heating at 50 °C for 1 day, and decomposition was observed in this experiment instead. For more details on these experiments, see the Ph.D thesis of Dr. Eirin Langseth.[92] Based on previous work performed in our group and the work described in Chapter 4 (*vide infra*), it seems like there is a strong preference for protolytic cleavage of Au-C(sp^2) bonds over Au-C(sp^3) bonds, this will be further discussed in Chapter 4. For example, in previous work performed in the Tilset group, treating AuMe$_2$(tpy) with TfOH at low temperatures led to a selective protolytic cleavage of the Au-C(sp^2) bond and no protolytic cleavage of the Au-Me bond occurred.[38]
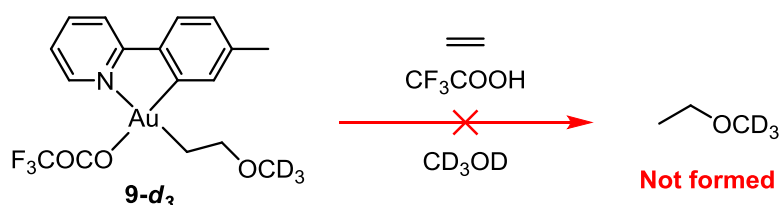
Scheme 41. Treatment of **9-*d$_3$*** with CF_3COOH in the presence of ethylene did not lead to any formation of the ether product expected upon protodeauration.

2.9 Conclusions

The work described in this chapter covers a detailed study of the functionalization of alkenes at complex **2** furnishing several new Au(III) complexes bearing *β*-functionalized C(sp^3) ligands. The complexes have been carefully characterized by several methods such as NMR, MS (including HRMS), X-ray diffraction analysis and elemental analysis. Insight into the scope and regiochemistry of the nucleophilic addition to alkenes at Au(III) was obtained. Different alkenes with various substitution patterns have been investigated, ranging from ethylene to more substituted alkenes such as the trisubstituted alkene 2-methyl-2-butene. Several different oxygen based nucleophiles were investigated ranging from CF_3COOH and CH_3COOH, which represent rather harsh acidic conditions, to H_2O and the alcohol based nucleophiles MeOH, EtOH, *i*-PrOH, and *t*-BuOH. In all reactions studied, the reaction occurs in the position *trans* to tpy-*N*, reflecting the strong thermodynamic preference of having the higher *trans* influence C(sp^3) ligand *trans* to the weaker *trans* influence tpy-*N*, and not *trans* to the higher *trans* influence tpy-*C*. The lower *trans* influence OCOCF$_3$ ligand therefore always remains in place *trans* to tpy-*C*. Furthermore, in all reactions discussed in this chapter, the nucleophilic addition

always occurres at the most substituted site of the double bond. However, a co-worker found one exception with 1,5-hexadiene (See M.Sc. Ihlefeldt's master thesis[102]). The insight gained through this study is of great importance for further development and understanding of Au(III) catalysis and functionalization of alkenes at Au(III).

2.10 Experimental

The experimental procedures for the complexes that are not included in Paper I are found herein.

General procedures

Complex **2** was prepared by a previously reported procedure.[89] CH_2Cl_2 was purified using a MB SPS-800 solvent purifying system from MBraun. CD_2Cl_2 was dried over 3Å molecular sieves. All other reagents and solvents were used as received. All complexes were synthesized in air. As a precaution, all syntheses were performed in the absence of light. NMR spectra were obtained on AVII600 and AVIIIHD800 instruments at ambient temperature. ^1H and ^{13}C NMR spectra have been referenced relative to the residual solvent signals (CD_2Cl_2: $\delta(^1H)$ 5.34, $\delta(^{13}C)$ 53.84) The peaks in the ^1H NMR spectra were assigned by the aid of 2D NMR techniques such as COSY, HSQC, HMBC, and NOESY according to the numbering scheme shown in Figure 1. Mass spectra (ESI) were obtained on a Bruker maXis II ETD spectrometer by Osamu Sekiguchi (University of Oslo).

Synthesis of [Au(tpy)$_2$]$^+$[OCOCF$_3$]$^-$

MeOH (10 mL) was added to complex **2** (100.3 mg, 0.1696 mmol, 1.0 equiv). 2-methyl-2-butene (40 μL, 0.38 mmol, 2.2 equiv) was added, the flask was sealed with a glass stopper, and the reaction mixture was stirred at ambient temperature in the absence of light for two days. After two days, a purple precipitate was observed by visual inspection. The reaction mixture was filtered and the volatiles were removed under reduced pressure. The remaining solid was then dissolved in CH_2Cl_2, layered with pentane, and stored in a fridge (*ca.* 10 ^oC) furnishing small amounts (a few mg) of a white precipitate. The white precipitate was collected, dried under reduced pressure, and investigated by NMR. Based on NMR characterization, the white solid is tentatively assigned to be [Au(tpy)$_2$]$^+$[OCOCF$_3$]$^-$.

^{1}H NMR (600 MHz, CD_2Cl_2): δ 8.86 (br. s, 2H, **H^6**), 8.25 (m, 2H, **H^4**), 8.16 (d, 2H, *J* = 8.1 Hz, **H^3**), 7.78-7.81 (m, 6H, **H^5**, **H$^{3'}$** and **H$^{6'}$**), 7.38 (d, 2H, *J* = 7.9 Hz, **H$^{4'}$**), 2.53 (s, 6H, Ar**CH$_3$**).

^{13}C NMR (151 MHz, CD_2Cl_2): δ 163.1 (Ar**C**), 148.2 (Ar**C**), 147.7 (Ar**C**), 144.3 (Ar**C**), 143.0 (Ar**C**), 141.3 (Ar**C**), 135.2 (Ar**C**), 130.2 (Ar**C**), 126.0 (Ar**C**), 125.5 (Ar**C**), 121.8 (Ar**C**), 22.1 (Ar**CH$_3$**). O**CO**CF$_3$ was not observed.

Synthesis of Au(OCOCH₃)₂(tpy)

Complex **2** (50.0 mg, 0.0846 mmol) and CH_3COOH (5 mL) was added to a round bottom flask and the reaction mixture was heated at reflux for 7 days. The solvent was removed under reduced pressure and small amounts of Au(OCOCH₃)₂(tpy) (5.0 mg, 0.010 mmol, 12 %) was obtained as a white solid upon crystallization from CH_3COOH and H_2O (*ca.* 1:1) at *ca.* 10 °C. Au(OCOCH₃)₂(tpy) has also been prepared by another method by a co-worker.[104]

¹H NMR (800 MHz, CD_2Cl_2): δ 8.60 (dd, 1H, *J* = 5.8, 0.7 Hz, **H⁶**), 8.11 (ddd, 1H, *J* = 8.0, 7.6, 1.4 Hz, **H⁴**), 7.84 (d, 1H, *J* = 8.1 Hz, **H³**), 7.43 (d, 1H, *J* = 7.8, **H³'**), 7.42 (ddd, 1H, *J* = 7.5, 5.9, 1.2 Hz, **H⁵**), 7.22 (d, 1H, *J* = 7.5 Hz, **H⁴'**), 7.02 (s, 1H, **H⁶'**), 2.44 (s, 3H, ArC**H₃**), 2.23 (s, 3H, OCOC**H₃** *trans* to tpy-*N*), 2.11 (s, 3H, OCOC**H₃** *trans* to tpy-*C*).

¹³C NMR (201 MHz, CD_2Cl_2): δ 176.8 (O**C**OCH₃ *trans* to tpy-*C*), 175.2 (O**C**OCH₃ *trans* tp tpy-*N*), 165.6 (Ar**C**), 148.5 (Ar**C**), 143.4 (Ar**C**), 143.4 (Ar**C**), 142.4 (Ar**C**), 139.5 (Ar**C**), 130.5 (Ar**C**), 130.2 (Ar**C**), 125.3 (Ar**C**), 123.9 (Ar**C**), 121.0 (Ar**C**), 24.6 (OCO**C**H₃ *trans* to tpy-*C*), 22.4 (OCO**C**H₃ *trans* to tpy-*N*), 22.3 (Ar**C**H₃).

Chapter 3 – Metallacycle formation at Au(III)

3.1 General introduction and scope of the chapter

This chapter covers the synthesis, characterization, and mechanism of formation of Au(III) metallacycle complexes **15** and **16** (Figure 13). The first part of this chapter concerning complex **15** is described in Paper II. Two other co-workers, M.Sc. Franziska Stefanie Ihlefeldt and M.Sc. Erlend Solbakken Aunan, have contributed to the work described in this chapter and their work is described in section 3.5 and 3.6.1.[102, 105, 106] The DFT calculations presented in this chapter were performed by Dr. Ainara Nova and Dr. David Balcells (University of Oslo).
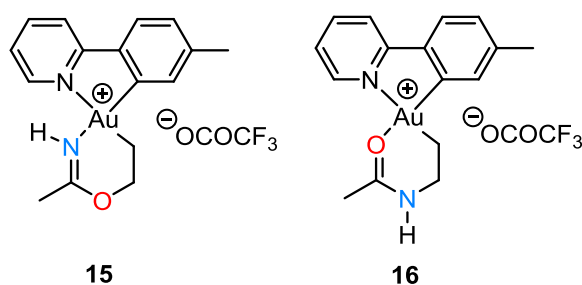
Figure 13. Au(III) metallacycle complexes **15** and **16** described in this chapter.

As discussed previously, alkene activation at Au(III) is a topic which is rapidly increasing in popularity. In Chapter 2, the functionalization of alkenes at Au(OCOCF$_3$)$_2$(tpy) (**2**) was presented. Following the work in Chapter 2, the alkene functionalization is taken one step further: herein not only the alkene (ethylene) is incorporated into the gold complex; the cheap and readily available building blocks H$_2$O and MeCN are also incorporated by utilizing both the coordination site *trans* to tpy-*N* and *trans* to tpy-*C* in complex **2**, forming Au(III) metallacycle complexes **15** and **16** (Figure 13).

Acetonitrile is not only a versatile solvent, it is also a very useful reagent and building block in organic synthesis.[107] For example, there is a wide variety of methods to convert acetonitrile into acetamide,[107] including gold catalysis.[108] Gold catalyzed hydration of more sophisticated nitriles into amides has also been reported.[109] Acetonitrile can also undergo acid catalyzed alcoholysis and it can be used as a building block to make various heterocycles.[107] In this chapter, the use of acetonitrile as a building block for the synthesis of Au(III) metallacycle complexes will be described.

3.2 Synthesis and characterization of metallacycle complex 15

Au(III) metallacycle complex **15** was discovered by serendipity; in an attempt of recrystallizing a reaction mixture containing complexes **3**, **11**, and **12** from acetonitrile, small amounts of a crystalline material was obtained. When investigating these crystals by single crystal X-ray diffraction analysis it was revealed that **15** was formed. Initially, it was not clear whether it was **15**, **15'**, or **16** (Figure 14)

which was obtained. Due to the similar electron density of O and N they can be hard to distinguish only by X-ray diffraction analysis. However, upon performing multinuclear 1D and 2D NMR together with MS, structure optimizations by DFT (see Paper II for details), and elemental analysis, the structure could firmly be assessed to be **15**.[vii]
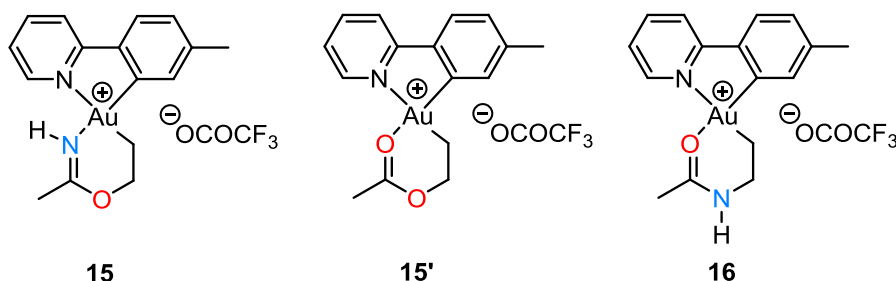
Figure 14. Initially considered Au(III) metallacycles.

Based on the findings that complex **15** was formed from crystallizing a reaction mixture of **3**, **11**, and **12** from acetonitrile, a synthesis protocol for **15** was developed. Upon simply stirring **3** in wet acetonitrile at ambient temperature for 5 days, **15** could be obtained in good yields (78-79%, Scheme 42, left). Complex **15** could also be prepared in comparable yield (79-80%) in one step from **2**, by stirring a mixture of **2** and ethylene in wet acetonitrile for 7 days at ambient temperature (Scheme 42, right). Thus, an efficient synthetic protocol has been developed where the three small, readily available building blocks ethylene, acetonitrile, and water are incorporated into the Au(III) metallacycle complex **15** in just one step, which is a nice example of small molecule activation at Au(III).
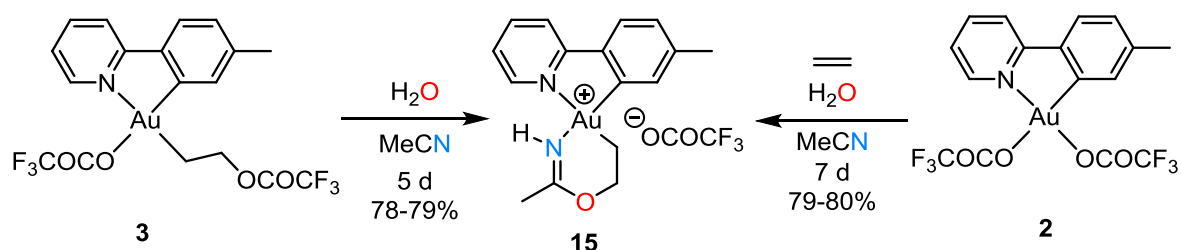
Scheme 42. Synthesis of **15** from either **2** or **3**. Both reactions were performed at ambient temperature.

Complex **15** was characterized by multinuclear NMR, MS, XRD (*vide infra*), and elemental analysis. The characterization of **15** is discussed in detail in Paper II and only some selected key data are discussed here. High resolution mass spectrometry established the elemental composition of the cation of **15**, showing that the metallacycle unit only contains one O atom and thereby ruling out structure **15'** (Figure 14). In the ^{1}H NMR spectrum of complex **15**, the characteristic CH_2Cl_2 unit originating from

---

[vii] Complex **15** was also discovered independently by Dr. Eirin Langseth in a reaction treating **2** with ethylene in CH_3CN. In this reaction **15** was obtained in a mixture with other products and was not isolated or characterized (See Dr. Langseth's Ph.D. thesis for details).[92]

ethylene (or $CH_2CH_2OCOCF_3$ in **3**) is observed at δ 4.34 and δ 2.73. The methyl group in the metallacycle unit, originating from acetonitrile, is found at δ 2.51 and the metallacycle-*NH* is found at δ 10.28. In the ^{19}F NMR spectrum of **15** one single resonance is observed at δ −78.1, corresponding to $^-OCOCF_3$. In a ^1H-^{15}N HMBC experiment two different signals arising from two different N atoms are observed. One resonance is observed at δ −129 with a correlation to H^6, originating from tpy-*N*. At δ −212, a resonance that has a correlation to the broadened NH resonance (δ 10.28) and the metallacycle methyl group (δ 2.51) is observed, originating from the metallacycle-*NH*. Finally, in a ^1H-^1H NOESY experiment a NOE correlation between NH and H^6 is observed, meaning that they are close in space, and indicating the formation of **15** and not **16**.

There was a possibility that a gold mediated or gold catalyzed hydration of acetonitrile to acetamide could be involved in the reaction forming complex **15**. Two experiments were performed to probe whether this could be the case or not. First, treating complex **3** with acetamide in CH_2Cl_2 did not lead to any formation of complex **15** (Scheme 43, top). Furthermore, treating complex **3** with non-labelled acetamide and CD_3CN furnished mainly **15-*d₃*** and only small amounts of non-labelled **15** (Scheme 43, bottom). Both these experiments indicate that the metallacycle is formed from **3**, CD_3CN, and H_2O and not from **3** and acetamide.
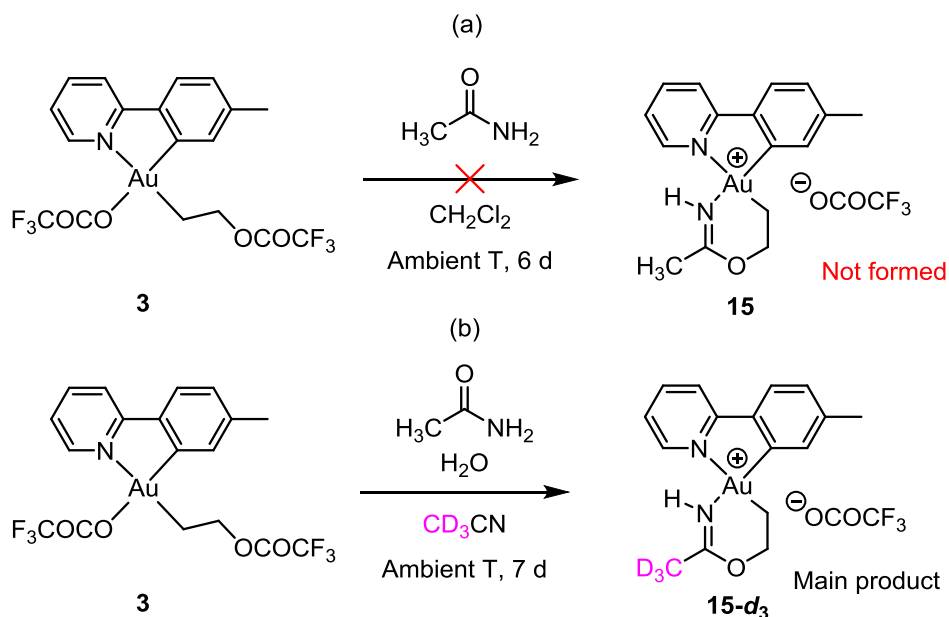
Scheme 43. Experiments probing for the potential role of acetamide being involved in the formation of complex **15**.

3.3 DFT calculations on the reaction mechanism forming complex 15

To gain more insight into the mechanism of formation of complex **15**, DFT calculations were performed. The DFT calculations were performed by Dr. Ainara Nova and Dr. David Balcells (University of Oslo). Scheme 44 shows a possible mechanism for the formation of **15**. The relative free energy of all the intermediates in Scheme 44 has been assessed by DFT calculations showing that they are all

accessible under the reaction conditions. The unobserved cationic ethylene complex **A** is generated from either **2** or **3**, in agreement with previous findings.[90] Then a nucleophilic addition of water to ethylene in **A** can generate **12** (**TSA-12** = 16.2 kcal mol^{-1}), in agreement with findings in Chapter 2 and Paper I where it was demonstrated that **12** could be generated either by adding water to **3** or by reacting **2** with ethylene and water. This step is also in agreement with the findings of Atwood and co-workers described in Chapter 1.[98] Then the OCOCF$_3$ ligand *trans* to tpy-*C* can undergo an exchange with MeCN to give complex **B**, which is closely related to AuMe(MeCN)tpy (with MeCN *trans* to tpy-*C*) which has been prepared previously in the Tilset group.[110] Following this, cyclization by an intramolecular attack of the hydroxyethyl-*O* atom at the nitrile-*C* atom and concomitant loss of CF$_3$COOH yields **C**. Finally, protonation of the metallacycle-*N* with CF$_3$COOH gives complex **15**. The transition state going from **B** to **C** (**TSB-C**) has also been computed and it shows that cyclization is triggered by the deprotonation of the hydroxyl group by an external trifluoroacetate with a free energy barrier that should be surpassable at room temperature (See Scheme 44 and Figure 15).
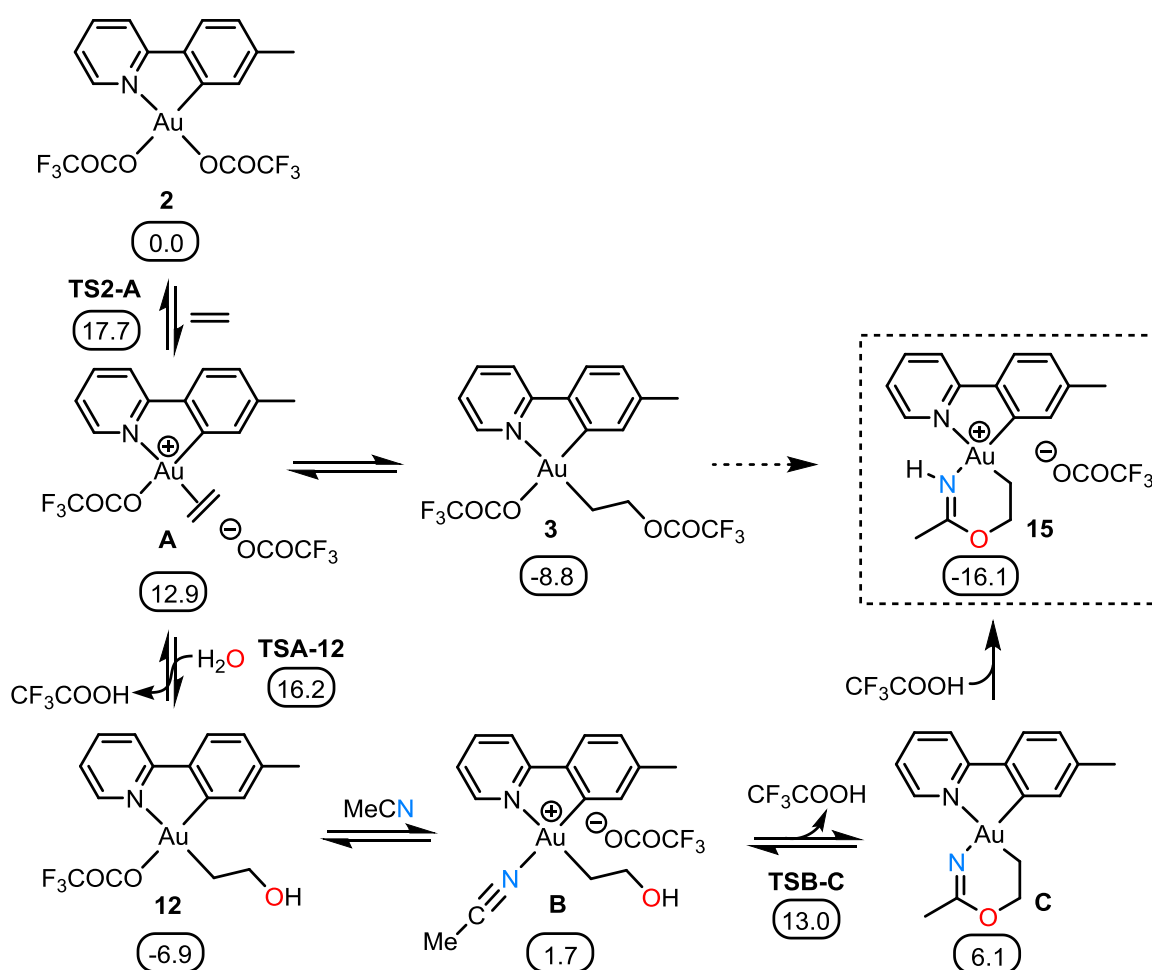
Scheme 44. Suggested reaction mechanism for the formation of complex **15**. Free energies, obtained from DFT calculations in acetonitrile, are given in kcal mol^{-1}. The energies of $^-$OCOCF$_3$, CF$_3$COOH, MeCN, ethylene, and H$_2$O have been included in the calculations where needed to maintain mass and charge balance. The DFT calculations were performed by Dr. Ainara Nova and Dr. David Balcells (University of Oslo). Computational details are given in Paper II.
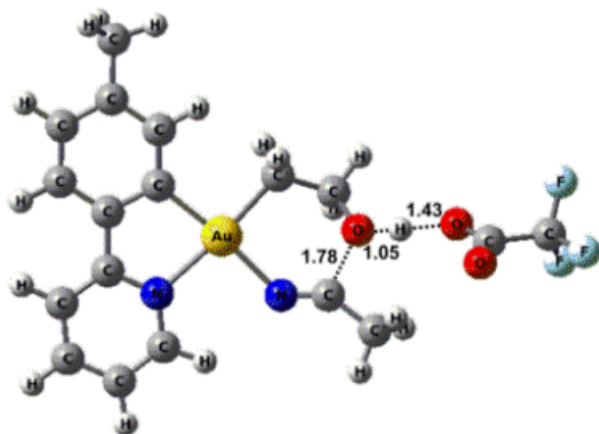
Figure 15. Optimized geometry for **TSB-C** with selected bond distances (Å).

3.4 Attempts at catalysis and further reactivity of complex 15

An eventual reductive elimination from complex **15** would generate 2-methyl-2-oxazoline, which is an important heterocyclic ring structure (Scheme 45, right). However, heating **15** in wet CD$_3$CN (70 $^\circ$C) did not lead to any formation of 2-methyl-2-oxazoline. Instead, a release of acetamide and concomitant formation of **15**-**d_3** was observed (Scheme 45 and Figure 16). Heating complex **2** in wet CD$_3$CN also furnished acetamide (acetamide-d_3 was formed since CD$_3$CN is used), so the formation of acetamide may not necessarily need to have **15** present. However, the non-labelled acetamide formed in the reaction in Scheme 45 should stem from complex **15** since the reaction medium is deuterated acetonitrile and the only source of non-labelled acetamide is from **15**.
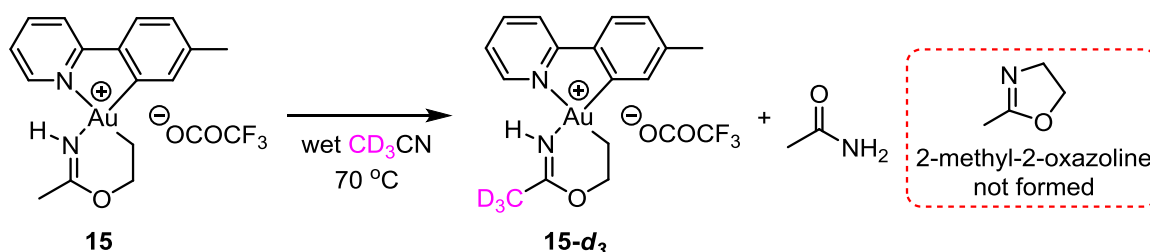
Scheme 45. Heating **15** in CD$_3$CN leads to release of acetamide and concomitant formation of **15**-**d_3**.

The mechanism for the release of acetamide from complex **15** and the concomitant regeneration of the metallacycle **15**-**d_3** has not been studied further. However, one possible explanation may be that the metallacycle opens up to form **15-Open** (Scheme 46). **15-Open** would then formally be a complex where acetamide has reacted as an O-nucleophile in a reaction with ethylene at **2** in the same way as the reactions discussed in Chapter 2. Then, as described in the introduction, we know that the nucleophilic addition of $^-$OCOCF$_3$ to ethylene at **2** forming **3** is reversible. If the same principles are true for the related product **15-Open**, complex **A** could be generated from **15-Open**. Finally, from **A**, complex **15**-**d_3** could be constructed by reaction with CD$_3$CN and H$_2$O, and acetamide would be released. The possibility of formation of **15-Open** was further supported by DFT calculations where it

was shown that the free energy of **15-Open** in acetonitrile (relatively to that of **2**) is –6.5 kcal mol^{-1}, which should make **15-Open** thermodynamically accessible compared to that of **15** (–16.1 kcal mol^{-1}). The kinetics of forming **15-Open** from **15** was however not investigated, and further studies need to be performed in order to support this hypothesis.
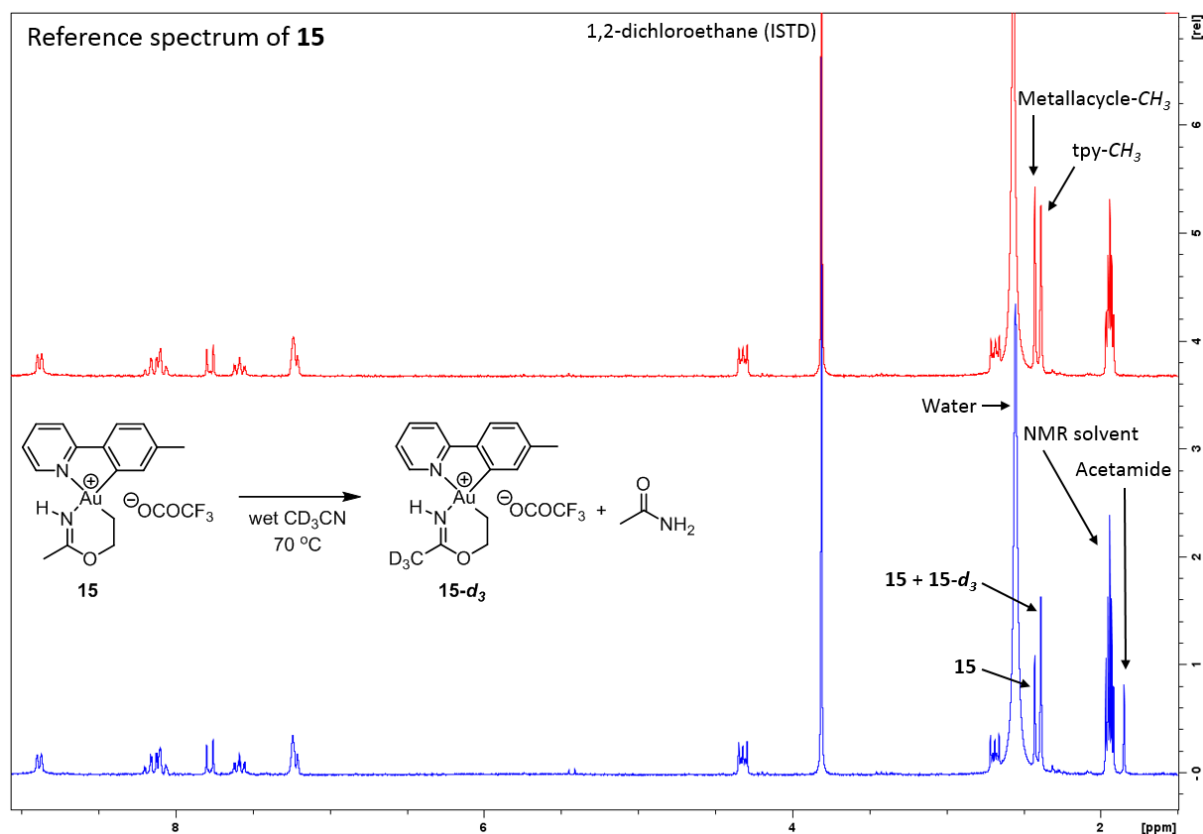
Figure 16. Stacked ^{1}H NMR (200 MHz, CD$_3$CN) spectra showing the reactivity of **15** in CD$_3$CN. Top: Reference spectrum of **15**. Bottom reaction mixture after heating **15** in CD$_3$CN for one day furnishing a mixture of **15**, **15-d_3**, and acetamide.

Addition of acid to **15** was also investigated to see if 2-methyl-2-oxazoline could be liberated. Upon adding HNTf$_2$ to a solution of **15** in CD$_2$Cl$_2$, no formation of 2-methyl-2-oxazoline was observed and further attempts at liberating 2-methyl-2-oxazoline were not performed.
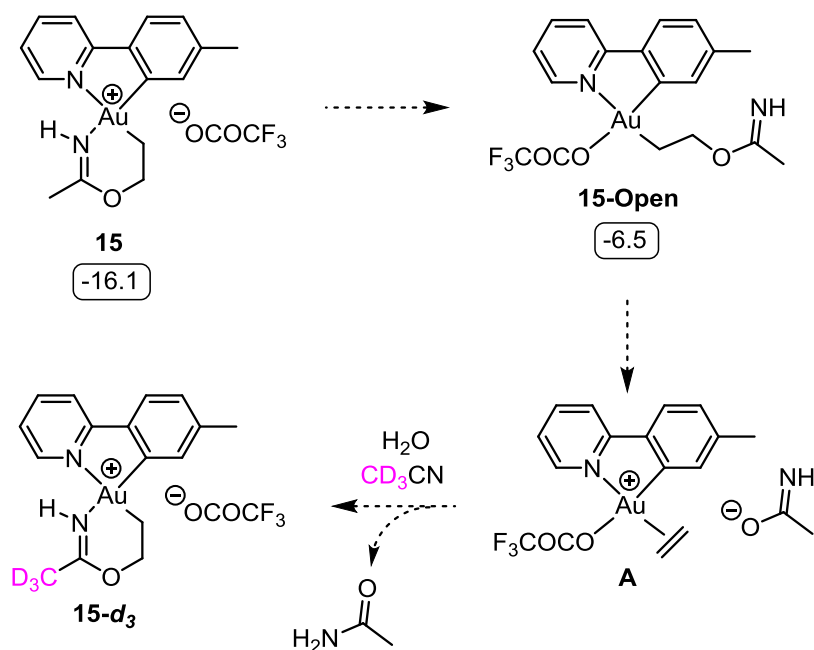
Scheme 46. Possible explanation of how acetamide and **15-d_3** are generated when heating **15** in CD_3CN. Free energies (relative to that of **2**) obtained from DFT-calculations in acetonitrile are given in kcal mol^{-1}. The DFT calculations were performed by Dr. Ainara Nova utilizing the same methodology as those in Scheme 44.

3.5 Other alkenes investigated by co-workers

M.Sc. Erlend Solbakken Aunan worked on this project during his bachelor degree studies. He found that it was possible to form metallacycle complex **15-*i*Pr** upon utilizing 3-methyl-1-butene instead of ethylene (Scheme 47).[106]
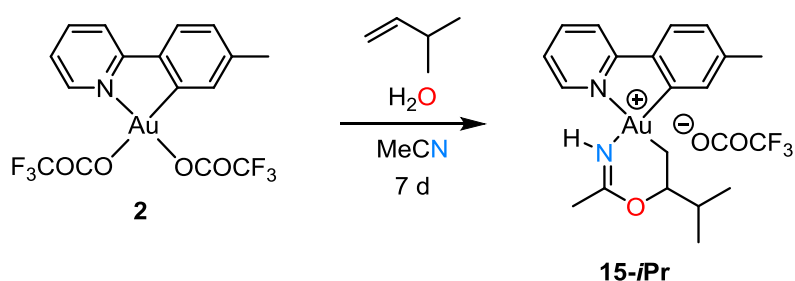
Scheme 47. Metallacycle formation by utilizing 3-methyl-1-butene instead of ethylene.[106]

Styrene was also investigated in the reaction depicted in Scheme 47 by M.Sc. Franziska Stefanie Ihlefeldt and Susan Dalzell. They found that upon utilizing styrene instead of ethylene, no Au(III) metallacycle complex could be obtained. However, they found that the dimer **15-Styrene** was formed instead (Scheme 48).[105] The reasons behind why dimer formation occur instead of metallacycle formation has not been investigated yet. Until now, 3-Methyl-1-butene is the only other alkene than ethylene that has successfully been incorporated in a metallacycle of the same type as **15**, and further work will be needed in order to achieve a full overview of the scope of this reaction.
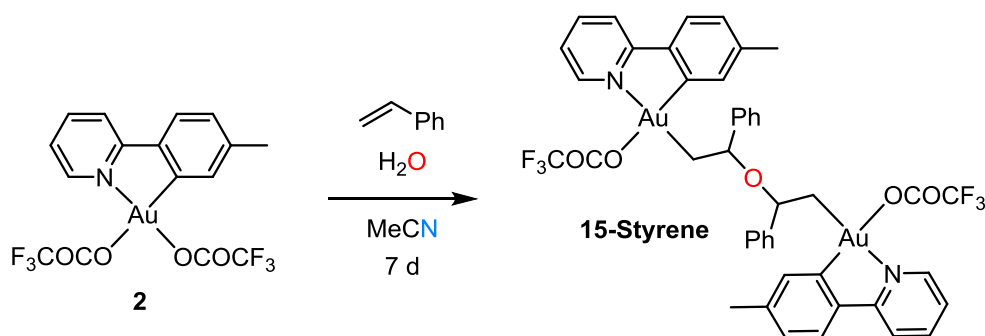
Scheme 48. Reacting **2** with styrene and water in acetonitrile led to formation of dimer **15-Styrene** instead of a metallacycle complex.[105]

3.6 Synthesis and characterization of metallacycle complex 16

3.6.1 Background

At approximately the same time as the author of this thesis synthesized metallacycle complex **15**, there was a related discovery by another member of the research group, M.Sc. Franziska Stefanie Ihlefeldt. In an attempt to perform insertion reactions with styrene in acetonitrile, a complex similar to **15** was obtained. The reaction conditions were somewhat different; in this case CF_3COOH was added to the reaction mixture and styrene was used instead of ethylene. A synthetic protocol for synthesizing the newly discovered complex was developed by M.Sc. Ihlefeldt and the product was carefully characterized as **16-Styrene** (Scheme 49),[102] which differ from complex **15** in the placement of the metallacylce-*O* and the metallacycle-*NH*.
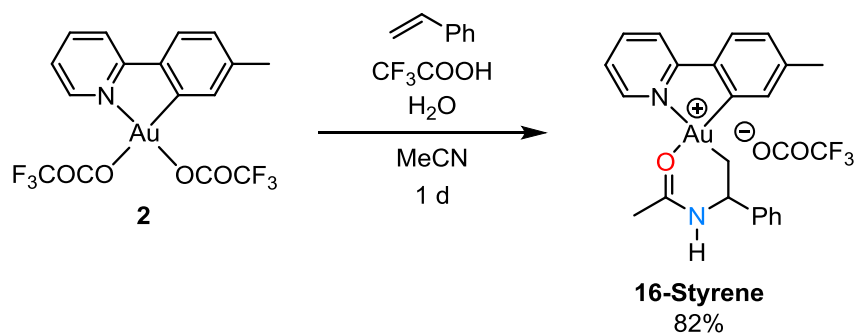
Scheme 49. Synthesis of **16-Styrene**.[102]

3.6.2 Synthesis and characterization of metallacycle complex 16

In order to probe whether the two different 6-membered metallacycle rings obtained in complexes **15** and **16-Styrene** were due to the change of the alkene from ethylene to styrene or due to the addition of CF_3COOH to the reaction mixture, or a combination of these factors, the author investigated the reaction with ethylene utilizing the conditions described in Scheme 49. Upon stirring complex **2** in MeCN with H_2O, CF_3COOH, and ethylene added for 10 days, complex **16** was formed (Scheme 50). The reasons why the reaction with ethylene forming **16** is that much slower than the reaction with styrene forming **16-Styrene** have not been investigated, but it is probably related to the

fact that the double bond in styrene is more activated than that of ethylene. This experiment shows that the addition of CF$_3$COOH has a remarkable effect on outcome of the reaction, and this will be further discussed in Section 3.7.
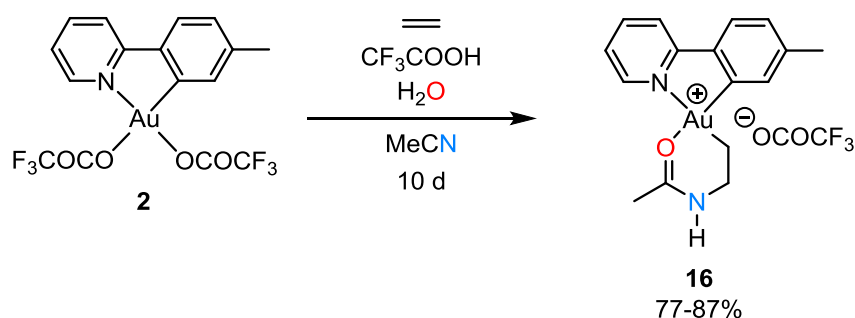
Scheme 50. Synthesis of complex **16**.

A one pot microwave synthesis of **16** from Au(OCOCH$_3$)$_3$ was also developed (Scheme 51). Upon mixing Au(OCOCH$_3$)$_3$ with tpyH in a mixture of H$_2$O, MeCN, and CF$_3$COOH (1:7:7) and bubbling ethylene through the mixture followed by microwave heating, complex **16** could be obtained. After the reaction, the crude mixture reveals a mixture of different products including **16**, and after extraction, washing and recrystallization complex **16** could be isolated in low to moderate yields (17-49%). The yields of the reaction varied quite a lot under the same reaction conditions and could probably be improved by further optimization of the reaction conditions and/or the work up.
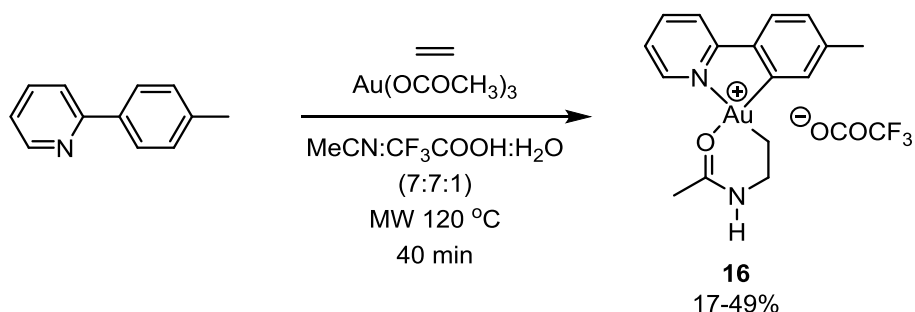
Scheme 51. One-pot synthesis of complex **16** from Au(OCOCH$_3$)$_3$, tpyH, MeCN, CF$_3$COOH, and H$_2$O.

It was also discovered that complex **15** could be converted into complex **16**. Upon heating **15** in CD$_3$CN with excess CF$_3$COOH and H$_2$O added at 50 °C for one day, full conversion of **15** into **16-d_3** was obtained. Acetamide was also formed in this reaction (Scheme 52).

Complex **16** was characterized by NMR, MS, and X-ray diffraction analysis. High resolution mass spectrometry of the cation of **16** revealed that the complex has the same elemental composition as **15**, but the ^{1}H NMR spectrum of **16** is clearly different than that of **15**. In the ^{1}H NMR spectrum of complex **16**, the characteristic CH$_2$CH$_2$ unit is observed as in complex **15**. The NCH$_2$ moiety is found at a significantly lower ppm value than that observed for OCH$_2$ in **15** (δ 4.34 in **15** and δ 3.47 in **16**), reflecting the weaker electron withdrawing N atom compared to the O atom. The AuCH$_2$ resonance in

16 is found at δ 2.69, which is similar to that of **15** (δ 2.73). In the ^{1}H NMR and ^{13}C NMR spectra of **16**, there are several broadened resonances present. The broadening is especially present in samples of **16** which are carefully dried; addition of CF_3COOH to these samples reduces the broadening (see Figure A14, Figure A23, and Figure A26, Appendix V). Among the broadened resonances in the ^{1}H NMR spectrum are the metallacycle-*CH$_3$* (δ 2.40), AuCH$_2$ (δ 2.69), H^6 (δ 8.75), and NH. The resonance of NH is broadened so much that it is barely visible at *ca.* δ 11.8. In the ^{13}C NMR spectrum of **16**, the resonances of the carbons in the CH$_2$CH$_2$ unit and OC̲CH$_3$N are significantly broadened. A possible explanation for this broadening will be discussed in Section 3.8. In the ^{19}F NMR spectrum of **16**, one single resonance is observed at δ −78.2, similar to that of **15** (δ −78.1), corresponding to $^-$OCOCF$_3$. In a ^{1}H-^{15}N HMBC experiment[viii], two different N atoms are observed. At δ −122 the resonance of tpy-*N* is found, similar to that of **15** (δ −129) and at δ −242 the resonance of the metallacycle-*NH* is found, at a slightly lower ppm value than that of **15** (δ −212). In a ^{1}H-^{1}H NOESY experiment,[viii] a NOE is observed between the metallacycle-*NH* and the metallacycle-*CH$_3$*, and between the metallacycle-*NH* and NCH$_2$, in agreement with structure **16**. Furthermore, no NOE correlations between the protons in the tpy ligand and the metallacycle-*NH* was observed, which is in full agreement with the placement of NH in the metallacycle **16** compared to that of **15**.
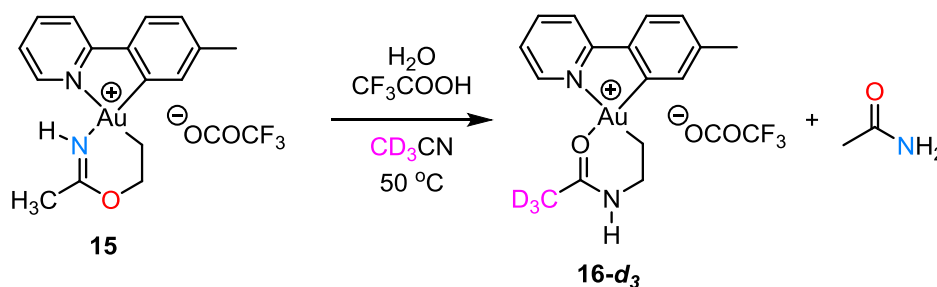
Scheme 52. Conversion of complex **15** into complex **16-*d$_3$*.**

3.7 DFT calculations on the reaction mechanism forming complex 16

DFT calculations on the reaction mechanism forming complex **16** from complex **2** were performed by Dr. Ainara Nova (University of Oslo). Scheme 53 shows a possible mechanism for the formation of **16** (the postulated mechanism for the formation of **15** from **2** is also included for comparison). The relative energy of all the intermediates in Scheme 53 have been assessed by DFT calculations, showing that they are all accessible under the reaction conditions. The mechanism of formation of complex **16** is similar to the Ritter reaction where a carbocation (*e.g.* generated from an alkene) is reacted with a nitrile and water under acidic conditions to form an amide.[111, 112]

---

viii CF$_3$COOH (*ca.* 0.7 equivalents) was added to the NMR sample used for the ^{1}H-^{15}N HMBC and ^{1}H-^{1}H NOESY experiments.
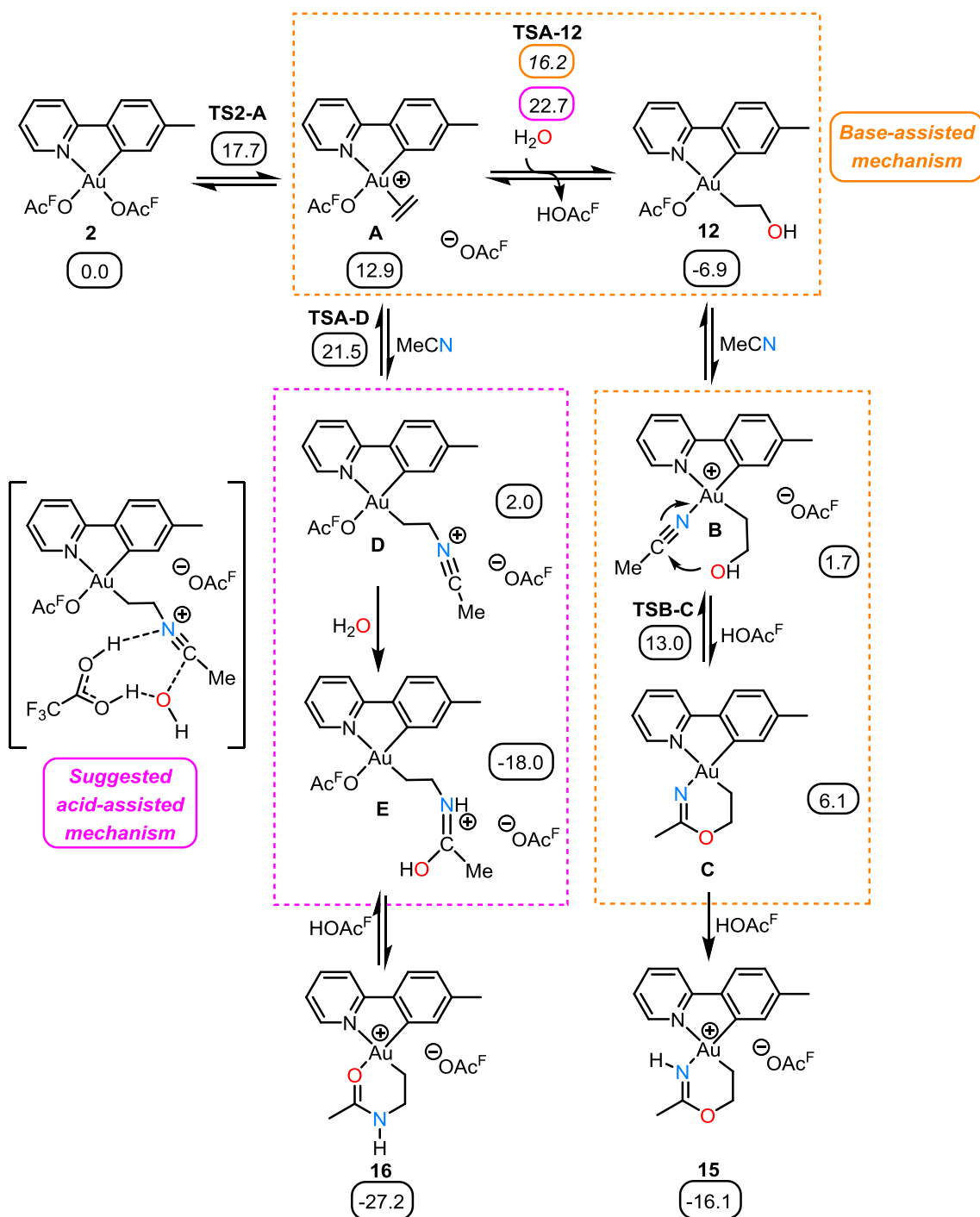
Scheme 53. Suggested reaction mechanism for the formation of **15** and **16** from **2**. Free energies, obtained from DFT calculations in acetonitrile, are given in kcal mol^{-1}. OAc^F = OCOCF$_3$. The energies of CF$_3$COOH, $^-$OCOCF$_3$, MeCN, and H$_2$O have been included in the calculations where needed to maintain mass and charge balance. The DFT calculations were performed by Dr. Ainara Nova by utilizing the same methodology as those in Scheme 44 and Paper II.

Analogously to the mechanism of forming complex **15**, complex **A** is first generated by substituting the $^-$OCOCF$_3$ ligand *trans* to tpy-*N* with ethylene. The next step differs in the mechanism forming **16** compared to that of **15**. In the mechanism forming **15**, H$_2$O acts as a nucleophile adding to ethylene at **A** forming **12**, and this mechanism is believed to be base assisted (that is; $^-$OCOCF$_3$ acts as a weak base abstracting one of the H's originating from H$_2$O). However, in the presence of excess CF$_3$COOH,

$^-$OCOCF$_3$ is not able to act as a base and the free energy barrier for this reaction becomes significantly higher (**TSA-12** = 22.7 kcal mol^{-1}, compared to 16.2 kcal mol^{-1} with $^-$OCOCF$_3$ assistance) and the pathway with the lower free energy barrier is then the nucleophilic addition of MeCN to ethylene at **A** (**TSA-D** = 21.5 kcal mol^{-1}) leading to complex **D** (Scheme 53, left frame). Following this, addition of water to the former MeCN unit furnishes complex **E**. This reaction is thought to be acid-assisted where one molecule of CF$_3$COOH effectively transfers one of the protons from water to the N atom of the former MeCN unit. Finally, a substitution of the $^-$OCOCF$_3$ ligand *trans* to tpy-*C* with the O-atom and a concomitant loss of CF$_3$COOH furnishes complex **16**.

3.8 Possibly dynamic behavior in solution.

As mentioned previously, broadening of the resonances were observed both in the ^{1}H NMR and ^{13}C NMR spectra of complex **16**. In addition to this, crosspeaks which are probably due to chemical exchange were observed in the NOESY spectrum of **16**. Crosspeaks with the same phase as the diagonal in a NOESY spectrum can be due to chemical exchange.[113] Several cross peaks of this type were observed in the NOESY spectrum of **16**. It appears that these crosspeaks are correlating some of the resonances of **16** with what was initially believed to be trace impurities present in the sample (see one example in Figure 17). However, in light of the chemical exchange crosspeaks observed in the NOESY spectrum, these resonances might instead be because **16** is able to interconvert to another species in solution during the time scale of the NMR experiment.
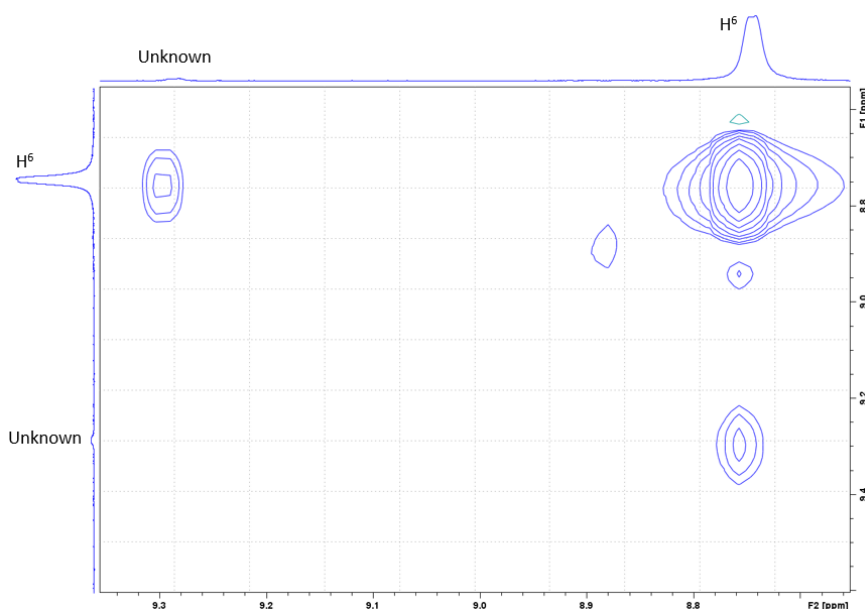
Figure 17. NOESY (600 MHz, CD$_2$Cl$_2$, mixing time = 1 s) of complex **16**. Close up on what is believed to be crosspeaks due to chemical exchange. The unknown species is suggested to be **16-Open**.

Due to time limitations, this phenomenon was not studied further. But one hypothesis of what may be occurring is illustrated in Scheme 54 (left). Here it is suggested that the metallacycle opens up to

form **16-Open** (analogously to what was suggested to happen in **15**) which can formally be regarded as an ethylene insertion product where acetamide acted as a N nucleophile in a reaction with ethylene at **2**, analogously to the reactions described in Chapter 2. The free energy of **16-Open** was calculated by DFT calculations (in acetonitrile, relatively to **2**) by Dr. Ainara Nova and was found to be –26.5 kcal mol^{-1}. This is rather close to, but slightly higher than, the calculated free energy of **16** (–27.2 kcal mol^{-1}) making it plausible that this complex is formed. However, it should be taken into account that the kinetics of forming **16-Open** from **16** were not investigated and further work will have to be undertaken to further support this hypothesis.
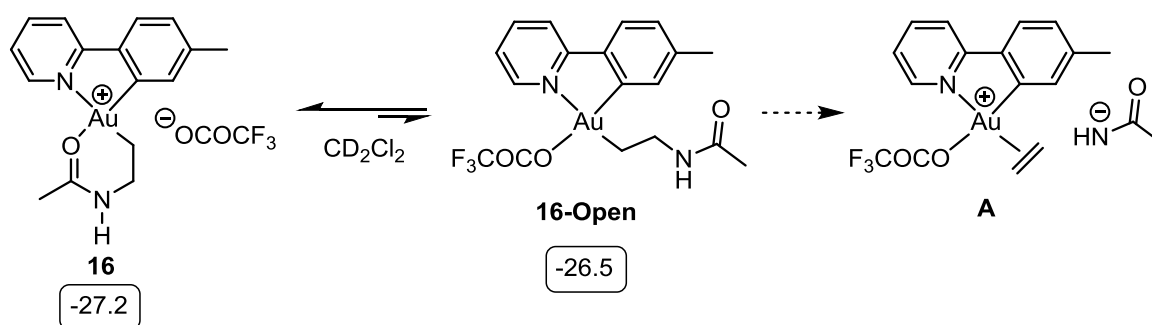
Scheme 54. Hypothetical solution behavior of **16**. Free energies (relative to that of **2**) obtained from DFT calculations in acetonitrile are given in kcal mol^{-1}. The DFT calculations were performed by Dr. Ainara Nova utilizing the same methodology as those in Scheme 44.

The behavior depicted in Scheme 54 may also explain the formation of acetamide as a side product in the reactions involving **16** as well as **15**, which was discussed previously. As already mentioned, the nucleophilic addition of $^-$OCOCF$_3$ to ethylene at **2** forming **3** is reversible. If the same principles are true for the related product **16-Open**, complex **A** (Scheme 54, right) could be generated. Finally, from complex **A**, complex **16** could be constructed by reacting it with CD$_3$CN, H$_2$O, and CF$_3$COOH, and acetamide would be released.

3.9 Crystallographic structure determination of complexes 15 and 16

Complexes **15** and **16** were characterized by single crystal X-ray diffraction analyses. The crystallographic structure determinations were performed by Dr. Sigurd Øien-Ødegaard (University of Oslo). The ORTEP plots of complexes **15** and **16** are shown in Figure 18 and Figure 19, and selected metrical parameters are given in Table 3. The molecular structures of **15** and **16** are in agreement with the other characterization data on the complexes. In **15**, a metallacycle where the N atom is coordinated to Au is observed whereas in **16** the O atom is coordinated to Au. In both complexes, a hydrogen bonding interaction between H2 and O2 is observed, with a donor-acceptor (N2⋯O2) distance of 2.8708(2) Å (**15**) and 2.7688(1) Å (**16**) (Figure 19). The directionality of the hydrogen bonding interactions in **15** and **16** are in full agreement with the assigned structures. As can be seen from Figure 18, both complexes exhibit the nearly square planer geometry which is typical for Au(III)

complexes. In both complexes, the N1-Au1-C1 angle for the tpy chelate deviates slightly from the idealized 90° to 80.60(10)° (**15**) and 81.73(6)° (**16**), in agreement with previous findings.[89, 90] The chelate angle of the six membered ring metallacycle, C2-Au1-N2 (**15**) and C2-Au1-O1(**15**), is close to the idealized 90° for both complexes, but slightly larger for **16** (92.37(6)°) than for **15** (89.54(11)°). The Au1-N1 and Au1-C1 distances are within the range of that reported previously for related Au(III) complexes.[89, 90] The Au1-C2 distances of 2.042(3) Å and 2.0361(16) Å for **15** and **16**, respectively, are similar to that of the ethylene insertion products reported previously[90] and the related complexes described in Chapter 2. The Au1-N2 bond of 2.092(3) Å in **15** is similar to that of the Au-N bond *trans* to tpy-*C* in AuMe(MeCN)(tpy)[110] (2.088(5) Å, see ESI Paper II) and the Au1-O1 bond of 2.0985(12) Å in **16** is similar to that of Au-O bond *trans* to tpy-*C* in **2** (2.111(5) Å).[89]
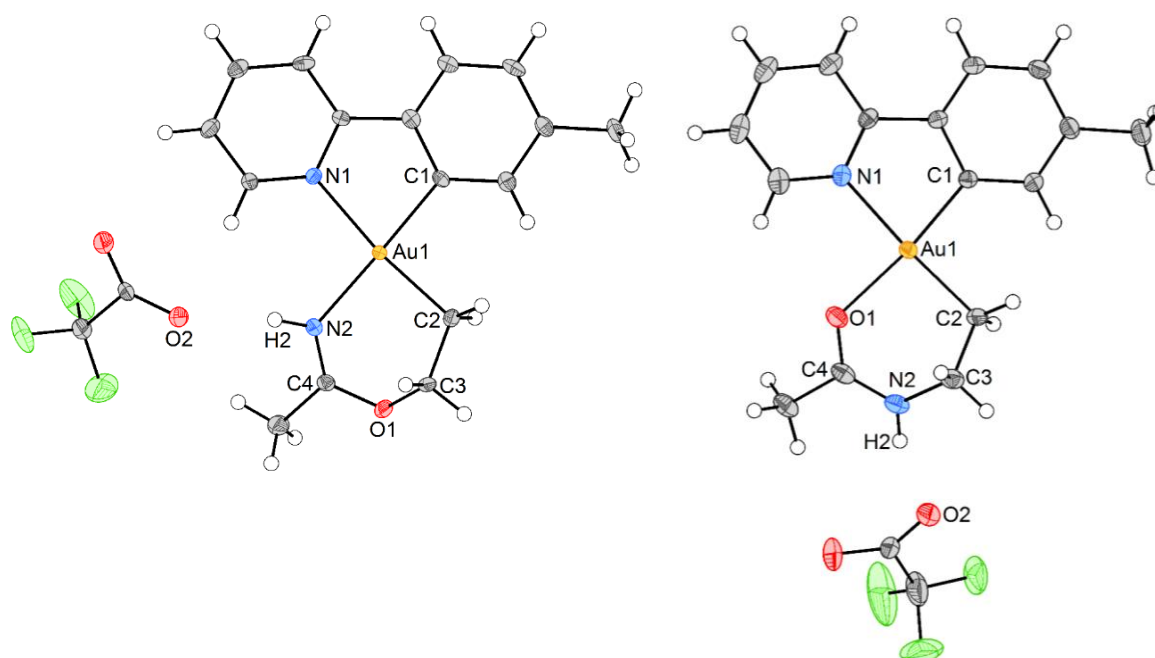
Figure 18. ORTEP plot of **15** (left) and **16** (right) with 50% ellipsoids. The CF$_3$ group in **16** is disordered (not shown). The crystallographic structure determinations were performed by Sigurd Øien-Ødegaard.
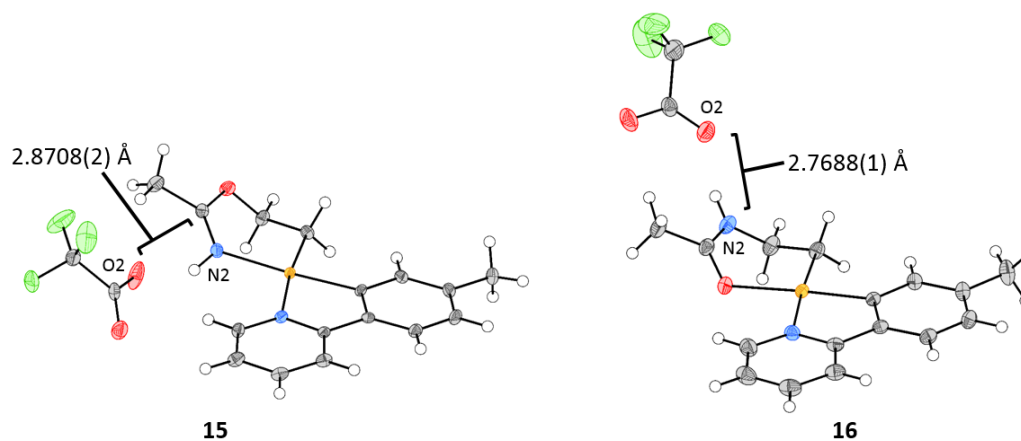
Figure 19. ORTEP plots of **15** (left) and **16** (right) showing the hydrogen bond interactions.

Table 3. Selected bond distances [Å], angles, and torsional angles [Å] for **15** and **16**.

Bond distances [Å]	**15**	Bond distances [Å]	**16**
Au1-N1	2.126(2)	Au1-N1	2.1129(14)
Au1-C1	2.019(3)	Au1-C1	1.9921(16)
Au1-N2	2.092(3)	Au1-O1	2.0985(12)
Au1-C2	2.042(3)	Au1-C2	2.0361(16)
C2-C3	1.510(4)	C2-C3	1.521(2)
C3-O1	1.449(4)	C3-N2	1.466(2)
O1-C4	1.332(3)	N2-C4	1.307(2)
C4-N2	1.284(4)	C4-O1	1.278(2)
O2···N2	2.8708(2)	O2···N2	2.7688(1)
Angles [º]		Angles [º]	
N2-Au1-N1	97.43(9)	O1-Au1-N1	91.86(5)
N1-Au1-C1	80.60(10)	N1-Au1-C1	81.73(6)
C1-Au1-C2	92.39(12)	C1-Au1-C2	94.02(7)
C2-Au1-N2	89.54(11)	C2-Au1-O1	92.37(6)
C1-Au1-N2	174.24(12	C1-Au1-O1	173.44(6)
N1-Au1-C2	172.99(11)	N1-Au1-C2	175.71(6)
Au1-C2-C3-O1	60.2(3)	Au1-C2-C3-N2	55.47(18)
Au1-N2-C4-O1	26.5(5)	Au1-O1-C4-N2	39.7(2)
C2-C3-O1-C4	−70.8(4)	C2-C3-N2-C4	−62.7(2)
N2-C4-O1-C3	21.8(5)	O1-C4-N2-C3	7.4(3)

3.10 Conclusions

The synthesis of Au(III) metallacycle complexes **15** and **16** from complex **2** by utilizing both the coordination site *trans* to tpy-*N* and *trans* to tpy-*C* were presented. Complexes **15** and **16** were characterized by multinuclear NMR, MS (including HRMS), elemental analysis, and X-ray diffraction analysis. It was found that CF_3COOH plays a major role in the synthesis of the two complexes; if CF_3COOH is added to the reaction mixture complex **16** is formed, and if CF_3COOH is not added, complex **15** is formed instead. DFT calculations revealed that two different mechanisms are operating under the different reaction conditions. In both complexes **15** and **16**, the simple and readily available building blocks ethylene, MeCN, and H_2O have been incorporated, which is a nice example of small molecule activation at Au(III). In addition to that, it proved possible to prepare complex **16** in a one pot procedure from $Au(OCOCH_3)_3$, tpyH, ethylene, MeCN, H_2O, and CF_3COOH.

3.11 Experimental

The experimental details for the content of Chapter 3 that are not described in Paper II are found herein.

General procedures

Complex **2** was prepared by a previously reported procedure.[89] $Au(OCOCH_3)_3$ was purchased from ABCR. CH_2Cl_2 and MeCN were purified using a MB SPS-800 solvent purifying system from MBraun. CD_2Cl_2 was dried over 3Å molecular sieves. Ethylene 3.5 was purchased from Hydro Gas. Distilled water was used in all reactions and workups. All other reagents and solvents were used as received. All reactions were performed in air. As a precaution, all syntheses were performed in the absence of light. NMR spectra were obtained on DPX200, AVI600, and AVII600 instruments at ambient temperature. ^1H and ^{13}C NMR spectra have been references relative to the residual solvent signals (CD_2Cl_2: $\delta(^1H)$ 5.34, $\delta(^{13}C)$ 53.84). The ^{15}N NMR chemical shifts have been calibrated using $MeNO_2$ as an external standard at 0 ppm by adding a closed capillary containing $MeNO_2$ to the NMR sample of interest. ^{19}F NMR has been referenced relative to $CFCl_3$ by using C_6F_6 (−164.9 ppm with respect to $CFCl_3$ at 0 ppm) as an internal standard by adding 0.5-1 μL C_6F_6 to the NMR sample of interest. The peaks in the ^1H NMR spectra were assigned by the aid of 2D NMR techniques such as COSY, HSQC, HMBC, and NOESY according to the numbering scheme shown in Figure 1. Mass spectra (ESI) were obtained on a Bruker maXis II ETD spectrometer by Osamu Sekiguchi (University of Oslo).

Reactivity of 15 in CD_3CN

Complex **15** (4.7 mg, 0.0083 mmol) was dissolved in wet CD_3CN and transferred to a NMR tube. 1,2-dichloroethane was added as an internal standard (ISTD). The solution was heated at 70 °C for 1 day and then investigated by ^1H NMR. A mixture of **15-d_3** and **15** (*ca*. 0.4:0.6) together with acetamide was observed by ^1H NMR. The presence of acetamide was confirmed by spiking the sample with an authentic sample of acetamide. MS (ESI, CD_3CN) *m/z* (rel.%): 451 (**15**−$OCOCF_3$, 100), 454 (**15-d_3**, 75).

Reactivity of $Au(OCOCF_3)_2(tpy)$ in MeCN

Complex **15** (5.3 mg, 0.0090 mmol, 1.0 equiv) was dissolved in wet CD_3CN and transferred to a *J*-Young NMR tube. 1,2-dichloroethane (1 μL, ISTD) was added. The reaction mixture was heated at 70 °C for 1 day. ^1H NMR of the reaction mixture revealed that acetamide-d_3 (*ca*. 3 equiv based on NMR integration of the NH_2 protons against the internal standard) was formed. At this point, >50 % of **1** had decomposed into unknown products.

Reactivity of 15 towards HNTf$_2$ in CD$_2$Cl$_2$

Complex **15** (4.9 mg, 0.0087 mmol, 1.0 equiv) was dissolved in CD$_2$Cl$_2$. HNTf$_2$ (5 mg, 0.02 mmol, 2 equiv) was added and the reaction was monitored by ^{1}H NMR. After 1 day, there were two products present in addition to **15**. Based on their chemical shifts one of them is probably **3**, the other unknown. 2-Methyl-2-oxazoline was not formed.

Synthesis of 16 from 2

Complex **2** (51.8 mg, 0.0876 mmol, 1.0 equiv.) was dissolved in acetonitrile (4 ml). CF$_3$COOH (0.50 mL, 6.5 mmol, 74 equiv.) and water (10 μL, 0.55 mmol, 6.3 equiv.) was added. Ethylene was bubbled through the solution for two minutes, and the flask was sealed with a glass stopper. The reaction mixture was stirred at ambient temperature in the absence of light for 10 days. The volatiles were removed under reduced pressure and the remaining solid was dissolved in CH$_2$Cl$_2$ and filtered. The solvent was removed under reduced pressure yielding **16** (43.0 mg, 0.0762 mmol, 87%) as a white solid. NB: It is difficult and sometimes impossible to get rid of all the excess CF$_3$COOH, therefore the yield might be overestimated.

^{1}H NMR (600 MHz, CD$_2$Cl$_2$): δ 11.8 (br. s, 1H, N**H**), 8.75 (br. d, 1H, J = 3.8 Hz, **H^6**), 8.11 (ddd, 1H, J = 8.0, 7.7, 1.6 Hz, **H^4**), 7.99 (d, 1H, J = 8.2 Hz, **H^3**), 7.70 (d, 1H, J = 7.9 Hz, **H$^{3'}$**), 7.60 (ddd, 1H, J = 7.5, 5.4, 0.8 Hz, **H^5**), 7.24-7.25 (m, 2H, **H$^{4'}$** and **H$^{6'}$**), 3.47 (m, 2H, NC**H$_2$**), 2.69 (br. m, 2H, AuC**H$_2$**), 2.44 (s, 3H, ArC**H$_3$**), 2.40 (br. s, 3H, OCC**H$_3$**N).

^{1}H NMR (600 MHz, CD$_2$Cl$_2$ with *ca.* 0.7 equiv CF$_3$COOH added): δ 9.47 (br. s, 1H, N**H**), 8.76 (d, 1H, J = 5.2 Hz, **H^6**), 8.13 (ddd, 1H, J = 8.0, 7.7, 1.5 Hz, **H^4**), 8.00 (d, 1H, J = 8.1 Hz, **H^3**), 7.71 (d, 1H, J = 7.9 Hz, **H$^{3'}$**), 7.62 (ddd, 1H, J = 6.9, 6.1, 0.8 Hz, **H^5**), 7.26 (d, 1H, J = 7.9, **H$^{4'}$**), 7.20 (s, 1H, **H$^{6'}$**), 3.46 (m, 2H, NC**H$_2$**), 2.71 (m, 2H, AuC**H$_2$**), 2.44 (s, 3H, ArC**H$_3$**), 2.42 (s, 3H, OCC**H$_3$**N).

^{19}F NMR (188 MHz, CD$_2$Cl$_2$): δ −78.2.

^{13}C NMR (151 MHz, CD$_2$Cl$_2$): δ 175 (br, O**C**CH$_3$NH), 161.0 (br. q, J = *ca.* 35 Hz, O**C**OCF$_3$), 160.6, 145.7, 143.1, 142.4, 140.7, 135.8, 132.0, 129.6, 126.1, 124.3, 120.4, 38.1 (br., HN**C**H$_2$), 34.0 (br., Au**C**H$_2$), 22.5, 21.9. Several of the peaks are broadened and the resonance at δ 175 is barely visible due to broadening. OCO**C**F$_3$ was not observed.

^{15}N(^{1}H) NMR (600 MHz, CD$_2$Cl$_2$ with *ca.* 0.7 equiv CF$_3$COOH added): δ −122 (**N$_{tpy}$**), −242 (**N**H).

MS (ESI, MeCN): *m/z* (rel.%): 451 ([M−OCOCF$_3$]$^+$, 100).

HRMS (ESI, MeCN): Found 451.1080; calcd. for C$_{16}$H$_{18}$AuN$_2$O 451.1079.

Synthesis of 16 from Au(OCOCH₃)₃

Au(OCOCH₃)₃ (196.2 mg, 0.5244 mmol, 1.04 equiv) was added to a microwave vessel. A mixture of water (1 mL), CF₃COOH (7 mL), MeCN (7 mL), and tpyH (100 μL, 0.504 mmol, 1.00 equiv) was added. Ethylene was bubbled through the mixture for 1 minute and the vessel was sealed and the reaction mixture was heated in a microwave at 120 °C for 40 min. After the reaction, a brownish mixture was obtained. CH₂Cl₂ (15 mL) was added and the solution was filtered. The mixture was transferred to a separation funnel and water (10 mL) was added. The organic phase was collected and the water phase was extracted with CH₂Cl₂ (2 x 10 mL). The combined organic phases were washed with water (3 x 10 mL), dried over Na₂SO₄, and filtered. The solvent was removed under reduced pressure furnishing a dark oil. The dark oil was redissolved in CH₂Cl₂ and filtered through celite furnishing a yellow solution. CH₂Cl₂ was again removed under reduced pressure and the remaining yellow oil was crystallized from CH₂Cl₂/pentane furnishing **16** (139.6 mg, 0.2474 mmol, 49%) as a white solid. NB: It is difficult and sometimes impossible to get rid of all the excess CF₃COOH, therefore the yield might be overestimated.

Conversion of 15 into 16-*d₃*
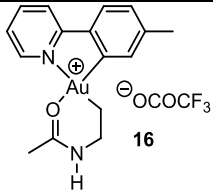
Complex **15** (5.0 mg, 0.0089 mmol, 1.0 equiv) was dissolved in CD₃CN and added to a NMR tube. CF₃COOH (50 μL, 0.065 mmol, 73 equiv) and H₂O (1 μL, 0.06 mmol, 7 equiv) was added. The sample was heated at 50 °C for 1 day. Investigation by ¹H NMR after 1 day of heating revealed that all of **15** was converted into **16-*d₃***. Acetamide was also formed. The presence of **16-*d₃*** and acetamide was confirmed by spiking the sample with authentic samples of **16** and acetamide.

Crystallographic structure determination

Crystals suitable for X-ray diffraction analysis of **16** were grown by the vapor diffusion technique.[114] A small vial containing **16** dissolved in CH₂Cl₂ was placed in a capped larger vial containing pentane and placed in a refrigerator (*ca*. 10 °C) slowly producing crystals of **16**.

Single crystal diffraction data for complex **16** was acquired on a Bruker D8 Venture equipped with a Photon 100 detector and using Mo Kα radiation (λ = 0.71073 Å) from an Incoatec iμS microsource. Data reduction was performed with the Bruker Apex3 Suite,[115] the structure was solved with ShelXT[116] and refined with ShelXL.[117] Olex2 was used as user interface.[118] The cif files were edited with enCIFer v1.4,[119] and molecular graphics were produced with Diamond v4.4.0.[120] The crystallographic structure determination was performed by Dr. Sigurd Øien-Ødegaard.

Table 4. Crystal and refinement data for complex **16**.

Crystal data	
Identification code	msh-454_pl
Chemical formula	$C_{16}H_{18}AuN_2O \cdot C_2F_3O_2$
M_r	564.31
Crystal system, space group	Monoclinic, $C2/c$
Temperature (K)	100
a, b, c (Å)	12.8485(7), 21.8433(12), 14.0317(11)
α, β, γ (°)	90, 109.346(1), 90
V (Å^3)	3715.7 (4)
Z	8
Radiation type	Mo $K\alpha$
μ (mm^{-1})	7.97
Crystal size (mm)	0.15 x 0.09 x 0.08
Data Collection	
Diffractometer	Bruker D8 Venture, CMOS detector diffractometer
Absorption correction	Multi-scan SADABS-2014/5 (Bruker,2014/5) was used for absorption correction. wR2(int) was 0.0704 before and 0.0379 after correction. The Ratio of minimum to maximum transmission is 0.7652. The $\lambda/2$ correction factor is Not present.
T_{min}, T_{max}	0.572, 0.747
No. of measured, independent and observed [I > 2σ(I)] reflections	46041, 9013, 7801
R_{int}	0.026
$(\sin\theta/\lambda)$max (Å^{-1})	0.835
Refinement	
$R[F^2 > 2\sigma(F^2)]$, $wR(F^2)$, S	0.017, 0.053, 1.19
No. of reflections	9013
No. of parameters	264
No. of restraints	0
H-atom treatment	H-atom parameters constrained
	$w = 1/[\sigma^2(F_o^2) + (0.0281P)^2 + 0.5356P]$ where $P = (F_o^2 + 2F_c^2)/3$
$\Delta\rho_{max}$, $\Delta\rho_{min}$ (e Å^{-3})	1.00 $-$1.96

Chapter 4 – Catalytic transformation of acetylene at Au(III)

4.1 General introduction and scope of the chapter

In this chapter the catalytic transformation of acetylene into vinyl trifluoroacetate (**17**) at Au(III) will be presented (Scheme 55). The first part of this chapter, which covers the catalytic transformation of acetylene into **17** with Au(OCOCF$_3$)$_2$(tpy) (**2**) as a precatalyst, is described in Paper III. The work presented in Section 4.4 is described in Paper IV. The remaining results presented herein are preliminary studies where other Au(III) complexes and nucleophiles have been investigated to gain insight into the scope of the reaction. The DFT calculations presented in this chapter were performed by Dr. Ainara Nova and Dr. David Balcells (University of Oslo). The initial experimental studies leading to the work presented herein were performed at École Polytechnique Fédérale de Lausanne (EPFL) in Lausanne, Switzerland together with Dr. Eirin Langseth in the group of Professor Paul Dyson under the guidance of Professor Gábor Laurenczy. These experiments are also described in the Ph.D thesis of Dr. Eirin Langseth.[92]
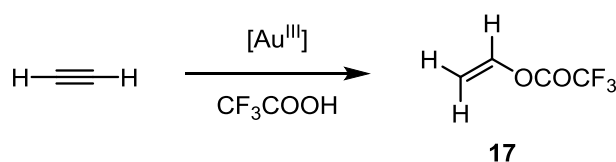
Scheme 55. Au(III) catalyzed transformation of acetylene into vinyl trifluoroacetate (**17**).

Lately, acetylene has become less used as a C$_2$ building block in western countries, due to the availability of less expensive hydrocarbons, such as ethylene, from petrochemical feedstocks.[54, 121] However, acetylene is still an important building block, and in countries where cheap coal is available acetylene is still in frequent use.[54, 121] For example, in China the production of vinyl chloride, which is the monomer used for producing polyvinyl chloride (PVC), is based on the acetylene hydrochlorination process (See Chapter 1, section 1.2.3).[54, 121] Traditionally, the acetylene hydrochlorination reaction has been performed with a mercury(II) chloride catalyst supported on carbon,[54, 121] but recently a commercial process utilizing a supported Au catalyst was developed.[52]

Vinyl trifluoroacetate (**17**) is also produced from acetylene. Until now, a mercury catalyzed process has been used, and there are several patented processes available.[122, 123] The catalyst used for this reaction is mercuric oxide, which is a very toxic mercury compound.[53] It is desirable to replace these mercury processes with more environmentally friendly processes and to the author's knowledge, there are currently no Au catalyzed processes for this reaction described in the literature.

4.2 Catalytic transformation of acetylene

After the discovery of the formal insertion of ethylene into the Au-O bond *trans* to tpy-*N* in complex **2**[90] (section 1.4, Chapter 1) a natural continuation was to investigate this reaction with acetylene. When bubbling acetylene through a mixture of complex **2** in CF$_3$COOD, an immediate reaction occurred. The reaction was monitored by ^{1}H NMR (Figure 20) and less than 5 minutes after the addition of acetylene, *ca*. 50% of **2** had reacted to form Au(III) vinyl complex **18** (Scheme 56, *vide infra*). In addition, signals of **17-*d*** appeared as two doublets at δ 7.18 and δ 5.19, mutually coupled with a *trans* $^3J_{HH}$ = 13.6 Hz, which indicates that an *anti* addition of CF$_3$COOD to acetylene has occurred. At this point, the yield of **17-*d*** (determined by NMR integration against an internal standard) was ca 20% based on the initial amount of **2**. Finally, traces of tpyD$_2$$^+$ and (1*E*,3*E*)-1,4-bis(trifluoroacetoxy)-1,3-butadiene (**19**) were observed (Scheme 56). After 30 minutes reaction time, all of **2** had reacted and complex **18** was the only tpy-containing Au species observed in solution. The yield of **17-*d*** had increased to 200%, based on the initial amount of **2**. Furthermore, the amounts of tpyD$_2$$^+$ and **19** had increased to *ca.* 40% and 50% of the quantity of **18**, respectively. The reaction was monitored for 24 hours, and at that point **17-*d*** (together with traces of **17**), the diene **19**, and tpyD$_2$$^+$ were the only species that could be detected by ^{1}H NMR and all of **18** had decomposed. At this point, tpyD$_2$$^+$ and **19** were formed in essentially quantitative yields and it will be seen later that these two species are decomposition products formed during the catalysis. A dark brown to black precipitate had also formed inside the NMR tube at this point, which is a clear sign of decomposition of the molecular gold complexes. The estimated turnover numbers for the formation of **17-*d***, based on integration of the NMR resonances of **17-*d*** against an internal standard in multiple experiments, were 13-15 per Au. A control experiment (See ESI, Paper III) established that no reaction occurred between acetylene and CF$_3$COOD in the absence of complex **2** or other Au sources during the time frame of these reactions, and it is clear that Au is needed in order for this transformation to occur.
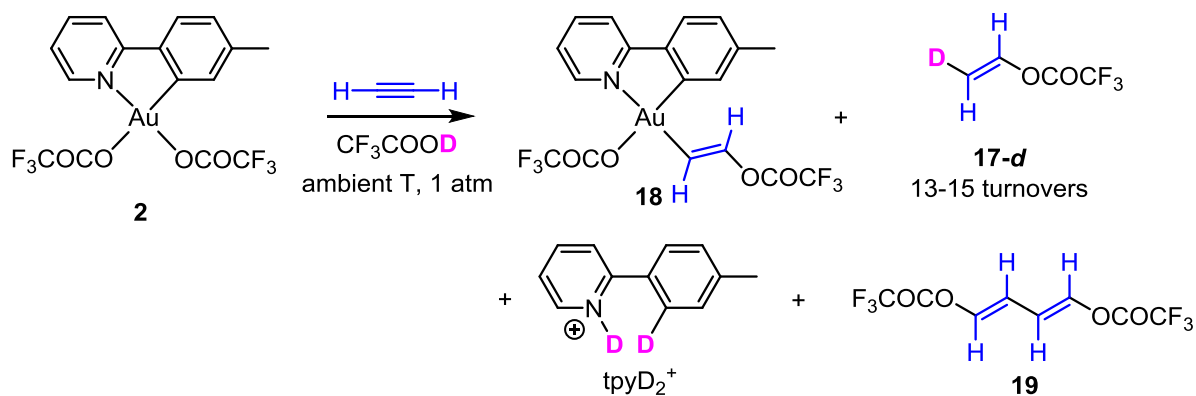
Scheme 56. Reaction between complex **2** and acetylene in CF$_3$COOD.
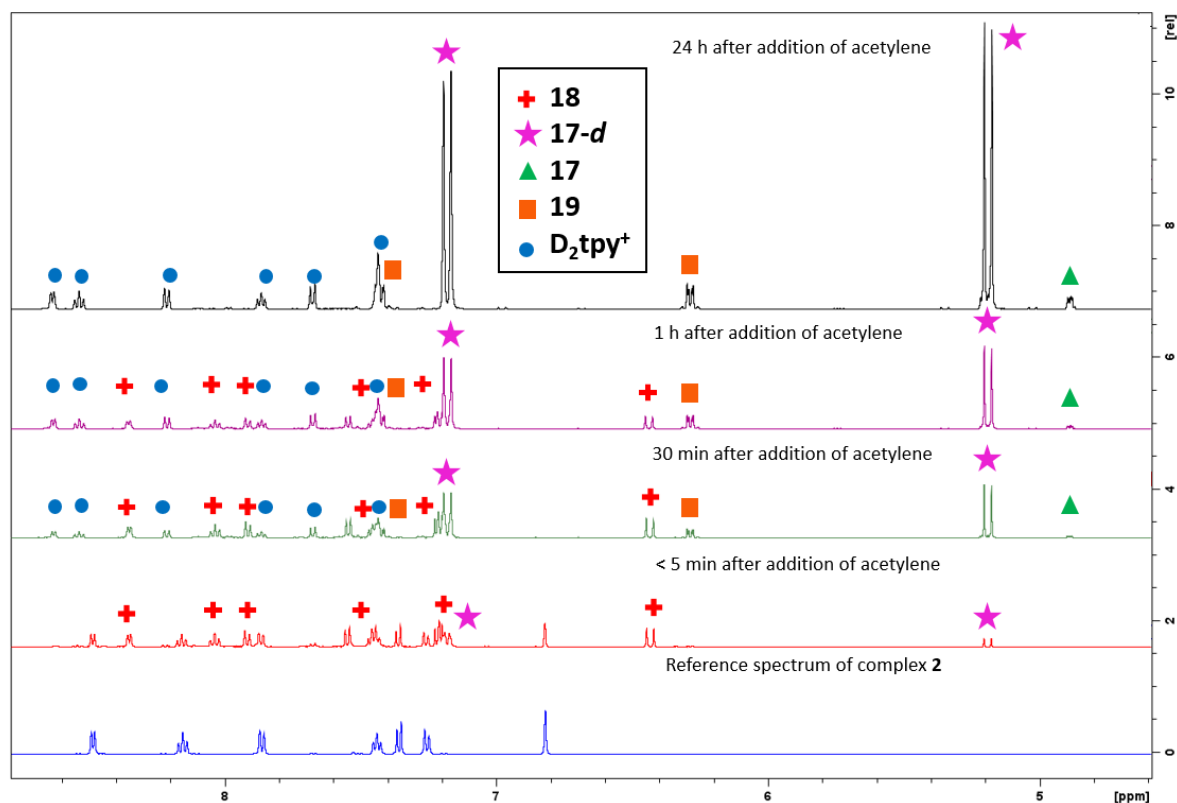
Figure 20. Stacked ^{1}H NMR (500 MHz, CF$_3$COOD) spectra of the catalytic transformation of acetylene into **17-d** in CF$_3$COOD, with **2** as precatalyst, showing the reaction development. Only the aromatic and the vinylic regions are shown.

The catalytic trifluoroacetoxylation of acetylene could also be performed in a mixture of CF$_3$COOH and CD$_2$Cl$_2$ (CD$_2$Cl$_2$:CF$_3$COOH, 6:1 (v:v)), leading to the formation of the same products as before, but without deuterium incorporation; **17** is formed instead of **17-d**, and tpyH$_2^+$ is formed instead of tpyD$_2^+$. The turnover numbers were 11-16 per Au, however, it was discovered that upon cooling the reaction mixture to *ca.* 0 $^\circ$C while bubbling through acetylene, the turnovers could be increased to 21-24. This may be due to the combination of different effects such as increased acetylene solubility and possibly slower rates of catalyst decomposition at lower temperature. The identity of **17** was confirmed in a ^{1}H NMR experiment, where a NMR sample was spiked with a commercial sample of **17** after the catalysis. The diene (**19**) has neither been isolated nor been previously described, but its identity is inferred from the ^{1}H NMR and ^{1}H-^{1}H COSY spectra of the reaction mixture after the catalysis. The ^{1}H NMR spectrum of **19** exhibit one well defined resonance with a complicated splitting pattern at δ 6.30 in CF$_3$COOD (δ 6.35 in CD$_2$Cl$_2$, see Figure 20 and ESI Paper III) which shows a COSY correlation to a resonance with the same appearance and intensity (although partly overlapping with signals from the tpy ligand) at *ca.* δ 7.4 (*ca.* 7.5 in CD$_2$Cl$_2$). The observed spectrum, especially the splitting pattern, strongly resembles that of the nonfluorinated analogue of **19**, (1*E*,3*E*)-1,4-diacetoxy-1,3-butadiene (See ESI, Paper III).

4.2.1 Synthesis and characterization of the acetylene insertion product 18

It was possible to isolate the acetylene insertion product **18** from the reaction mixture in 40-42 % yield upon reacting **2** with acetylene in CF_3COOH at 0 °C (Scheme 57, left). Complex **18** was characterized by NMR, MS, and X-ray diffraction analysis. The ^1H NMR spectrum of **18** is in full agreement with that observed in the catalysis experiments. The two characteristic doublets corresponding to the two vinylic protons are observed at *ca.* δ 7.2 (overlapping with tpy-*H*) and δ 6.43, mutually coupled with a *trans* $^3J_{HH}$ = 12.8 Hz, which indicates that the addition of $^-OCOCF_3$ has occurred in an *anti* fashion. In the ^{13}C NMR spectrum of **18**, two pairs of quartets are observed, corresponding to the carbons in the two $OCOCF_3$ groups. A ^1H-^1H NOESY experiment show that the insertion of acetylene has occurred *trans* to tpy-*N*; a NOE is observed between the vinylic proton α Au and H$^{6'}$. In the ^{19}F NMR spectrum of **18**, two resonances are observed at δ −77.1 and δ −77.5. A ^{19}F-^1H HOESY experiment established that the resonance at δ -77.1 arises from the $OCOCF_3$ ligand *trans* to tpy-*C*. Addition of *ca.* 1 equiv of CF_3COOH to the solution caused the signal at δ −77.1 to broaden, whereas the free CF_3COOH gave rise to a broadened resonance at δ −78.2 (See Paper III). This broadening suggest the kinetic availability of the coordination site *trans* to tpy-*C*, in agreement with that observed for complex **2** and **3**,[90] which provides an additional coordination site for incoming substrates. The availability of the coordination site *trans* to tpy-*C* was demonstrated in Chapter 3, where the preparation of metallacycle complexes **15** and **16** were described, utilizing both the coordination site *trans* to tpy-*N* and *trans* to tpy-*C*.
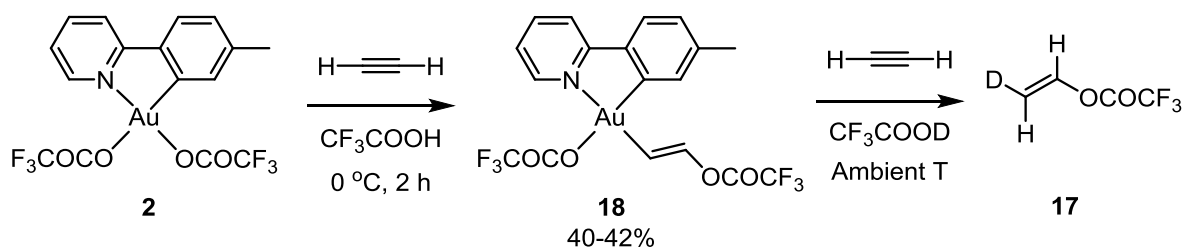
Scheme 57. Synthesis of Au(III) vinyl complex **18** (left) and catalytic trifluoroacetoxylation of acetylene at **18** (right).

The ORTEP plot of complex **18** is shown in Figure 21 and selected metrical parameters are given in Table 5. The crystallographic structure determination was performed by Dr. Sigurd Øien-Ødegaard. The crystal structure contains two molecules of **18** in the asymmetric unit and the metric parameters are given for the complex with the lower uncertainties in the bond lengths and angles. The crystal structure exhibits open channels that contains disordered solvent molecules. The molecular structure is in full agreement with that observed by NMR; the formal insertion of acetylene has occurred in the position *trans* to tpy-*N* and the resulting vinyl group has a *trans* (*E*) geometry. Complex **18** has the slightly distorted square planar geometry which is commonly observed for Au(III) complexes. The N1-Au1-C1 chelate angle deviates slightly from the idealized 90° to 82.7(5)°, in agreement with that observed for previously reported related complexes[89, 90] and the complexes described in Chapters 2

and 3. The Au-ligand distances Au-N1, Au-C1, and Au-O1 are within the range of that reported previously for related complexes,[89, 90] and the complexes described in this thesis. The Au-C(sp^2) bond (Au1-C2) of 2.027(13) Å is slightly shorter than the Au-C(sp^3) bond *trans* to tpy-*N* in the closely related complex **3**[90] (2.042(3) Å), but in the range of that reported for Au-C(sp^2) bonds in other structurally characterized Au(III) vinyl complexes (2.004(19)-2.083(9) Å).[44, 45, 48] The C2-C3 bond distance of 1.293(19) Å is quite close to the typical bond distance for 1,2-disubstituted double bonds (1.312(11) Å in average)[124] and is the shortest of those reported for other structurally characterized Au(III) vinyl complexes ranging from 1.311(3)-1.344(6) Å.[44, 45, 48]
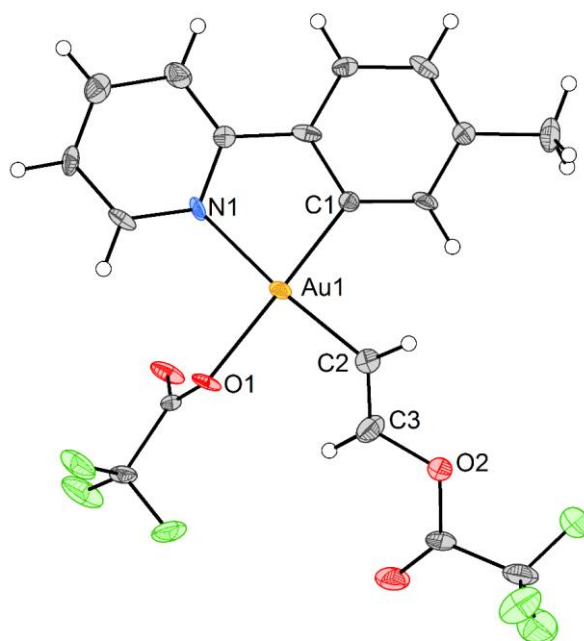
Figure 21. ORTEP plot of **18** with 50% ellipsoids. Disordered solvent molecules are omitted for clarity. The crystallographic structure determination was performed by Dr. Sigurd Øien-Ødegaard.

Table 5. Selected bond distances [Å] and angles [°] for **18**. The asymmetric unit consists of two complexes and the metrical parameters are given for the complex with the lower uncertainties in the bond distances and bond angles.

Bond distances [Å]		Angles [°]	
Au1-N1	2.070(11)	O1-Au1-N1	96.5(4)
Au1-C1	2.007(11)	N1-Au1-C1	82.7(5)
Au1-O1	2.110(8)	C1-Au1-C2	92.2(5)
Au1-C2	2.027(13)	C2-Au1-O1	88.6(5)
C2-C3	1.293(19)	C1-Au1-O1	179.0(4)
C3-O2	1.450(18)	N1-Au1-C2	173.2(5)
		Au1-C2-C3	123.2(11)
		C2-C3-O2	115.3(14)
		Au1-C2-C3-O2	175.7(9)

Au(III) vinyl complex **18** appears to be a plausible intermediate in the catalytic cycle, as protolytic cleavage of the Au-vinyl bond would release **17** and regenerate complex **2**, as depicted in the simple,

putative catalytic cycle in Scheme 58. Surprisingly, it was found that complex **18** was stable in CF$_3$COOD. Even after several days in CF$_3$COOD at ambient temperature, no hint of **17-*d*** nor any formation of complex **2** was observed upon ^{1}H NMR monitoring, indicating that the protolytic cleavage of the Au-vinyl bond does not occur under these conditions. This experiment therefore appears to rule out the simple mechanism depicted in Scheme 58. However, when acetylene is added to the mixture of **18** in CF$_3$COOD, catalysis occurred (11-12 turnovers per Au, Scheme 57, right). The reaction depicted in Scheme 57 (right) was monitored by ^{1}H NMR and no formation of complex **2** (or any other intermediates) could be observed. If a protolytic cleavage of the Au-vinyl bond *trans* to tpy-*N* would occur, complex **2** is expected to be observed by ^{1}H NMR.
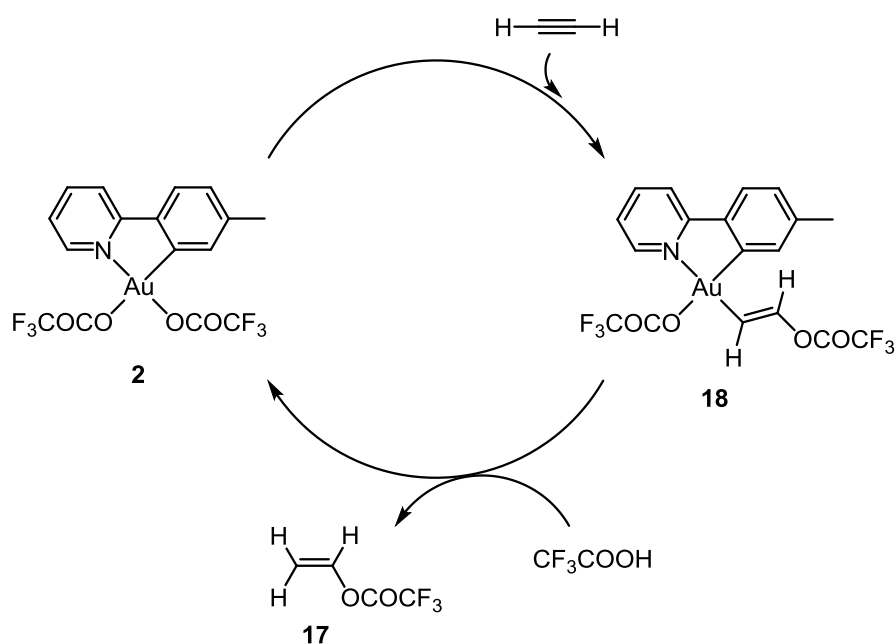
Scheme 58. Initially considered putative catalytic cycle for the trifluoroacetoxylation of acetylene.

4.2.2 Synthesis and characterization of a Au(III) C-bonded enolate complex and its involvement in the catalysis

Based on the results presented in Chapter 2, we were interested in whether the product of the catalysis (**17**) would react with the precatalyst **2**. Upon stirring complex **2** and **17** in CF$_3$COOH at ambient temperature for 6 days, the Au(III) C-bonded enolate complex **20** was formed (Scheme 59). The mechanism of formation of complex **20** has not been investigated, but one hypothesis is that it is formed *via* **20'** (Scheme 59) which would be the expected product of a nucleophilic addition of $^-$OCOCF$_3$ to vinyl trifluoroacetate at **2**, based on the previous findings described in Chapter 2. The net elimination of trifluoroacetic anhydride from **20'** will then furnish complex **20**. Upon monitoring the reaction forming complex **20** from complex **2** by ^{1}H NMR, no intermediates could be observed.
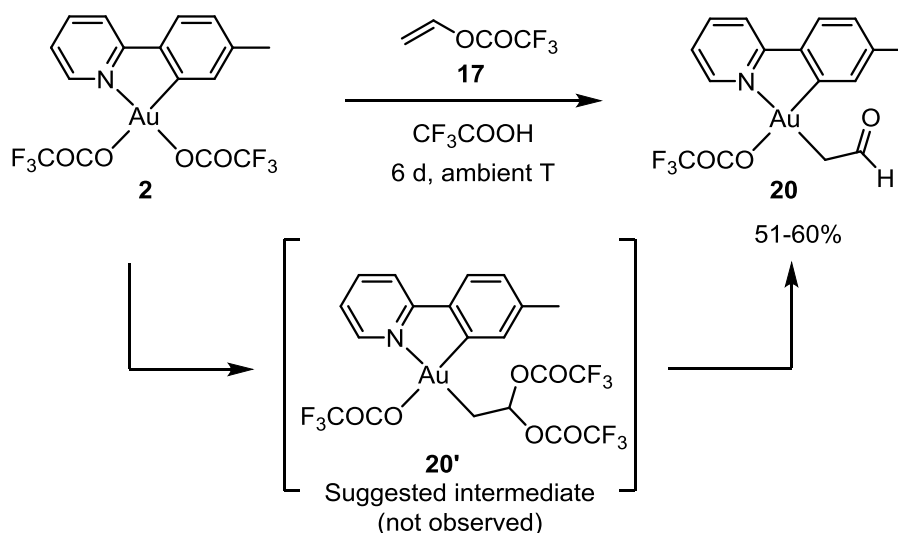
Scheme 59. Synthesis of the C-bonded Au(III) enolate complex **20**.

Complex **20** was characterized by NMR, MS, X-ray diffraction analysis, and elemental analysis. The ^{1}H NMR spectrum of **20** exhibits some characteristic resonances; at δ 9.92 the resonance of the formyl proton is found as a triplet ($^3J_{HH}$= 4.6 Hz) and at δ 3.14 the two methylene protons are found as a doublet ($^3J_{HH}$ = 4.6 Hz). In the ^{19}F NMR spectrum of **20**, one single resonance is observed at δ −77.1 corresponding to the OCOCF$_3$ ligand *trans* to tpy-*C*, which is the same ppm value as that of the OCOCF$_3$ ligand *trans* to tpy-*C* in **18** and similar to that observed for complexes **2**[89] and **3**.[90] Furthermore, one pair of quartets corresponding to the carbons of the OCOCF$_3$ ligand is observed in the ^{13}C NMR spectrum of **20** and the resonance of the carbonyl carbon is found at δ 200.2. When dissolving complex **20** in CF$_3$COOD, ^{1}H NMR analysis revealed that **20** undergoes H/D exchange with the deuterated solvent to form **20-d_2** (Scheme 60), presumably by a keto/enol tautomerization. This was evident by ^{1}H NMR, as an exchange of the methylene protons with deuterium led to a decrease of the signal intensity of the corresponding ^{1}H NMR resonance with concomitant apparent loss of coupling and the conversion of the triplet of the formyl proton into a singlet (See ESI, Paper III). The approximate half-life of this process was found to be 25 min by ^{1}H NMR integration.
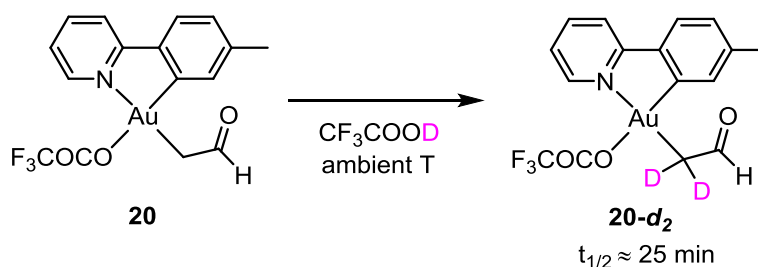
Scheme 60. H/D exchange in complex **20**.

The ORTEP plot of complex **20** is shown in Figure 22 and metrical parameters are given in Table 6. The structure based on the X-ray diffraction analysis of **20** is in full agreement with that observed by NMR;

the presence of the C-bonded enolate *trans* to tpy-*N* is evident. Two other closely related Au(III) acetonate complexes have been reported previously by Fan and co-workers: (ppy)Au(X)(CH$_2$COMe) (X = Cl or NO$_3$, with CH$_2$COMe *trans* to ppy-*N*).[80] Complex **20** exhibits the slightly distorted square planar geometry which is commonly observed for Au(III) complexes, with the five membered ring chelate angle N1-Au1-C1 deviating slightly from the idealized 90° to 81.69(9)°, similarly to the other complexes described in this thesis and previously reported related complexes.[89, 90] The Au-ligand bond distances Au1-N1, Au1-C1, and Au-O1 are also similar to that reported for other related complexes.[89, 90] The Au-C(sp^3) bond distance, Au1-C2 (2.069(2) Å), is quite similar to that found for the related Au(III) acetonate complexes (2.067(7) Å for X = Cl and 2.059(5) Å for X = NO$_3$).[80] The C2-C3 bond of 1.468(3) Å and the C3-O2 double bond of 1.212(3) Å are quite close to the corresponding distances in aldehydes (1.510(8) Å and 1.192(5) Å, respectively).[124]
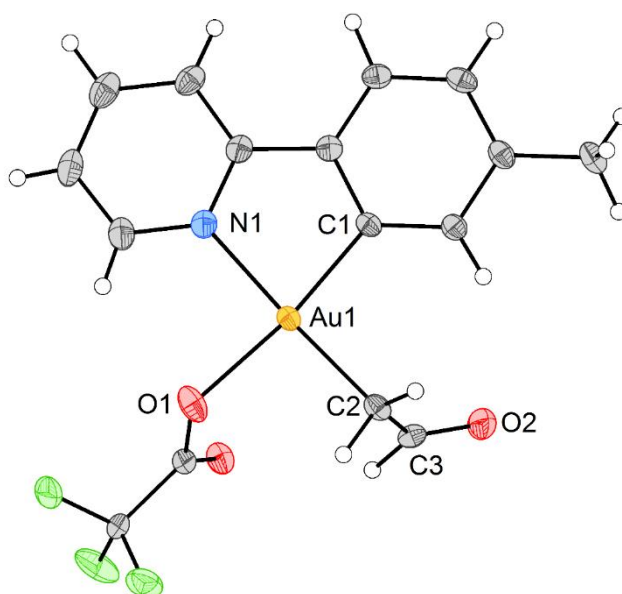
Figure 22. ORTEP plot of complex **20** with 50% ellipsoids. The OCOCF$_3$ ligand is disordered (not shown).

Table 6. Selected bond distances [Å] and angles [°] for **20**.

Bond distances [Å]		Angles [°]	
Au1-N1	2.090(2)	O1-Au1-N1	91.19(8)
Au1-C1	2.006(2)	N1-Au1-C1	81.69(9)
Au1-O1	2.1016(17)	C1-Au1-C2	95.22(9)
Au1-C2	2.069(2)	C2-Au1-O1	91.90(8)
C2-C3	1.468(3)	C1-Au1-O1	171.73(8)
C3-O2	1.212(3)	N1-Au1-C2	176.91(8)
		Au1-C2-C3	108.68(16)
		C2-C3-O2	125.8(2)
		Au1-C2-C3-O2	111.9(2)

Complex **20** could also be formed by treating **18** with water in the presence of CF$_3$COOH. This reaction has only been performed as a NMR experiment, and therefore no yield is reported (Scheme 61, for

details, see ESI, Paper III). The possibility of forming small amounts of complex **20** during the catalytic reactions, either by hydrolysis of complex **18** (in the presence of CF₃COOH) or upon reaction of complex **2** with **17**, could potentially be a problem for the catalysis. However, it was found that complex **20** could also act as a catalyst for the trifluoroacetoxylation of acetylene, so formation of traces of **20** during the catalysis should not be any problem. Performing the acetylene trifluoroacetoxylation reaction with complex **20** as precatalyst in CF₃COOD, led to 7 turnovers of **17-*d***, which is a bit lower than that obtained with complexes **2** and **18** (Scheme 61). During the reaction, substantial decomposition to form several unidentified compounds occurred.
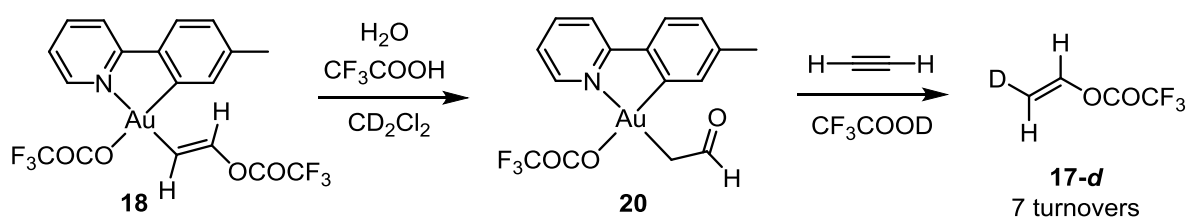
Scheme 61. Hydrolysis of complex **18** leading to complex **20** (left) and the performance of complex **20** in the catalytic trifluoroacetoxylation of acetylene (right). Both experiments were performed at ambient T.

4.2.3 Catalysis *trans* to tpy-*C*

The finding that complex **18** is stable in CF₃COOD over several days led us to think that the actual catalysis might happen in the position *trans* to tpy-*C*, and not *trans* to tpy-*N*, as was first suggested. This is in agreement with the finding that **20** (with CH₂CHO *trans* to tpy-*N*), in addition to **2** and **18** (with CH=CHOCOCF₃ *trans* to tpy-*N*), could catalyze the acetylene trifluoroacetoxylation, since all these complexes have an available coordination site *trans* to tpy-*C*. This was further demonstrated in an experiment where Au(NTf₂)(Me)(tpy) was generated *in situ* from the previously reported AuBrMe(tpy)[89] (with Me *trans* to tpy-*N*) and AgNTf₂ and found to cause the formation of **17** from acetylene and CF₃COOH (although only *ca*. 1 turnover was obtained). No detectable intermediates could be observed, however, several other unidentified products were obtained. Based on these findings, a modified reaction mechanism was postulated. As can be seen in Scheme 62, a double insertion mechanism is now suggested and this mechanism seems to be in agreement with all the experimental results obtained so far. Here, the first insertion *trans* to tpy-*N* generates the isolated Au(III) vinyl complex **18** (step a) which does not undergo protolytic cleavage (step b), in agreement with the experimental findings. Instead, a second insertion occurs (step c), this time *trans* to tpy-*C*, to give the unobserved divinyl complex **21**. Finally, protolytic cleavage of the Au-vinyl bond *trans* to tpy-*C* in **21** releases the product **17** with concomitant regeneration of catalytically active **18** (step d). Thus, the operating catalytic cycle involves complexes **18** and **21**, whereas complex **2** is just a precatalyst. The unobserved divinyl complex **21** is in good agreement with the formation of the diene **19**, which could be formed from **21** by reductive elimination.

70
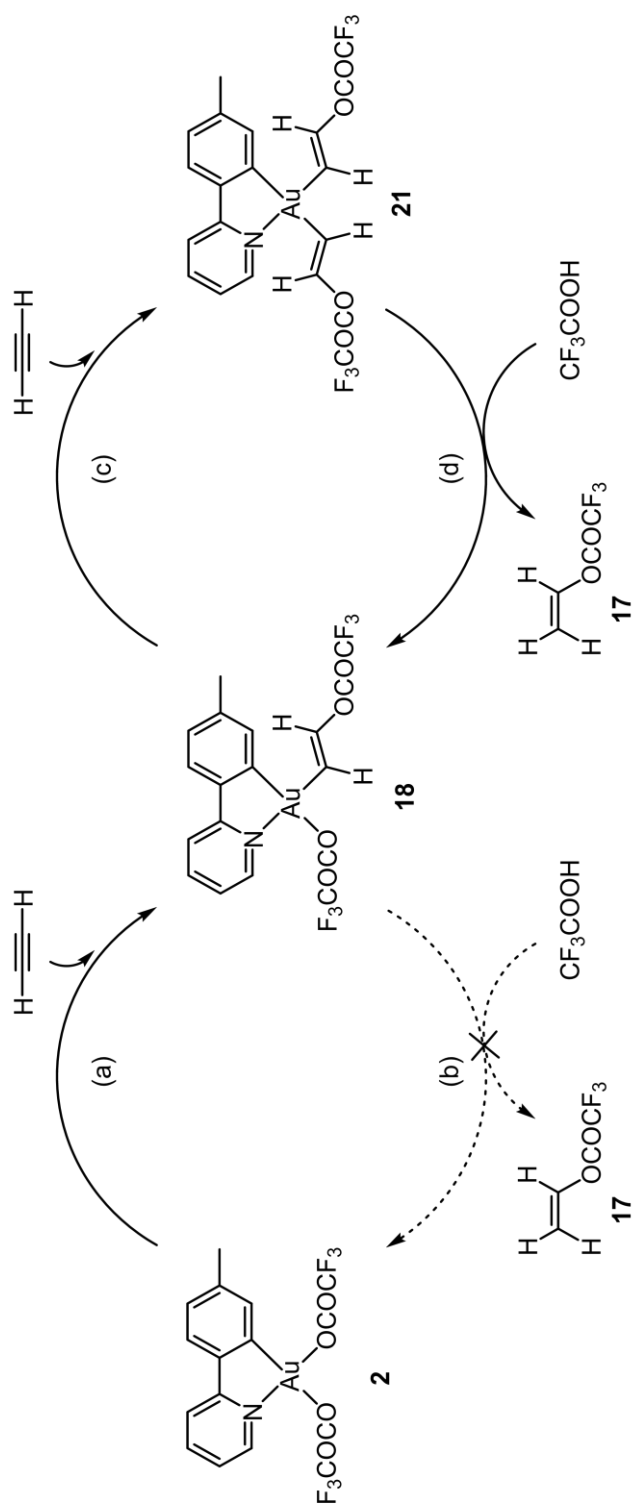
Scheme 62. Postulated double insertion mechanism for the trifluoroacetoxylation of acetylene catalyzed by **18**, with **2** as a precatalyst.

Two deuterium labelling experiments (Scheme 63) were designed to further support the suggested catalytic cycle shown in Scheme 62. If the double insertion mechanism in Scheme 62 operates, then the reaction of **18** with acetylene-d_2 and CF$_3$COOH would lead to the formation of vinyltrifluoroacetate-d_2 ((Z)CHD=CD(OCOCF$_3$), **17-d_2**) from catalysis *trans* to tpy-*C* during all catalytic cycles, including the first cycle. In contrast, catalysis *trans* to tpy-*N* would give non-deuterated **17** during the first cycle, and then **17-d_2** in the following cycles. Acetylene-d_2 was generated from CaC$_2$ and D$_2$O and then bubbled through a NMR tube containing complex **18** and CF$_3$COOH in CD$_2$Cl$_2$. Monitoring the reaction by ^{1}H NMR revealed that **17-d_2** was formed as the predominant product during the first turnover, as was inferred by the appearance of one broad resonance at δ 4.96 for the proton *trans* to OCOCF$_3$ in **17-d_2** (Scheme 63, top). There was no indication of **17** which would arise from protolytic cleavage of the Au-vinyl bond *trans* to tpy-*N* during the first and most diagnostic turnover. However, after the first turnover and later in the catalysis, resonances corresponding to acetylene-d_0 and acetylene-d_1 slowly appeared. At the same time, resonances of **17** and **17-d_1** appeared in the ^{1}H NMR spectrum, presumably due to H/D exchange on acetylene in solution or π-bonded at Au. The findings from this labelling experiment supports the mechanism depicted in Scheme 62 where the active site of the catalysis is *trans* to tpy-*C*, but the occurrence of some residual reactivity *trans* to tpy-*N* cannot be excluded completely. Because of the complications of the (presumably Au-promoted) H/D exchange on acetylene a complementary experiment which circumvents this problem was designed (Scheme 63, bottom). When complex **18-d_2** (prepared from **2** and acetylene-d_2 in CF$_3$COOH, see ESI, Paper III) was reacted with acetylene and CF$_3$COOH in CD$_2$Cl$_2$, no evidence of formation of unlabeled **18** was observed by ^{1}H NMR, neither during the first turnover nor later during the reaction. This indicates that the trifluoroacetoxylation of acetylene is occurring *trans* to tpy-*C*, while the vinyl group *trans* to tpy-*N* remains intact. Protolytic cleavage of the Au-vinyl bond *trans* to tpy-*N* in **18-d_2** would furnish **2** which then would undergo insertion of non-labelled acetylene *trans* to tpy-*N* to form **18**. Furthermore, signals arising from **19** could also be observed in the ^{1}H NMR spectrum of this reaction at δ 6.35 and *ca.* δ 7.5. But in this case, the splitting patterns were simplified compared to that observed previously; the resonance of the proton *β* to OCOCF$_3$ in **19** now resembles a doublet of triplets with a *trans* $^3J_{HH}$ coupling of 12.2 Hz and a $^3J_{HD}$ coupling of 1.4 Hz. The resonance of the proton *α* to OCOCF$_3$ (which is partly overlapping with the protons from the tpy-ligand) resembles a doublet (See ESI, Paper III). This suggest that **19-d_2** has been formed *via* reductive elimination of one vinyl-d_2 group *trans* to tpy-*N* and one vinyl-d_0 group *trans* to tpy-*C*.

The finding that the complexes **2**, **18**, **20**, and Au(Me)(NTf$_2$)(tpy) all catalyze the trifluoroacetoxylation of acetylene can now readily be explained; catalysis proceeds *via* coordination of acetylene *trans* to tpy-*C*, followed by nucleophilic attack by $^-$OCOCF$_3$ and then protolytic cleavage of the Au-vinyl bond

trans to tpy-*C* releases the product **17**. Because of the considerably higher *trans* influence of the tpy-*C* than tpy-*N*, the Au-vinyl bond *trans* to tpy-*C* in **21** should be more prone to protolytic cleavage than the one *trans* to tpy-*N*. These effects will be further discussed in section 4.2.4.
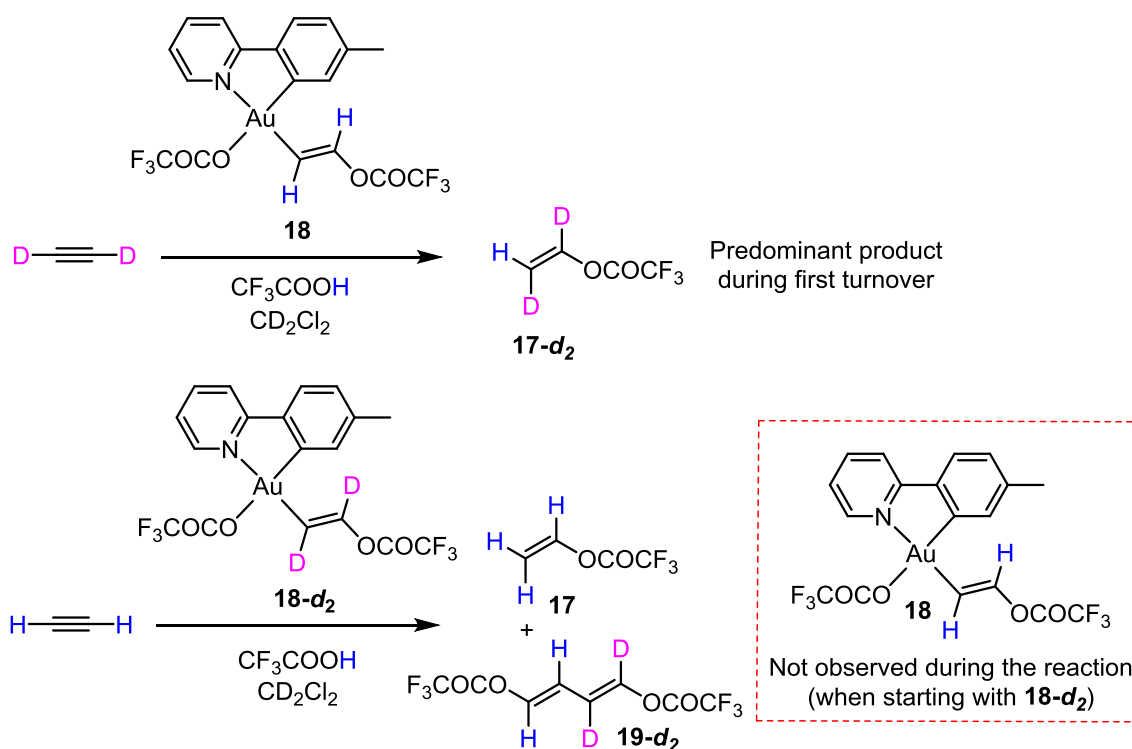
Scheme 63. Deuterium labeling experiments supporting the hypothesis that the catalysis occurs *trans* to tpy-*C*. Both experiments were performed at ambient T.

4.2.4. DFT calculations on the reaction mechanism and decomposition pathway

The mechanism of the trifluoroacetoxylation of acetylene was also investigated by DFT calculations. The DFT calculations were performed by Dr. Ainara Nova and Dr. David Balcells (University of Oslo). The mechanism of the ethylene insertion reported previously[90] laid the foundation for the DFT calculation on the acetylene system, and the same mechanism was considered; first associative substitution of $OCOCF_3$ with acetylene followed by intermolecular (*anti*) nucleophilic addition of $^-OCOCF_3$ to the coordinated acetylene. Both the reaction *trans* to tpy-*N* and *trans* to tpy-*C* were investigated computationally using **2** as the energy base level. The first step of the reaction, the nucleophilic addition, has a rather similar energy profile both *trans* to tpy-*N* and *trans* to tpy-*C*, with energies for **22** and **22c** of *ca.* 18 kcal mol^{-1} (Scheme 64). The nucleophilic addition step is however both kinetically and thermodynamically preferred *trans* to tpy-*N*, which is in agreement with the experimental findings where the formal insertion of acetylene *trans* to tpy-*N* in complex **2**, forming complex **18**, was observed during the catalysis. The reaction is clearly irreversible as can be seen from the reverse energy barrier which is >40 kcal mol^{-1}, in contrast to the ethylene insertion (see Chapter 1) where the nucleophilic addition of $^-OCOCF_3$ to ethylene at complex **2** was found to be reversible.[90]
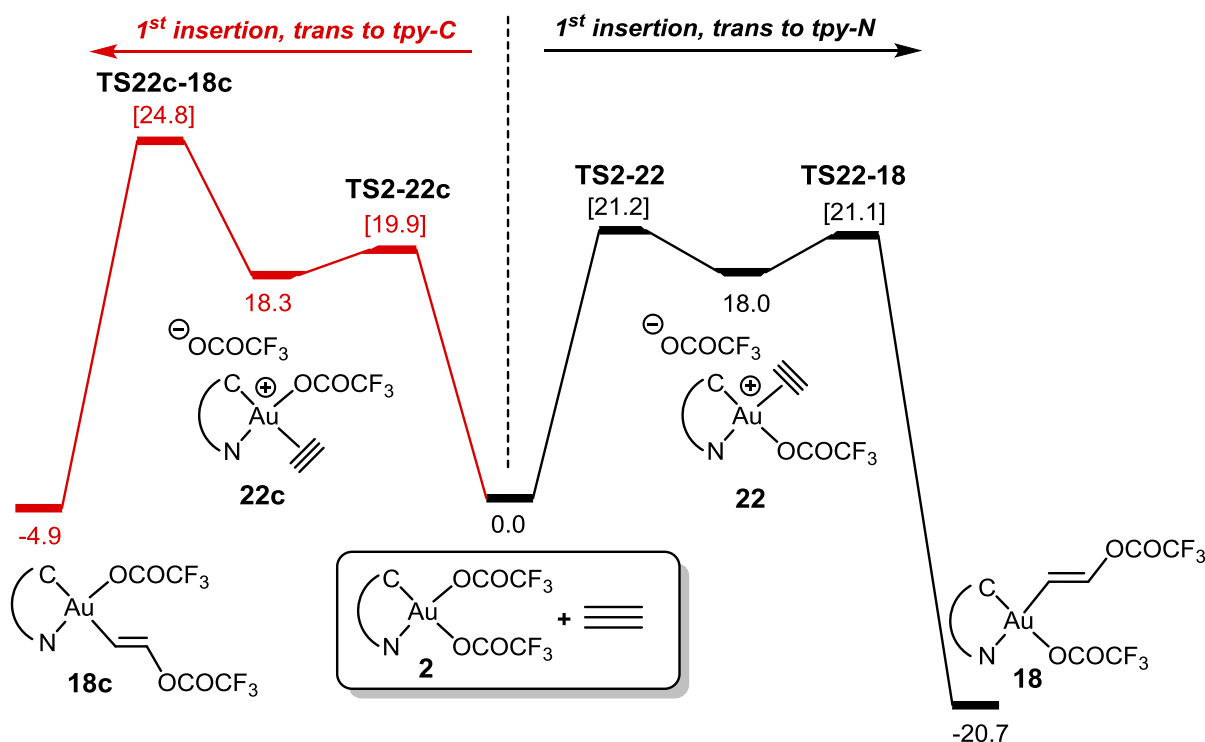
Scheme 64. Free energy profile in kcal mol^{-1} for the first insertion of acetylene *trans* to tpy-*C* (left, red) and *trans* to tpy-*N* (right, black). The energies of all minima and transition states in [brackets] are computed in CF$_3$COOH. Computational details and transition state geometries can be found in Paper III. DFT calculations by Dr. Ainara Nova and Dr. David Balcells.

As mentioned previously, complex **18** did not undergo protolytic cleavage of the Au-vinyl bond in CF$_3$COOH. Therefore, it was suggested that instead a second insertion of acetylene *trans* to tpy-*C* could occur to form **21**, and then the Au-vinyl bond *trans* to tpy-*C* can undergo protolytic cleavage to form **17** and regenerate complex **18**. These steps were investigated by DFT calculations with **18** as the energy base level. As can be seen from Scheme 65, the protolytic cleavage of the Au-vinyl group *trans* to tpy-*N* has a free energy barrier of 24.8 kcal mol^{-1} (**TS18-23**). Even though this reaction barrier seems surpassable, it appears to be too high for a reaction that occur readily at ambient temperature. The second insertion of acetylene *trans* to tpy-*C* has a slightly lower free energy barrier of 22.7 kcal mol^{-1}. This free energy barrier is 2.1 kcal mol^{-1} lower than that found for the same process at **2**, where the position *trans* to tpy-*N* is occupied by an OCOCF$_3$ ligand. This energy difference, combined with that the site *trans* to tpy-*N* is blocked (at least towards reactivity through the coordination/nucleophilic attack pathway) allows the second insertion, this time *trans* to tpy-*C*, to occur giving divinyl complex **21**. The free energy barrier for the protolytic cleavage of the Au-vinyl bond *trans* to tpy-*C* has a rather low free energy barrier (14.3 kcal mol^{-1}), which is in agreement with that **21** could not be observed during the catalysis. The protolytic cleavage leads to the formation of **25**. From **25**, substitution of coordinated **17** by $^-$OCOCF$_3$ promotes the forward, strongly exergonic reaction regenerating the active catalyst **18** ($\Delta G = -19.7$ kcal mol^{-1}, not shown in Scheme 65, see ESI, Paper III).

2nd insertion trans to tpy-C + protolytic cleavage trans to tpy-C

Protolytic cleavage trans to tpy-N

Protolytic cleavage of Au-C(tpy)

TS18-23 [24.8]

TS18-24 [19.3]

17.5

24

TS24-21 [22.7]

17.1

23

2 + **17**

-1.5

0.0

18 + CF₃COOH

-6.2

21

TS21-25 [8.1]

-2.4

25

TS21-26 [9.9]

5.7

26
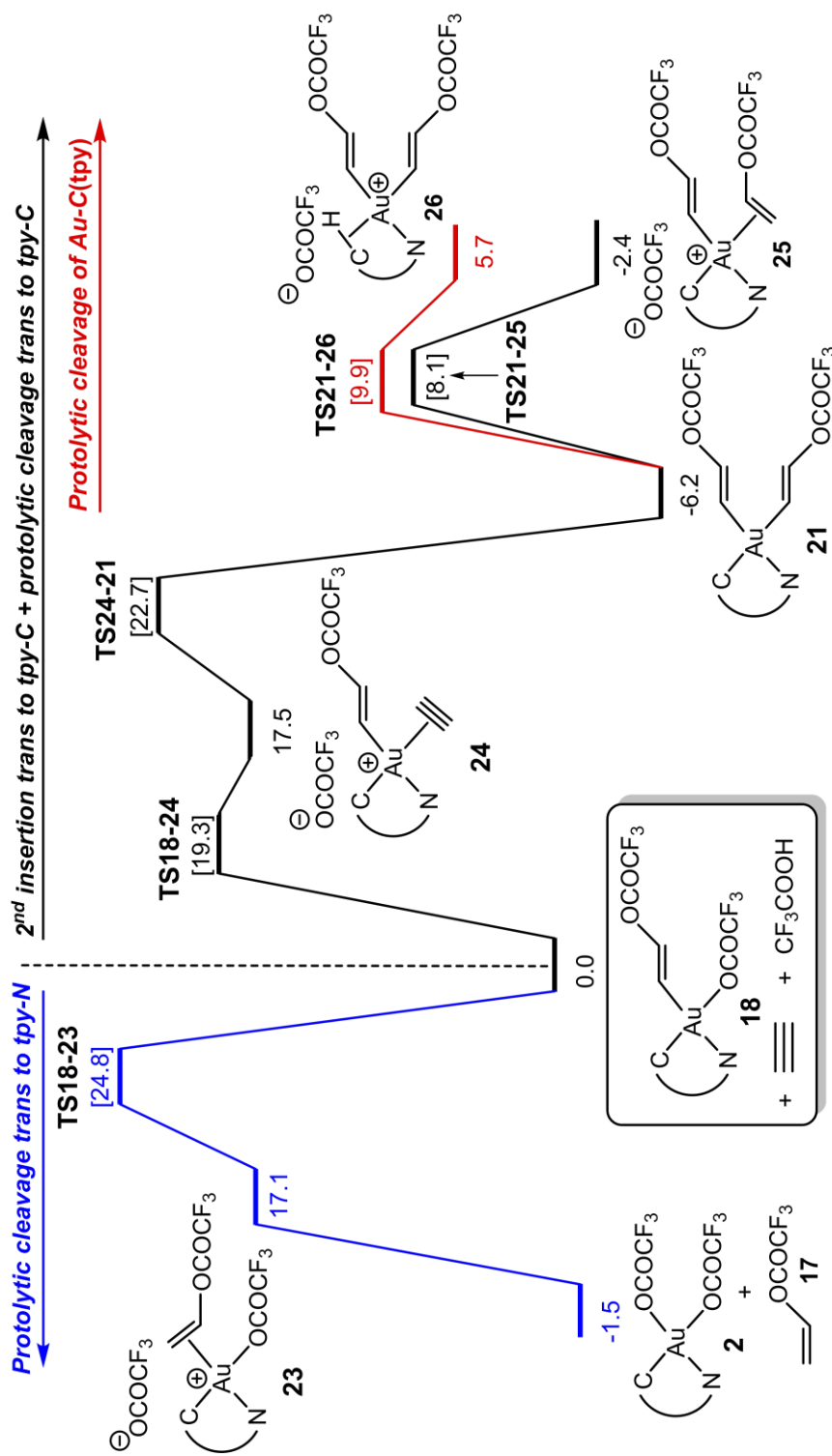
Scheme 65. Free energy profile in kcal mol⁻¹ for the protolytic cleavage of the Au-vinyl bond *trans* to tpy-C in **18** (left, blue), the insertion of acetylene into the Au-O bond *trans* to tpy-C in **18** (right, black), and protolytic cleavage of Au-C(tpy) (right, red) in **21**. The energies of all minima and transition states in [brackets] are computed in CF₃COOH. Computational details and transition state geometries can be found in Paper III. To maintain mass balance, the energies of additional CF₃COOH and/or acetylene have been included in the calculation where needed. The DFT calculations were performed by Dr. Ainara Nova and Dr. David Balcells.

The more facile protolytic cleavage of the Au-vinyl bond *trans* to tpy-*C* (**TS21-25**; $\Delta G^{\ddagger} = 14.3$ kcal mol^{-1}) than that *trans* to tpy-*N* in **21** ($\Delta G^{\ddagger} = 26.8$ kcal mol^{-1}, not shown in Scheme 65, see ESI, Paper III) can be explained by the larger *trans* effect of the aryl-*C* part of the chelate compared to the pyridine-*N* part. In agreement with this, the Au-C(tpy) bond in **21** is also prone to protolytic cleavage, as it is *trans* to the high *trans* influence vinyl-*C* ligand. The free energy barrier for this protolytic cleavage is 16.1 kcal mol^{-1} (**TS21-26**, Scheme 65) which is just 1.8 kcal mol^{-1} higher than the protolytic cleavage of the Au-vinyl bond *trans* to tpy-*C* (**TS21-25**; $\Delta G^{\ddagger} = 14.3$ kcal mol^{-1},) releasing the product of the catalysis (**17**). This difference in free energy, although quite small, for the two transition states explains why catalysis can occur; protolytic cleavage of the Au-vinyl bond *trans* to tpy-*C* to yield **17** is preferred over catalyst decomposition. However, the small difference in the free energy barrier for these two processes explain why decomposition occurs with this system. Protolytic cleavage of the Au-C(tpy) bond will lead to the tricoordinated Au(III) species **21H** (Scheme 66) which is assumed to undergo further decomposition. Previous findings in the Tilset research group demonstrates that AuMe$_2$(tpy) undergoes selective protolytic cleavage of the Au-C(tpy) bond at -78 $^{\circ}$C followed by reductive elimination of ethane from the resulting putative 3-coordinated species (protolytic cleavage of the Au-Me bonds was not observed at all).[38] If complex **21** behaves analogously, the tricoordinated **21H** will undergo reductive elimination to give the diene **19**, followed by complete decomposition furnishing tpyH$_2$$^+$ and Au(s) (the mode of eventual Au(s) formation from Au(I) is unknown, but a dark brown to black precipitate forms during the course of the reaction, see Scheme 66).
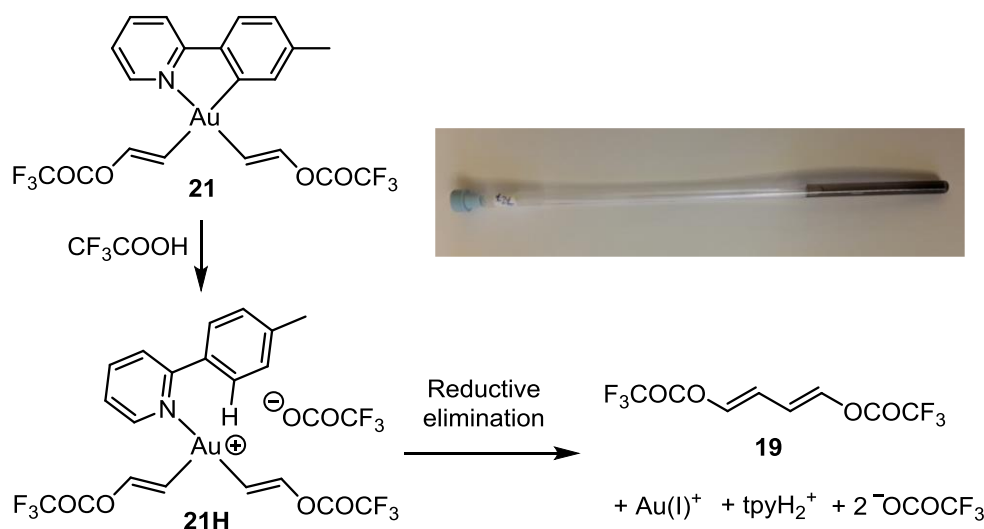
Scheme 66. Left and bottom: Suggested decomposition pathway from **21** *via* **21H** leading to the diene **19**. Top right: photography of the NMR tube after 24 hours of catalysis, visually demonstrating the decomposition.

Overall, the computational results are in full agreement with the proposed catalytic cycle shown in Scheme 62. The formal insertion of acetylene *trans* to tpy-*N* in **2** should be regarded as an activation

of the precatalyst and then the catalytic trifluoroacetoxylation takes place *trans* to tpy-*C* in the activated catalyst **18**.

4.2.5 Involvement of the Au particles in the catalysis

Decomposition occurred during the course of the catalysis to form dark brown to black Au particles (See Scheme 66). Work presented in this chapter (for example; the deuterium labelling experiments, the observation of the vinyl complex **18**, and the decomposition product **19**), clearly shows that this catalysis is a homogenous process where the catalysis is happening at molecular Au(III) complexes in agreement with the mechanism in Scheme 62. However, it cannot be completely ruled out whether there is some catalytic contribution from the Au particles formed because of decomposition during the catalysis. It is especially important to check for this since there are several heterogeneous processes where Au is used to activate alkynes towards nucleophilic addition, such as the acetylene hydrochlorination process developed by Hutchings and co-workers.[52, 56, 125] The Au particles originating from the catalyst decomposition were isolated and their reactivity was investigated under the same conditions as the homogenous system described in this chapter (see ESI, Paper III for details). The Au particles did indeed show some activity and small amounts of vinyl trifluoroacetate were formed. The results were compared with the outcome of the homogenous system and it was found that the Au particles may be responsible for 4-13% of the total production of **17**.

4.2.6 Computational study on acetylene *vs.* ethylene

To gain further insight into why the reaction of complex **2** with acetylene in CF_3COOH is catalytic, while the same reaction with ethylene is not, the thermodynamics of the three fundamental steps in the catalytic cycle, ligand substitution, nucleophilic attack and protolytic cleavage (steps a-c in Scheme 67) were computed and compared for both ethylene and acetylene (Table 7). The DFT calculations were performed by Dr. Ainara Nova and Dr. David Balcells (University of Oslo). The substitution of $OCOCF_3$ with acetylene and ethylene (step a) shows only small variations in free energy changes for the two substrates, both in the position *trans* to tpy-*N* and the position *trans* to tpy-*C*. In contrast to this, the nucleophilic addition (step b) at both acetylene and ethylene *trans* to tpy-*N* is more favorable than *trans* to tpy-*C* (by *ca.* 16 kcal mol^{-1}). Furthermore, the nucleophilic addition to coordinated acetylene is favored over addition to coordinated ethylene by *ca.* 16 kcal mol^{-1} for both the reactions *trans* to tpy-*N* and *trans* to tpy-*C*. The thermodynamic preference for nucleophilic addition to acetylene over ethylene can be explained by the fact that there is a lower energy penalty associated with breaking one π-bond component in a triple bond, compared to breaking the π-bond in a double bond, and by the fact that nucleophilic addition to acetylene generates a stronger Au-C(*sp^2*) bond than the Au-C(*sp^3*) bond resulting from nucleophilic addition to ethylene.[30, 76] These energy differences have consequences for the insertion reactions (steps a+b, Scheme 67). A reversible insertion reaction of

ethylene is predicted and observed *trans* to tpy-*N*,[90] whereas with acetylene an irreversible insertion occurs *trans* to tpy-*N*. The insertion *trans* to tpy-*C* (step a+b, Scheme 67) is endergonic for ethylene but exergonic for acetylene. The protolytic cleavage (step c, Scheme 67) is thermodynamically preferred *trans* to tpy-*C* by *ca.* 17 kcal mol^{-1} for both ethylene and acetylene, and is exergonic in all cases. Changing the ligands X in Scheme 67 and Table 7 from OCOCF$_3$ to CH=CHOCOCF$_3$ and CH$_2$CH$_2$OCOCF$_3$ lead only to small changes in the thermodynamics.
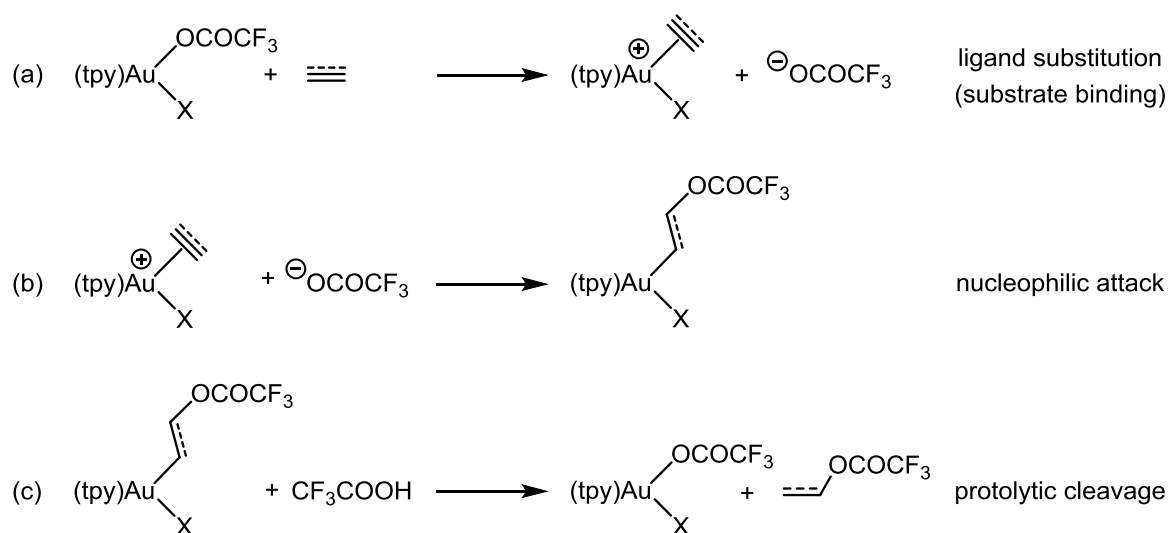
Scheme 67. The three fundamental reaction steps (a-c) for the (catalytic) trifluoroacetoxylation of acetylene and ethylene.

Table 7. Calculated free energy changes (kcal mol^{-1}) for reactions a-c in Scheme 67. These values have been computed by using the same methodology and without considering ion-pairs to facilitate comparison (see ESI, Paper III). Therefore the data may differ slightly from those in section 4.2.4 and the previously published work on ethylene.[90]

-X	Reaction	Acetylene		Ethylene	
		trans to tpy-*C*	*trans* to tpy-*N*	*trans* to tpy-*C*	*trans* to tpy-*N*
-OCOCF$_3$	(a)	24.5	23.7	23.6	22.4
	(b)	−29.4	−44.4	−12.5	−29.4
	(c)	−17.3	−1.5	−22.1	−4.0
-CH=CHOCOCF$_3$	(a)	22.0	21.8		
	(b)	−28.3	−43.9		
	(c)	−15.9	−0.1		
-CH$_2$CH$_2$OCOCF$_3$	(a)			21.3	17.0
	(b)			−11.7	−25.6
	(c)			−20.6	−2.5

As discussed previously, a simple catalytic cycle for acetylene where ligand substitution and nucleophilic addition *trans* to tpy-*N* is followed by a protolytic cleavage of the Au-vinyl bond will not occur. With ethylene, however, the insertion *trans* to tpy-*N* (previously shown to be reversible[90]) is most favorable, but after reversal the less favorable insertion *trans* to tpy-*C* could in principle occur to furnish **18c-alk** (See Scheme 68), provided that the following protolytic cleavage of the Au-C(sp^3) bond could help in driving this reaction forward. However, the free energy barrier for the protolytic cleavage

of the Au-C(sp^3) bond in **18c-alk** was found to be 23.7 kcal mol^{-1} (Scheme 68, top) which is too high since the formation of **18c-alk** from **2** is already endergonic by 11.1 kcal mol^{-1} (= ΔG^a+ ΔG^b, see Table **7**, entries for ethylene, X = OCOCF$_3$, *trans* to tpy-*C*). When the free energy barrier for the protolytic cleavage of the Au-vinyl bond in **18c** was calculated, it was found to be significantly lower ($\Delta G^{\ddagger}$ = 14.5 kcal mol^{-1}, Scheme 68, bottom), indicating that there is a kinetic preference for cleaving the Au-C(sp^2) bond in **18c** over the Au-C(sp^3) bond in **18c-alk** ($\Delta\Delta G^{\ddagger}$=9.2 kcal mol^{-1}). This is in agreement with previous findings made in the Tilset group, for example in the previously mentioned AuMe$_2$(tpy) where a selective protolytic cleavage of the Au-C(sp^2) bond was observed upon treatment with TfOH at low temperatures.[38] As mentioned previously, the protolytic cleavage releasing the product must be favorable over the protolytic cleavage of the Au-C(tpy) for catalysis to occur instead of decomposition. For complex **21** it is shown that protolytic cleavage of the Au-vinyl bond is preferred over the Au-C(tpy) bond (Scheme 65). However, for **18c-alk**, the opposite preference is predicted; the protolytic cleavage of the Au-C(tpy) (Au-C(sp^2)) bond is assumed to be favored over protolytic cleavage of the Au-C(sp^3) bond, and no catalysis can be achieved with this system.
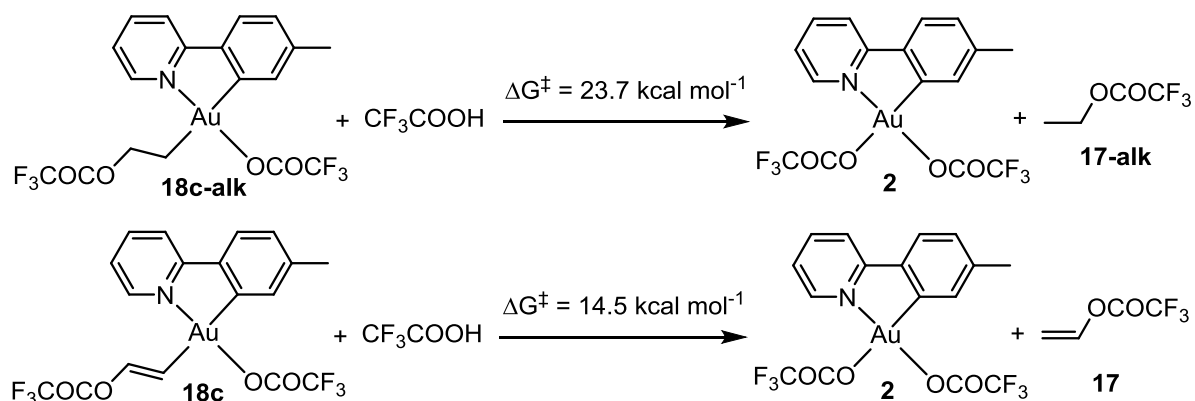
Scheme 68. Protolytic cleavage of the Au-C(sp^3) bond in **18c-alk** (top) and the Au-C(sp^2) bond in **18c** (bottom). The DFT calculations were performed by Dr. Ainara Nova and Dr. David Balcells (University of Oslo).

4.3 Other (*N,C*) cyclometalated Au(III) complexes investigated in the catalytic trifluoroacetoxylation of acetylene

To gain further insight into the scope of the acetylene transformation (Scheme 55), other (*N,C*) cyclometalated Au(III) complexes were investigated in this reaction. Complexes **1**, **2-OMe**, **2-CF₃**, and **2-Me₂** (Figure 23) were investigated under the same conditions used for complex **2**. The results are summarized in Table 8 (see Section 4.8) and Figure 23. Complexes **2-OMe**, **2-Me₂**, and **1** have been prepared previously in the Tilset group.[88, 94, 95] Complex **2-CF₃** was prepared by the author in collaboration with M.Sc. Knut Hylland.[97]
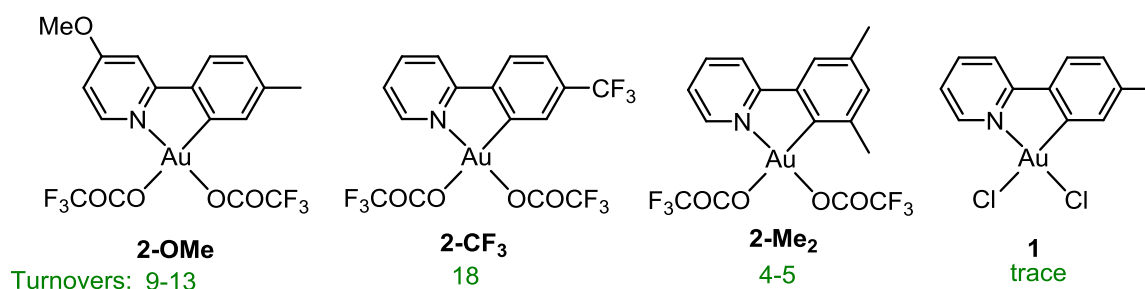
Figure 23. Other (*N,C*) cyclometalated Au(III) complexes[88, 94, 95, 97] investigated in the catalytic trifluoroacetoxylation of acetylene.

Upon bubbling acetylene through a solution of complex **2-OMe** in CF_3COOD, **17-*d*** was formed in similar, but slightly lower turnover numbers than with complex **2** (9-13 turnover per Au after 24 h for **2-OMe**, compared to 13-15 for **2**). By monitoring the reaction by ^{1}H NMR it seems that the reaction with **2-OMe** as precatalyst proceeded in a similar way to the reaction with complex **2**. After 1 hour reaction time, all of **2-OMe** was consumed and a vinyl complex analogous to **18** is formed as the only Au-containing species in solution. The vinyl complex was not isolated or characterized, but based on the reactivity of **2**, it is assumed to have the vinyl group *trans* to pyridine-*N*. Furthermore, the decomposition products **19** and [2-(*p*-tolyl)(4-methoxypyridine)]D_2^+ (**L$_2$-OMe**) together with **17-*d*** (*ca.* 3 turnovers per Au) were observed, in agreement with the previous observations for complex **2** (see Scheme 56). The reaction was monitored by ^{1}H NMR for 24 hours, and at that point **17-*d*** (together with traces of **17**), **19**, and **L$_2$-OMe** were the only species that could be detected in the solution by ^{1}H NMR. The presence of **L$_2$-OMe** was confirmed by spiking the NMR sample with an authentic sample of **L$_2$-OMe$_2$**.

The fluorinated analogue of complex **2**, complex **2-CF$_3$**, gave higher turnover numbers than both complexes **2** and **2-OMe**. After 24 hours, 18 turnovers per Au were achieved and at this point there is still a vinyl complex (analogous to complex **18**) present in solution, and nearly all the acetylene is used up. Based on this, the turnovers for this reaction would probably be higher if it was not limited by the amount of acetylene initially added to the solution. Further work on optimizing the method for measuring the turnover numbers for this complex has not been performed yet. The reaction using **2-CF$_3$** as the precatalyst seems to proceed in a similar manner to that of **2-OMe** and **2**, and both **19** and [2-(4-(trifluoromethyl)phenyl)pyridine)]D_2^+ (**L$_2$-CF$_3$**) were observed by ^{1}H NMR as decomposition products. The presence of **L$_2$-CF$_3$** was confirmed by spiking the reaction with an authentic sample of **L$_2$-CF$_3$**.

In the case of the more sterically encumbered complex **2-Me$_2$**, the turnovers of **17-*d*** were significantly lower (4-5 turnovers after 24 hours) than that obtained with complexes **2**, **2-OMe**, and **2-CF$_3$**. The reaction was monitored by ^{1}H NMR and *ca.* 20 minutes after the acetylene addition all of **2-Me$_2$** was

consumed and there was only small amounts of the vinyl complex of **2-Me₂** left in the solution. One hour after addition of acetylene, all of the vinyl complex had decomposed. At this point there are two ligand-containing decomposition products present in the reaction mixture, one of them being [2-(3,5-dimethylphenyl)(pyridine)]D₂⁺ (**L₂-Me₂**) the other one unknown, in a 2:1 ratio, respectively (Figure 24). The presence of this new decomposition product indicates that there might be an additional decomposition pathway to that observed with complexes **2**, **2-OMe**, and **2-CF₃**, which may explain the low turnover numbers obtained when using this complex as precatalyst. The unknown decomposition product has not yet been characterized. The presence of **L₂-Me₂** was confirmed by spiking the reaction mixture with an authentic sample of **L₂-Me₂**.
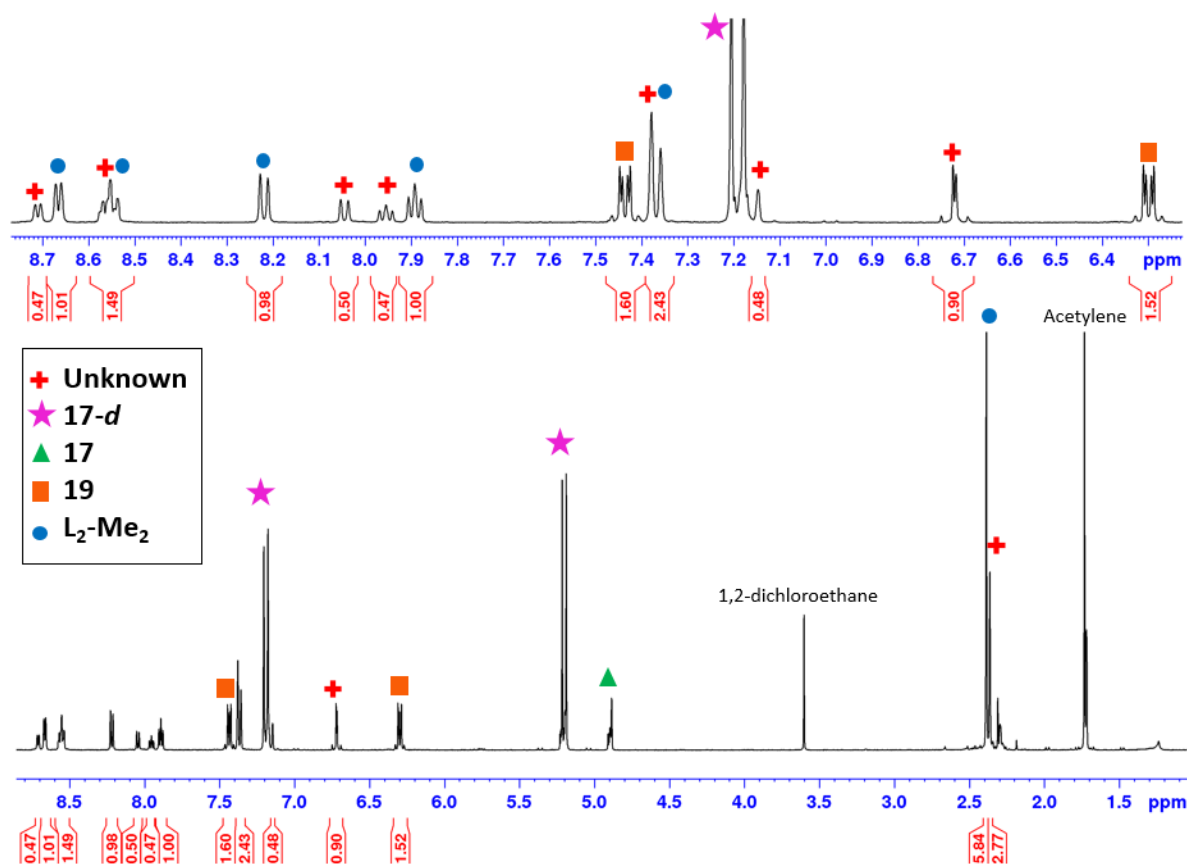
Figure 24. ^{1}H NMR (500 MHz, CF₃COOD) spectrum of the reaction mixture after 24 h catalysis with **2-Me₂** as precatalyst.

The dichloro complex **1** was also investigated under the same reaction conditions as the other complexes. With complex **1** as precatalyst, only traces of **17-d** was formed after 24 h reaction time. This might be due to the limited solubility of complex **1** in CF₃COOD or due to that the Cl ligands in **1** are less labile than the OCOCF₃ ligands in the complexes investigated previously, or a combination of these two factors. To further activate complex **1** towards acetylene functionalization, **1** was treated with *ca.* 1 equivalent of AgNTf₂ in CD₂Cl₂ (Scheme 69). One species is formed selectively, and based on the broadening of the resonance of the proton α to tpy-*N* (H^6) in the ^{1}H NMR spectrum acquired directly after mixing, it is suggested that the species formed is **1-NTf₂**, where the chloride ligand *trans*

to tpy-*C* has been abstracted, but no further experiments have been carried out to support this hypothesis. Upon adding CF_3COOH and acetylene to this mixture, formation of **17** (3 turnovers per Au after 24 hours, Scheme 69 and Table 8) occurred, together with the appearance of several other unidentified species.
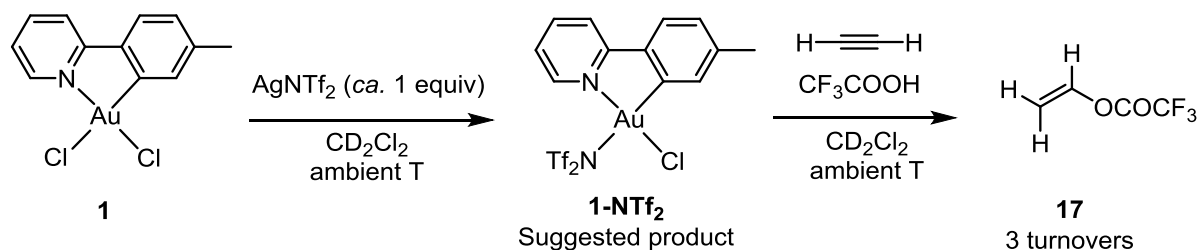
Scheme 69. AgNTf$_2$ promoted chloride abstraction at **1** and the performance of the complex in the catalytic trifluoroacetoxylation of acetylene.

4.4 A more robust (*N,C,C*) Au(III) pincer complex as catalyst

The Au(III) (*N,C,C*) pincer complex **27** was also investigated in the catalytic trifluoroacetoxylation of acetylene (Scheme 70). The synthesis and characterization of complex **27** will be presented in Chapter 5. In complex **27**, the "unproductive" coordination site *trans* to tpy-*N* is blocked by the $C(sp^3)$ alkyl ligand and if the pincer complex would be active in the catalytic transformation of acetylene this would further support the mechanism depicted in Scheme 62. Furthermore, the introduction of the pincer ligand should lead to a more stable complex than that of the (*C,N*) cyclometalated complexes; the tridentate ligand should make the protolytic cleavage of the Au-$C(sp^2)$ bond less favorable. The reductive elimination step (leading to decomposition) should also be less favorable due to the sp^3 hybridization of the alkyl-*C trans* to pyridine-*N*.[30, 31, 126] When bubbling acetylene through a solution of complex **27** in CF$_3$COOD, the formation of **17-*d*** did indeed occur. No formation of any Au(III) vinyl complex could be observed by ^{1}H NMR, in agreement with the proposed mechanism for the tpy-system; catalysis occured *trans* to aryl-*C* and no accumulation of **21** was observed in the reaction with **2** as precatalyst. Furthermore, the decomposition product that was always observed when using the (*C,N*)Au(OCOCF$_3$)$_2$ complexes, the diene (**19**), was also not observed. This is in full agreement with previous results where it was suggested that **19** is formed *via* reductive elimination from Au(III) divinyl complex **21**, and starting from complex **27** it should not be possible to form such a divinyl complex. The turnover numbers for the acetylene trifluoroacetoxylation reaction with **27** as catalyst (Scheme 70) were determined as previously described and compared with the results obtained with the tpy-system. Turnover numbers of 3.0, 5.0, and 18 (average number of multiple experiments) were obtained after 30 minutes, 1 hour, and 24 hours, respectively, whereas, with complex **2** 1.8, 3.1, and 14 turnovers were obtained, respectively (see ESI Paper IV). The larger turnover numbers obtained with complex **27** could be because complex **27** is more active than complex **2**. However, as mentioned

previously, with complex **2** substantial decomposition occurred during the catalysis and after 24 hours reaction time, complete decomposition was observed, so this difference might be due to a higher concentration of catalyst **27** in solution compared to that of **2**. Indeed it was found that when using complex **27**, a maximum of 10% decomposition was observed after 24 hours of catalysis in multiple experiments, indicating that complex **27** is much more stable under the catalysis conditions than complex **2**. Furthermore, at this stage nearly all the acetylene is used up in the reaction with **27**, indicating that the turnovers for complex **27** could be significantly higher if further optimization of the reaction conditions were performed. The differing degree of decomposition obtained with the two complexes **2** and **27** as (pre)catalysts could also be observed visually; the NMR tube with **2** as precatalyst contained a larger amount of Au-particles (as observed by visual inspection) than the NMR tube with **27** as catalyst after 24 hours reaction time (Figure 25).
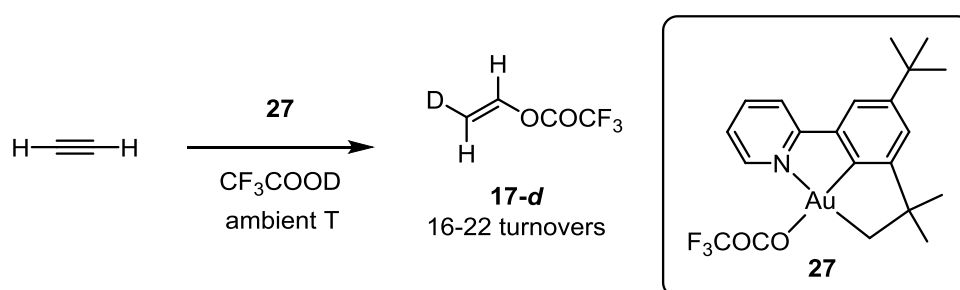
Scheme 70. The performance of the (*N,C,C*) Au(III) pincer complex **27** in the catalytic trifluoroacetoxylation of acetylene.

Figure 25. NMR tubes containing the reaction mixtures after 24 hours catalysis starting with **2** (top) and **27** (bottom), visually demonstrating the differing degree of decomposition (*i.e.* formation of dark brown to black Au-particles) in the two systems.

4.4.1 DFT calculations on the reaction mechanism when using complex 27 as catalyst

The acetylene trifluoroacetoxylation at complex **27** was investigated by DFT calculations. The DFT calculations were performed by Dr. Ainara Nova (University of Oslo). The free energy profile of the acetylene trifluoroacetoxylation at **27** was calculated (Scheme 71) and compared to that of **18** (starting with **2** as precatalyst, see Scheme 64 and Scheme 65). The transition states for the acetylene functionalization with complex **27** does not differ much from that obtained with complex **18** ($\Delta\Delta G^{\ddagger}$ <1 kcal mol^{-1}). However, the difference in the free energy barrier for the protolytic cleavage of the Au-vinyl bond (forming the product **17**) and the protolytic cleavage of the Au-C(aryl) bond (leading

to decomposition) is larger than that of the tpy-system ($\Delta\Delta G^{\ddagger}$ = 4.8 kcal mol^{-1} compared to 1.8 kcal mol^{-1} for the tpy-system). This should make protolytic cleavage of the Au-C(aryl) bond less favorable in the system starting with complex **27** than in the tpy-system starting with complex **2**, hence increasing the catalyst robustness. This is in full agreement with the experimental results obtained with complex **27**, where a maximum of *ca.* 10% decomposition of complex **27** was observed after 24 hours of catalysis in multiple experiments. In comparison, full decomposition was observed after 24 hours of catalysis when using complex **2** as precatalyst**.**
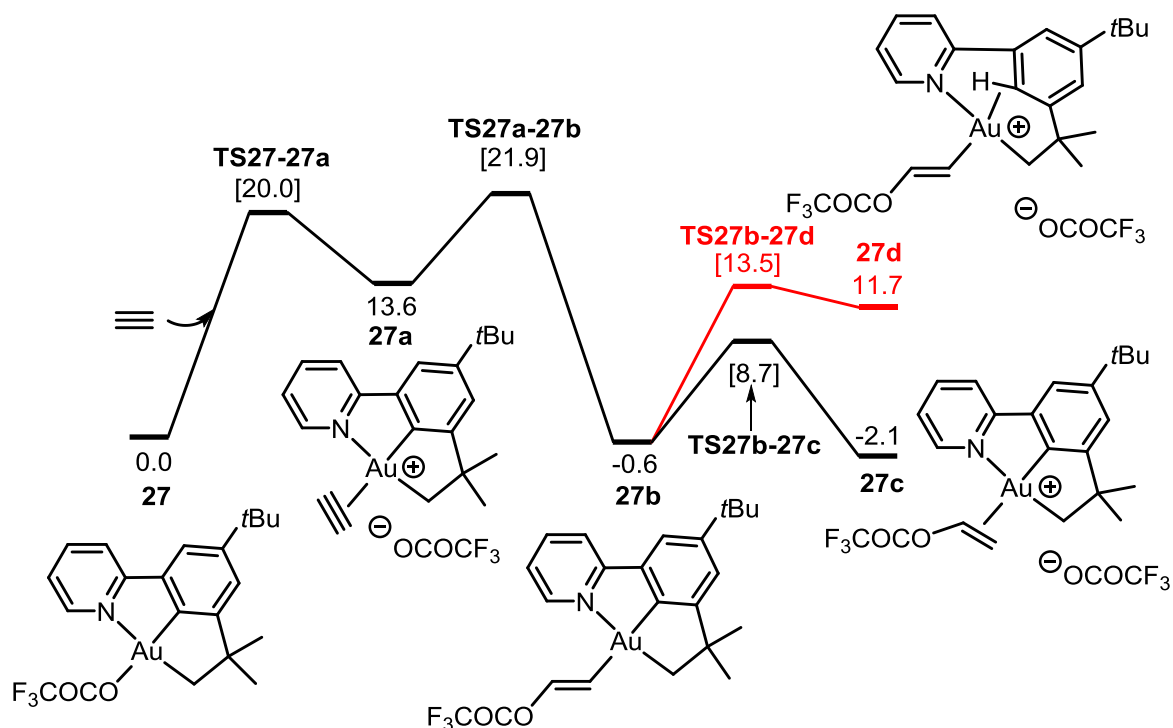
Scheme 71. Free energy profile in kcal mol^{-1} for the trifluoroacetoxylation of acetylene at **27** (in black) and the protolytic cleavage of the Au-C(arylpyridine) bond (in red). The energies of all minima and transition states in [brackets] are computed in CF$_3$COOH. To maintain mass balance, the energies of additional CF$_3$COOH and/or acetylene have been included in the calculations where needed. Computational details are given in Paper IV. The calculations were performed by Dr. Ainara Nova.

4.5 Other solvents/nucleophiles investigated

Due to the successful reactions of alkenes with various nucleophiles at complex **2**, it was desirable to investigate other nucleophiles than $^-$OCOCF$_3$ for the reactions with acetylene at complexes **2** and **27**. The experiments described in this section are all preliminary experiments where further work is needed to understand all the details. However, the experiments give a brief insight into the scope and limitations of the functionalization of acetylene with other nucleophiles and could potentially lead to other interesting projects in the future.

4.5.1 Acetic acid

Upon bubbling acetylene through a solution of complex **2** in CD$_3$COOD, the solution went from colourless to yellow. However, no immediate reaction was observed by ^{1}H NMR after *ca.* 10 minutes,

in contrast to that observed for the analogous reaction in CF_3COOD. After 2 days, small amounts of two vinylic products (<1 turnover) were observed in solution as two doublets at δ 5.22 (J = 13.7 Hz, minor product) and δ 4.85 (J = 14.0 Hz, major product) in the ^1H NMR spectrum (the coupling partners of the two doublets could not be observed, probably due to overlap with the aromatic protons, Scheme 72). Spiking the reaction mixture with commercial **17** showed that the minor vinylic product at δ 5.22 was **17-d**. The major product is thought to be (*E*)-vinyl acetate-d_4 (**28-d₄**). At this point, the sample contained a brown precipitate which was probably Au particles. By ^1H NMR, $tpyD_2^+$ was the main tpy-containg species observed in solution together with other unidentified decomposition products.
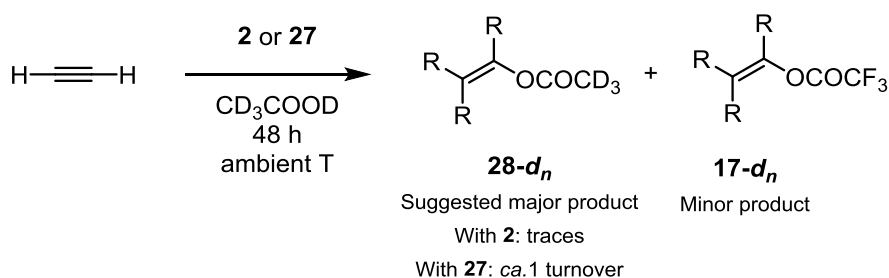
Scheme 72. Reactivity of acetylene at complexes **2** and **27** in CD_3COOD. R = H or D.

Since complex **27** was found to be a more robust catalyst than complex **2** for the acetylene trifluoroacetoxylation, complex **27** was also investigated in the reaction depicted in Scheme 72. Upon monitoring the reaction of **27** with acetylene and CD_3COOD by ^1H NMR, it could again be seen that two different vinylic species were formed. Upon comparing the ^1H NMR chemical shifts in both reactions, it is believed that it is the same compounds that has been formed as in the reaction with **2**. However, it seems that the deuterium from CD_3COOD has not ended up selectively *trans* to the $OCOCH_3$ or $OCOCF_3$ group (Scheme 72 and Figure 26), in contrast to that observed for the reactions of acetylene in CF_3COOD with **2** and **27** as (pre)catalysts. The coupling partners of these vinylic resonances were identified by a ^1H-^1H COSY experiment as overlapping signals at δ 7.25-7.30 (Figure 26). Based on the appearance of the ^1H NMR spectrum, several different isomers with the protons and deuteriums placed at different positions is thought to be formed in this reaction. It is not known whether this is due to loss of selectivity of the reaction, or if it is due to a (possibly gold catalyzed) H/D exchange on acetylene. However, after two days, acetylene-d_1 was observed together with a significant increase of the amount of CD_3COOH, which could indicate the latter scenario (see Figure 26). After two days, **28-d$_n$** was formed in *ca*. 1 turnover while only traces of **17-d$_n$** was formed (<0.2 turnovers). This represents rather low turnovers, but upon further optimization of the reaction conditions, these might be improved.
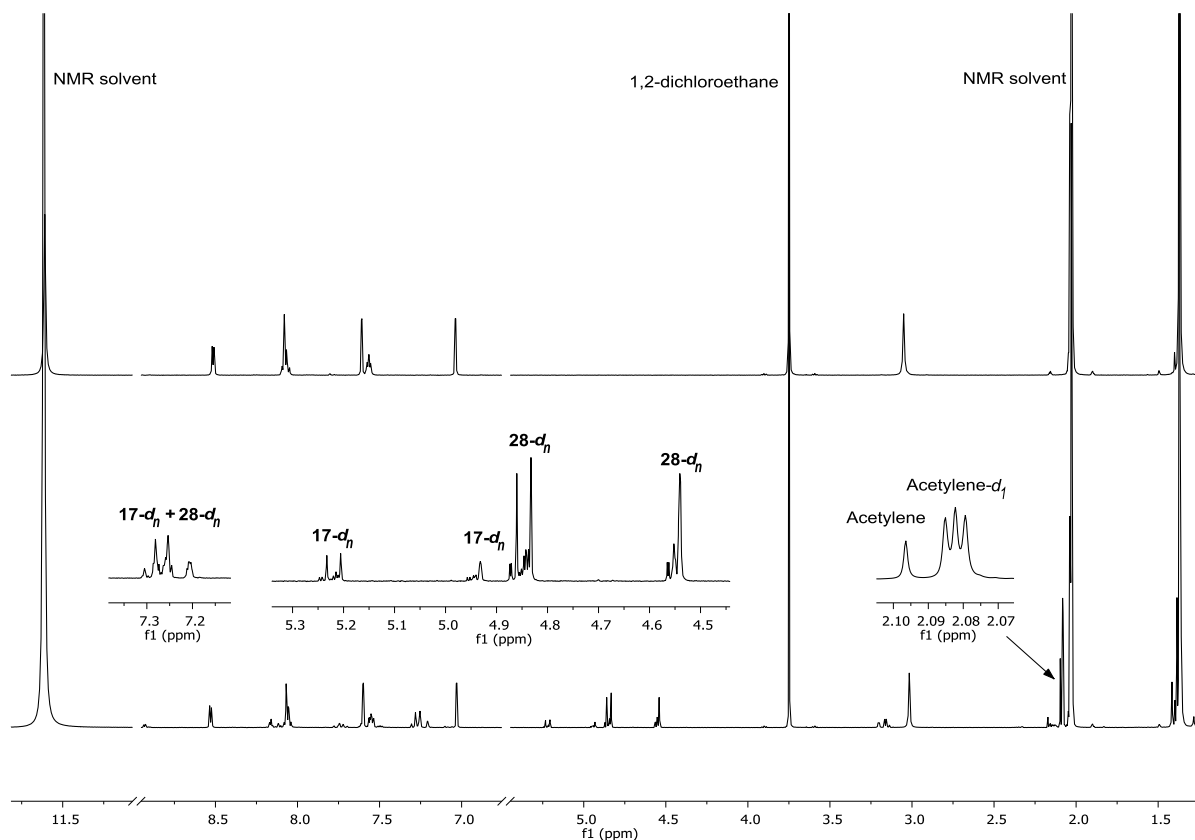
Figure 26. Stacked [^1]H NMR (500 MHz, CD$_3$COOD) spectra of the reaction of **27** with acetylene in CD$_3$COOD. Top: Reference spectrum of **27** in CD$_3$COOD. Bottom: Reaction mixture after 2 days. The insets shows the two vinylic products formed (**17-d_n** and **28-d_n**). Parts of the spectra have been omitted to improve clarity.

4.5.2 Trifluoroethanol

Due to the successful reaction of complex **2** with ethylene in CF$_3$CD$_2$OD,[90] we were interested in whether it was possible undertake the same reaction with acetylene, catalytically. Upon bubbling acetylene through a solution of complex **2** in CF$_3$CD$_2$OD and monitoring the reaction by [^1]H NMR, a complex reaction mixture containing traces of one or two vinylic product(s) were obtained after 1 day reaction time. Several tpy-containing species, one of them being tpyH, were also observed. Due to these less promising results, this reaction was not investigated further.
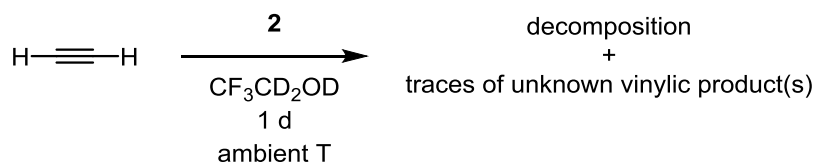
Scheme 73. Reactivity of acetylene and complex **2** in CF$_3$CD$_2$OD.

4.5.3 Methanol

To investigate if it is possible to produce methyl vinyl ether (**29**, Scheme 74) catalytically from acetylene and methanol at gold, the reaction of complex **2** and acetylene was investigated in CD$_3$OD and monitored by [^1]H NMR. Upon bubbling acetylene through a solution of complex **2** in CD$_3$OD, an

immediate reaction occurred. A well-defined species appeared in the vinylic region of the ^{1}H NMR spectrum with resonances at δ 3.94-3.96, δ 4.13-4.17 and δ 6.49-6.53 (Figure 27, top) and during the first 5 hours of the reaction the amount of this product increased with time. After extended reaction time, a decrease in the amount of this product was observed together with concomitant appearance of another species at δ 1.19-1.24 and δ 4.53-4.55 (Figure 27, bottom), the appearance of the latter resonances (Figure 27, bottom) suggest that they might originate from oligomeric or polymeric species. Based on previous findings with the acetylene reaction and the alkene reactions described in Chapter 2, it is suggested that the products formed in this reaction are a mixture of methyl vinyl ethers with the protons and deuteriums placed at different positions (**29-d_n**, Scheme 74) and that the polymer/oligomer product is likely to be polymethyl ether (**29$_n$**, Scheme 74). However, further studies to support this hypothesis have not been performed yet. The estimated turnover numbers (of **29-d_n** and **29$_n$** combined) after *ca.* 2 days is 2. At this point the main tpy-containing species in solution is tpyH and all of **2** has been consumed. A brown precipitate was observed by visual inspection which is probably due to Au particles.

Scheme 74. Suggested products from the reaction between **2** or **27** and acetylene in CD$_3$OD. R = H or D.

Figure 27. ^{1}H NMR (500 MHz, CD$_3$OD) of the two products formed in the reaction between complex **2**, acetylene and CD$_3$OD. Top: The vinylic products **29-d_n**. Bottom: The polymeric/oligomeric product **29$_n$**.

The reaction depicted in Scheme 74 was also performed with complex **27** instead of complex **2**. The same products were formed as with **2**, but significantly higher turnovers were achieved (14 turnovers after 1 day combining the products **29-d_n** and **29$_n$**. Furthermore, no Au particles could be observed by

visual inspection during the time interval in which the reaction was performed, in contrast to the reaction starting with **2** where a brown precipitate appeared after 1 day. After 1 week, 27 turnovers were achieved and at this point all the acetylene was used up. A white precipitate was also formed during the reaction which might be oligomers or polymers which have precipitated out of the solution.

4.6 Conclusions

The catalytic trifluoroacetoxylation of acetylene using **2** as precatalyst was presented. The mechanism of the transformation was studied both experimentally and computationally. Catalysis occurs *via* a double insertion mechanism where first a formal insertion of acetylene into the Au-O bond *trans* to tpy-*N* in **2** occured to furnish the active catalyst **18** (Scheme 75). In complex **18** the Au-vinyl bond *trans* to tpy-*N* does not undergo protolytic cleavage, instead a second insertion occurs; this time *trans* to tpy-*C* to give divinyl complex **21**. Finally, a protolytic cleavage of the Au-vinyl bond *trans* to tpy-*C* releases the product **17** and regenerates complex **18**. Turnovers up to around 20 could be achieved with the system using **2** as a precatalyst. It was discovered that decomposition is initiated by protolytic cleavage of the Au-C(tpy) bond leading to tpyH$_2^+$, the diene **19**, and Au particles. DFT calculations showed that the free energy barrier of the protolytic cleavage of the Au-C(tpy) bond (leading to decomposition) was only 1.8 kcal mol^{-1} higher than that of the protolytic cleavage of the Au-vinyl bond (leading to product formation), explaining why decomposition occurs readily with this system.
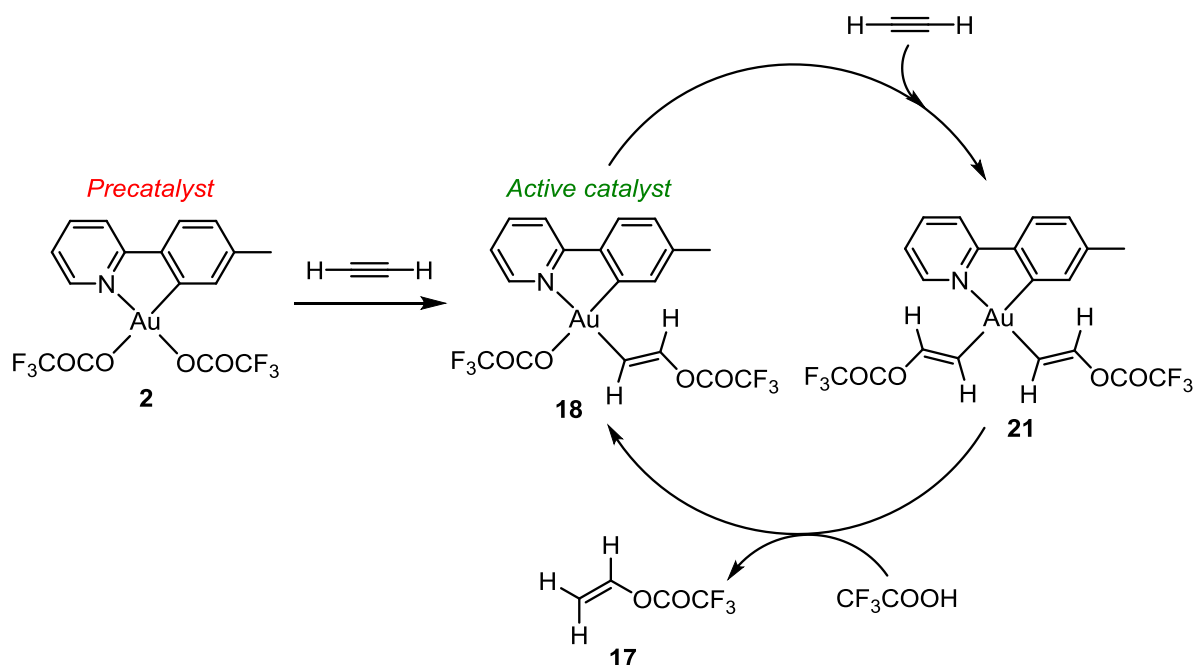
Scheme 75. Proposed mechanism for the catalytic trifluoroacetoxylation of acetylene with **2** as precatalyst.

Several other complexes were found to catalyze the acetylene trifluoroacetoxylation. All these complexes have a OCOCF$_3$ ligand *trans* to aryl-*C* where catalysis can occur. Complex **27** performed best of the complexes tested and a maximum of *ca*. 10% decomposition was obtained after 24 hours of

catalysis with this complex. Compared to the system starting with complex **2** (where complete decomposition occurred after 24 hours of catalysis), this is a significant improvement. Indeed, DFT calculations showed that with complex **27**, the difference in the free energy barrier of the protolytic cleavage of the Au-C(aryl) bond and the protolytic cleavage of the Au-vinyl bond is larger than that of the tpy-system (1.8 kcal mol^{-1} *vs.* 4.8 kcal mol^{-1} with **2** and **27**, respectively), explaining the increased robustness obtained with complex **27**.

Other nucleophiles were also investigated in the reaction with acetylene, and preliminary studies with acetic acid, trifluoroethanol, and methanol were performed. Of the tested nucleophiles, trifluoroethanol gave the least promising results. The reactions with acetic acid and methanol seems more promising; small amounts of what appears to be vinyl acetate (**28**), methyl vinyl ether (**29**), and the polymeric/oligomeric species **29**$_n$ could be obtained with **2** as precatalyst. Switching to **27** as catalyst led to higher turnovers of **28**, **29**, and **29**$_n$, again showing that complex **27** is a better catalyst than complex **2**.

4.7 Experimental

The experimental details for the content of Chapter 4 that are not described in Paper III or Paper IV are found herein.

General procedures

Complexes **1** and **2** were prepared according to previously reported procedures.[88, 89] Complexes **2-OMe**, **2-Me₂**, and **2-CF₃** were prepared according to unpublished procedures developed in the Tilset research group.[94, 95, 97] The preparation of complex **27** is described in Paper IV and Chapter 5. NMR solvents were purchased from Sigma Aldrich, Eurisotop, and Larodan. Acetylene 2.6 was purchased from AGA and Praxiar and passed through a double cooling trap at −78 °C (dry ice/acetone) prior to use. CD_2Cl_2 was dried over molecular sieves prior to use. All other reagents were used as received. As a precaution, all reactions were performed in the absence of light. AgNTf₂ was weighed out under argon. ^{1}H NMR spectra were recorded on Bruker Avance DPX200, DPX300 and DRX500. ^{1}H NMR spectra have been referenced relative to the residual solvent signals (CD_2Cl_2: $\delta(^1H)$ 5.34; CF₃COOD: $\delta(^1H)$ 11.50; CD₃OD: $\delta(^1H)$ 3.31; CD₃COOD $\delta(^1H)$ 2.03; CF₃CD₂OD $\delta(^1H)$ 3.88).

^{1}H NMR chemical shifts for compounds 17 and 17-*d*

The ^{1}H NMR chemical shifts for **17** and **17-*d*** are given for the compounds in the reaction mixture obtained after catalysis (when using complex **2** as precatalyst):

^{1}H NMR (500 MHz, CD_2Cl_2:CF_3COOH, 6:1 (v:v)) of **17**: δ 7.28 (dd, 1H, $^3J_{trans}$ = 13.7 Hz, $^3J_{cis}$ = 6.1 Hz, C**H**OCOCF$_3$), δ 5.27 (dd, 1H, $^3J_{trans}$ = 13.7 Hz, $^2J_{gem}$ = 2.7 Hz, **H** *cis* to OCOCF$_3$), δ 4.98 (dd, 1H, $^3J_{cis}$ = 6.1 Hz, $^2J_{gem}$ = 2.7 Hz, **H** *trans* to OCOCF$_3$).

^{1}H NMR (500 MHz, CF_3COOD) of **17-*d***: δ 7.18 (d, 1H, $^3J_{trans}$ = 13.6 Hz, C**H**OCOCF$_3$), δ 5.19 (d, 1H, $^3J_{trans}$ = 13.6, C**H**D).

Preliminary catalytic testing of complexes 1, 2-OMe, 2-CF$_3$, and 2-Me$_2$

5.0 mg of the Au(III) complex of interest was dissolved in CF_3COOD (0.7 mL) and transferred to a NMR tube. 1,2-dichloroethane (1 µL) was added as an internal standard (ISTD). A reference ^{1}H NMR spectrum (500 MHz or 300 MHz, CF_3COOD) was recorded. The internal standard was integrated against the peaks of the Au(III) complexes. Acetylene was bubbled through the solution for 1 min at ambient temperature and the reaction was monitored by ^{1}H NMR. After 24 hours, the turnover numbers (TONs) were determined by integration of the most upfield peak of vinyl trifluoroacete-*d* (**17-*d***) in the ^{1}H NMR spectrum against the peak of the ISTD. The results are summarized in Table 8. Due to limited solubility of complex **1** in CF_3COOD the turnovers could only roughly be estimated for this complex.

Preliminary catalytic testing of complex 1 + AgNTF$_2$

Complex **1** (5.0 mg, 0.011 mmol, 1.0 equiv.) was suspended in CD_2Cl_2. AgNTf$_2$ (5.0 mg, 0.013, 1.2 equiv) was added and the solution was transferred to a NMR tube. 1,2-Dichloroethane (1 µL, ISTD) was added. A reference ^{1}H NMR spectrum (500 MHz, CD_2Cl_2) was recorded and one major product was observed in the solution which was tentatively assigned to be AuCl(NTf$_2$)(tpy) with NTf$_2$ *trans* to tpy-*C*. The internal standard was integrated against the peaks of the Au(III) complex. CF_3COOH (100 µL) was added and another ^{1}H NMR spectrum was recorded. At this point there was at least two tpy-containing species present. Acetylene was bubbled through the solution for 1 minute. After 24 h, the TONs were determined by integration of the most upfield peak of vinyl trifluoroacete (**17**) in the ^{1}H NMR spectrum against the peak of the ISTD (See Table 8).

Table 8: Experimentally determined TONs[ix] for the formation of **17-*d*** (**17** for the last entry) using **2**, **2-OMe**, **2-CF₃**, **2-Me₂**, **1**, and **27** as (pre)catalysts. The reported values for $n_{product}$ are given as the average of all the experiments, and the error bars indicate the largest deviation from the average observed. The TONs are calculated from the minimum and maximum values of $n_{product}$ determined. [a]In this experiment nearly all acetylene was used after 24 h and at this point there were still non-decomposed gold complexes in solution, so the turnovers are probably underestimated. [b]Only one repetition of this experiment was performed. In all the experiments the presence of **17-*d*** (or **17**) was confirmed by spiking the NMR sample with an authentic sample of **17**.

	n_{Au} [mmol]	$n_{product}$ [mmol]	TON
2 (from Paper II)	0.0085	0.12 ± 0.01	13-15
2-OMe	0.0080	0.090 ± 0.019	9-13
2-CF₃	0.0077	0.14	18[a,b]
2-Me₂	0.0083	0.038 ± 0.005	4-5
1	0.011	trace	<1[b]
27 (from Paper IV)	0.0087	0.016 ± 0.004	16-22[a]
1 + AgNTf₂	0.011	0.028	3[b]

Reactivity of 2 towards acetylene in CD₃COOD

Complex **2** (5.0 mg, 0.0085 mmol) was suspended in CD₃COOD and transferred to a NMR tube. 1,2-Dichloroethane (1 µL, ISTD) was added. A reference ^{1}H NMR spectrum (500 MHz, CD₃COOD) was recorded. Acetylene was bubbled through the solution for 1 minute and the reaction was monitored by ^{1}H NMR. No immediate reaction was observed after *ca.* 10 minutes. After 2 days, small amounts (<1 turnover) of two vinylic species could be observed by ^{1}H NMR at δ 5.22 (*J* = 13.7 Hz, minor product) and δ 4.85 (*J* = 14.0 Hz, major product). The coupling partners of these two resonances could not be observed, probably due to overlap with the resonances for the tpy ligand. The resonance at δ 5.22 was found to be **17-*d*** by spiking of the NMR sample with commercial **17** and the resonance at δ 4.85 is thought to be from *(E)*-vinyl acetate-*d₄* (**28-*d₄***).

Reactivity of 27 towards acetylene in CD₃COOD

Complex **27** (5.0 mg, 0.0087 mmol) was suspended in CD₃COOD and transferred to a NMR tube. 1,2-Dichloroethane (1 µL, ISTD) was added. A reference ^{1}H NMR spectrum (500 MHz, CD₃COOD) was recorded. Acetylene was bubbled through the solution for 1 minute and the reaction was monitored by ^{1}H NMR. After 2 days, two vinylic species could be observed by ^{1}H NMR at δ 5.21-5.25, δ 4.93-4.96, δ 7.25-7.30 (minor product) and δ 4.83-4.87, δ 4.54-4.56, δ 7.25-7.30 (major product, *ca.* 1 turnover, Scheme 74). Based on the chemical shift of the two vinylic species, they are thought to be several different isomers of **17-*d*ₙ** and **28-*d*ₙ** with different degree of deuteration and location of the deuterium.

[ix] It should be considered that the turnover numbers might be affected by sources of error such as the lack of full control of the bubbling rate of acetylene, rate of mixing, convection rates, evaporation of volatile components (during the addition of acetylene or later in the experiment), inaccurate integration of the ^{1}H NMR spectrum etc.

Reactivity of 2 towards acetylene in CF$_3$CD$_2$OD

Complex **2** (5.0 mg, 0.0085 mmol) was dissolved in CF$_3$CD$_2$OD and transferred to a NMR tube. 1,2-Dichloroethane (1 µL, ISTD) was added. A reference ^{1}H NMR spectrum (500 MHz, CF$_3$CD$_2$OD) was recorded. Acetylene was bubbled through the solution for 1 minute and the reaction was monitored by ^{1}H NMR. After bubbling acetylene through the solution the colour changed from colourless to orange. After 1 day reaction time, a complex reaction mixture was obtained. Traces one of two unknown vinylic product(s) at δ 6.45 (J = 14.3 Hz) and δ 4.34 (J = 14.2 Hz) was observed. Several tpy-containing species were observed, one of them being tpyH, the others unknown. Further investigation of this reaction was not performed.

Reactivity of 2 towards acetylene in CD$_3$OD

Complex **2** (5.0 mg, 0.0085 mmol) and CD$_3$OD was added to a NMR tube. 1,2-Dichloroethane (1 µL, ISTD) was added. A reference ^{1}H NMR spectrum (500 MHz, CD$_3$OD) was recorded. Acetylene was bubbled through the solution for 1 minute and the reaction was monitored by ^{1}H NMR. Upon adding acetylene, the solution changed from colourless to yellow and an immediate reaction occurred. A well-defined new species appeared in the vinylic region of the ^{1}H NMR spectrum at δ 3.94-3.96, δ 4.13-4.17 and δ 6.49-6.53 and is thought originate from **29-d_n** with various degree of deuteration and placement of the deuteriums(s). During the first 5 hours, the amounts of **29-d_n** increased with time. After extended reaction times the amounts of **29-d_n** decreased and concomitant formation of a product at δ 1.19-1.24 and δ 4.53-4-55, which is thought to be the oligomeric or polymeric species **29$_n$**, was observed. After 2 days, the combined TONs for all the products (**29-d_n** and **29$_n$**) was found to be 2. At this point the main tpy-containing species in solution is tpyH and all of **2** has been consumed. A brown precipitate was observed by visual inspection which was probably due to Au-particles.

Reactivity of 27 towards acetylene in CD$_3$OD

Complex **27** (5.0 mg, 0.0087 mmol) was suspended in CD$_3$OD and transferred to a NMR tube. 1,2-Dichloroethane (1 µL, ISTD) was added. A reference ^{1}H NMR spectrum (500 MHz, CD$_3$OD) was recorded. Acetylene was bubbled through the solution for 1 minute and the reaction was monitored by ^{1}H NMR. The same products were formed as reported for the analogous reaction with **2**, but higher TONs were achieved. After 1 day, 14 turnovers were observed (combining the products **29-d_n** and **29$_n$**) and at this point no Au-particles could be observed by visual inspection. After 1 week, 27 TONs were measured, and at this point nearly all the acetylene is used up. A white precipitate was also formed, which could be oligomer or polymer which has precipitated out of the solution.

# Chapter 5 – C(sp^3)-H activation at Au(III): synthesis of a Au(III) (*N*,C,C) pincer complex

5.1 General introduction and scope of the chapter

Pincers are tridentate ligands that occupy adjacent binding sites in metal complexes.[127, 128] The use of pincers as ligands in metal complexes have gained a lot of popularity due to their ability of stabilizing the metal center.[7, 127, 128] There are several reports of Au(III) pincer complexes, the most widely explored type being the (*C,N,C*) pincer complexes derived from 2,6-diarylpyridines.[7] Other examples of Au(III) pincer complexes reported include the cationic complexes of the type (*C,N,N*) and (*N,C,N*).[7] Very recently, our group reported the first cationic mononuclear phosphino-amido Au(III) (*P,N,P*) pincer complexes.[129] As is also the case for Au(III) (*C,N*) cyclometalated complexes, Au(III) pincer complexes have traditionally been synthesized *via* transmetalation from organomercury compounds.[7, 78] A few years ago, Nevado and co-workers reported the synthesis of (*N,C,C*) Au(III) pincer complexes based on the 2-biphenylpyridine framework.[12] These were synthesized *via* a two-step mercury-free protocol by first coordinating the gold precursor to the pyridine-*N*, followed by microwave assisted cyclometalation to furnish the pincer complex (Scheme 76).[12]
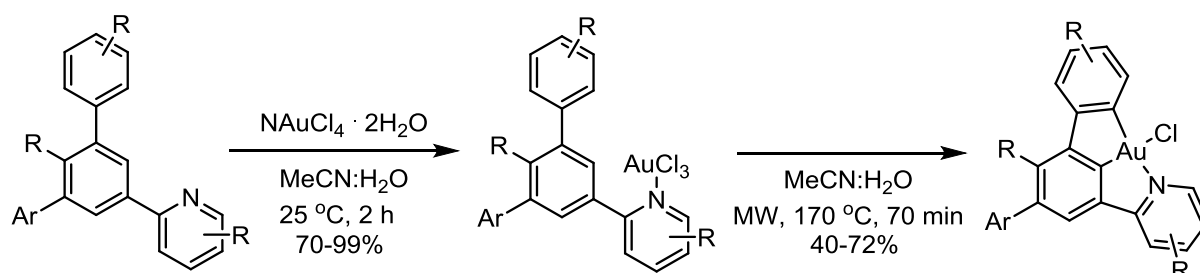
Scheme 76. Synthesis of Au(II) (*N,C,C*) pincer complexes reported by Nevado and co-workers.[12]

Most of the examples of cyclometalations at Au(III) reported in the literature involve a C(sp^2)-H activation, and there are only few examples of C(sp^3)-H activation at Au(III).[7, 78] Cinellu and co-workers reported the synthesis of a (*N,N,C*) Au(III) pincer complex *via* AgBF$_4$ assisted C(sp^3)-H activation from (6-(*tert*-butyl)-2,2'-bipyridine)AuCl$_3$ (Scheme 77).[130]
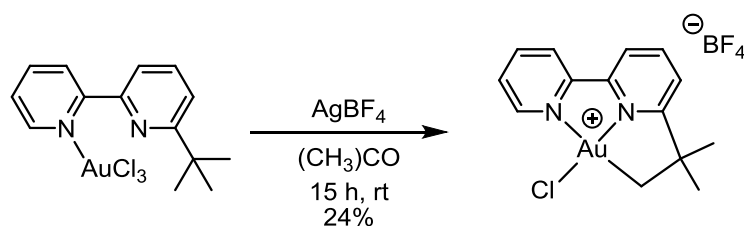
Scheme 77. AgBF$_4$ assisted C(sp^3)-H activation furnishing a Au(III) (*N,N,C*) pincer complex.[130]

Figure 28 shows two examples of (*C,N*) cyclometalated Au(III) complexes prepared *via* C(*sp³*)-H activation reported by Vicente and co-workers and Fan and co-wokers, respectively.[80, 131]

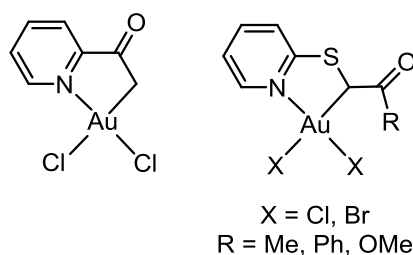X = Cl, Br
R = Me, Ph, OMe

Figure 28. Au(III) (*N,C*) cyclometalated complexes synthesized *via* C(*sp³*)-H activation.[80, 131]

In this chapter, the one-pot synthesis of a (*N,C,C*) Au(III) pincer complex *via* both C(*sp²*)-H and C(*sp³*)-H activation will be presented. The mechanism of the C(*sp³*)-H activation has been investigated by DFT calculations by Dr. Ainara Nova, and will also be discussed herein. The ligands described in this chapter have been prepared by M.Sc. Knut Hylland. The work presented in this chapter is covered in Paper IV.

5.2 Synthesis and characterization of Au(III) (*N,C,C*) pincer complex 27

Previous studies in the Tilset group showed that using the more sterically crowded ligand 2-(3,5-dimetylphenyl)pyridine to synthesize a (*N,C*) Au(III) bis(trifluoroacetate) complex gave complex **2-Me₂** (Figure 10, Chapter 1)[94, 95, 132] which was more distorted from the ideal square planar geometry than the corresponding complex with the tpy-ligand (complex **2**).[90] We were therefore interested in what the resulting product would be using the even more sterically crowded ligand 2-(3,5-di-*tert*-butylphenyl)pyridine. The reaction was performed utilizing the same reaction conditions as was used for the synthesis of complex **2**, and it turned out that cyclometalation occurred. However, as was immediately evident from ¹H NMR and ¹⁹F NMR, the expected cyclometalation product, a Au(OCOCF₃)₂(arylpyridine) type complex (**27a**, Scheme 78), was not formed. Instead, both a C(*sp²*)-H activation at the aryl group and a C(*sp³*)-H activation at one of the *tert*-butyl groups had occurred forming Au(III) (*N,C,C*) pincer complex **27** (Scheme 78).
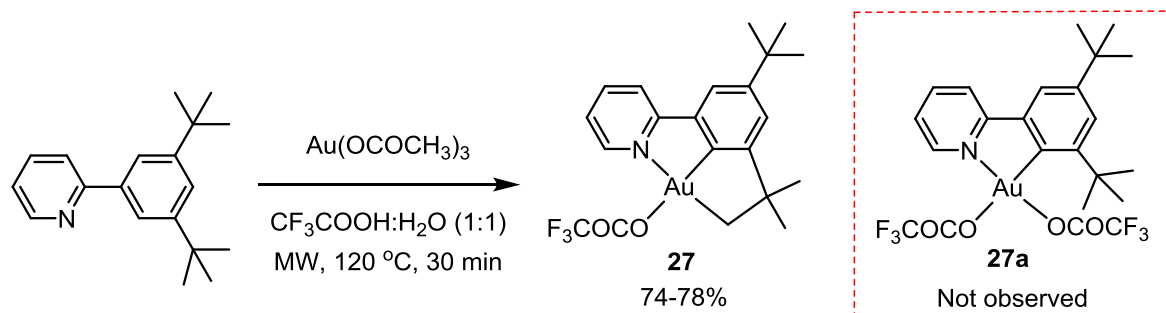
Scheme 78. Synthesis of Au(III) pincer complex **27**.

Complex **27** was characterized by NMR, MS, elemental analysis, and X-ray diffraction analysis. In the ¹H NMR spectrum of **27** in CD₂Cl₂, 6 different aromatic protons (all integrating for one H) are observed,

94

clearly indicating that cyclometalation of the aryl ligand has occurred. Three different resonances are found in the aliphatic region. At δ 3.16, the characteristic resonance of the two AuCH$_2$ protons from the *tert*-butyl methyl group which underwent C-H activation is found and at δ 1.40 the two unreacted methyl groups from the same *tert*-butyl group are observed. At δ 1.39, the resonance of the unreacted *tert*-butyl group is found. In the ^{19}F NMR spectrum of **27**, one single resonance is found at δ −76.9 corresponding to the OCOCF$_3$ group *trans* to aryl-*C*, similar to that that observed for OCOCF$_3$ *trans* to tpy-*C* in **2**,[89] **3**,[90] and **4**[90] (all at δ −77.0) and the other related complexes described in this thesis. The ORTEP plot of complex **27** is given in Figure 29 and selected metrical parameters are given in Table 9. The molecular structure of complex **27** is in full agreement with that observed by NMR. Complex **27** exhibits the typical square planar geometry which is commonly observed for Au(III) complexes. The N1-Au1-C1 chelate angle deviates from the idealized 90° to 80.36(13)°. The C1-Au1-C2 chelate angle also deviates from the idealized 90° to 81.66(15)°, which is smaller than that of the related (*N*,*N*,*C*) pincer complex reported by Cinellu and co-workers (84.0 (3)°).[130] The Au1-N1 and Au1-O1 bond lengths are similar to, but on the long side of, that reported for related Au(III) arylpyridine complexes.[89, 90] The Au-C1 bond length of 1.944(3) Å is slightly shorter than the corresponding Au-C(aryl) bond in the related complex **2** (1.995(7) Å),[89] indicating that the aryl ligand is slightly more tightly bound in complex **27** than in complex **2**, which may contribute to the observed increased robustness of **27** compared to **2** during catalysis (see Section 4.4). The Au-C2 bond length of 2.049(4) Å is in the range of that reported for related complexes with C(*sp^3*) bonded ligands *trans* to pyridine-*N*,[90] including the complexes described in Chapter 2, and is slightly longer than that of the related pincer complex reported by Cinellu and co-workers (2.028(7)Å).[130]
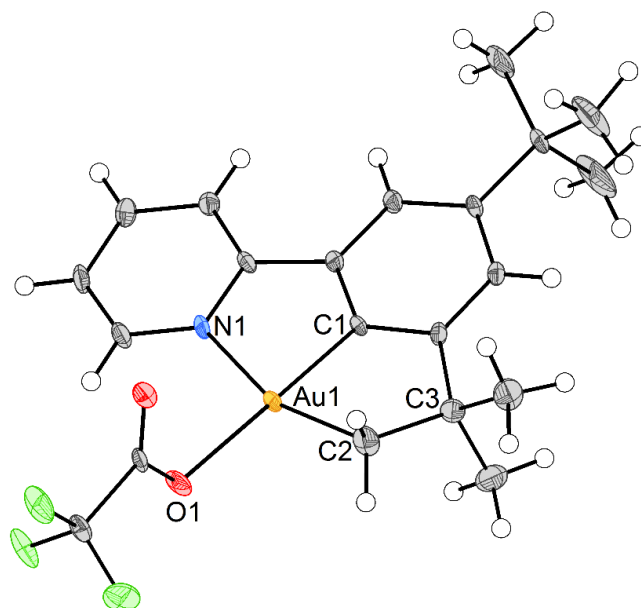

Figure 29. ORTEP plot of **27** with 50% ellipsoids. The crystallographic structure determination was performed by Dr. David Wragg and Dr. Sigurd Øien-Ødegaard.

Table 9. Selected bond distances [Å] and angles [º] for **27**.

Bond distances [Å]		Angles [º]	
Au1-N1	2.135(3)	O1-Au1-N1	99.62(11)
Au1-C1	1.944(3)	N1-Au1-C1	80.36(13)
Au1-O1	2.119(3)	C1-Au1-C2	81.66(15)
Au1-C2	2.049(4)	C2-Au1-O1	98.30(14)
C2-C3	1.557(6)	C1-Au1-O1	179.34(13)
		N1-Au1-C2	161.36(14)

Complex **27** could also be synthesized without microwave heating using prolonged reaction time forming **27** in slightly lower yields (58-62% compared to 74-78% for the microwave method, see ESI, Paper IV for details). This indicates that the microwave irradiation is not needed for the C(sp^3)-H activation, but that it speeds up the reaction compared to conventional heating.

5.3 DFT calculations on the C(sp^3)-H activation step forming 27

DFT calculations on the C(sp^3)-H activation step forming complex **27** from **27a** were performed by Dr. Ainara Nova (University of Oslo). The free energy profile with **27a** as energy reference is shown in Scheme 79. Even though complex **27a** is not observed experimentally, it is expected to be formed upon cyclometalation. As can be seen from Scheme 79, going from **27a** to **27** is a highly exergonic reaction (ΔG = −22.5 kcal mol^{-1}).
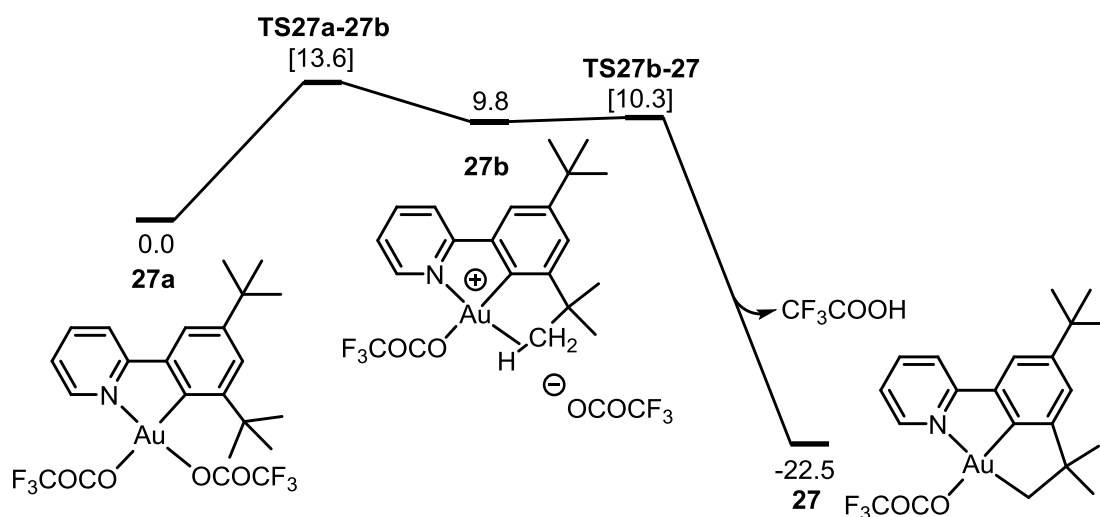
Scheme 79. Free energy profile (in kcal mol^{-1}) for the C(sp^3)-H activation step forming **27** from **27a**, in CF$_3$COOH. The DFT calculations were performed by Dr. Ainara Nova. To maintain mass balance, the energy of additional CF$_3$COOH have been included in the calculations where needed. Computational details are given in Paper IV.

Compared to complex **2**, the optimized geometry of complex **27a** deviates even more from the ideal square planar geometry (Figure 30 and ESI, Paper IV and Paper III). The F$_3$COCO-Au-OCOCF$_3$ angle deviates more from the idealized 90º in complex **27a** than in complex **2** (82.3º in **27a** *vs.* 88.0º in **2**). The same is observed to the *cis* C(aryl)-Au-OCOCF$_3$ angle which is 103.5º in **27a** and 94.6º in **2**. The

96

steric repulsion between the *tert*-butyl group *ortho* to Au and the OCOCF$_3$ ligand *trans* to pyridine-*N* forces C3 out of the Au-C(1)-C(2) plane by 9.1° (Figure 30), probably favoring the associate substitution of the OCOCF$_3$ ligand *trans* to pyridine-*N* with the *tert*-butyl group to give the agostic intermediate **27b**. The agostic intermediate **27b** has an activated C-H bond (d(C-H) = 1.18 Å in **27b** *vs.* 1.09 in **27a**, Figure 30). The ligand substitution step, going from **27a** to the agostic intermediate **27b**, is an endergonic reaction with a rather low free energy barrier (**TS27a-27b** = 13.6 kcal mol^{-1}) and is followed by an almost barrierless proton abstraction by ⁻OCOCF$_3$ to furnish Au(III) (*N,C,C)* pincer complex **27** (Scheme 79). Bourissou and co-workers recently reported experimental and theoretical evidence for C-H agostic interactions at Au(III) centers, in agreement with the proposed intermediate **27b**.[32, 33, 100]
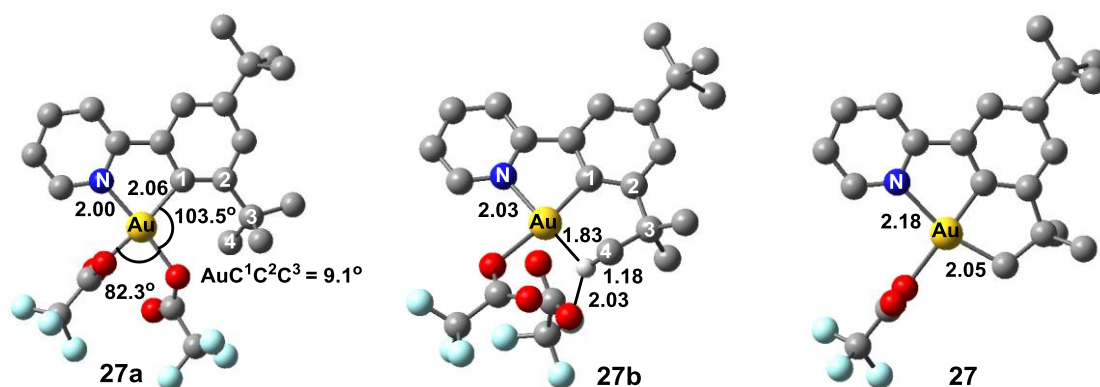
Figure 30. Optimized geometries for **27a**, **27b**, and **27**. The DFT calculations were performed by Dr. Ainara Nova.

5.4 Reactivity of Au(III) (*N,C,C*) pincer complex 27

As was described in Chapter 4, complex **27** could be used as a catalyst for the acetylene trifluoroacetoxylation reaction. Indeed, complex **27** was found to be a significantly more robust catalyst than the originally investigated precatalyst **2** and a maximum of *ca*. 10% decomposition of the catalyst (compared to complete decomposition when starting with **2**) under the catalysis conditions was obtained after 24 hours catalysis when using **27** as catalyst. A natural continuation was then to investigate the reactivity of complex **27** towards ethylene in CF$_3$COOH. As was mentioned in the introduction, reacting ethylene with complex **2** in CF$_3$COOH led to the formal insertion of ethylene into the Au-O bond *trans* to tpy-*N* in **2** forming complex **3**, but no catalysis could be achieved simply because the protolytic cleavage of the Au-C(sp^3) bond does not occur. In complex **27**, the position *trans* to pyridine-*N* is blocked, and we were interested in whether we could obtain any reactivity *trans* to aryl-*C* instead. However, upon reacting complex **27** with ethylene in CF$_3$COOD, no reaction could be observed, even at elevated temperatures (70 °C).

5.5 Attempt at synthesizing a Au(III) (*C,N,C*) pincer complex

After the successful synthesis of Au(III) (*N,C,C*) pincer complex **27**, we were interested in whether 2-(*tert*-butyl)-6-(*p*-tolyl)pyridine would react analogously to form Au(III) (*C,N,C*) pincer complex **30**

(Scheme 80). Upon reacting 2-(*tert*-butyl)-6-(*p*-tolyl)pyridine with $Au(OCOCH_3)_3$ under the same reaction conditions as **27** (Scheme 80), no Au(III) (*C,N,C*) pincer complex could be obtained and only the protonated ligand ([2-(*tert*-butyl)-6-(*p*-tolyl)pyridine]H$^+$) could be isolated from the reaction mixture. A co-worker undertook several more attempts to try to achieve a Au(III) (*C,N,C*) pincer complex with this ligand system, but did not succeed (See ESI, Paper IV). Furthermore, DFT calculations were performed to investigate why the synthesis of the (*C,N,C*) pincer complex in Scheme 80 failed, these results are included in Paper IV and will not be discussed herein.
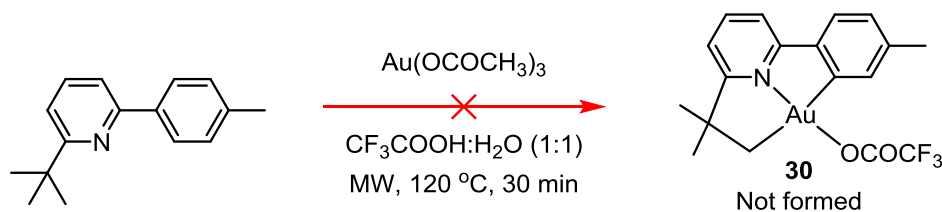
Scheme 80. Attempted synthesis of a Au(III) (*C,N,C*) pincer complex.

5.6 Conclusions

The synthesis of Au(III) (*N,C,C*) pincer complex **27** *via* both C(sp^2)-H activation, which is common at Au(III), and C(sp^3)-H activation, which is a rare process at Au(III), has been presented. Complex **27** can be prepared in a good yield both under microwave conditions and with conventional heating. The formation of complex **27** under the reaction conditions is in agreement with DFT calculations showing that forming complex **27** from the corresponding $Au(OCOCF_3)_2$(arylpyridine) complex (**27a**) is an exergonic process with surpassable free energy barriers.

5.7 Experimental

The experimental details for the reactions in Chapter 5 that are not included in Paper IV are described herein.

General procedures

CF_3COOD was purchased form Sigma Aldrich and used as received. Ethylene 3.5 was purchased from Hydro Gas. NMR spectra were recorded on Bruker Avance DRX500.

Reactivity of 27 towards ethylene

Complex **27** (5.0 mg, 0.0087 mmol) was dissolved in CF_3COOD and transferred to a NMR tube. 1,2-Dichloroethane was added as an internal standard (ISTD) and a reference ^{1}H NMR spectrum (500 MHz, CF_3COOD) was recorded. Ethylene was bubbled through the solution for 1 minute and the reaction was monitored by ^{1}H NMR. No reaction could be observed by ^{1}H NMR either after 4 days at ambient T or after heating at 70 ^{o}C for *ca*. 14 hours.

Chapter 6 – Generation of Au(III) η^1 and η^3 allyl complexes

6.1 General introduction and scope of the chapter

The allyl ligand is a very popular ligand and transition metal allyl complexes have been thoroughly studied.[76, 133] The allyl ligand can adopt several modes of coordination and some of the most common types are shown in Figure 31.[76, 133] The two monomeric structures are the most common where either an η^1 allyl complex or an η^3 allyl complex is formed with the allyl ligand acting as a one electron donor X-type ligand and a three electron donor LX-ligand, respectively.[76, 133] In this chapter, the generation and characterization of η^1 and η^3 allyl Au(III) complexes will be presented. Much of the work presented in this chapter are preliminary studies where further work will be needed to fully understand the systems studied.

An η^1 allyl complex   An η^3 or π allyl complex   Bridging allyl complexes
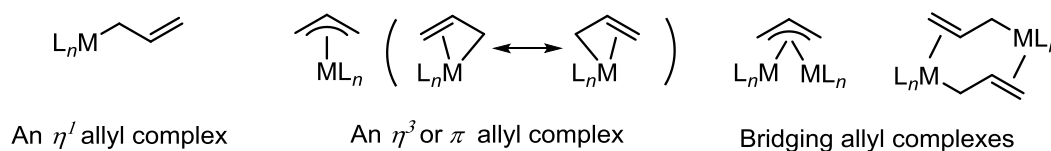
Figure 31. Common binding modes seen in allyl complexes.[76, 133]

To determine whether coordination of an alkene to Au has occurred or not, NMR and single crystal X-ray diffraction analysis are two very important tools. As discussed in Chapter 1, there are only a few examples of Au(III) complexes reported in the literature and to the author's knowledge, there are no reports in the literature of any well characterized Au(III) η^3 allyl complexes. The only related complex reported is η^3 aryl complex **C** (Figure 32) prepared by Bourissou and co-workers.[42] In Table 10, the ^{1}H NMR chemical shifts of the vinylic protons of a selection of Au(III) alkene complexes (Figure 32) are listed.[38, 39, 42, 92, 134] One example of a Au(III) arene complex is also included together with one Au(I) alkene complex. For most of the Au(III) complexes, the resonances of the vinylic protons move to higher ppm values upon coordination to Au (as compared to the free alkene, Table 10).[38, 39, 92] There are however a few examples where the resonances of the vinylic protons move to lower ppm values, including the Au(III) arene complex **C** and the Au(I) tris(ethylene) complex **D**.[42, 134] For complex **B-norbornene**, a small change of δ(^{1}H$_{vinyl}$) to a lower ppm value was observed.[39]

B(C$_6$F$_5$)$_3$ is a strong Lewis acid and is used in organogold chemistry for abstracting ligands at Au and thereby creating an open coordination site where *e.g.* an alkene or alkyne can coordinate.[7, 31] Two examples of the use of B(C$_6$F$_5$)$_3$ in Au(III) chemistry are given in Scheme 81. Bochmann and co-workers abstracted a trifluoroacetate ligand from a (*C,N,C*)AuOCOCF$_3$ complex, followed by coordination of an alkyne (Scheme 81, top).[7, 40] This strategy was also used for the synthesis of the Au(III) alkene complexes **B** depicted in Figure 32 (see Scheme 2, Chapter 1).[39] Bourissou and co-workers abstracted

a methyl ligand from a (*P,C*)AuMe$_2$ complex, followed by coordination of 2,6-dimethylpyridine (Scheme 81, bottom).[99]
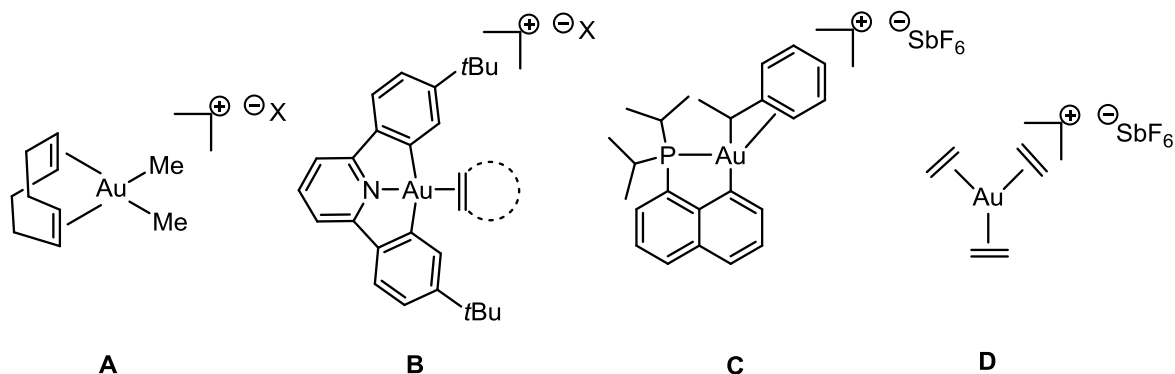

Figure 32. Selected Au(I) and Au(III) alkene and arene complexes.[38, 39, 42, 92, 134] In **A**, X = BAr^F, OTf, or NTf$_2$. In **B**, X = (C$_6$F$_5$)$_3$B(OCOCF$_3$) and alkene = ethylene, cyclopentene, or norbornene.

Table 10. ^{1}H NMR chemical shifts (in CD$_2$Cl$_2$) for the vinylic (or aromatic in the case of **C**) protons in Au(I) and Au(III) alkene and arene complexes **A-D** in Figure 32.[38, 39, 42, 92, 134] Δδ = δ$_{bound}$ − δ$_{free.}$ In **C**, δ$_{free}$ is from the related [(*P,C*)AuPh]$^+$[SBF$_6$]$^-$.[42]

	δ(^{1}H$_{vinyl}$)	Δδ
A-BAr^F	6.29 (0 °C)	+ 0.74
A-OTf	6.39 (0 °C)	+ 0.84
A-NTf$_2$	6.38 (rt)	+ 0.83
B-ethylene	6.29 (-70 °C)	+ 0.91
B-cyclopentene	6.31 (-40 °C)	+ 0.56
B-norbornene	5.97 (-40 °C)	−0.22
C	4.94 (25 °C)	−1.26
D	6.49 (0 °C)	−0.46
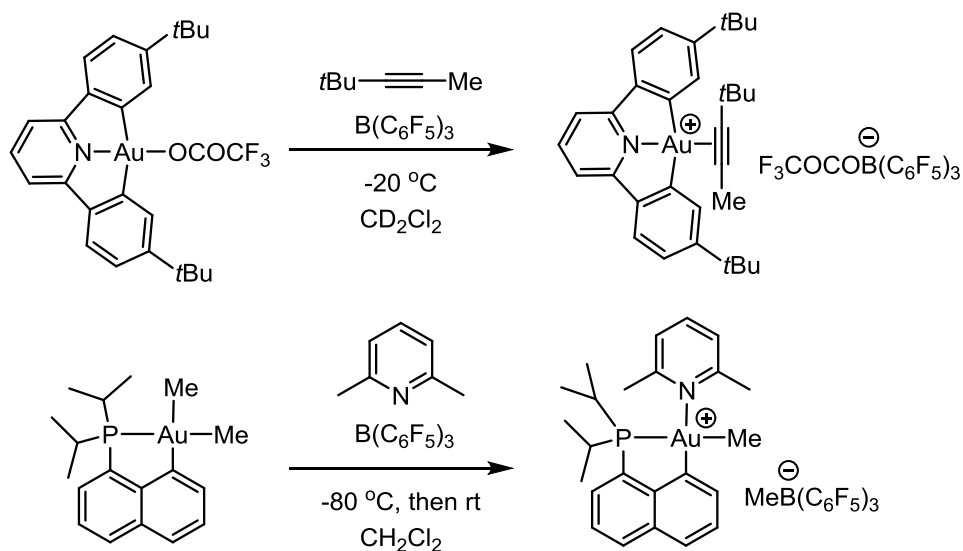
Scheme 81. Two examples of the use of B(C$_6$F$_5$)$_3$ for abstracting either a trifluoroacetate ligand (top) or a methyl ligand (bottom) from Au.[40, 99]

6.2 Reactivity of β-OMe Au(III) alkyl complexes towards B(C₆F₅)₃

Upon adding *ca.* 1 equivalent of B(C$_6$F$_5$)$_3$ to a solution of **6b** in CD$_2$Cl$_2$, an immediate reaction occurred as could be observed by ^{1}H NMR (Scheme 82 and Figure 33). One major product was formed together with small amounts of side products and/or decomposition products (*ca.*10%). Large changes in the ^{1}H NMR spectrum were observed after the addition of B(C$_6$F$_5$)$_3$. The resonances of CH$_3$^{d} and CH$_3$^{e} have moved to higher ppm values from δ 0.98-1.00 (overlapping resonances) to δ 2.08 and δ 2.59. The resonances for H^a and H^b have also moved to higher ppm values (from δ 2.43-2.46 and δ 2.30 to δ 3.66 for H^a and from δ 3.35 to δ 5.76 for H^b). The resonance for H^c is not present in the ^{1}H NMR spectrum and no well-defined resonance for the OMe group is observed. However, two broadened resonances are observed at δ 4.02 and δ 3.55, the origin of these resonances is unknown, but they might originate from an adduct of B(C$_6$F$_5$)$_3$ and MeOH. Based on NMR characterization, it is suggested that a double bond has formed *via* B(C$_6$F$_5$)$_3$ promoted elimination of MeOH from **6b** to either η^1 allyl complex **31a** or η^3 allyl complex **31b** (Scheme 82). The fate of the OCOCF$_3$ ligand remains unknown. The obtained product after reaction of **6b** with B(C$_6$F$_5$)$_3$ decomposed over time into at least two different decomposition products, which complicated the characterization of the product. The exact identity of the ligand (in **31a**) or anion (in **31b**) X remains uncertain, but it is probably an adduct of B(C$_6$F$_5$)$_3$ and MeOH and/or ⁻OCOCF$_3$.
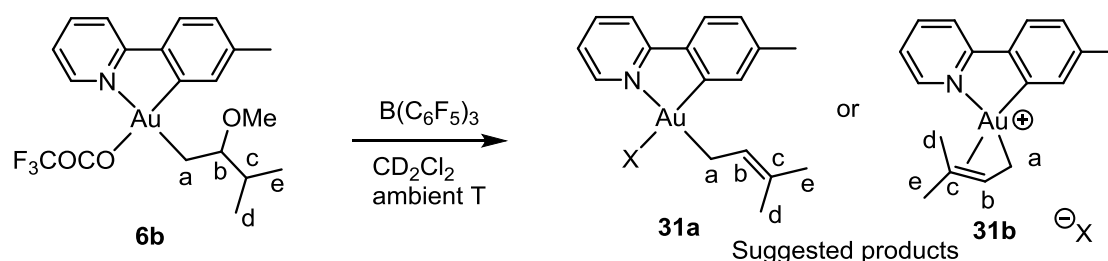
Scheme 82. Reactivity of **6b** towards B(6$_6$F$_5$)$_3$. X = unknown. The atoms of the ligand *trans* to tpy-*N* have been labelled a-e to simplify the NMR discussions.

In the ^{1}H-^{1}H NOESY spectrum of **31a/b** (Figure 34) a NOE between H^a and H$^{6'}$ is observed which is in agreement with both structures **31a** and **31b**. Furthermore, a NOE between CH$_3$^{e} and H^6 is observed, and upon increasing the intensity of the NOESY spectrum, a weak NOE between CH$_3$^{d} and H^6 could also be observed. These observations might indicate a coordination of the double bond to Au *trans* to tpy-*C*, which is in agreement with structure **31b**. Therefore, it is thought that the product of the reaction of **6b** with B(C$_6$F$_5$)$_3$ is **31b**, but further characterization will have to be performed in order to confidently assign the product of the reaction. Complex **31b** has not been isolated from the CD$_2$Cl$_2$ solution in which it was generated. The reaction depicted in Scheme 82 was also performed with complex **5b** (see Chapter 2) to investigate if **5b** would react analogously to that of **6b**. However, treating **5b** with B(C$_6$F$_6$)$_3$ led to the formation of a complicated reaction mixture and no products could be identified.
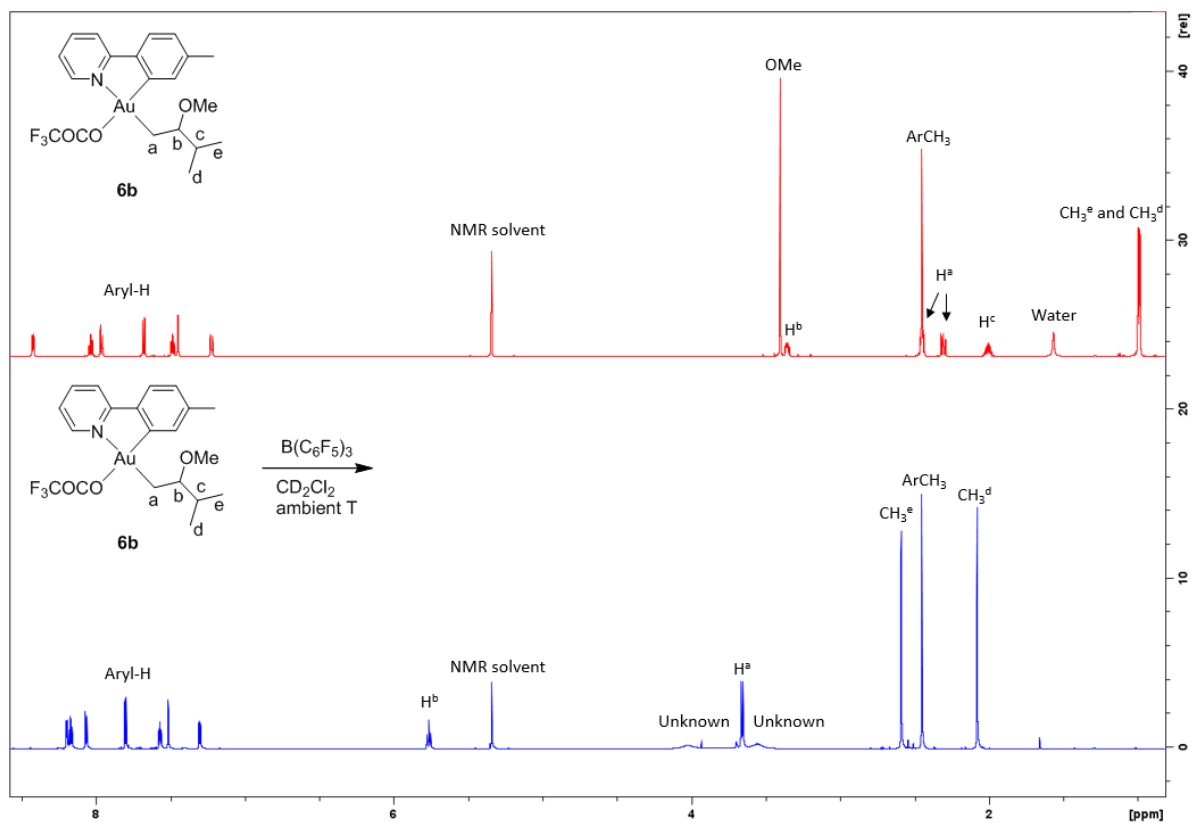
Figure 33. Stacked ^{1}H NMR (600 MHz (top) or 800 MHz (bottom), CD$_2$Cl$_2$) spectra showing the reaction between **6b** and B(C$_6$F$_5$)$_3$. Top: Reference spectrum of **6b** (NB: the actual sample of **6b** used did not contain water). Bottom: Spectrum acquired *ca.* 20 min after addition of B(C$_6$F$_5$)$_3$.
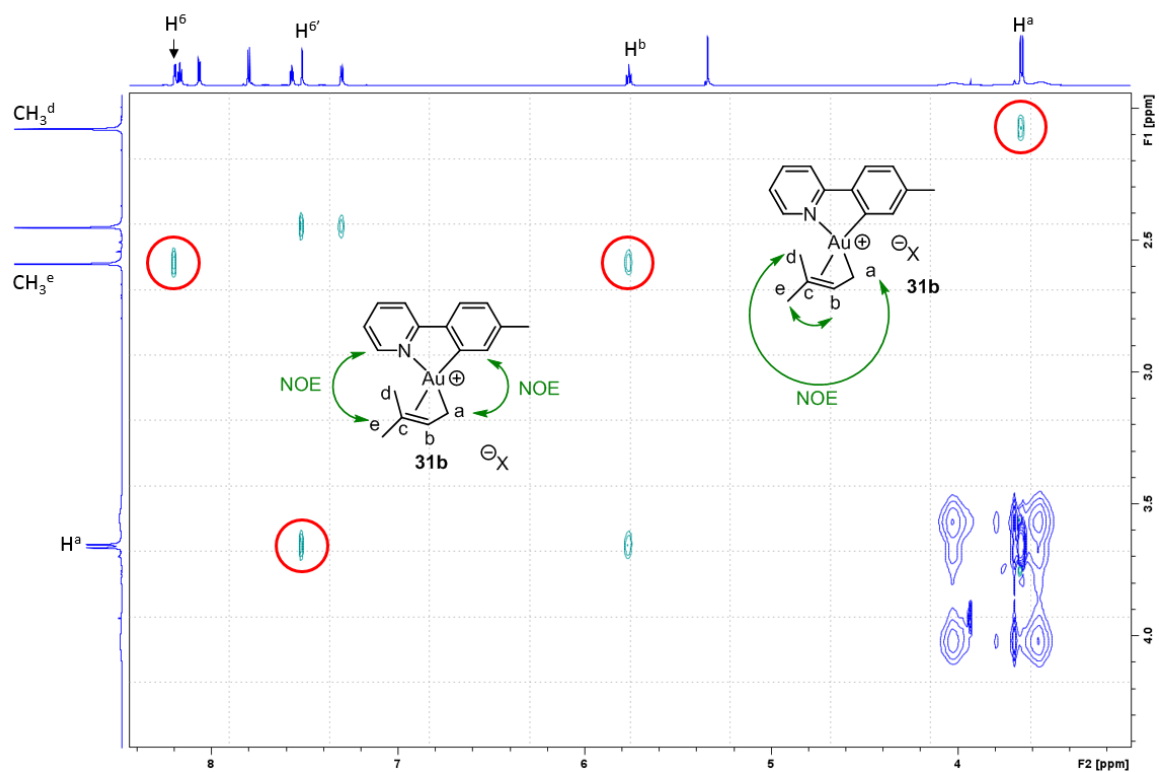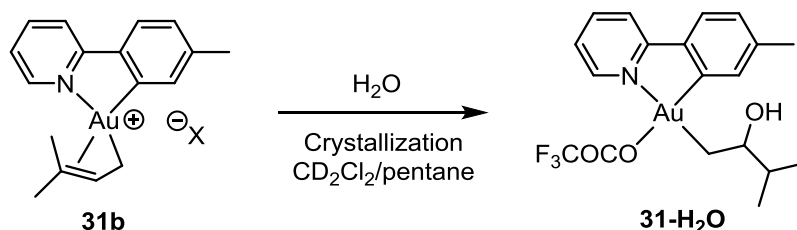

Figure 34. ^{1}H-^{1}H NOESY (800 MHz, CD$_2$Cl$_2$, mixing time = 1 s) of Au(III) complex **31b**. Close up on the NOE between CH$_3$^{e} and H^6, between CH$_2$^{a} and H$^{6'}$, and CH$_3$^{d} and CH$_2$^{a}. X = unknown.

102

In an attempt at growing crystals of complex **31b**, crystals of **31-H₂O** was obtained instead (Scheme 83). It is assumed that a molecule of water has added across the double bond in **31b** furnishing **31-H₂O** (Scheme 83).

Scheme 83. Suggested pathway to complex **31-H₂O**. X = unknown.

The ORTEP plot of complex **31-H₂O** is given in Figure 35 and selected metrical parameters are given in Table 11. As can be seen from the molecular structure of **31-H₂O**, the addition of water to the double bond in **31b** has occurred in a non-Markovnikov manner, in contrast to that observed for the reactions described in Chapter 2. Intramolecular hydrogen bonding interaction between the OH group and the OCOCF₃ ligand, with a donor acceptor distance (O2···O3) of 2.6767(1) Å, is observed in **31-H₂O**. Complex **31-H₂O** has co-crystallized with B(C₆F₅)₃·H₂O (Figure 36). The water molecule in B(C₆F₅)₃·H₂O shows an intermolecular hydrogen bonding interaction with the OH group in **31-H₂O**, with a donor acceptor distance (O4···O2) of 2.4853(1) Å.
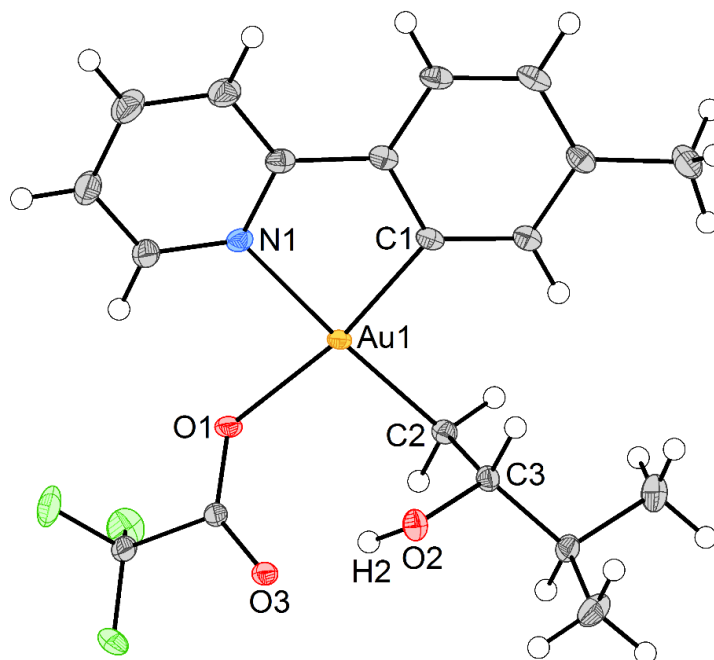
Figure 35. ORTEP plot of **31-H₂O** with 50% ellipsoids. B(C₆F₅)₃·H₂O was removed for clarity. For full structure including the co-crystallized B(C₆F₅)·H₂O, see Figure 36.

Table 11. Selected bond distances [Å] and angles [°] for **31-H₂O**.

Bond distances [Å]		Angles [°]	
Au1-N1	2.1190(14)	O1-Au1-N1	90.30(5)
Au1-C1	2.0026(16)	N1-Au1-C1	81.85(6)
Au1-O1	2.1189(12)	C1-Au1-C2	93.53(7)
Au1-C2	2.0497(16)	C2-Au1-O1	94.68(6)
C2-C3	1.524(2)	C1-Au1-O1	170.20(6)
C3-O2	1.4424(19)	N1-Au1-C2	173.97(6)
O2⋯O3	2.6767(1)		
O2⋯O4	2.4853(1)		
O4⋯B1	1.5546(1)		
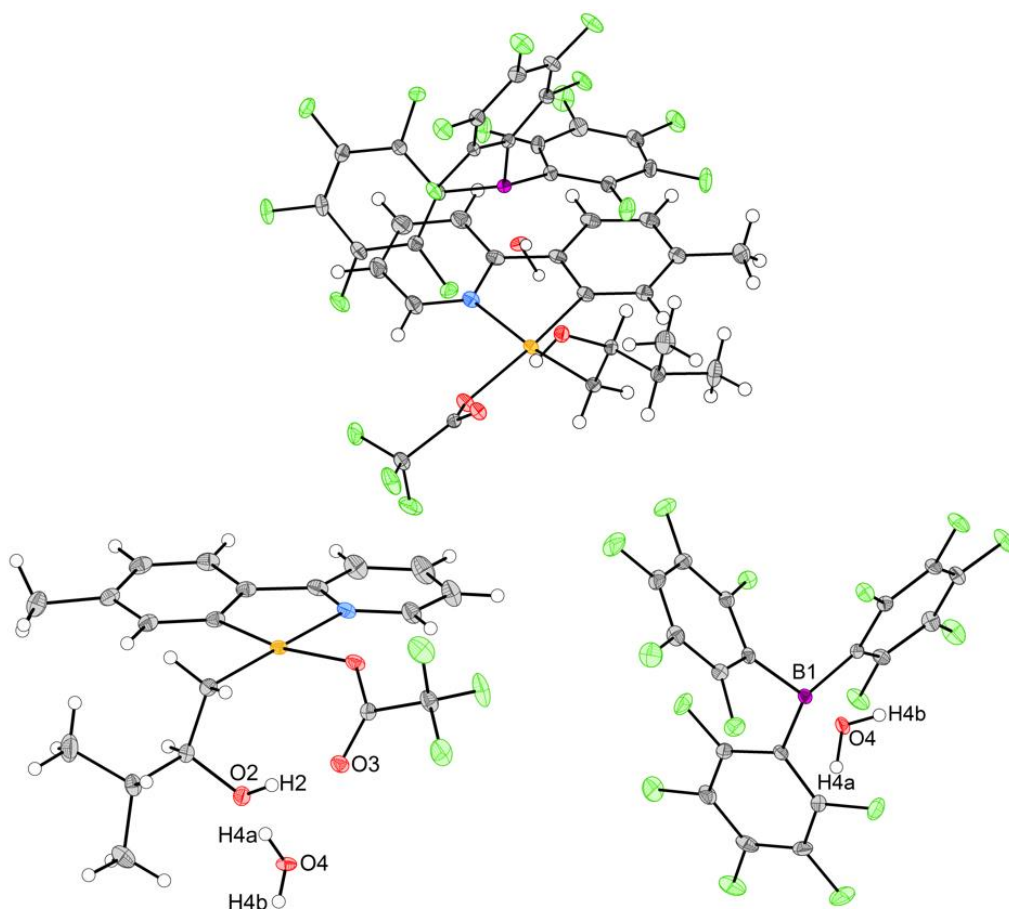
Figure 36. ORTEP plots of **31-H₂O** with 50% ellipsoids. Left: **31-H₂O** and its interaction with the co-crystallized water molecule. Top: **31-H₂O** and B(C₆F₅)₃·H₂O. Right: The co-crystallized B(C₆F₅)₃·H₂O moiety.

Complex **31-H₂O** has the nearly square planar geometry which is commonly observed for Au(III) complexes, with the N1-Au1-C1 chelate angle deviating from the idealized 90° to 81.85(6)°. The Au-ligand distances, Au1-N1, Au1-C1, and Au1-O1 are similar to those of the related complexes discussed in Chapter 2. The Au-C2 bond distance in **31-H₂O** (2.0497 Å) is similar to that reported for the closely related complex **6b** (2.055(9) Å). Unfortunately, attempts at growing crystals of complex **31b** under dry conditions has not yet led to crystals of sufficient quality for crystallographic structure determination.

104

6.3 Synthesis and characterization of Au(III) η^1 allyl complex 32

It was desirable to synthesize a Au(III) complex analogous to that of **31a**, but without substituents on the double bond of the allyl group and with a Cl or Br ligand *trans* to tpy-*C*. In this putative complex, abstraction of the halide *trans* to tpy-*C* (*e.g.* with an Ag(I) salt) would lead to an open coordination site where the double bond of the allyl group could coordinate. Complex **32**, with an η^1 allyl group *trans* to tpy-*N* and Br *trans* to tpy-*C*, was synthesized by using the previously reported monoalkylation procedure[89] developed in the Tilset research group (Scheme 84). Reacting complex **2** with allylmagnesium bromide led to complex **32** in 52-69% yield. Complex **32** was characterized by NMR, MS, elemental analysis and X-ray diffraction analysis (*vide infra*). In the ^{1}H NMR spectrum of **32**, the characteristic resonances of the protons on the allyl ligand are observed; the resonances of the three vinylic protons are found at δ 6.28 (H^b, see labelling Scheme 84), δ 5.48 (H^c), and δ 5.02 (H^d) with $^3J_{trans}$ = 17.0 Hz, $^3J_{cis}$ = 10.0 Hz, and $^2J_{geminal}$ = 2.2 Hz. The two H^a are found as a doublet at δ 3.39. A ^{1}H-^{1}H NOESY experiment established that the η^1 allyl ligand is located *trans* to tpy-*N*; a NOE is observed between H$^{6'}$ and H^a, H$^{6'}$ and H^b, and H$^{6'}$ and H^c. The observed selectivity is in agreement with that reported previously in the Tilset group with reactions analogous to that in Scheme 84 (see Chapter 1).[89] The presence of Br was confirmed by MS (including HRMS).
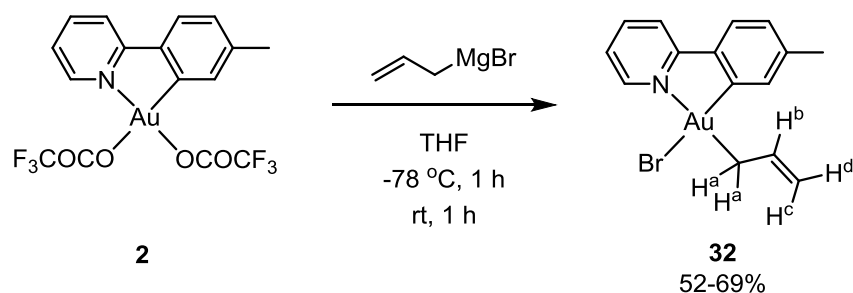
Scheme 84. Synthesis of η^1 allyl complex **32**. The protons of the allyl ligand have been labelled a-d to simplify the NMR discussions.

6.4 Generation and characterization of a Au(III) η^3 allyl complex

Upon adding AgNTf$_2$ to a solution of complex **32** in CD$_2$Cl$_2$ an immediate reaction was observed by ^{1}H NMR (Figure 37); transformation of **32** into one major product together with traces of what is believed to be a decomposition product (*ca.* 5-10%) was observed. The product of the reaction is thought to be complex **33**, where the double bond of the η^1 allyl ligand in **32** now has coordinated at the open coordination site generated *trans* to tpy-*C* (by abstraction of Br with Ag$^+$) to form a η^3 bonded allyl ligand. Complex **33** was characterized by NMR and X-ray diffraction analysis (*vide infra*). Comparing the ^{1}H NMR spectrum of complex **33** with that of complex **32** (Figure 37 and Table 12) shows that H^b and H^d are found at higher ppm values in **33** compared to in **32** (Δδ = 0.22 (H^b) and 0.66 (H^d)) whereas, H^c is observed at a lower ppm value in **33** compared to **32** (Δδ = −0.18). The two H^a are

found at a higher ppm value going from **32** to **33** ($\Delta\delta$ = 0.41). The downfield shift of the resonances of H^b and H^d are similar to, or smaller than, the corresponding shifts for the vinylic protons of Au(III) alkene complexes **A**, **B-ethylene**, **and B-cyclopentene** in Figure 32 ($\Delta\delta$ = 0.56-0.84, Table 10). The upfield shift of H^c is similar to, or slightly smaller than, that of complexes **B-norbornene** and **D** ($\Delta\delta$ = −0.22 and −0.46, respectively, Figure 32 and Table 10). Complex **33** can be described by the two Lewis structures **33** and **33'** (Scheme 85). The NMR data suggest that **33** is the main contributing structure; three protons are observed in the vinylic region (H^b, H^c, and H^d; see Table 12) of the ^{1}H NMR spectrum and the two H^a are found at a significantly lower ppm value. This can be explained by the thermodynamic preference of having the high *trans* influence C(sp^3) end of the allyl ligand *trans* to the lower *trans* influence ligand tpy-*N*, instead of the higher *trans* influence tpy-*C*.
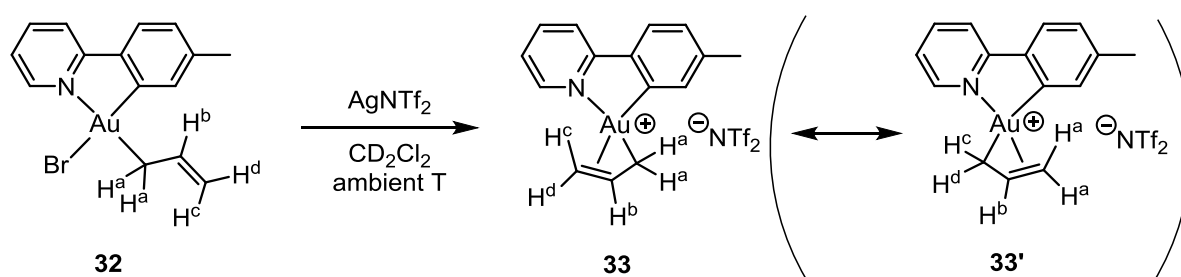
Scheme 85. Generation of complex **33** from **32** and AgNTf$_2$. The protons of the allyl ligand have been labelled a-d to simplify the NMR discussions.

Complex **33** slowly decomposes at ambient temperature and NMR characterization was therefore performed at lower temperature (7 °C). At 7 °C, the resonances of H^a, H^d, and H^6 are significantly broadened (Figure A43, Appendix V). Several of the resonances in the ^{13}C NMR spectrum are also broadened including C^6, $C^{6'}$, C^b, $C^{c,d}$, and C^a (Figure A44, Appendix V). Furthermore, the resonance at *ca*. δ 151, which probably belongs to C-Au, is broadened into the baseline and could only be observed indirectly by a ^{1}H-^{13}C HMBC experiment. It is worth noticing that the broadened resonances are associated with the atoms close to the Au center. The broadening observed in the ^{1}H NMR and ^{13}C NMR spectra could indicate a dynamic behavior during the time scale of the NMR experiments, but further work will be needed in order to get a proper insight into these processes. In the ^{1}H-^{1}H NOESY spectrum of complex **33** (Figure 38), a NOE correlation between H^a and $H^{6'}$ and between H^b and $H^{6'}$ is observed. Furthermore, a NOE between H^d and H^6 is observed, indicating a coordination of the double bond to Au. In contrast, H^c (bonded to the same C as H^d) shows a NOE with $H^{6'}$, but upon increasing the intensity of the peaks in the NOESY spectrum, what appears to be a weak NOE between H^c and H^6 becomes visible. These observations might indicate an interconversion between **33**, with the allyl ligand bound in an η^3 fashion, and the corresponding η^1 complex during the time scale of the NMR experiment. Another possible explanation could be that a bridging dimeric species like that shown to the right in Figure 31 is formed in solution. Based on only the NMR characterization, it cannot

be determined for certain whether the monomeric complex **33** or a bridging dimeric complex has been formed. Complex **33** has not been isolated from the CD$_2$Cl$_2$ solution in which it was generated.

Table 12. δ(^{1}H) for the allylic moiety of complexes **32**, **31b**, and **33**. Δδ = δ$_{33}$ − δ$_{32}$.

	32	31b	33 (Δδ)
H^a	δ 3.39	δ 3.66	δ 3.80 (+0.41)
H^b	δ 6.28	δ 5.76	δ 6.50 (+0.22)
H^c	δ 5.48	-	δ 5.30 (−0.18)
H^d	δ 5.02	-	δ 5.68 (+0.66)
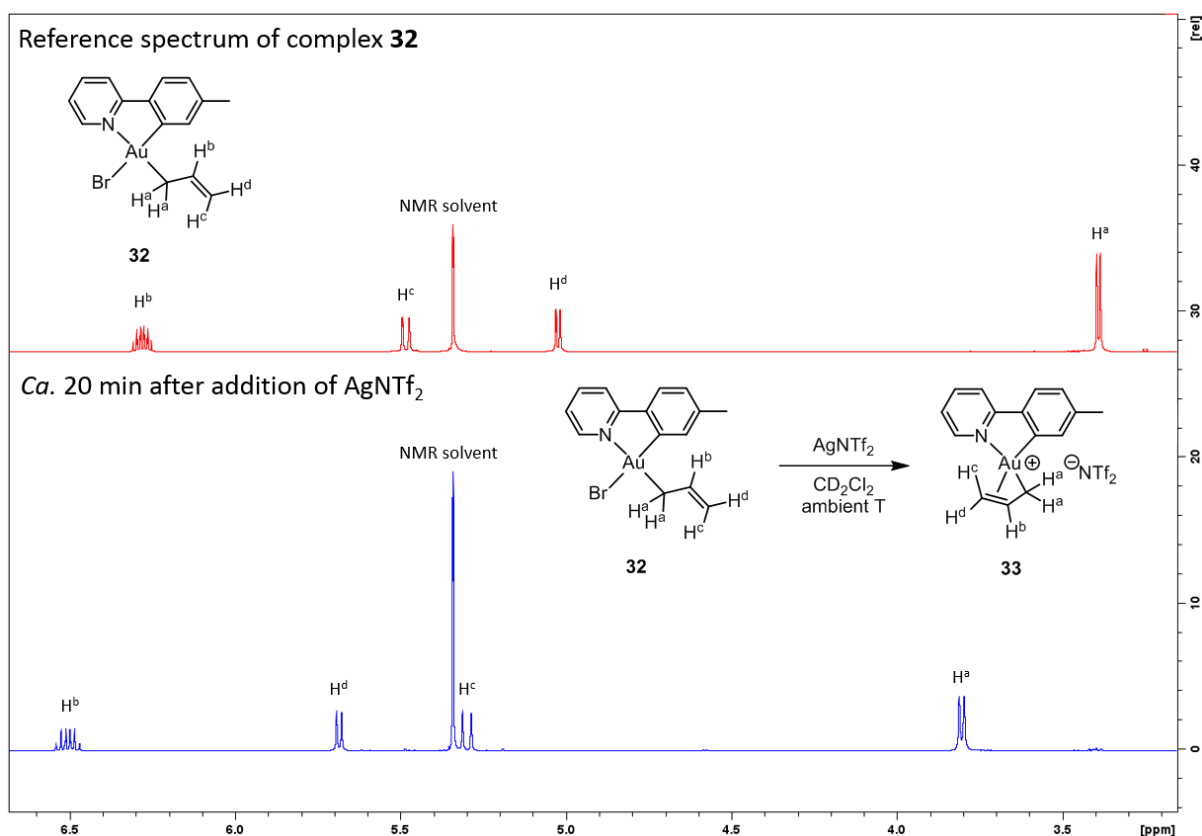
Figure 37. Stacked ^{1}H NMR (800 MHz (top) or 600 MHz (bottom), CD$_2$Cl$_2$) spectra of the reaction of **32** with AgNTf$_2$ forming complex **33**. Top: Reference spectrum of complex **32**. Bottom: Spectrum acquired *ca.* 20 min after addition of AgNTf$_2$. Only parts of the ^{1}H NMR spectra are shown.
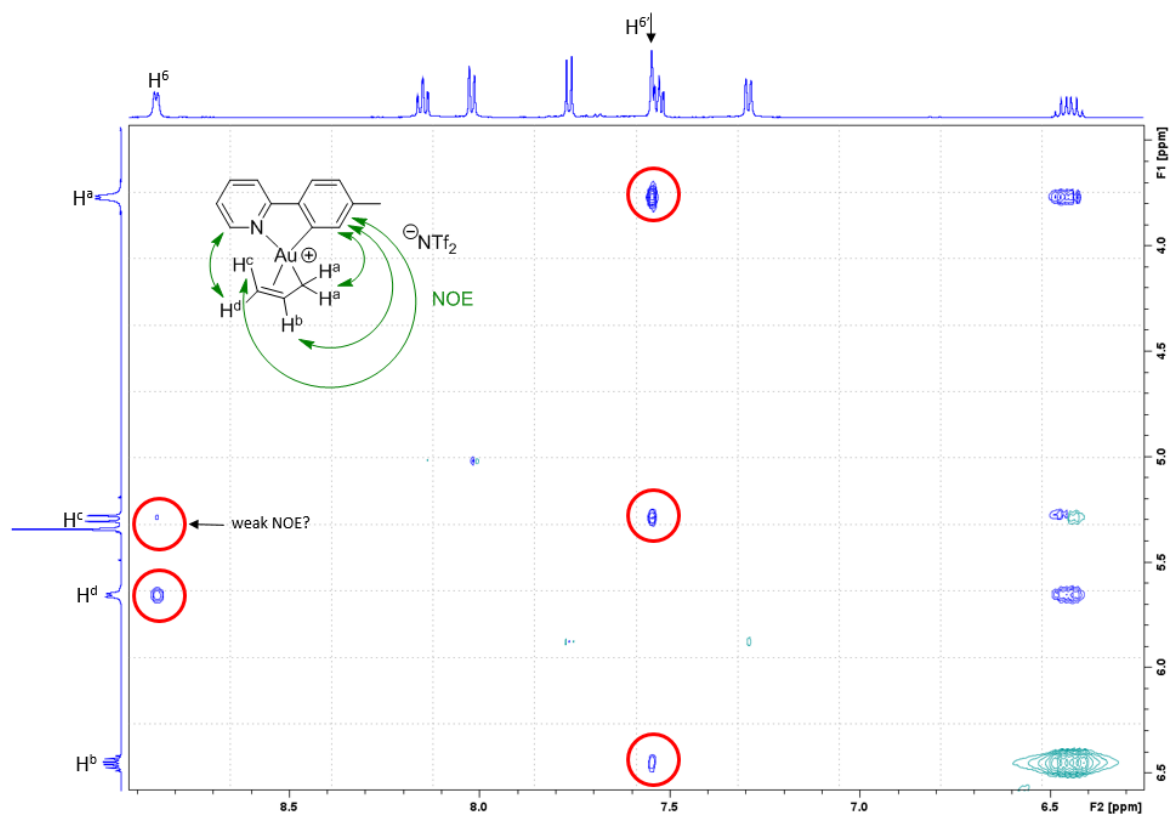
Figure 38. ^{1}H-^{1}H NOESY (600 MHz, CD$_2$Cl$_2$, mixing time = 1 s) of complex **33**.

6.5 Crystallographic structure determination of complexes 32 and 33

The crystals of complexes **32** and **33** were not of sufficient quality to be measured at our home facility for single crystal X-ray diffraction analysis. However, we got the chance to perform measurements at the Swiss-Norwegian beamline (SNBL, BM01) at the European Synchrotron Radiation Facility (ESRF) in Grenoble, France, and the molecular structures of complexes **33** and **32** were obtained. The measurements at ESRF were performed with help from Dr. Dmitry Chernyshov and the structures were solved by Dr. Sigurd Øien-Ødegaard.

The preliminary molecular structure of complex **32** is shown in Figure 39. The structure is in full agreement with that observed by NMR; the η^1 allyl ligand is located *trans* to tpy-*N* and Br is located *trans* to tpy-*C*. Due to complex twinning in the measured crystal, the refinement is not completed yet. Metrical parameters are therefore not given.

The ORTEP plot of complex **33** is given in Figure 40 and metrical parameters are given in Table 13. The molecular structure of complex **33** is in agreement with the structure that was predicted based on the NMR analysis. The formation of a monomeric species with the double bond of the allyl ligand coordinated to Au, *trans* to tpy-*C*, is evident.
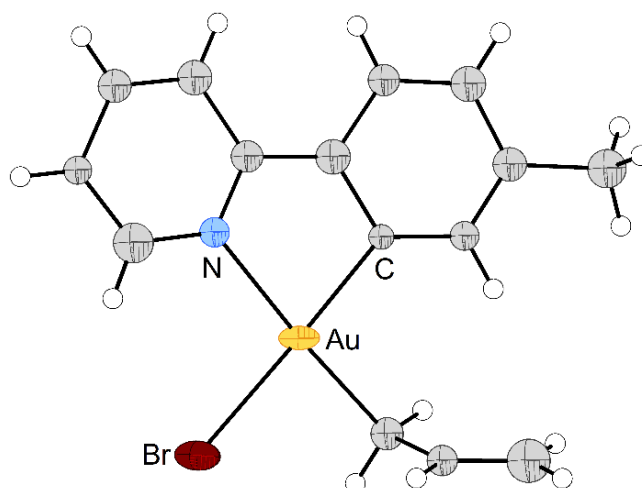
Figure 39. Preliminary molecular structure of complex **32**. Due to complex twinning in the measured crystal, the refinement is not completed yet. The data set was obtained with help from Dr. Dmitry Chernyshov (SNBL, ESRF).

Because of the η^3 allyl ligand, complex **33** deviates more from the ideal square planar geometry than the other complexes presented in this thesis. The C1-Au1-N1, C4-Au1-N1, C2-Au1-C4, and C1-Au1-C2 angles all deviate from the idealized 90° to 81.0(7)°, 110.0(8)°, 65.3(8)°, and 103.8(8)°, respectively. The C3-C4 bond length of 1.23(4) Å is significantly shorter than the C2-C3 bond length of 1.42(3) Å, indicating that the double bond character has been retained upon coordination to Au, in agreement with the NMR observations. The Au1-C2 bond length of 2.065(19) Å is shorter than the Au1-C3 and Au1-C4 bond lengths (2.21(2) Å and 2.35(2) Å, respectively), indicating that C2 is more tightly bound to Au than C3 and C4. The ellipsoids of C3 and C4 are more elongated than that of C2, because of a higher dynamic disorder, indicating a looser coordination the double bond to Au (Figure 41).
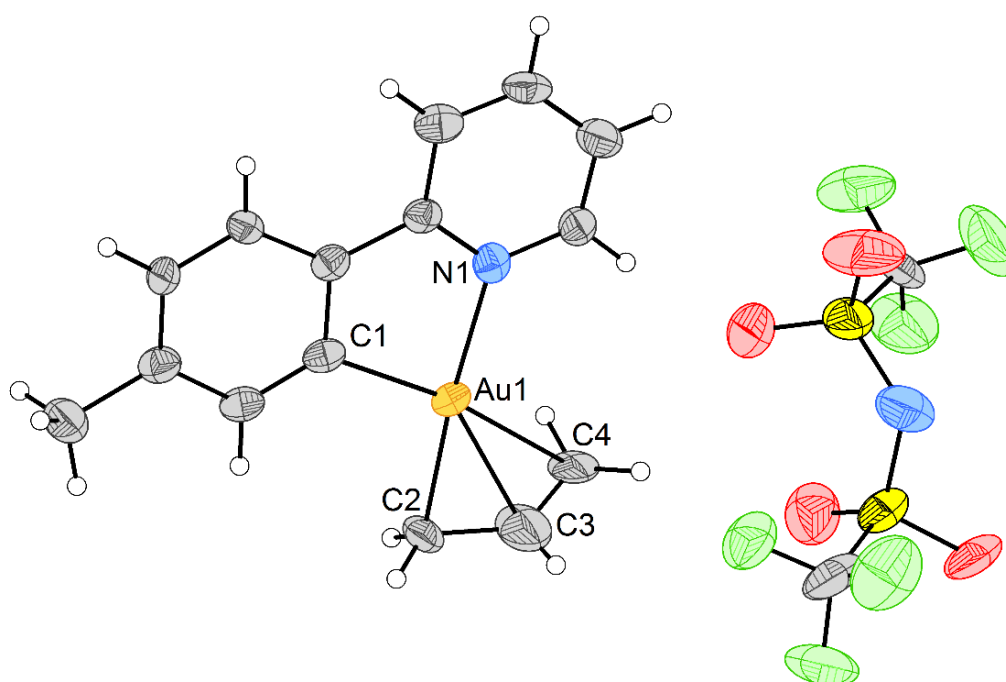
Figure 40. ORTEP plot of complex **33** with 50% ellipsoids. The data set was obtained with help from Dr. Dmitry Chernyshov (SNBL, ESRF) and the structure was solved by Dr. Sigurd Øien-Ødegaard.

Table 13. Selected bond distances [Å] and angles [º] for complex **33**.

Bond distances [Å]		Angles [º]	
Au1-N1	2.117(16)	C4-Au1-N1	110.0(8)
Au1-C1	2.04(2)	N1-Au1-C1	81.0(7)
Au1-C2	2.065(19)	C1-Au1-C2	103.8(8)
Au1-C3	2.21(2)	C2-Au1-C4	65.3(8)
Au1-C4	2.35(2)	C2-Au1-C3	38.6(9)
C2-C3	1.42(3)	C3-Au1-C4	31.2(9)
C3-C4	1.23(4)	C1-Au1-C4	166.2(9)
		N1-Au1-C2	175.2(7)
		C2-C3-C4	129(3)
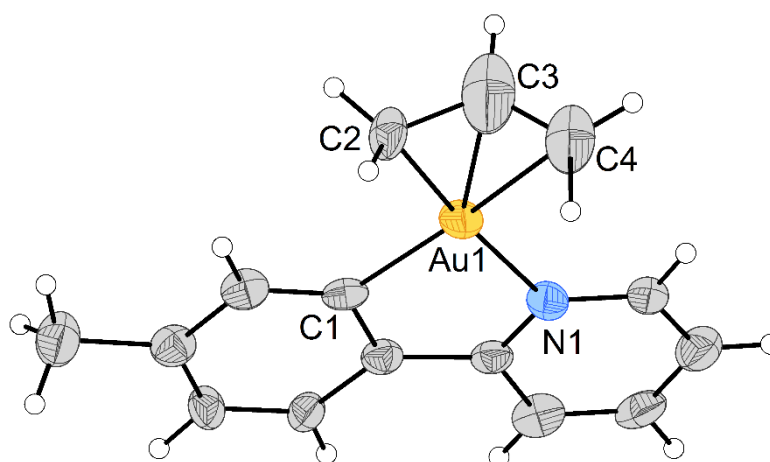
Figure 41. ORTEP plot of the cation of complex **33** with 50% ellipsoids showing the dynamic disorder of C3 and C4.

6.6 Conclusions

In conclusion, the generation of Au(III) η^1 and η^3 allyl complexes have been presented. Whereas the η^1 allyl complex **32** has been thoroughly characterized, there are still more work to be done on the η^3 allyl complexes to confidently be able to assign their structures. Good indications of the formation Au(III) η^3 allyl complexes have however been obtained by NMR characterization and single crystal X-ray diffraction analysis, and further work will hopefully lead to a better understanding of the structure and behavior of this class of Au(III) complexes.

6.7 Experimental

The experimental details for the reactions described in Chapter 6 are included herein.

General procedures

Complex **2** was synthesized as reported previously.[89] CD_2Cl_2 was dried over molecular sieves prior to use. CH_2Cl_2 and THF were purified using a MB SPS-800 solvent purifying system from MBraun. All solvents (including NMR solvents) utilized inside the glove box were dried over molecular sieves and degassed by the freeze pump thaw method prior to use. Distilled water was used in the work up of complex **32**. All other reagents and solvents were used as received. An inert atmosphere glove box of the type UNIlab Pro from MBraun was used. All glassware were dried prior to use and all reactions were performed under argon in the absence of light, except for the work up of complex **32**. NMR spectra were recorded on Bruker Avance AVI600 and AVIIIHD800. ^1H and ^{13}C NMR spectra have been referenced relative to the residual solvent signals (CD_2Cl_2: $\delta(^1H)$ 5.34, $\delta(^{13}C)$ 53.84). The peaks in the ^1H NMR spectra were assigned by the aid of 2D NMR techniques such as COSY, HSQC, HMBC, and NOESY according to the numbering scheme shown in Figure 1. Mass spectra (ESI) were obtained on a Bruker maXis II ETD spectrometer by Osamu Sekiguchi (University of Oslo). Elemental analysis was performed by Microanalytisches Laboratorium Kolbe, Mülheim an der Ruhr, Germany.

Generation of complex 31b

Complex **6b** (5 mg, 0.009 mmol, 1 equiv) was dissolved in CD_2Cl_2 and added to $B(C_6F_5)_3$ (6 mg, 0.01 mmol, 1 equiv) inside a glove box. The solution was transferred to a NMR tube, and the NMR tube was taken out of the glove box. After *ca*. 20 min, the reaction mixture was investigated by ^1H NMR. One major product was formed together with *ca.* 10% impurities and/or decomposition products (determined by ^1H NMR integration). The major product is tentatively assigned to be complex **31b**. Due to decomposition over time, only NMR characterization was performed. Complex **31b** has not been isolated from the CD_2Cl_2 solution in which it was generated.

^1H NMR (800 MHz, CD_2Cl_2): δ 8.20 (d, 1H, *J* = 5.4 Hz, **H⁶**), 8.17 (ddd, 1H, *J* = 8.0, 7.6, 1.5 Hz, **H⁴**), 8.07 (d, 1H, *J* = 8.2 Hz, **H³**), 7.80 (d, 1H, *J* = 7.8 Hz, **H³'**), 7.57 (ddd, 1H, *J* = 7.4, 5.5, 1.2 Hz, **H⁵**), 7.51 (s, 1H, **H⁶'**), 7.30 (d, 1H, *J* = 7.8 Hz, **H⁴'**), 5.76 (t, *J* = 9.6 Hz, **H^b**), 4.02 (br. s, unknown), 3.66 (d, 2H, *J* = 9.6 Hz, **H^a**), 3.55 (br. s, unknown), 2.59 (s, 3H, CH₃^e), 2.45 (s, 3H, ArCH₃), 2.08 (s, 3H, CH₃^d).

^{13}C NMR (201 MHz, CD_2Cl_2): δ 21.8 (Ar**C**H₃), 21.9 (s, 3H, CH₃^d), 26.4 (s, 3H, CH₃^e), 46.2 (**C**H₂^a), 111.9 (**C**H^b), 121.7 (Ar**C**H), 125.3 (Ar**C**H), 126.8 (Ar**C**H), 130.4 (Ar**C**H), 137.3 (Ar**C**H), 143.5 (Ar**C**H), 147.8 (Ar**C**H). Quaternary carbons are not given because the ^{13}C NMR spectrum was very crowded due to decomposition with time.

Reactivity of complex 5b towards B(C₆F₅)₃

Complex **5b** (5 mg, 0.008 mg, 1 equiv) was dissolved in CD_2Cl_2 and added to $B(C_6F_5)_3$ (6 mg, 0.01 mmol, 1 equiv) inside a glove box. The solution was transferred to a NMR tube, and the NMR tube was taken out of the glove box. Investigation of the reaction by ^{1}H NMR immediately after mixing revealed that all of **5b** had reacted to form a complicated reaction mixture. At least three different species have been formed and there are several resonances in the vinylic region of the ^{1}H NMR spectrum. The products of the reaction have not been identified.

Synthesis of complex 32

Complex **2** (200.0 mg, 0.3383 mmol, 1.0 equiv) was dissolved in THF and cooled down to *ca*. -78 °C (dry ice/acetone). Allyl magnesium bromide (0.50 mL 1.0 M solution in Et_2O, 0.50 mmol, 1.5 equiv) was added and the solution was stirred at *ca.* −78 °C in the absence of light for 1 h, followed by stirring at ambient temperature for 1 h. The volatiles were removed under reduced pressure and the remaining solid was dissolved in CH_2Cl_2 (50 mL). The solution was filtered and washed with distilled water (4 x 25 mL, pH ≈ 7). CH_2Cl_2 (100 mL) was added and the organic phase was dried over Na_2SO_4 and filtered. The solvent was removed under reduced pressure and the resulting solid was purified by flash chromatography (silica gel 60, CH_2Cl_2) furnishing complex **32** (99.7 mg, 0.205 mmol, 61%) as a white solid.

^{1}H NMR (800 MHz, CD_2Cl_2): δ 9.54 (ddd, 1H, J = 5.5, 1.5, 0.7 Hz, **H⁶**), 7.99 (ddd, 1H, J = 8.0, 7.5, 1.6 Hz, **H⁴**), 7.92 (d, 1H, J = 8.1 Hz, **H³**), 7.69 (d, 1H, J = 7.8 Hz, **H³'**), 7.52 (s, 1H, **H⁶'**), 7.43 (ddd, 1H, J = 7.4, 5.6, 1.2 Hz, **H⁵**), 7.23 (dq, 1H, J = 7.8, 0.7 Hz, **H⁴'**), 6.28 (ddt, 1H, $^3J_{trans}$ = 17.0 Hz, $^3J_{cis}$ = 10.0 Hz, $^3J_{Ha-Hb}$ = 8.2 Hz, **Hᵇ**), 5.48 (ddt, 1H, $^3J_{trans}$ = 17.0 Hz, $^2J_{gem}$ = 2.2 Hz, $^4J_{Ha-Hc}$ = 0.9 Hz, **Hᶜ**), 5.02 (dd, 1H, $^3J_{cis}$ = 10.0 Hz, $^2J_{gem}$ = 2.2 Hz, **Hᵈ**), 3.39 (d, 1H, $^3J_{Ha-Hb}$ = 8.1 Hz, **Hᵃ**), 2.48 (s, 3H, Ar**CH₃**).

¹³C NMR (201 MHz, CD_2Cl_2): δ 161.9 (Ar**C**), 149.5 (Ar**C**), 149.3 (Ar**C**), 142.6 (Ar**C**), 141.5 (Ar**C**), 141.0 (Ar**C**), 139.0 (**CH**ᵇ), 130.7 (Ar**C**), 128.8 (Ar**C**), 125.6 (Ar**C**), 124.2 (Ar**C**), 119.9 (Ar**C**), 114.9 (**CH₂**ᶜ,ᵈ), 34.2 (**CH₂**ᵃ), 22.1 (Ar**CH₃**). The resonance at δ 149.5 appear as a doublet due to insufficient ^{1}H decoupling.

MS (ESI, MeCN): *m/z* (rel. %): 508/510 ([M+Na]⁺, 8/8), 406 ([M−Br]⁺, 100), 360 (27).

HRMS (ESI, MeCN): Found: 507.9944; calcd. for $C_{15}H_{15}Au^{79}BrNNa$: 507.9946, Found: 406.0864; calcd. for $C_{15}H_{15}AuN$ 406.0865.

Elemental analysis: Anal. calcd. for $C_{15}H_{15}AuBrN$: C, 37.06; H, 3.11; N, 2.88. Found: C, 37.17; H, 3.10; N, 2.82.

Generation of complex 33

Complex **32** (5 mg, 0.01 mmol, 1 equiv) was dissolved in CD_2Cl_2 and added to $AgNTf_2$ (6 mg, 0.02 mmol, 2 equiv) inside a glove box. A white precipitate was formed immediately after the addition to $AgNTf_2$. The solution was transferred to a NMR tube and the NMR tube was taken out of the glove box. ^{1}H NMR *ca.* 20 minutes after mixing revealed that one major product (**33**) was formed together with small amounts (*ca.* 5-10%) of what is believed to be a decomposition product. Complex **33** has not been isolated and was only characterized in the CD_2Cl_2 solution in which it was generated in. Complex **33** decomposes over time at ambient temperature, therefore the NMR characterization was performed at 7 °C.

^{1}H NMR (600 MHz, CD_2Cl_2, 27 °C): δ 8.84 (d, 1H, J = 5.2 Hz, **H⁶**), 8.16 (ddd, 1H, J = 8.0, 7.8, 1.5 Hz, **H⁴**), 8.03 (d, 1H, J = 8.2, **H³**), 7.78 (d, 1H, J = 8.0 Hz, **H³'**), 7.56 (s, 1H, **H⁶'**), 7.53 (ddd, 1H, J = 7.5, 5.7, 1.2 Hz, **H⁵**), 7.31 (dq, 1H, J = 7.9, 0.6 Hz, **H⁴'**), 6.50 (ddt, 1H, $^3J_{trans}$ = 15.9 Hz, $^3J_{cis}$ = 8.9 Hz, $^3J_{Ha-Hb}$ = 8.9 Hz, **H^b**), 5.68 (d, 1H, $^3J_{cis}$ = 8.9 Hz, **H^d**), 5.30 (d, 1H, $^3J_{trans}$ = 15.8 Hz, **H^c**), 3.80 (d, 1H, $^3J_{Ha-Hb}$ = 8.9 Hz, **H^a**), 2.46 (s, 3H, ArC**H₃**).

^{1}H NMR (600 MHz, CD_2Cl_2, 7 °C): δ 8.85 (br. d, 1H, J = 5.3 Hz, **H⁶**), 8.15 (ddd, 1H, J = 8.0, 7.7, 1.5 Hz, **H⁴**), 8.02 (d, 1H, J = 8.2, **H³**), 7.76 (d, 1H, J = 7.9 Hz, **H³'**), 7.55 (s, 1H, **H⁶'**), 7.53 (ddd, 1H, J = 7.5, 5.7, 1.2 Hz, **H⁵**), 7.29 (d, 1H, J = 7.9 Hz, **H⁴'**), 6.45 (ddt, 1H, $^3J_{trans}$ = 15.9 Hz, $^3J_{cis}$ = 8.9 Hz, $^3J_{Ha-Hb}$ = 8.9 Hz, **H^b**), 5.65 (br. d, 1H, $^3J_{cis}$ = 8.5 Hz, **H^d**), 5.29 (d, 1H, $^3J_{trans}$ = 15.8 Hz, **H^c**), 3.77 (br. d, 1H, $^3J_{Ha-Hb}$ = 8.2 Hz, **H^a**), 2.44 (s, 3H, ArC**H₃**).

^{13}C NMR (151 MHz, CD_2Cl_2, 7 °C): δ 162.3 (br., Ar**C**), 153.1 (br., **C**H⁶), *ca.* 151 (Ar**C**), 143.9 (Ar**C**), 142.8 (**C**H⁴), 141.3 (Ar**C**), 135.5 (br., **C**H⁶'), 134.6 (br., **C**H^b), 130.0 (**C**H⁴'), 126.2 (**C**H³'), 125.4 (**C**H⁵), 121.0 (**C**H³), 119.9 (q, J = 322.2 Hz, **C**F₃), 106.1 (br., **C**H₂^{c,d}), 49.8 (br., **C**H₂^a), 21.7 (Ar**C**H₃). The resonance at *ca.* δ 151 was broadened into the baseline, and was only observed indirectly in a ^{1}H-^{13}C HMBC experiment.

Crystallographic structure determination of complexes 31-H₂O, 32, and 33

Single crystal diffraction data for complex **31-H₂O** was acquired by Dr. Sigurd Øien-Ødegaard on a Bruker D8 Venture equipped with a Photon 100 detector and using Mo Kα radiation (λ = 0.71073 Å) from an Incoatec iµS microsource. Data reduction was performed with the Bruker Apex3 Suite,[115] the structure was solved with ShelXT[116] and refined with ShelXL.[117] Olex2 was used as user interface.[118] The cif files were edited with enCIFer v1.4,[119] and molecular graphics were produced with Diamond v4.4.0.[120] Data sets for complexes **32** and **33** were obtained at the Swiss-Norwegian beamline (SNBL, BM01)[135] at the European Synchrotron Radiation Facility (ESRF) in Grenoble, France. For complex **33**, two crystals were measured and the two data sets were merged after data reduction using least-

squares fitting of common reflections in XPREP.[115] The measurements at ESRF were performed with help from Dr. Dmitry Chernyshov (SNBL, ESRF) and crystal structures were solved by Dr. Sigurd Øien-Ødegaard.

Complex 31-H₂O

Crystals suitable for single crystal X-ray diffraction analysis of complex **31-H₂O** was obtained by placing a solution of **31b** generated *in situ* from **6b** and $B(C_6F_5)_3$ in CD_2Cl_2 in a small vial. The small vial was placed inside a capped larger vial containing pentane and placed inside a fridge (*ca.* 10 ^{o}C) , slowly yielding crystals of **31-H₂O**.

Complex 33

Complex **33** was generated *in situ* from complex **32** (5 mg, 0.01 mmol, 1 equiv) and $AgNTf_2$ (7 mg, 0.02 mmol, 2 equiv) in CH_2Cl_2 (1-2 mL) inside a glove box. After 1-2 minutes, the solution was filtered and the filtrate was distributed between two small vials. Each of the vials were placed in one capped larger vial each containing pentane, and placed in a freezer inside the glove box (−36 ^{o}C) slowly yielding crystals of **33**. The vials were taken out of the glovebox (while still cold and closed) and placed in a dry ice-cooled dewar. The crystals were mounted in a cold room at 4 ^{o}C by Dr. Sigurd Øien-Ødegaard with help from Dr. Kaare Bjerregaard-Andersen (Bio[3]- Chemical Life Sciences, University of Oslo) and stored in a dewar cooled by liguid nitrogen which was shipped to ESRF. The crystals were kept in the cooled dewar until they were measured.

Complex 32

Crystals suitable for single crystal X-ray diffraction analysis of complex **32** were obtained by placing a solution of **32** in a small vial placed inside a capped larger vial containing pentane. The vial was placed inside a freezer (−36 ^{o}C) slowly yielding crystals of **32**. The crystals of **32** were also measured at ESRF and for simplicity, they were mounted and shipped the same way as the crystals of **33**, even though complex **32** is not sensitive to air or moisture.

Table 14. Crystal and refinement data for Au(III) complex **31-H$_2$O**.
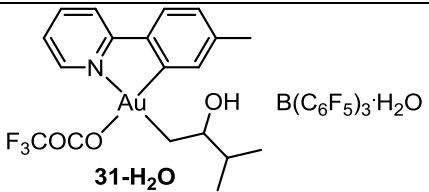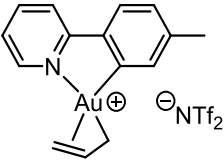
Crystal data	
Identification code	msh-406
Chemical formula	C$_{19}$H$_{21}$AuF$_3$NO$_3$·C$_{18}$BF$_{15}$·H$_2$O
M_r	1095.34
Crystal system, space group	Triclinic, P-1
Temperature (K)	100
a, b, c (Å)	11.2540(7), 12.3431(7), 14.8317(9)
α, β, γ (°)	110.695(1), 97.054(1), 103.275(1)
V (Å^3)	1828.15(19)
Z	2
Radiation type	Mo $K\alpha$
μ (mm^{-1})	4.16
Crystal size (mm)	0.33 x 0.12 x 0.01
Data Collection	
Diffractometer	Bruker D8 Venture, CMOS detector diffractometer
Absorption correction	Multi-scan SADABS2014/5 (Bruker, 2014/5) was used for absorption correction. wR2(int) was 0.1308 before and 0.0374 after correction. The Ratio of minimum to maximum transmission is 0.7037. The λ/2 correction factor is Not present.
T$_{min}$, T$_{max}$	0.525, 0.746
No. of measured, independent and observed [I > 2σ(I)] reflections	37401, 10681, 10113
R_{int}	0.025
(sin θ/λ)max (Å^{-1})	0.704
Refinement	
$R[F^2 > 2\sigma(F^2)]$, $wR(F^2)$, S	0.017, 0.038, 1.05
No. of reflections	10681
No. of parameters	573
No. of restraints	0
H-atom treatment	H atoms treated by a mixture of independent and constrained refinement
	$w = 1/[\sigma^2(F_o^2) + (0.009P)^2 + 1.548P]$ where $P = (F_o^2 + 2F_c^2)/3$
Δρ$_{max}$, Δρ$_{min}$ (e Å^{-3})	0.80, -0.77

Table 15. Crystal and refinement data for Au(III) complex **33**.

	33
Crystal data	
Identification code	msh-628-isotropic_tw
Chemical formula	$C_{15}H_{15}AuN \cdot C_2F_6NO_4S_2$
M_r	686.40
Crystal system, space group	Monoclinic, $P2_1/n$
Temperature (K)	100
a, b, c (Å)	6.8423(4), 12.3649(7), 24.7602(11)
α, β, γ (°)	90, 96.956(4), 90
V (Å^3)	2079.40 (19)
Z	4
Radiation type	Synchrotron radiation, $\lambda = 0.78487$ Å
μ (mm^{-1})	9.47
Crystal size (mm)	0.04 x 0.03 x 0.01
Data Collection	
Diffractometer	BM01-ESRF[135]
Absorption correction	Multi-scan (Crysalis, Oxford Diffraction, 2017)
T_{min}, T_{max}	0.897,1.000
No. of measured, independent and observed [$I > 2\sigma(I)$] reflections	2230, 2230, 1883
R_{int}	0.100
$(\sin \theta/\lambda)$max (Å^{-1})	0.505
Refinement	
$R[F^2 > 2\sigma(F^2)]$, $wR(F^2)$, S	0.071, 0.149, 1.26
No. of reflections	2230
No. of parameters	291
No. of restraints	102
H-atom treatment	H-atom parameters constrained
	$w = 1/[\sigma^2(F_o^2) + (0.0204P)^2 + 46.196P]$ where $P = (F_o^2 + 2F_c^2)/3$
$\Delta\rho_{max}$, $\Delta\rho_{min}$ (e Å^{-3})	2.12, -1.28

Chapter 7 – Future prospects

7.1 Scope of the Chapter

There are still a lot of opportunities to follow up in the project presented in this thesis. Indeed, it was very difficult for the author of this thesis to let go of the lab work, since there were so many interesting things to do! In this chapter, ideas for possible future work are presented. This chapter is organized in such a way that possible future work is discussed chapterwise.

7.2 Chapter 2

A natural continuation of the chemistry presented in Chapter 2 would be to try to move from stoichiometric functionalization of alkenes to catalysis, as this would lead to very useful methods for preparing ethers and esters from simple and readily available building blocks. One idea could, for example, be to replace the C(sp^2) end of the chelating tpy ligand with a C(sp^3) ligand (Scheme 86, left) to see if it is possible to circumvent the kinetic preference for protolytic cleavage of Au-C(sp^2) over Au-C(sp^3). Another idea could be to tune the donor properties of the tpy ligand in complex **2** by investigating different substituents on the phenyl pyridine skeleton (Scheme 86, right). However, some work has already been performed in the Tilset group on the latter, and so far no catalysis could be achieved *via* this strategy.[95] Furthermore, expanding the scope of the reactions presented in Chapter 2 even more by investigating other alkenes and nucleophiles is desirable.

R = H, Alkyl, Aryl, etc.   R = EWG or EDG
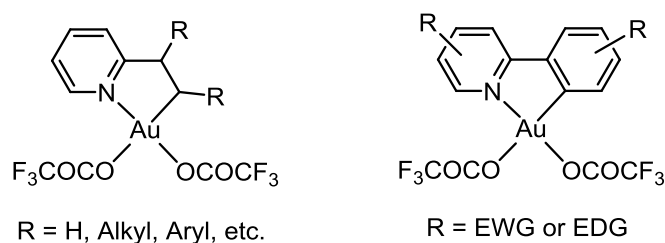
Scheme 86. Possible complexes that could be investigated in the reactions presented in Chapter 2. EWG = electron withdrawing group; EDG = electron donating group.

7.3 Chapter 3

Following the successful synthesis of the two metallacycle complexes **15** and **16** by reaction of complex **2** with ethylene, MeCN, and H_2O (in the presence of CF_3COOH for complex **16**), there is a lot of interesting work that could be undertaken in the continuation of this project. For example, it would be interesting to investigate other nitriles than acetonitrile in the reaction as well as other alkenes. The alkenes 3-methyl-1-butene and styrene have already been investigated by other co-workers,[102, 106] and there are several other alkenes which could be tested out. A co-worker investigated the metallacycle formation by changing the tpy ligand in complexes **15** and **16** with 2-(3,5-dimethylphenyl)pyridine,[136] and it would be interesting to investigate several different ligands

with different donor properties to see if that has an effect on the metallacycle formation. It could also be of interest to investigate the metallacycle formation reaction with acetylene instead of ethylene. The finding that both complexes **15** and **16** release acetamide upon heating in CD₃CN could be further investigated; these complexes might be utilized as catalysts for hydration of more sophisticated nitriles into amides. Further attempts at achieving reductive elimination of the metallacycle unit to release the heterocyclic product could also be carried out.

7.4 Chapter 4

In Chapter 4, the Au(III) catalyzed acetylene trifluoroacetoxylation reaction was presented. Au(III) (*N,C,C*) pincer complex **27** (Figure 42) was found to be the best catalyst for this reaction. However, due to the limitations of the currently used method for the turnover measurements for this reaction, the full potential of complex **27** could not be assessed. A new and improved method for the turnover measurements (for example a method using gas chromatography) should be developed for this reaction. Even though complex **27** was found to be a significantly improved catalyst comparing to that of using complex **2** as a precatalyst, one could try to find an even better catalyst. Of the (*N,C*) Au(III) complexes investigated, complex **2-CF₃** (with a CF₃ substituent on the arylpyridine ligand, Figure 42) was found to be most robust towards the catalysis conditions. Perhaps adding a CF₃ group to the arylpyridine ligand in complex **27** (**27-CF₃**, Figure 42) could lead to an even better catalyst?
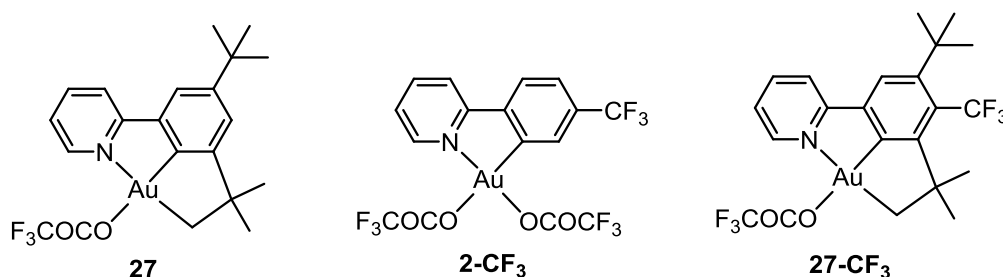
Figure 42. Left and middle: Complexes **27** and **2-CF₃**. Right: Suggested improved catalyst (**27-CF₃**) for the acetylene trifluoroacetoxylation.

Several preliminary experiments where different nucleophiles were investigated in the reaction with acetylene were presented in Chapter 4. Good indications of formation of vinyl acetate and methyl vinyl ether were obtained, and these are results that it would be interesting to investigate further. Finally, investigation of various substituted alkynes are of great interest.

7.5 Chapter 5

Following the successful synthesis of Au(III) (*N,C,C*) pincer complex **27** presented in Chapter 5, it would be of interest to expand the scope of this reaction, since developing a broad method to give easy access to Au(III) pincer complexes is of large interest. It would be interesting to investigate the ligands shown in Figure 43 to see if C(sp^3)-H activation can be achieved with these ligands as well, or if the

steric bulk of the *tert*-butyl ligands is needed for the C(sp^3)-H activation to occur. Finally, it would be interesting to further investigate the potential of complex **27** in catalysis. A co-worker has very recently started investigating complex **27** in catalysis and promising results have already been obtained.
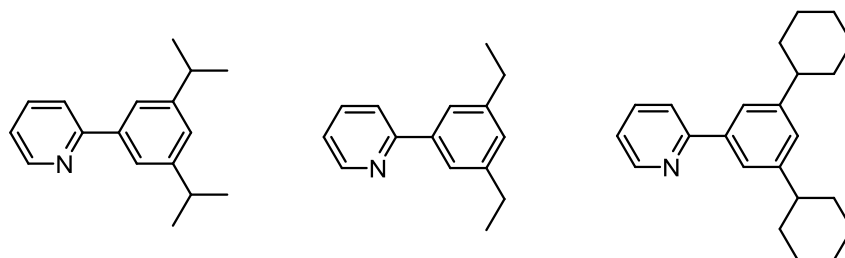
Figure 43. Ligands of interest to investigate if formation of a (*N,C,C*) Au(III) pincer complex is possible.

7.6 Chapter 6

Since the majority of the work described in Chapter 6 is not completed yet, future work will of course be to finish the work started in Chapter 6. For the η^3 allyl complex **33** there are clearly some dynamic behavior occurring during the time scale of the NMR experiment, and it would be interesting to investigate this more to gain further insight into the nature of Au(III) η^3 allyl complexes. Following this, it would be interesting to investigate the η^3 allyl complexes computationally, for example to learn more about the bonding in these complexes. It is also desired to study the reactivity of these complexes further, *e.g.* nucleophilic addition to the η^3 allyl complexes could be investigated. Complex **33** was generated by treating complex **32** with AgNTf$_2$. Following this, it would be interesting to investigate other Ag(I) salts in this reaction. Finally, it would be interesting to check if it is possible generate the Au(III) bis(η^3 allyl) complex shown in Scheme 87. A suggested path to this complex is proposed in Scheme 87 and both the proposed steps are based on previous work performed in the Tilset research group.[38, 89, 92]
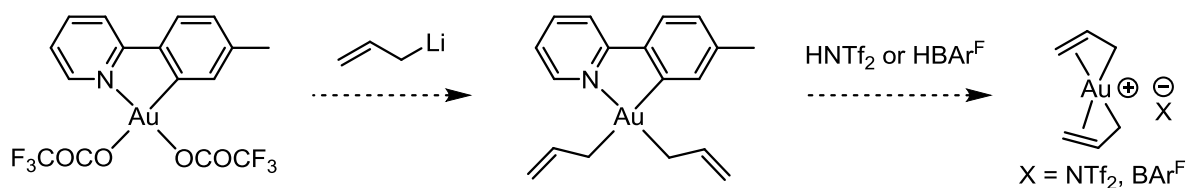
Scheme 87. Suggested route to Au(III) bis(η^3 allyl) complexes.

Even though it is sad to leave this fascinating project now, I hope that this project will continue to develop in the hands of other co-workers in the Tilset group, and I look forward to see what the next steps forward will be in gold chemistry and catalysis.

References

[1]   S. A. Cotton, *Chemistry of Precious Metals*, Blackie Academic and Professional, 1st ed., **1997**.

[2]   C. Louis, O. Pluchery, *Gold Nanoparticles for Physics, Chemistry and Biology*, Imperial College Press, 1st ed., **2012**.

[3]   G. Rayner-Canham, T. Overton, *Descriptive Inorganic Chemistry*, Freeman, 4th ed., **2006**.

[4]   C. F. Shaw, *Chem. Rev.* **1999**, *99*, 2589-2600.

[5]   P. J. Barnard, S. J. Berners-Price, *Coord. Chem. Rev.* **2007**, *251*, 1889-1902.

[6]   B. Bertrand, M. R. M. Williams, M. Bochmann, *Chem. Eur. J.* **2018**, *24*, 11840-11851.

[7]   R. Kumar, C. Nevado, *Angew. Chem. Int. Ed.* **2017**, *56*, 1994-2015.

[8]   E. E. Langdon-Jones, S. J. A. Pope, *Chem. Commun.* **2014**, *50*, 10343-10354.

[9]   C. Bronner, O. S. Wenger, *Dalton Trans.* **2011**, *40*, 12409-12420.

[10]   D. Di, A. S. Romanov, L. Yang, J. M. Richter, J. P. H. Rivett, S. Jones, T. H. Thomas, M. Abdi Jalebi, R. H. Friend, M. Linnolahti, M. Bochmann, D. Credgington, *Science* **2017**, *356*, 159-163.

[11]   S. Lentijo, G. Aullón, J. A. Miguel, P. Espinet, *Dalton Trans.* **2013**, *42*, 6353-6365.

[12]   R. Kumar, A. Linden, C. Nevado, *Angew. Chem. Int. Ed.* **2015**, *54*, 14287-14290.

[13]   K.-H. Wong, K.-K. Cheung, M. C.-W. Chan, C.-M. Che, *Organometallics* **1998**, *17*, 3505-3511.

[14]   R. J. Puddephatt, *The Chemistry of Gold*, Elsevier, **1978**.

[15]   H. Schmidbaur, K. C. Dash, *Adv. Inorg. Chem.* **1982**, *25*, 239-266.

[16]   F. Mohr, *Gold Bulletin* **2004**, *37*, 164-169.

[17]   M. Jansen, *Chem. Soc. Rev.* **2008**, *37*, 1826-1835.

[18]   J. Lin, S. Zhang, W. Guan, G. Yang, Y. Ma, *J. Am. Chem. Soc.* **2018**, *140*, 9545-9550.

[19]   G. Brauer, *Handbook of Preparative Inorganic Chemistry*, Academic Press, 2nd ed., **1965**.

[20]   F. Habashi, *Hydrometallurgy* **2005**, *79*, 15-22.

[21]   A. S. K. Hashmi, *Chem. Rev.* **2007**, *107*, 3180-3211.

[22]   H. Schmidbaur, A. Schier, *Organometallics* **2010**, *29*, 2-23.

[23]   A. S. K. Hashmi, F. D. Toste, *Modern Gold Catalyzed Synthesis*, Wiley-VCH, Weinheim, **2012**.

[24]   T. Lauterbach, A. M. Asiri, A. S. K. Hashmi, *Adv. Organomet. Chem.* **2014**, *62*, 261-297.

[25]   Z. Li, C. Brouwer, C. He, *Chem. Rev.* **2008**, *108*, 3239-3265.

[26]   A. Arcadi, *Chem. Rev.* **2008**, *108*, 3266-3325.

[27]   A. S. K. Hashmi, G. J. Hutchings, *Angew. Chem. Int. Ed.* **2006**, *45*, 7896-7936.

[28]   M. Chiarucci, M. Bandini, *Beilstein J. Org. Chem.* **2013**, *9*, 2586-2614.

[29]   R. Dorel, A. M. Echavarren, *Chem. Rev.* **2015**, *115*, 9028-9072.

[30]   D. Balcells, O. Eisenstein, M. Tilset, A. Nova, *Dalton Trans.* **2016**, *45*, 5504-5513.

[31]   M. Joost, A. Amgoune, D. Bourissou, *Angew. Chem., Int. Ed.* **2015**, *54*, 15022-15045.

[32]   F. Rekhroukh, L. Estévez, S. Mallet-Ladeira, K. Miqueu, A. Amgoune, D. Bourissou, *J. Am. Chem. Soc.* **2016**, *138*, 11920-11929.

[33]   F. Rekhroukh, L. Estévez, C. Bijani, K. Miqueu, A. Amgoune, D. Bourissou, *Angew. Chem. Int. Ed.* **2016**, *55*, 3414-3418.

[34]   C. Blons, A. Amgoune, D. Bourissou, *Dalton Trans.* **2018**, *47*, 10388-10393.

[35]   A. J. Chalk, *J. Am. Chem. Soc.* **1964**, *86*, 4733-4734.

[36]   D. Belli Dell'Amico, F. Calderazzo, R. Dantona, J. Straehle, H. Weiss, *Organometallics* **1987**, *6*, 1207-1210.

[37]   D. M. P. Mingos, J. Yau, S. Menzer, D. J. Williams, *Angew. Chem. Int. Ed.* **1995**, *34*, 1894-1895.

[38]   E. Langseth, M. L. Scheuermann, D. Balcells, W. Kaminsky, K. I. Goldberg, O. Eisenstein, R. H. Heyn, M. Tilset, *Angew. Chem. Int. Ed.* **2013**, *52*, 1660-1663.

[39]   N. Savjani, D.-A. Roşca, M. Schormann, M. Bochmann, *Angew. Chem. Int. Ed.* **2013**, *52*, 874-877.

[40]   L. Rocchigiani, J. Fernandez-Cestau, G. Agonigi, I. Chambrier, P. H. M. Budzelaar, M. Bochmann, *Angew. Chem. Int. Ed.* **2017**, *56*, 13861-13865.

[41]   F. Rekhroukh, L. Estévez, C. Bijani, K. Miqueu, A. Amgoune, D. Bourissou, *Organometallics* **2016**, *35*, 995-1001.

[42]   F. Rekhroukh, C. Blons, L. Estévez, S. Mallet-Ladeira, K. Miqueu, A. Amgoune, D. Bourissou, *Chem. Sci.* **2017**, *8*, 4539-4545.

[43]   I. Chambrier, L. Rocchigiani, D. L. Hughes, P. M. H. Budzelaar, M. Bochmann, *Chem. Eur. J.* **2018**, *24*, 11467-11474.

[44]   O. A. Egorova, H. Seo, Y. Kim, D. Moon, Y. M. Rhee, K. H. Ahn, *Angew. Chem. Int. Ed.* **2011**, *50*, 11446-11450.

[45]   M. Melchionna, M. Nieger, J. Helaja, *Chem. Eur. J.* **2010**, *16*, 8262-8267.

[46]   A. Pintus, L. Rocchigiani, J. Fernandez-Cestau, P. H. M. Budzelaar, M. Bochmann, *Angew. Chem. Int. Ed.* **2016**, *55*, 12321-12324.

[47]   D. A. Roşca, D. A. Smith, D. L. Hughes, M. Bochmann, *Angew. Chem. Int. Ed.* **2012**, *51*, 10643-10646.

[48]   R. Kumar, J. P. Krieger, E. Gómez-Bengoa, T. Fox, A. Linden, C. Nevado, *Angew. Chem. Int. Ed.* **2017**, *56*, 12862-12865.

[49]   A. Pujol, M. Lafage, F. Rekhroukh, N. Saffon-Merceron, A. Amgoune, D. Bourissou, N. Nebra, M. Fustier-Boutignon, N. Mézailles, *Angew. Chem.* **2017**, *129*, 12432-12435.

[50]   D.-A. Roşca, J. Fernandez-Cestau, J. Morris, J. A. Wright, M. Bochmann, *Sci. Adv.* **2015**, DOI: 10.1126/sciadv.1500761.

[51]   G. C. Bond, P. A. Sermon, G. Webb, D. A. Buchanan, P. B. Wells, *J. Chem. Soc., Chem. Commun.* **1973**, 444b-445.

[52]   P. Johnston, N. Carthey, G. J. Hutchings, *J. Am. Chem. Soc.* **2015**, *137*, 14548-14557.

[53]   K. S. Egorova, V. P. Ananikov, *Organometallics* **2017**, *36*, 4071-4090.

[54]   I.-T. Trotuş, T. Zimmermann, F. Schüth, *Chem. Rev.* **2014**, *114*, 1761-1782.

[55]   G. J. Hutchings, *J. Catal.* **1985**, *96*, 292-295.

[56]   M. Conte, A. F. Carley, C. Heirene, D. J. Willock, P. Johnston, A. A. Herzing, C. J. Kiely, G. J. Hutchings, *J. Catal.* **2007**, *250*, 231-239.

[57]   A. S. K. Hashmi, G. J. Hutchings, *Angew. Chem. Int. Ed.* **2006**, *45*, 7896-7936.

[58]   H. Masatake, K. Tetsuhiko, S. Hiroshi, Y. Nobumasa, *Chem. Lett.* **1987**, *16*, 405-408.

[59]   A. S. K. Hashmi, M. Rudolph, *Chem. Soc. Rev.* **2008**, *37*, 1766-1775.

[60]   C. Obradors, A. M. Echavarren, *Chem. Commun.* **2014**, *50*, 16-28.

[61]   D. Wang, R. Cai, S. Sharma, J. Jirak, S. K. Thummanapelli, N. G. Akhmedov, H. Zhang, X. Liu, J. L. Petersen, X. Shi, *J. Am. Chem. Soc.* **2012**, *134*, 9012-9019.

[62]   M. Jia, M. Bandini, *ACS Catal.* **2015**, *5*, 1638-1652.

[63]   J. H. Teles, S. Brode, M. Chabanas, *Angew. Chem. Int. Ed.* **1998**, *37*, 1415-1418.

[64]   D. J. Gorin, B. D. Sherry, F. D. Toste, *Chem. Rev.* **2008**, *108*, 3351-3378.

[65]   S. L. Crawley, R. L. Funk, *Org. Lett.* **2006**, *8*, 3995-3998.

[66]   R. O. C. Norman, W. J. E. Parr, C. B. Thomas, *J. Chem. Soc., Perkin Trans. 1* **1976**, 1983-1987.

[67]   M. Rudolph, A. S. K. Hashmi, *Chem. Commun.* **2011**, *47*, 6536-6544.

[68]   Y. Fukuda, K. Utimoto, *Synthesis* **1991**, *1991*, 975-978.

[69]   A. S. K. Hashmi, L. Schwarz, J. H. Choi, T. M. Frost, *Angew. Chem. Int. Ed.* **2000**, *39*, 2285-2288.

[70]   Y. Liu, F. Song, Z. Song, M. Liu, B. Yan, *Org. Lett.* **2005**, *7*, 5409-5412.

[71]   H. Schmidbaur, A. Schier, *Arab. J. Sci. Eng.* **2012**, *37*, 1187-1225.

[72]   A. S. K. Hashmi, J. P. Weyrauch, M. Rudolph, E. Kurpejović, *Angew. Chem. Int. Ed.* **2004**, *43*, 6545-6547.

[73]   A. Dar, K. Moss, S. M. Cottrill, R. V. Parish, C. A. McAuliffe, R. G. Pritchard, B. Beagley, J. Sandbank, *J. Chem. Soc., Dalton Trans.* **1992**, 1907-1913.

[74]   D. Aguilar, M. Contel, R. Navarro, E. P. Urriolabeitia, *Organometallics* **2007**, *26*, 4604-4611.

[75]   H. von Wachenfeldt, A. V. Polukeev, N. Loganathan, F. Paulsen, P. Rose, M. Garreau, O. F. Wendt, D. Strand, *Dalton Trans.* **2015**, *44*, 5347-5353.

[76]   Hartwig, *Organotransition Metal Chemistry, From Bonding to Catalysis*, University Science Books, 1st ed., **2010**.

[77]   M. Albrecht, *Chem. Rev.* **2010**, *110*, 576-623.

[78]   W. Henderson, *Adv. Organomet. Chem.* **2006**, *54*, 207-265.

[79]   E. C. Constable, T. A. Leese, *J. Organomet. Chem.* **1989**, *363*, 419-424.

[80]   D. Fan, E. Meléndez, J. D. Ranford, P. F. Lee, J. J. Vittal, *J. Organomet. Chem.* **2004**, *689*, 2969-2974.

[81]   Y. Fuchita, H. Ieda, M. Yasutake, *J. Chem. Soc., Dalton Trans.* **2000**, 271-274.

[82]   J. Vicente, M. T. Chicote, M. D. Bermúdez, *J. Organomet. Chem.* **1984**, *268*, 191-195.

[83]   M. Nonoyama, K. Nakajima, K. Nonoyama, *Polyhedron* **1997**, *16*, 4039-4044.

[84]   P. A. Bonnardel, R. V. Parish, R. G. Pritchard, *J. Chem. Soc., Dalton Trans.* **1996**, 3185-3193.

[85]   H. Ieda, H. Fujiwara, Y. Fuchita, *Inorg. Chim. Acta* **2001**, *319*, 203-206.

[86]   M. A. Mansour, R. J. Lachicotte, H. J. Gysling, R. Eisenberg, *Inorg. Chem.* **1998**, *37*, 4625-4632.

[87]   W. Henderson, B. K. Nicholson, S. J. Faville, D. Fan, J. D. Ranford, *J. Organomet. Chem.* **2001**, *631*, 41-46.

[88]   A. P. Shaw, M. Tilset, R. H. Heyn, S. Jakobsen, *J. Coord. Chem.* **2011**, *64*, 38-47.

[89]   E. Langseth, C. H. Görbitz, R. H. Heyn, M. Tilset, *Organometallics* **2012**, *31*, 6567-6571.

[90]   E. Langseth, A. Nova, E. A. Tråseth, F. Rise, S. Øien, R. H. Heyn, M. Tilset, *J. Am. Chem. Soc.* **2014**, *136*, 10104-10115.

[91]   C. Blons, S. Mallet-Ladeira, A. Amgoune, D. Bourissou, *Angew. Chem. Int. Ed.* **2018**, *57*, 11732-11736.

[92]   E. Langseth, *Ph.D. thesis, University of Oslo* **2014**.

[93]   A. L. Sundsdal, *Master thesis, University of Oslo* **2014**.

[94]   L. P. Escrivá, *Unpublished results, University of Oslo* **2013**.

[95]   M. Philipp, *Unpublished results, University of Oslo* **2017**.

[96]   V. Levchenko, *Unpublished results, University of Oslo* **2017**.

[97]   K. Hylland, M. S. M. Holmsen, *Unpublished results, University of Oslo* **2017**.

[98]   C. E. Rezsnyak, J. Autschbach, J. D. Atwood, S. Moncho, *J. Coord. Chem.* **2013**, *66*, 1153-1165.

[99]   F. Rekhroukh, R. Brousses, A. Amgoune, D. Bourissou, *Angew. Chem. Int. Ed.* **2015**, *54*, 1266-1269.

[100]   J. Serra, P. Font, E. D. Sosa Carrizo, S. Mallet-Ladeira, S. Massou, T. Parella, K. Miqueu, A. Amgoune, X. Ribas, D. Bourissou, *Chem. Sci.* **2018**, *9*, 3932-3940.

[101]   M. J. Harper, E. J. Emmett, J. F. Bower, C. A. Russell, *J. Am. Chem. Soc.* **2017**, *139*, 12386-12389.

[102]   F. S. Ihlefeldt, *Master thesis, Department of Chemistry, University of Oslo* **2015**.

[103]   Y. Wencke, *Erasmus project, Department of Chemistry, University of Oslo* **2014**.

[104]   N. Tamosiunaite, *Unpublished results, University of Oslo* **2017**.

[105]   F. S. Ihlefeldt, S. Dalzell, *Unpublished results, Department of Chemistry, University of Oslo* **2016**.

[106]   E. S. Aunan, *Bachelor thesis, Department of Chemistry, University of Oslo* **2016**.

[107]   B. H. Hoff, *Synthesis* **2018**, *50*, 2824-2852.

[108]   Y.-M. Liu, L. He, M.-M. Wang, Y. Cao, H.-Y. He, K.-N. Fan, *ChemSusChem* **2012**, *5*, 1392-1396.

[109]   R. S. Ramón, N. Marion, S. P. Nolan, *Chem. Eur. J.* **2009**, *15*, 8695-8697.

[110]   E. A. Tråseth, *Master thesis, Department of Chemistry, University of Oslo* **2014**.

[111]   J. J. Ritter, P. P. Minieri, *J. Am. Chem. Soc.* **1948**, *70*, 4045-4048.

[112]   L. Kurti, B. Czako, *Strategic Applications of Named Reactions in Organic Synthesis*, Academic Press, 1st ed., **2005**.

[113]   T. D. W. Claridge, *High-Resolution NMR techniques in Organic Chemistry*, Elsevier, 2nd ed., **2009**.

[114]   B. Spingler, S. Schnidrig, T. Todorova, F. Wild, *CrystEngComm* **2012**, *14*, 751-757.

[115]   *Bruker APEX3, SAINT, SADABS, XPREP Ver. 2016.5-0*, Bruker AXS inc, Madison, Wisconsin, USA, **2016**.

[116]   G. Sheldrick, *Acta Crystallogr. Sect. A* **2015**, *71*, 3-8.

[117]   G. Sheldrick, *Acta Crystallogr. Sect. C* **2015**, *71*, 3-8.

[118]   O. V. Dolomanov, L. J. Bourhis, R. J. Gildea, J. A. K. Howard, H. Puschmann, *J. Appl. Crystallogr.* **2009**, *42*, 339-341.

[119]   F. H. Allen, O. Johnson, G. P. Shields, B. R. Smith, M. Towler, *J. Appl. Crystallogr.* **2004**, *37*, 335-338.

[120]   H. Putz, K. Brandenburg, *Diamond - Crystal and Molecular Structure Visualization, Ver. 4.4.0*, Crystal Impact: Kreuzherrenstr. 102, 53227 Bonn, Germany, **1997**.

[121]   H. Schobert, *Chem. Rev.* **2014**, *114*, 1743-1760.

[122]   J. B. Dickey, T. E. Stanin, **1950**, U.S. Patent 2525530.

[123]   T. L. Tolbert, W. A. Wadell, **1965**, U.S. Patent 3177243.

[124]   F. H. Allen, O. Kennard, D. G. Watson, L. Brammer, A. G. Orpen, R. Taylor, *J. Chem. Soc., Perkin Trans. 2* **1987**, *0*, S1-S19.

[125]   M. Conte, A. F. Carley, G. Attard, A. A. Herzing, C. J. Kiely, G. J. Hutchings, *J. Catal.* **2008**, *257*, 190-198.

[126]   W. J. Wolf, M. S. Winston, F. D. Toste, *Nat. Chem.* **2014**, *6*, 159.

[127]   E. Peris, R. H. Crabtree, *Chem. Soc. Rev.* **2018**, *47*, 1959-1968.

[128]   G. van Koten, *Top. Organomet. Chem.* **2013**, *40*, 1-20.

[129]   J. Grajeda, A. Nova, D. Balcells, Q. J. Bruch, D. S. Wragg, R. H. Heyn, A. J. M. Miller, M. Tilset, *Eur. J. Inorg. Chem.* **2018**, *2018*, 3113-3117.

[130]   M. A. Cinellu, A. Zucca, S. Stoccoro, G. Minghetti, M. Manassero, M. Sansoni, *J. Chem. Soc., Dalton Trans.* **1996**, 4217-4225.

[131]   J. Vicente, M. T. Chicote, M. I. Lozano, S. Huertas, *Organometallics* **1999**, *18*, 753-757.

[132]   E. A. Heen, *Unpublished results, Department of Chemistry, University of Oslo* **2014**.

[133]   R. H. Crabtree, *The Organometallic Chemistry of the Transition Metals*, Wiley, 5th ed., **2009**.

[134]   H. V. R. Dias, M. Fianchini, T. R. Cundari, C. F. Campana, *Angew. Chem. Int. Ed.* **2008**, *47*, 556-559.

[135]   V. Dyadkin, P. Pattison, V. Dmitriev, D. Chernyshov, *J. Synchrotron Rad.* **2016**, *23*, 825-829.

[136]   J. Nyrud, *Bachelor thesis, Department of Chemistry, University of Oslo* **2018**.

Appendices I-V

Appendix I: Paper I

Appendix II: Paper II

Appendix III: Paper III

Appendix IV: Paper IV

Appendix V: NMR spectra of unpublished compounds

Appendices I-V

Paper II

Small-molecule Activation at Au(III): Metallacycle Construction from Ethylene, Water, and Acetonitrile

Marte Sofie Martinsen Holmsen, Ainara Nova, David Balcells, Eirin Langseth, Sigurd Øien-Ødegaard, Eline Aasen Tråseth, Richard H. Heyn, and Mats Tilset

PAPER

Small-molecule activation at Au(III): metallacycle construction from ethylene, water, and acetonitrile†

Marte Sofie Martinsen Holmsen,[a] Ainara Nova,[b] David Balcells,[b] Eirin Langseth,‡[a] Sigurd Øien-Ødegaard,[a] Eline Aasen Tråseth,[a] Richard H. Heyn[c] and Mats Tilset*[a,b]

Incorporation of the simple, readily available, building blocks ethylene, water and acetonitrile into Au(tpy)(OCOCF₃)₂ (tpy = 2-(p-tolyl)pyridine) in a one-step reaction leads to high yields of a new 6-membered ring gold(III) metallacycle complex. The metallacycle has been characterized spectroscopically and crystallographically, and the mechanism of its formation has been investigated with the aid of DFT calculations.

Introduction

The functionalization of alkenes has great practical and economic value in catalysis, and as the simplest of such building blocks, ethylene is of particular interest.[1] Gold is known for its ability to π-coordinate and thereby activate alkenes and alkynes towards nucleophilic attack, which is considered to be a key step in gold catalysis.[2–8] However, there are only scarce reports of Au(III)-mediated functionalization of the simplest olefin, ethylene. One important example was provided by Atwood and co-workers (Scheme 1, top),[9] who demonstrated that ethylene and propylene could be functionalized stoichiometrically at the Au(III) complex Au(bipy)Cl₂⁺ (bipy = 2,2′-bipyridine) in water to furnish Au(III) hydroxyalkyl products that were observed in solution by ¹H NMR spectroscopy but not isolated. Reactions of ethylene and propylene with HAuCl₃ and AuCl₃(tppts) (tppts = 3,3′,3″-phosphanetriyltris-(benzenesulfonic acid) trisodium salt) led to Au(III) hydroxyalkyl species, which upon heating underwent gold reduction to the metal with concomitant formation of organic oxygenated products (alcohols, aldehyde or ketone).[9] More recently, Bochmann and co-workers (Scheme 1, bottom)[10] showed that ethylene slowly undergoes a formal insertion into the

[a]*Department of Chemistry, University of Oslo, P.O. Box 1033 Blindern, N-0315 Oslo, Norway. E-mail: mats.tilset@kjemi.uio.no*
[b]*Centre for Theoretical and Computational Chemistry (CTCC), Department of Chemistry, University of Oslo, P.O. Box 1033 Blindern, N-0315 Oslo, Norway*
[c]*SINTEF Materials and Chemistry, P.O. Box 124 Blindern, N-0314 Oslo, Norway*
†Electronic supplementary information (ESI) available: Full experimental and computational details, characterization data, and spectra. CCDC 1443527 and 1443528. For ESI and crystallographic data in CIF or other electronic format see DOI: 10.1039/c6dt01648k
‡Current address: SINTEF Materials and Chemistry, P.O. Box 124 Blindern, N-0314 Oslo, Norway.

Scheme 1 Reactions of ethylene at Au(III) complexes (OAc^F = OCOCF₃).

Au–OAc^F bond *trans* to the pyridine-N in a diarylpyridine CNC pincer complex to yield an Au(III) acetoxyalkyl complex (OAc^F = OCOCF₃).

Our group recently reported a combined experimental and computational study of the formal insertion of ethylene into an Au–O bond of Au(tpy)(OAc^F)₂ (**1**; tpy = 2-(p-tolyl)pyridine; Scheme 2, top).[11] Selective insertion into the Au–O bond *trans* to N of the chelating tpy ligand furnished Au(tpy)-(CH₂CH₂OAc^F)(OAc^F) (**2**). Although the *trans* to C coordination site is kinetically more accessible, the *trans* to N insertion product is thermodynamically favoured and is formed by nucleophilic attack by free ⁻OAc^F at the coordinated ethylene. This discovery led to further investigations, and herein we report that the coordinated and inserted ethylene molecule can undergo further functionalization due to the availability of the *trans* to C coordination site at Au.

Scheme 2 Formal insertion of ethylene into an Au−O bond of Au(tpy)(OAc^F)$_2$ (**1**)[11] and preparation of the metallacyclic Au(III) complex **3** from **1** and **2** (this work); (OAc^F = OCOCF$_3$).

Results and discussion

Synthesis and characterization

An attempt to crystallize a product mixture containing **2** from acetonitrile led instead to the isolation of small quantities of a new crystalline complex. Examination of these crystals by single-crystal X-ray diffraction revealed that the new complex was a Au(III) metallacycle **3** (Scheme 2, lower part). Synthesis of larger quantities of **3** in about 80% yield was possible simply by stirring **2** in wet acetonitrile for 5 days at ambient temperature. Alternatively, **3** can be obtained in comparable yields by dissolving **1** in acetonitrile and adding water and ethylene. Thus, an efficient synthetic protocol has been developed wherein the three small, readily available building blocks ethylene, water, and acetonitrile are incorporated into the Au(III) metallacycle complex **3** in just one step.

The molecular structure, based on the single-crystal X-ray analysis, clearly indicated a complex which contained a new 6-membered chelate ring. Although the X-ray data and the refined structure were of excellent quality, we were concerned about the even slightest possibility of a NH *vs.* O misassignment,[12,13] and sought additional and independent verification of the connectivity seen in the structure. Thus, the three alternatives **3**, **4**, and **5** in Scheme 3 were initially considered. The 6-ring chelates in these alternatives are formally derived from Au, ethylene, acetonitrile, and one (**3**, **4**) or two (**5**) equiv.
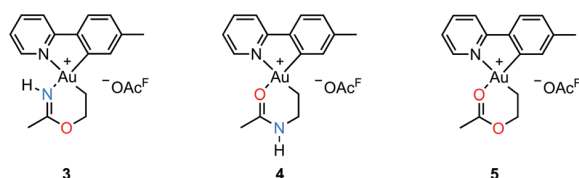
Scheme 3 Possible structures of the metallacyclic Au(III) complex.

of water. However, involvement of reagents arising from a (possibly gold) catalyzed hydrolysis of acetonitrile, or from impurities inadvertently present in this solvent, must also be considered.

By positive-ion high resolution mass spectrometry (HRMS), the parent ion at m/z = 451.1068 established the elemental composition $C_{16}H_{18}AuN_2O$ for the cation (calcd m/z = 451.1084), in accord with the presence of one N and one O atom in the chelate ring. This composition, which eliminates alternative **5**, was corroborated by elemental analysis. Support for the formulation of the *N,O*-containing chelate **3** was obtained by ^{1}H–^{15}N HMBC NMR spectroscopy. In the spectrum,¶ signals arising from two different N atoms are clearly observed. One signal at $\delta(^{15}N\{^1H\})$ = −212 arises from the chelate NH and correlates with the broadened ^{1}H signal of the NH group at $\delta(^1H)$ = 10.28 and with the signal from the metallacycle methyl group at $\delta(^1H)$ = 2.51, but not with the other protons of the metallacycle. The other ^{15}N signal at $\delta(^{15}N\{^1H\})$ = −129 arises from the N atom in the tpy ligand and has a correlation with the signal arising from the CH proton α to the pyridyl-N atom at $\delta(^1H)$ = 9.33. The ^{19}F NMR spectrum shows only one signal, arising from the $^-$OAc^F anion. So as to further unambiguously distinguish between alternatives **3** and **4**, a NOE experiment was performed. The ^{1}H–^{1}H NOESY spectrum¶ shows a clear NOE interaction between the NH proton at δ 10.28 and the CH proton at δ 9.33. These H atoms are therefore in close proximity, supporting the crystallographic analysis and verifying that **3** does indeed represent the structure of the metallacycle.

An ORTEP plot of the molecular structure of **3** is shown in Fig. 1, with selected bond distances and angles. The Au(III) centre has the expected square planar geometry. The deviation of the C9–Au–N1 bond angle in the tpy chelate from 90 to 80.60(10)° is typical, and the Au–ligand distances Au1–N1, Au1–C9, and Au1–C4 (sp^3) are within the ranges that have previously been observed for the related complexes Au(tpy)Me$_2$,[14] Au(tpy)(CH$_2$CH$_2$OAc^F)(OAc^F),[11] and Au(tpy)(CH$_2$CH$_2$OCH$_2$CF$_3$) (OAc^F).[11] The N5–C3 (1.284(4) Å) and C3–O2 (1.332(3) Å) bond distances are consistent with the corresponding average N═C (1.282 Å) and C–O (1.325 Å) in Pt(II) imino ether complexes.[15–22] ‖ These distances are, however, distinctly different from the distances in a [(tpa)Rh^{III}]$^{2+}$ (tpa = *N,N,N*-tri (2-pyridylmethyl)amine) analogue to **3**, in which the corresponding N–C and C–O bond distances are 1.245(19) and 1.374 (17) Å, respectively.[23] The directionality of the N5⋯O1A interaction between the NH of the 6-membered ring and the nearest O (O1A) of the trifluoroacetate anion suggests the presence of a hydrogen bond; in fact, the final refinement shows a donor–acceptor distance (N5⋯O1A) of 2.8708(2) Å. This is in excellent agreement with the proposed structure **3**. The crystal structure of **3** is monoclinic, but with β = 90°. In addition, it is twinned *via* a twofold rotation about the crystallographic *a*

¶See ESI pages S5, S13, and S14† for details.
‖No structural examples of Au imino ethers were found *via* SciFinder.
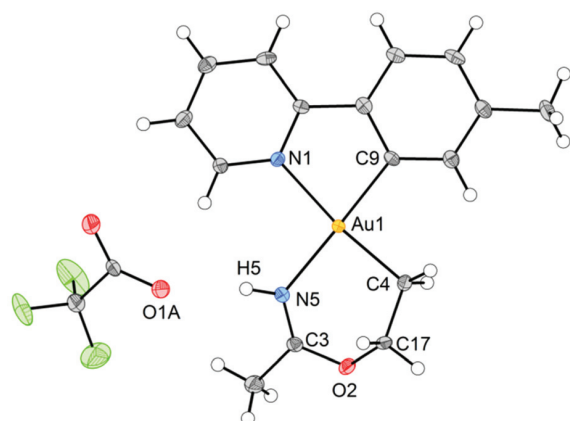
Fig. 1 ORTEP drawing of Au(III) complex **3**, with 50% probability ellipsoids. Selected bond distances (Å), angles, and torsional angles (°): Au1–C4, 2.042(3); Au1–C9, 2.019(3); Au1–N1, 2.126(2); Au1–N5, 2.092(3); C3–N5, 1.284(4); C3–O2, 1.332(3); C17–O2, 1.449(4); C4–C17, 1.510(4); O1A···N5, 2.8708(2); C4–Au1–C9, 92.39(12); C4–Au1–N5, 89.54(11); C9–Au1–N1, 80.60(10); N1–Au1–N5, 97.43(9); C4–Au1–N1, 172.99(11); C9–Au1–N5, 174.24(12); C3–O2–C17–C4, −70.8(4); Au1–C4–C17–O2, 60.2(3); Au1–N5–C3–O2, 26.5(5); C17–O2–C3–N5, 21.8(5).

Fig. 2 Packing diagram of structure **3** viewed along the *a* axis, showing stacking between the tpy ligands. The thermal ellipsoids are displayed at 50% probability, and H atoms are omitted for clarity.

Scheme 4 Potential role of acetamide in the formation of **3**.

Mechanistic studies by experiment and DFT calculations

Initial mechanistic experiments probed whether a gold-mediated or gold-catalyzed hydrolysis of acetonitrile to form acetamide might be involved in the process (Scheme 4). First, no formation of **3** was seen when **2** was treated with only acetamide in CH_2Cl_2 (Scheme 4A). Second, the reaction of **2** with wet acetonitrile-d_3 in the presence of acetamide led to the generation of **3-d_3** and a minor amount of **3** as inferred by integration of the metallacycle–methyl resonance at δ 2.51 in the ^{1}H NMR spectrum (Scheme 4B). These experiments suggest that acetonitrile, and not acetamide, is the main reactant in the formation of the metallacycle.

Scheme 5 shows a possible mechanism for the formation of **3**. The unobserved cationic ethylene complex **6** is generated from either **1** or **2**, in agreement with our previous findings.[11] The hydroxyethyl complex **7** is formed from **2** after nucleophilic attack by water, by analogy with Atwood's study,[9] and parallel to reaction of trifluoroethanol with **2**, which proceeds *via* **6** yielding **10**.[11] Acetonitrile substitution for the $^-OAc^F$ anion of **7** at the kinetically most accessible position[11] *trans* to tpy-C furnishes a crucial intermediate **8**, which undergoes cyclization by an intramolecular nucleophilic attack of the hydroxyethyl-O atom on the nitrile-C atom of acetonitrile, analogous to the alcoholysis of Pt(II)-coordinated nitriles to provide Pt(II) imino ethers.[20–22] An $^-OAc^F$ anion assisted proton transfer from O to N finally provides **3**. Close analogues of the putative intermediates **7** and **8** exist and support their mechanistic viability. The hydroxyethyl complex **7** is an analogue of Au(tpy)Me(OTf) and Au(tpy)Me(OAc); both have been structurally characterized as the pertinent stereoisomers with Me *trans* to N.[24] Complex **8** is closely related to [Au(tpy)Me(NCMe)][BF$_4$] (**9**) which has been prepared with the relevant stereochemistry at Au by bromide abstraction from AuBrMe(tpy) with AgBF$_4$ in acetonitrile.[25]

The relative stability of all intermediates shown in Scheme 5 has been assessed by means of DFT calculations, which show that they are all accessible under the experimental conditions.§ The TS from **8** to **11** has also been computed (**TS8-11**,

axis. The structure displays parallel displaced π–π stacking along the *a* direction, and the distance between the intersecting planes of the tpy ligands alternates between 3.42 and 3.44 Å (Fig. 2).

DFT calculations were performed on the cations of **3**, **4**, and **5** in order to further assist with the verification of the structure. Gratifyingly, comparisons of the crystallographic data with the optimized structures showed that the average r.m.s. deviations of the atomic positions were considerably smaller for **3** (average deviation 0.015 Å) than for **4** (0.022 Å) and **5** (0.032 Å), lending further support for the structural assignment.

---

§ For an estimation of the transition state energies involved in the transformation of **1** to **7**, see ref. 11.
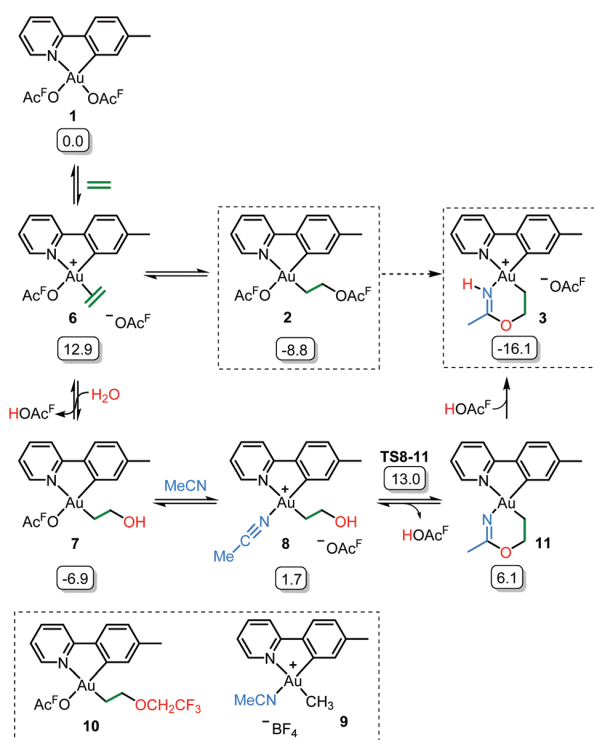
Scheme 5 Postulated reaction mechanism for the formation of **3** (OAc^F = OCOCF$_3$). Framed species have been characterized by X-ray diffraction in either this or previous (ref. 11) work. Free energies obtained from DFT calculations in acetonitrile are given in kcal mol^{-1}.
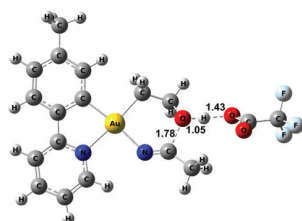
Fig. 3 Optimized geometry for **TS8-11** with selected bond distances (Å).

Fig. 3) and it shows that cyclization is triggered by the deprotonation of the hydroxyl group by an external $^-$OAc^F. This transition state is 13.0 kcal mol^{-1} higher than **1** and involves an effective energy barrier of 21.8 kcal mol^{-1} relative to **2**. The long experimental reaction time required for this transformation may be due to the existence of many equilibria, which are dependent on the different reactant concentrations.

Concluding remarks

An eventual reductive elimination from **3** would generate 2-methyl-2-oxazoline, with an important heterocyclic ring structure. Previously, 2-oxazolines have been prepared by Sawamura and coworkers[26–28] by Au(I) catalyzed asymmetric aldol reactions

of isocyanides and aldehydes. Hashmi and coworkers more recently[29,30] prepared oxazolines by Au(I)-catalyzed cycloisomerizations of propargyl amides. Interestingly, it has been recently reported that cyclometallated Au(III) aryl–pyridine complexes may act as efficient catalysts for the three-component synthesis of propargylic amines from aldehydes, secondary amines, and alkynes, and of substituted oxazoles from N-benzyl imines, alkynes, and acyl chlorides.[31,32] The [(tpa)Rh^{III}]$^{2+}$ analogue to **3** was synthesized in a two-step process by H$_2$O$_2$ oxidation of a coordinated ethylene, followed by reaction with acetonitrile and NH$_4$PF$_6$.[23] In this context, our one-step assembly of an oxazoline from an alkene, a nitrile, and water represents a new strategy with obvious possibilities in organic synthesis.[33]

In conclusion, the convenient and high-yield one-pot, four-component assembly of a new cationic metallacyclic Au(III) complex has been described. In the process, the three small, readily available building blocks ethylene, water, and acetonitrile have been incorporated into one product. The transformation demonstrates that both of the potentially labile coordination sites in Au(tpy)(OAc^F)$_2$ can be utilized – a fact that may be of importance for catalytic applications. The metallacycle is constructed in such a fashion that the high *trans*-effect (alkyl) end of the assembled chelate ligand occupies the position that is *trans* to the low *trans*-effect (N donor) of the tpy supporting ligand, and *vice versa*.

Experimental and computational section

General experimental methods

Gold(III) complexes **1** and **2** were prepared by previously reported procedures.[11,14] Distilled water was used. CH$_3$CN and CH$_2$Cl$_2$ were purified using a MB SPS-800 solvent purifying system from MBraun. The gold(III) complexes studied here are not sensitive to air, so inert atmosphere was not utilized, except for the synthesis of **9** which is described in the ESI.† NMR spectra were recorded on Bruker Avance DPX200, AVII400, DRX500, AVII600 and AV600 instruments at ambient temperature. ^{1}H and ^{13}C spectra have been referenced relative to the residual solvent signals. ^{19}F has been referenced to CFCl$_3$ by using C$_6$F$_6$ (−164.9 ppm with respect to CFCl$_3$ at 0 ppm) as an internal standard. The ^{15}N chemical shifts have been calibrated using MeNO$_2$ as an external standard at 0 ppm. The peaks in the ^{1}H NMR and ^{13}C NMR spectra were assigned by the aid of 2D NMR techniques such as HSQC, HMBC, COSY, NOESY, and ^{1}H–^{15}N HMBC according to the numbering scheme shown below. Mass spectra (ESI) were obtained on a Micromass QTOF II spectrometer and a Bruker Daltronics maXisII spectrometer. Elemental analysis was performed by Microanalytisches Laboratorium Kolbe, Mülheim an der Ruhr, Germany.

Preparation of [Au(tpy)(C–N)$^+$][$^-$OCOCF$_3$] (3) from 1. Au(tpy)(OCOCF$_3$)$_2$ (50.1 mg, 0.0847 mmol, 1.0 equiv.) was dissolved in acetonitrile (3 mL). Water (10 μL, 0.55 mmol, 6.5 equiv.) was added. Ethylene was bubbled through the solution at ambient pressure for two minutes, and the flask was sealed with a glass stopper. The reaction mixture was stirred at ambient temperature in the absence of light for 7 days. The reaction mixture was filtered and the volatiles were removed under reduced pressure furnishing 3 as a white solid (38.1 mg, 0.0675 mmol, 80%).

Preparation of [Au(tpy)(C–N)$^+$][$^-$OCOCF$_3$] (3) from 2. Au(tpy)-(CH$_2$CH$_2$OCOCF$_3$)(OCOCF$_3$) (50.1 mg, 0.0809 mmol, 1.0 equiv.) was dissolved in acetonitrile (3 mL). Water (10 μL, 0.55 mmol, 6.8 equiv.) was added. Ethylene was bubbled through the solution at ambient pressure for two minutes, and the flask was sealed with a glass stopper. The reaction mixture was stirred at ambient temperature in the absence of light for 5 days. The reaction mixture was filtered and the volatiles were removed under reduced pressure furnishing 3 as a white solid (35.8 mg, 0.0634 mmol, 78%). ^{1}**H NMR** (600 MHz, CD$_2$Cl$_2$): δ 10.28 (bs, 1H, **NH**), 9.33 (d, 1H, J = 5.4 Hz, **H^6**), 8.08 (ddd, 1H, J = 8.0, 7.5, 1.4 Hz, **H^4**), 7.96 (d, 1H, J = 8.0 Hz, **H^3**), 7.71 (d, 1H, J = 7.7 Hz, **H$^{3'}$**), 7.58 (ddd, 1H, J = 7.5, 5.6, 1.1 Hz, **H^5**), 7.23–7.25 (m, 2H, **H$^{4'}$** and **H$^{6'}$**), 4.34 (m, 2H, O**CH$_2$**), 2.73 (m, 2H, Au**CH$_2$**), 2.51 (s, 3H, OC**CH$_3$**), 2.44 (s, 3H, Ar**CH$_3$**). ^{13}**C NMR** (150 MHz, CD$_2$Cl$_2$): δ 175.2, 161.7, 149.8, 142.4, 142.3, 142.0, 141.9, 131.2, 129.4, 126.0, 124.9, 120.2, 66.5, 28.6, 22.0, 21.6. $^-$OCOCF$_3$ was not observed by ^{13}C NMR. ^{15}**N{^{1}H} NMR** (600 MHz, CD$_2$Cl$_2$): δ −129 (**N**(tpy)), −212 (**N**H, $|J|$ = 78 Hz), as observed by ^{1}H–^{15}N HMBC (see Fig. S12†). ^{19}**F NMR** (188 MHz, CD$_2$Cl$_2$): δ −78.1 (bs, C**F$_3$**). **MS** (ESI$^+$, MeCN): m/z (rel.%): 451 ([M − OCOCF$_3$]$^+$, 100). **MS** (ESI$^-$, MeCN): m/z (rel.%): 113 ([OCOCF$_3$]$^-$, 100) was observed among other unidentified peaks. **HRMS** (ESI$^+$, MeCN): Found: 451.1068; calcd for C$_{16}$H$_{18}$AuN$_2$O: 451.1084 (+0.0016). **HRMS** (ESI$^-$, MeCN): Found: 112.9859; calcd for C$_2$F$_3$O$_2$: 112.9856 (−0.0003). **Elemental analysis:** Anal. Calcd for C$_{18}$H$_{18}$AuF$_3$N$_2$O$_3$: C, 38.31; H, 3.22; N, 4.96. Found: C, 37.81; H, 3.19; N, 4.59.

Computational details

Calculations were carried out at the DFT level as implemented in the Gaussian09 software package.[34] The hybrid PBE0+GD3 functional[35,36] including Grimme's model for dispersion forces was used to optimize all geometries. This methodology was selected because previous studies have proven its solid performance in the modeling of Au(III) alkene complexes.[8,11,37] C, H, N and O were described with the all-electron triple-ζ 6-311+G** basis set,[38,39] whereas Au was described with the Stuttgart–Köln basis set including a small-core quasi-relativistic pseudopotential.[40,41] Geometries were fully optimized without any constraint. Vibrational frequencies were computed analytically to verify that the stationary points found were energy minima or transition states. All optimizations needed for the mechanism proposal were carried out in solvent (acetonitrile) using the SMD solvation model.[42] Complexes 3, 4 and 5 were optimized in gas phase with the aim of comparing their geometries with an X-ray crystal structure. Gibbs energies were obtained for T = 298.15 K and p = 1 atm. In the bimolecular steps, these energies were corrected for the 1 M standard state (T = 298.15 K and p = 24.465 atm). Further computational details are given in the ESI.†

Notes and references

1 M. Chiarucci and M. Bandini, *Beilstein J. Org. Chem.*, 2013, **9**, 2586–2614.
2 A. S. K. Hashmi, S. Schäfer, M. Wölfle, C. Diez Gil, P. Fischer, A. Laguna, M. C. Blanco and M. C. Gimeno, *Angew. Chem., Int. Ed.*, 2007, **46**, 6184–6187.
3 *Modern Gold Catalyzed Synthesis*, ed. A. S. K. Hashmi and F. D. Toste, Wiley-VCH, Weinheim, 2012.
4 A. S. K. Hashmi and G. J. Hutchings, *Angew. Chem., Int. Ed.*, 2006, **45**, 7896–7936.
5 R. E. M. Brooner and R. A. Widenhoefer, *Angew. Chem., Int. Ed.*, 2013, **52**, 11714–11724.
6 R. Dorel and A. M. Echavarren, *Chem. Rev.*, 2015, **115**, 9028–9072.
7 H. Schmidbaur and A. Schier, *Organometallics*, 2010, **29**, 2–23.
8 D. Balcells, O. Eisenstein, M. Tilset and A. Nova, *Dalton Trans.*, 2016, **45**, 5504–5513.
9 C. E. Rezsnyak, J. Autschbach, J. D. Atwood and S. Moncho, *J. Coord. Chem.*, 2013, **66**, 1153–1165.
10 N. Savjani, D.-A. Roşca, M. Schormann and M. Bochmann, *Angew. Chem., Int. Ed.*, 2013, **52**, 874–877.
11 E. Langseth, A. Nova, E. A. Tråseth, F. Rise, S. Øien, R. H. Heyn and M. Tilset, *J. Am. Chem. Soc.*, 2014, **136**, 10104–10115.
12 R. L. Harlow, *J. Res. Natl. Inst. Stand. Technol.*, 1996, **101**, 327–339.
13 A. Spek, *Acta Crystallogr., Sect. D: Biol. Crystallogr.*, 2009, **65**, 148–155.
14 E. Langseth, C. H. Görbitz, R. H. Heyn and M. Tilset, *Organometallics*, 2012, **31**, 6567–6571.
15 D. Giardina-Papa, F. P. Intini, C. Pacifico and G. Natile, *Inorg. Chem.*, 2013, **52**, 13058–13067.

16 D. Giardina-Papa, F. P. Intini, G. Natile and C. Pacifico, *Acta Crystallogr., Sect. C: Cryst. Struct. Commun.*, 2012, **68**, m300–m302.

17 T. G. Chulkova, P. V. Gushchin, M. Haukka and V. Y. Kukushkin, *Inorg. Chem. Commun.*, 2010, **13**, 580–583.

18 S. M. Sbovata, F. Bettio, C. Marzano, A. Tassan, M. Mozzon, R. Bertani, F. Benetollo and R. A. Michelin, *J. Inorg. Biochem.*, 2008, **102**, 882–891.

19 S. M. Sbovata, F. Bettio, M. Mozzon, R. Bertani, A. Venzo, F. Benetollo, R. A. Michelin, V. Gandin and C. Marzano, *J. Med. Chem.*, 2007, **50**, 4775–4784.

20 P. D. Prenzler, D. C. R. Hockless and G. A. Heath, *Inorg. Chem.*, 1997, **36**, 5845–5849.

21 R. Cini, P. A. Caputo, F. P. Intini and G. Natile, *Inorg. Chem.*, 1995, **34**, 1130–1137.

22 J. M. Casas, M. H. Chisholm, M. V. Sicilia and W. E. Streib, *Polyhedron*, 1991, **10**, 1573–1578.

23 B. de Bruin, M. J. Boerakker, R. de Gelder, J. M. M. Smits and A. W. Gal, *Angew. Chem., Int. Ed.*, 1999, **38**, 219–222.

24 A. Venugopal, A. P. Shaw, K. W. Törnroos, R. H. Heyn and M. Tilset, *Organometallics*, 2011, **30**, 3250–3253.

25 The synthesis, characterization, and X-ray structure of Au (tpy)(Me)(NCMe)$^+$BF$_4$$^-$ is given in the ESI.†

26 Y. Ito, M. Sawamura and T. Hayashi, *J. Am. Chem. Soc.*, 1986, **108**, 6405–6406.

27 Y. Ito, M. Sawamura, M. Kobayashi and T. Hayashi, *Tetrahedron Lett.*, 1988, **29**, 6321–6324.

28 Y. Ito, M. Sawamura, E. Shirakawa, K. Hayashizaki and T. Hayashi, *Tetrahedron Lett.*, 1988, **29**, 235–238.

29 A. S. K. Hashmi, J. P. Weyrauch, W. Frey and J. W. Bats, *Org. Lett.*, 2004, **6**, 4391–4394.

30 S. Doherty, J. G. Knight, A. S. K. Hashmi, C. H. Smyth, N. A. B. Ward, K. J. Robson, S. Tweedley, R. W. Harrington and W. Clegg, *Organometallics*, 2010, **29**, 4139–4147.

31 H. von Wachenfeldt, A. V. Polukeev, N. Loganathan, F. Paulsen, P. Rose, M. Garreau, O. F. Wendt and D. Strand, *Dalton Trans.*, 2015, **44**, 5347–5353.

32 K. K.-Y. Kung, V. K.-Y. Lo, H.-M. Ko, G.-L. Li, P.-Y. Chan, K.-C. Leung, Z. Zhou, M.-Z. Wang, C.-M. Che and M.-K. Wong, *Adv. Synth. Catal.*, 2013, **355**, 2055–2070.

33 *Oxazoles: Synthesis, Reactions, and Spectroscopy, Part B*, ed. D. C. Palmer, John Wiley & Sons, Inc., Hoboken, NJ, USA, 2004.

34 M. J. Frisch, G. W. Trucks, H. B. Schlegel, G. E. Scuseria, M. A. Robb, J. R. Cheeseman, G. Scalmani, V. Barone, B. Mennucci, G. A. Petersson, H. Nakatsuji, M. Caricato, X. Li, H. P. Hratchian, A. F. Izmaylov, J. Bloino, G. Zheng, J. L. Sonnenberg, M. Hada, M. Ehara, K. Toyota, R. Fukuda, J. Hasegawa, M. Ishida, T. Nakajima, Y. Honda, O. Kitao, H. Nakai, T. Vreven, J. A. Montgomery, Jr., J. E. Peralta, F. Ogliaro, M. Bearpark, J. J. Heyd, E. Brothers, K. N. Kudin, V. N. Staroverov, R. Kobayashi, J. Normand, K. Raghavachari, A. Rendell, J. C. Burant, S. S. Iyengar, J. Tomasi, M. Cossi, N. Rega, J. M. Millam, M. Klene, J. E. Knox, J. B. Cross, V. Bakken, C. Adamo, J. Jaramillo, R. Gomperts, R. E. Stratmann, O. Yazyev, A. J. Austin, R. Cammi, C. Pomelli, J. W. Ochterski, R. L. Martin, K. Morokuma, V. G. Zakrzewski, G. A. Voth, P. Salvador, J. J. Dannenberg, S. Dapprich, A. D. Daniels, Ö. Farkas, J. B. Foresman, J. V. Ortiz, J. Cioslowski and D. J. Fox, *Gaussian 09, Rev. D.01*, Gaussian, Inc., Wallingford CT, 2009.

35 C. Adamo and V. Barone, *J. Chem. Phys.*, 1999, **110**, 6158–6170.

36 S. Grimme, J. Antony, S. Ehrlich and H. Krieg, *J. Chem. Phys.*, 2010, **132**, 154104.

37 E. Langseth, M. L. Scheuermann, D. Balcells, W. Kaminsky, K. I. Goldberg, O. Eisenstein, R. H. Heyn and M. Tilset, *Angew. Chem., Int. Ed.*, 2013, **52**, 1660–1663.

38 R. Krishnan, J. S. Binkley, R. Seeger and J. A. Pople, *J. Chem. Phys.*, 1980, **72**, 650–654.

39 A. D. McLean and G. S. Chandler, *J. Chem. Phys.*, 1980, **72**, 5639–5648.

40 D. Figgen, G. Rauhut, M. Dolg and H. Stoll, *Chem. Phys.*, 2005, **311**, 227–244.

41 D. Figgen, K. A. Peterson, M. Dolg and H. Stoll, *J. Chem. Phys.*, 2009, **130**, 164108.

42 A. V. Marenich, C. J. Cramer and D. G. Truhlar, *J. Phys. Chem. B*, 2009, **113**, 6378–6396.

Supporting Information

Small-molecule activation at Au(III): metallacycle construction from ethylene, water, and acetonitrile

Marte Sofie Martinsen Holmsen,[a] Ainara Nova,[b] David Balcells,[b] Eirin Langseth,[a] Sigurd Øien,[a] Eline Aasen Tråseth,[a] Richard H. Heyn[c] and Mats Tilset*[ab]

[a]Department of Chemistry, University of Oslo, P.O. Box 1033 Blindern, N-0315 Oslo, Norway (e-mail of corresponding author: mats.tilset@kjemi.uio.no)

[b]Centre for Theoretical and Computational Chemistry (CTCC) Department of Chemistry, University of Oslo, P.O. Box 1033 Blindern, N-0315 Oslo, Norway

[c]SINTEF Materials and Chemistry, P.O. Box 124 Blindern, N-0314 Oslo, Norway.

Table of contents

Experimental Section

General procedures. Gold(III) complexes **1** and **2** and AuBrMe(tpy) were prepared by previously reported procedures.[1,2] Distilled water was used. CH_3CN and CH_2Cl_2 were purified using a MB SPS-800 solvent purifying system from MBraun. The gold(III) complexes studied here are not sensitive to air, so inert atmosphere was not utilized, except for the synthesis of **9**. NMR spectra were recorded on Bruker Avance DPX200, AVII400, DRX500, AVII600 and AV600 instruments at ambient temperature. ^{1}H and ^{13}C spectra have been referenced relative to the residual solvent signals. ^{19}F has been referenced to $CFCl_3$ by using C_6F_6 (-164.9 ppm with respect to $CFCl_3$ at 0 ppm) as an internal standard. The ^{15}N chemical shifts have been calibrated using $MeNO_2$ as an external standard at 0 ppm. The peaks in the ^{1}H NMR and ^{13}C NMR spectra were assigned by the aid of 2D NMR techniques such as HSQC, HMBC, COSY, NOESY, and ^{1}H-^{15}N HMBC according to the numbering scheme shown below. Mass spectra (ESI) were obtained on a Micromass QTOF II spectrometer and a Bruker Daltronics maXisII spectrometer. Elemental analysis was performed by Microanalytisches Laboratorium Kolbe, Mülheim an der Ruhr, Germany.

Numbering scheme used for reporting the NMR data.

[1]   E. Langseth, C. H. Görbitz, R. H. Heyn and M. Tilset, *Organometallics*, 2012, **31**, 6567-6571.
[2]   E. Langseth, A. Nova, E. A. Tråseth, F. Rise, S. Øien, R. H. Heyn and M. Tilset, *J. Am. Chem. Soc.*, 2014, **136**, 10104-10115.

Preparation of [Au(tpy)(C–N)$^+$][$^-$OCOCF$_3$] (3).

3
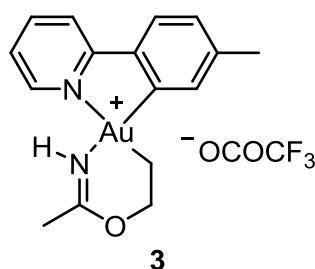
Preparation of 3 from 1. Au(tpy)(OCOCF$_3$)$_2$ (50.1 mg, 0.0847 mmol, 1.0 equiv.) was dissolved in acetonitrile (3 mL). Water (10 μL, 0.55 mmol, 6.5 equiv.) was added. Ethylene was bubbled through the solution at ambient pressure for two minutes, and the flask was sealed with a glass stopper. The reaction mixture was stirred at ambient temperature in the absence of light for 7 days. The reaction mixture was filtered and the volatiles were removed under reduced pressure furnishing **3** as a white solid (38.1 mg, 0.0675 mmol, 80%).

Preparation of 3 from 2. Au(tpy)(CH$_2$CH$_2$OCOCF$_3$)(OCOCF$_3$) (50.1 mg, 0.0809 mmol, 1.0 equiv.) was dissolved in acetonitrile (3 mL). Water (10 μL, 0.55 mmol, 6.8 equiv.) was added. Ethylene was bubbled through the solution at ambient pressure for two minutes, and the flask was sealed with a glass stopper. The reaction mixture was stirred at ambient temperature in the absence of light for 5 days. The reaction mixture was filtered and the volatiles were removed under reduced pressure furnishing **3** as a white solid (35.8 mg, 0.0634 mmol, 78%).

^{1}H NMR (600 MHz, CD$_2$Cl$_2$): δ 10.28 (bs, 1H, N**H**), 9.33 (d, 1H, J = 5.4 Hz, **H^6**), 8.08 (ddd, 1H, J = 8.0, 7.5, 1.4 Hz, **H^4**), 7.96 (d, 1H, J = 8.0 Hz, **H^3**), 7.71 (d, 1H, J = 7.7 Hz, **H$^{3'}$**), 7.58 (ddd, 1H, J = 7.5, 5.6, 1.1 Hz, **H^5**), 7.23-7.25 (m, 2H, **H$^{4'}$** and **H$^{6'}$**), 4.34 (m, 2H, OC**H$_2$**), 2.73 (m, 2H, AuC**H$_2$**), 2.51 (s, 3H, OCC**H$_3$**), 2.44 (s, 3H, ArC**H$_3$**).

^{1}H NMR (400 MHz, CD$_3$CN): δ 9.03 (bs, 1H, N**H**), 8.94 (d, 1H, J = 5.4 Hz, **H^6**), 8.15 (ddd, 1H, J = 8.0, 7.6, 1.5 Hz, **H^4**), 8.08 (d, 1H, J = 8.1 Hz, **H^3**), 7.77 (d, 1H, J = 8.4 Hz, **H$^{3'}$**), 7.58 (ddd, 1H, J = 7.3, 5.7, 1.3 Hz, **H^5**), 7.22-7.24 (m, 2H, **H$^{4'}$** and **H$^{6'}$**), 4.32 (m, 2H, OC**H$_2$**), 2.69 (m, 2H, AuC**H$_2$**), 2.43 (s, 3H, OCC**H$_3$**), 2.39 (s, 3H, ArC**H$_3$**).

^{13}C NMR (150 MHz, CD$_2$Cl$_2$): δ 175.2, 161.7, 149.8, 142.4, 142.3, 142.0, 141.9, 131.2, 129.4, 126.0, 124.9, 120.2, 66.5, 28.6, 22.0, 21.6. $^-$OCOCF$_3$ was not observed by ^{13}C NMR.

^{15}N{^{1}H} NMR (600 MHz, CD$_2$Cl$_2$): δ -129 (**N**(tpy)), -212 (**N**H, $|J|$ = 78 Hz), as observed by ^{1}H-^{15}N HMBC (see **Figure S12**).

^{19}F NMR (188 MHz, CD$_2$Cl$_2$): δ -78.1 (bs, C**F$_3$**).

MS (ESI⁺, MeCN): *m/z* (rel. %): 451 ([M-OCOCF₃]⁺, 100).

MS (ESI⁻, MeCN): *m/z* (rel. %): 113 ([OCOCF₃]⁻, 100) was observed among other unidentified peaks.

HRMS (ESI⁺, MeCN): Found: 451.1068; calcd for $C_{16}H_{18}AuN_2O$: 451.1084 (+0.0016).

HRMS (ESI⁻, MeCN): Found: 112.9859; calcd for $C_2F_3O_2$: 112.9856 (–0.0003).

Elemental analysis: Anal. Calcd for $C_{18}H_{18}AuF_3N_2O_3$: C, 38.31; H, 3.22; N, 4.96. Found: C, 37.81; H, 3.19; N, 4.59.

Comments to the ^{1}H-^{15}N HMBC Spectrum

In the ^{1}H-^{15}N HMBC spectrum, see **Figure S12**, signals arising from two different N atoms are clearly observed. One signal at $\delta(^{15}$N$\{^1$H$\})$ = -212 arises from the chelate NH and correlates with the broadened ^{1}H signal of the NH group at $\delta(^1$H$)$ = 10.28 and with the signal from the metallacycle methyl group at $\delta(^1$H$)$ = 2.51. No correlation of NH with OCH$_2$CH$_2$ was observed which is in agreement with the proposed structure **3**. The chemical shift of NH is in the range of what has been observed for Pt(II) imine complexes[3,4] and is shifted upfield compared to free 2-methyl-2-oxazoline ($\delta(^{15}$N$)$ = -167 ppm)[5] probably due to the coordination of N to Au. The $\left| {}^1J(^1$H-^{15}N$)\right|$ coupling constant of 78 Hz is within the range of what is observed for ketimines and protonated ketimines.[6] The other ^{15}N signal at $\delta(^{15}$N$\{^1$H$\})$ = -129 arises from the N atom in the tpy ligand and has a correlation with the signal arising from the CH proton α to the pyridyl-N atom at $\delta(^1$H$)$ = 9.33. This chemical shift is similar to what is observed for Au(ppy)Cl$_2$ (ppy = 2-phenylpyridine)[7] and Au(III) acetylpyridine and benzoylpyridine complexes[8] and is within the region where ^{15}N NMR shifts for azines are usually found and lies in the region between pyridine and protonated pyridine.[9,10]

[3] B. Longato, D. Montagner, G. Bandoli and E. Zangrando, *Inorg. Chem.*, 2006, **45**, 1805-1814.

[4] T. Chivers, K. McGregor and M. Parvez, *Inorg. Chem.*, 1993, **32**, 5119-5125.

[5] M. Witanowski, I. Stefaniak and G. A. Webb, *Annu. Rep. NMR Spectrosc.,* 1987, **18**, 213-737.

[6] M. Witanowski and G. A. Webb, eds., *Nitrogen NMR*, Springer US, Boston, MA, 1973.

[7] L. Pazderski, T. Pawlak, J. Sitkowski, L. Kozerski and E. Szłyk, *Magn. Reson. Chem.*, 2009, **47**, 932-941.

[8] D. Niedzielska, T. Pawlak, T Czubachowski and L. Pazderski, *J. Spectrosc.*, 2013, **2013**, Article ID 982832. DOI: 10.1155/2013/982832.

[9] W. von Philipsborn and R. Müller, *Angew. Chem. Int. Ed.*, 1986, **25**, 383-413.

[10] M. Witanowski, I. Stefaniak and G. A. Webb, *Annu. Rep. NMR Spectrosc.,* 1978, **7**, 117-244.

Preparation of [Au(tpy)(NCMe)Me$^+$][BF$_4^-$] (9).
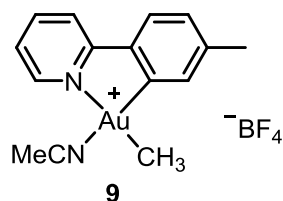
A solution of AuBrMe(tpy) (49 mg, 0.11 mmol, 1.0 equiv.) in CH$_2$Cl$_2$ (5 mL) was cooled to −78 °C. A solution of AgBF$_4$ (53 mg, 0.27 mmol, 2.5 equiv.) in acetonitrile (500 μL) was added. Stirring was continued for 5 minutes, and the solution was warmed to ambient temperature. The solvents were removed from the grayish mixture under reduced pressure. The pale greyish solid was dissolved in acetonitrile (10 mL) and filtered to furnish a clear, colorless solution. The solvent was removed under reduced pressure, leaving a light grey solid. Recrystallization by slow diffusion of ether layered on top of a concentrated solution of **9** in acetonitrile provided material for the single-crystal structure determination and for the spectroscopic characterization.

^{1}H NMR (CD$_3$CN, 500 MHz): δ 8.72 (d, J = 5.4 Hz, 1H, **H^6**), 8.18 (ddd, J = 7.8, 7.8, 1.2 Hz, 1H, **H^4**), 8.08 (d, J = 8.2 Hz, 1H, **H^3**), 7.76 (d, J = 8.3 Hz, 1H, **H$^{3'}$**), 7.61 (dd, J = 6.6, 6.6 Hz, 1H, **H^5**), 7.27 (s, 1H, **H$^{6'}$**), 7.26 (d, J = 7.2 Hz, 1H, **H$^{4'}$**), 2.39 (s, 3H, ArC**H$_3$**), 1.97 (s, 3H, NCC**H$_3$**), 1.51 (s, 3H, AuC**H$_3$**).

^{13}C NMR (CD$_3$CN, 150 MHz): δ 160.5, 148.7, 143.5, 143.4, 142.5, 136.6, 132.1, 130.7, 127.3, 126.1, 121.6, 21.8, 12.1, 1.3.

MS (ESI$^+$, MeCN): m/z (rel. %): 421([M-BF$_4$]$^+$,100).

HRMS (MeCN): Found: 421.0973, calcd for C$_{15}$H$_{16}$N$_2$Au 421.0979 (−1.4 ppm).

Mechanistic experiments on the role of acetamide.

Experiment in scheme 4A: A CH_2Cl_2 solution of **2** (1.0 equiv.) and acetamide (1.9 equiv.) were stirred for 6 days at ambient temperature. Volatiles were removed under reduced pressure and the remaining solid was investigated by ^{1}H NMR spectroscopy, which revealed that Au(III) complex **3** was not formed.

Experiment in scheme 4B: The metallacycle complex **3** was synthesized from **2** as already described, but in acetonitrile-d_3 with acetamide (3.1 equiv.) and water (6.6 equiv.) added. After 5 days the volatiles were removed under reduced pressure. The remaining solid was dissolved in CH_2Cl_2, filtered and CH_2Cl_2 was removed under reduced pressure yielding a white solid. Inspection of the white solid by ^{1}H NMR spectroscopy revealed that **3-d_3** was formed as the major product, together with minor amounts of **3** (ca 8% by ^{1}H-NMR integration) as inferred by the metallacycle-methyl resonance at δ 2.51 (CD_2Cl_2) in the ^{1}H NMR spectrum (see **Figure S14**).

Complex **3**
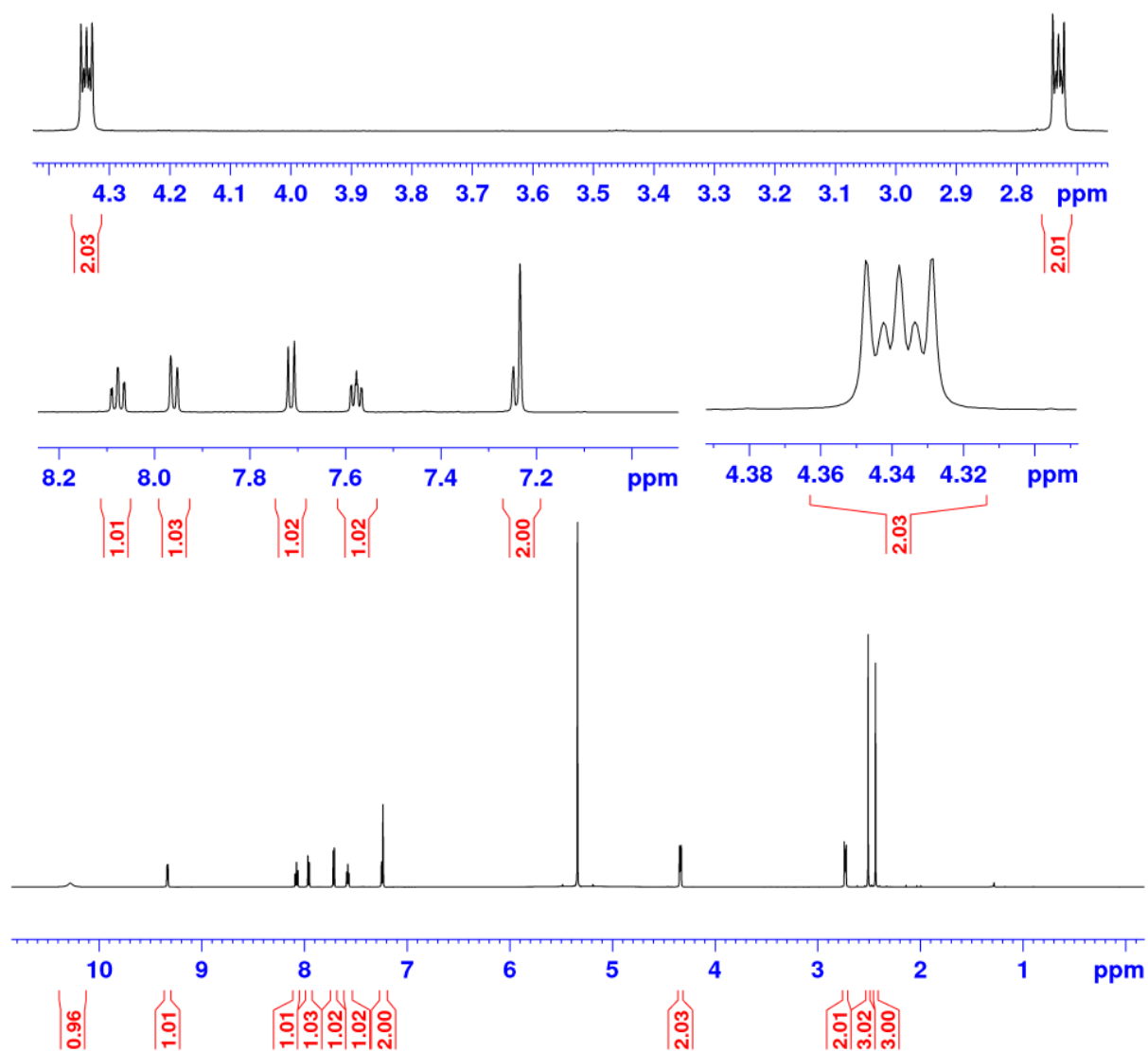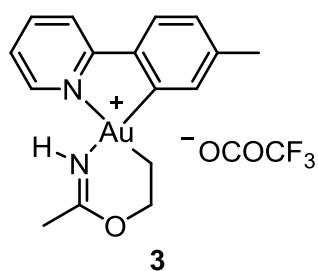
Figure S1. ^{1}H NMR (600 MHz, CD$_2$Cl$_2$) of Au(III) complex **3**.
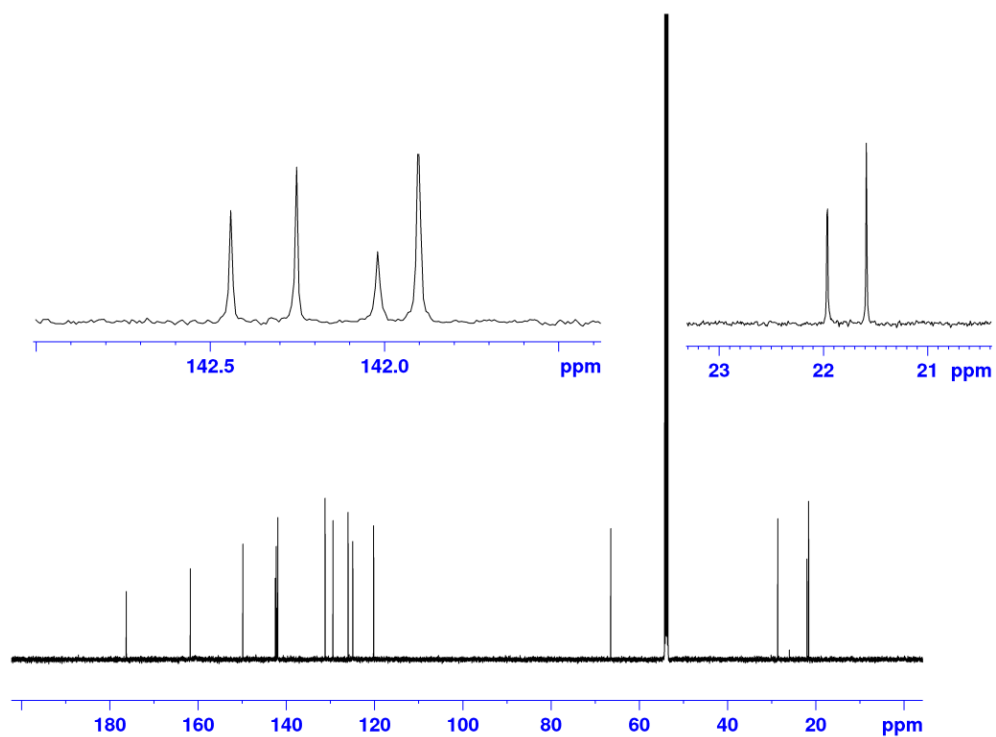
Figure S2. ^{13}C NMR(150 MHz, CD_2Cl_2, d1 = 10 s) of Au(III) complex **3**.

C6F6
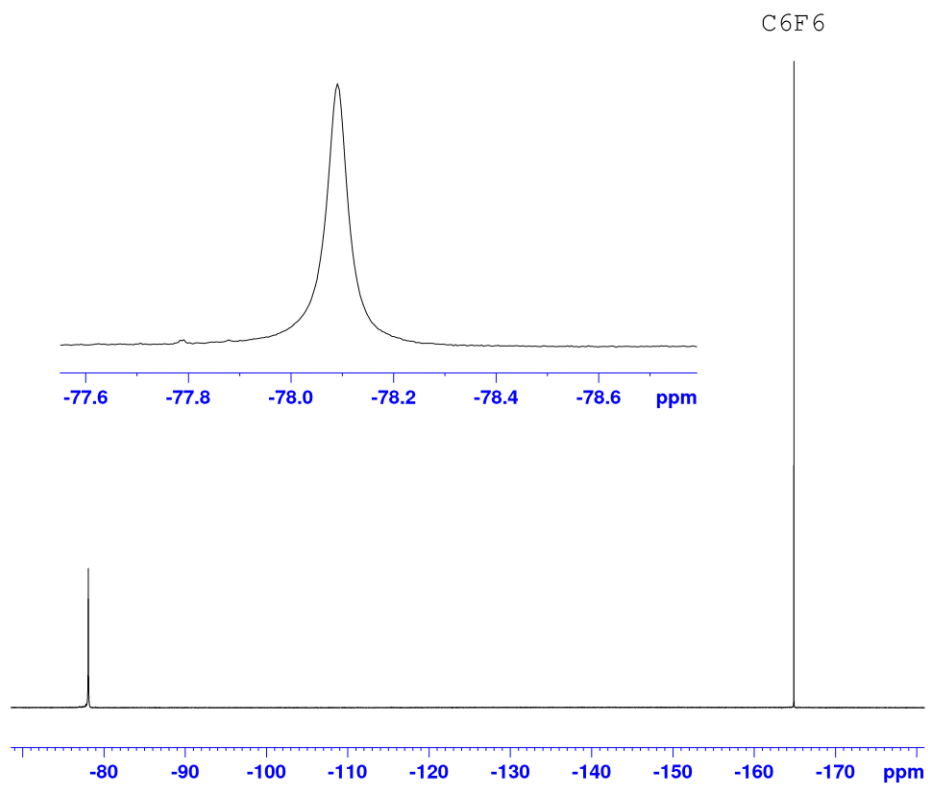
Figure S3. ^{19}F NMR (188 MHz, CD_2Cl_2) of Au(III) complex **3**.
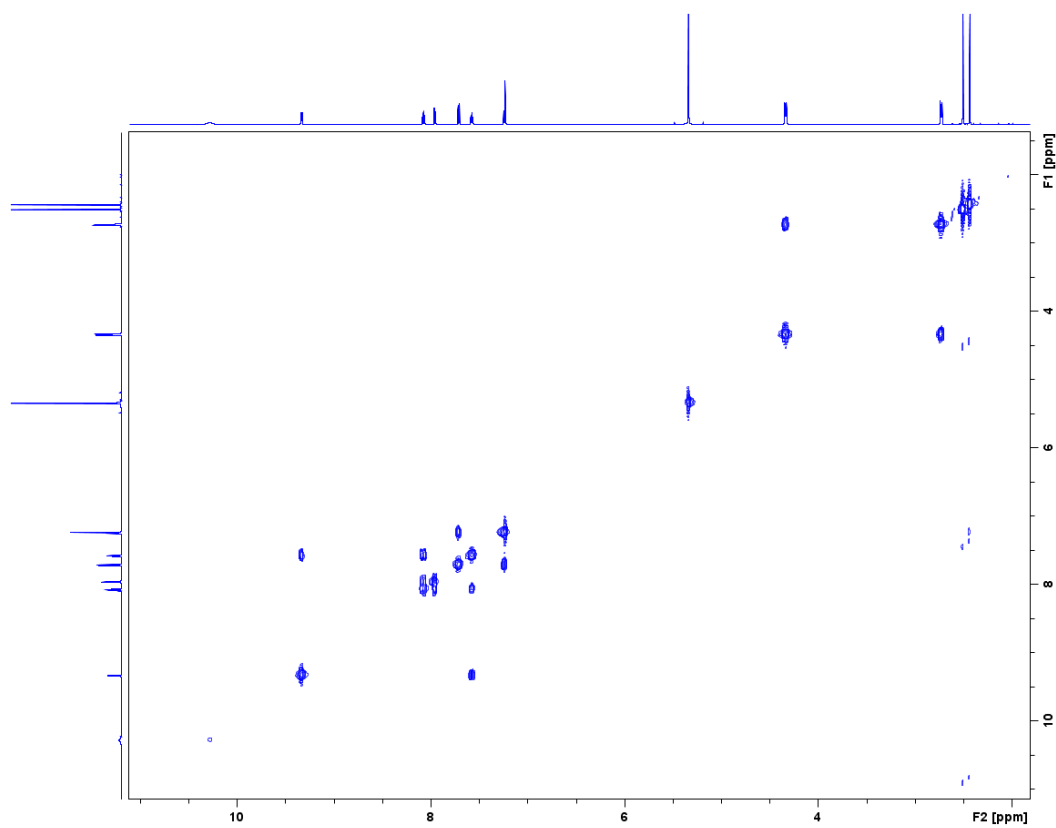
Figure S4. COSY (600 MHz, CD_2Cl_2) of Au(III) complex **3**.
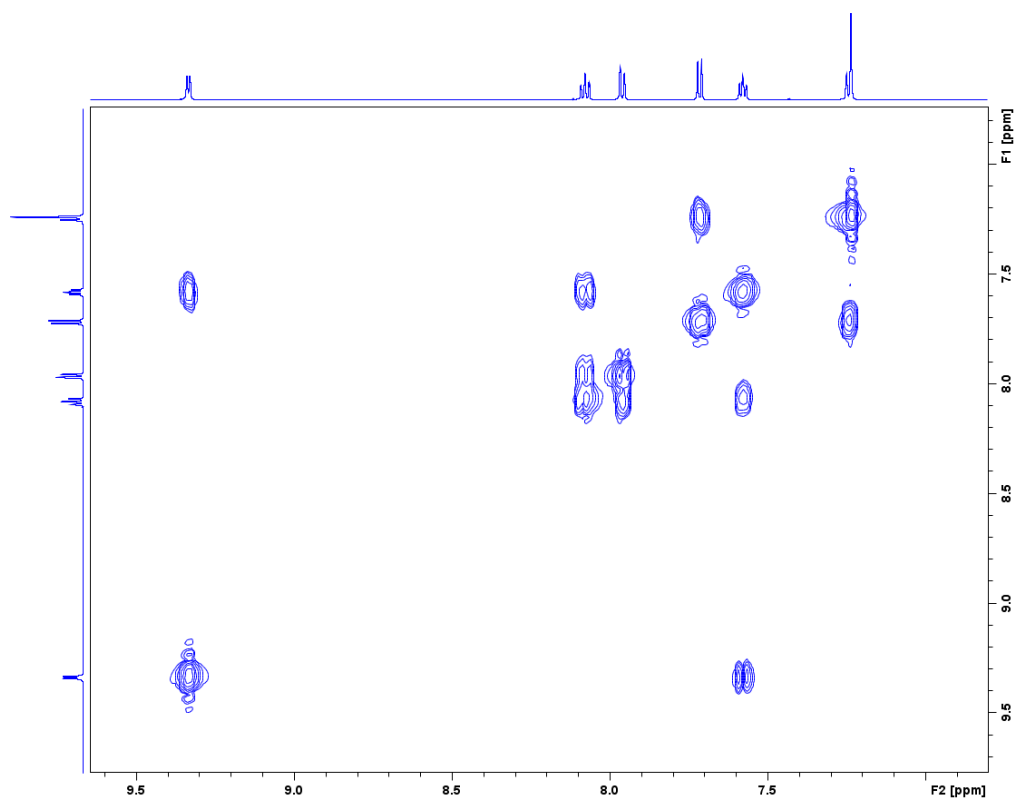
Figure S5. COSY (600 MHz, CD_2Cl_2) of Au(III) complex **3**. Close-up of the aromatic region.
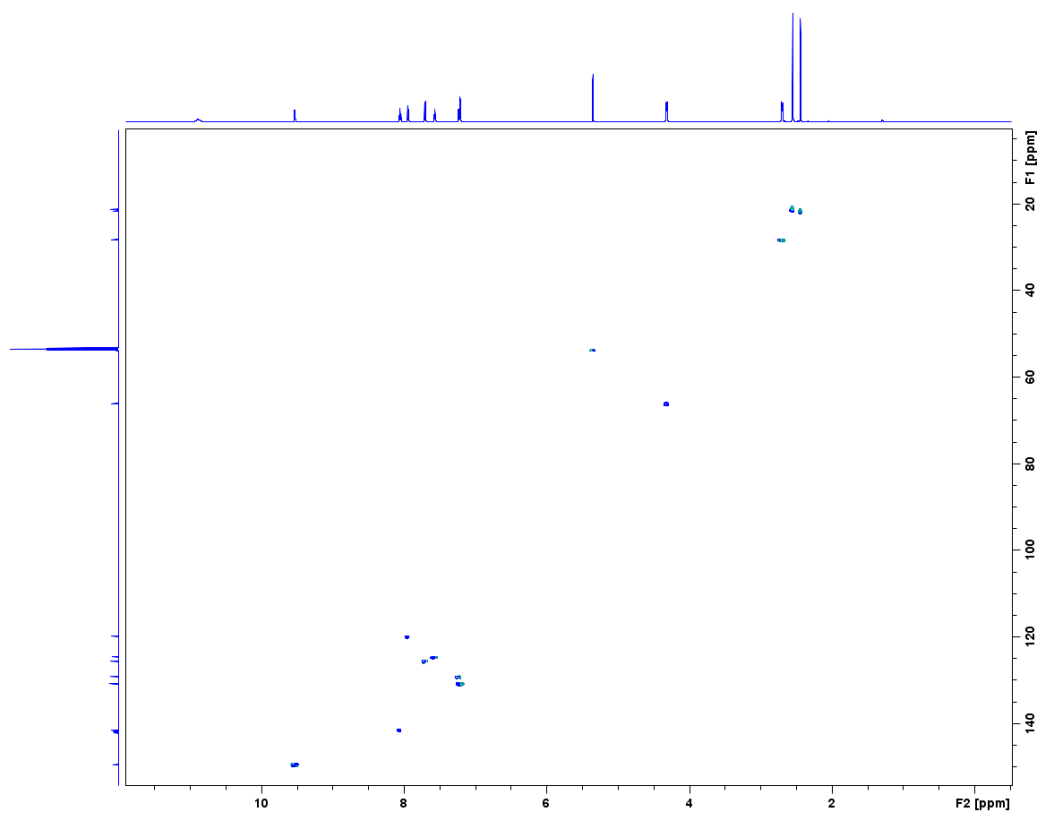
Figure S6. HSQC (600 MHz, CD$_2$Cl$_2$) of Au(III) complex **3**.
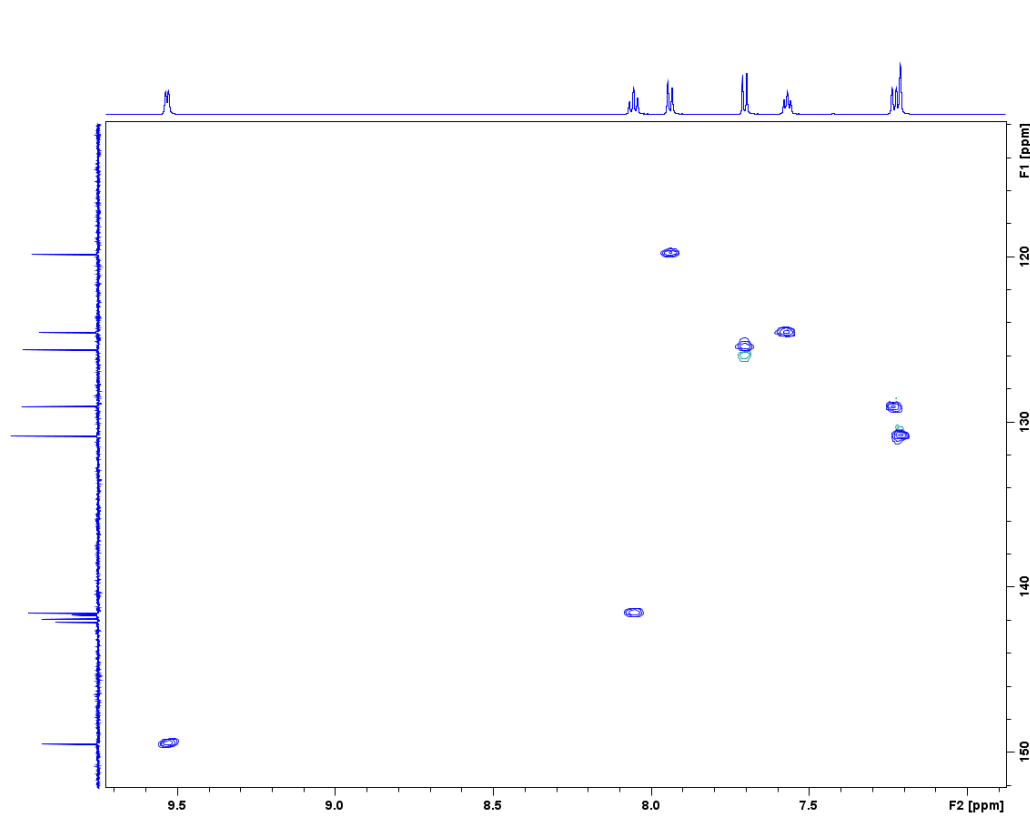
Figure S7. HSQC (600 MHz, CD$_2$Cl$_2$) of Au(III) complex **3**. Close-up of the aromatic region.
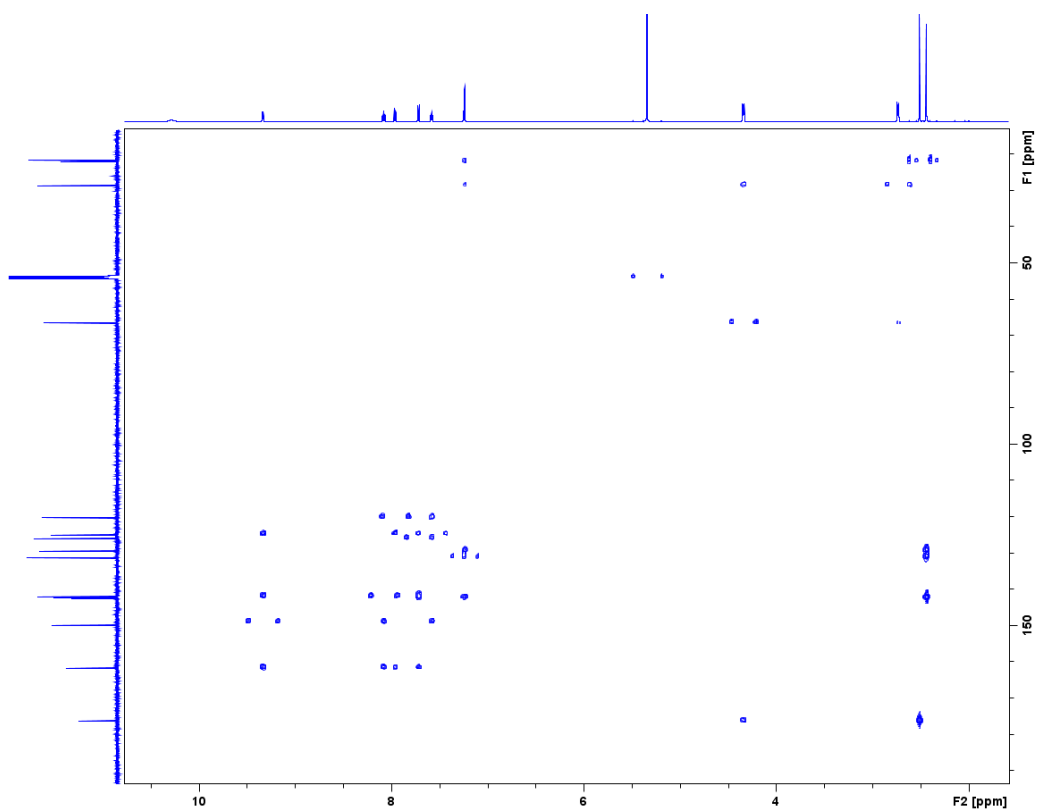
Figure S8. HMBC (600 MHz, CD$_2$Cl$_2$, no decoupling) of Au(III) complex **3**.
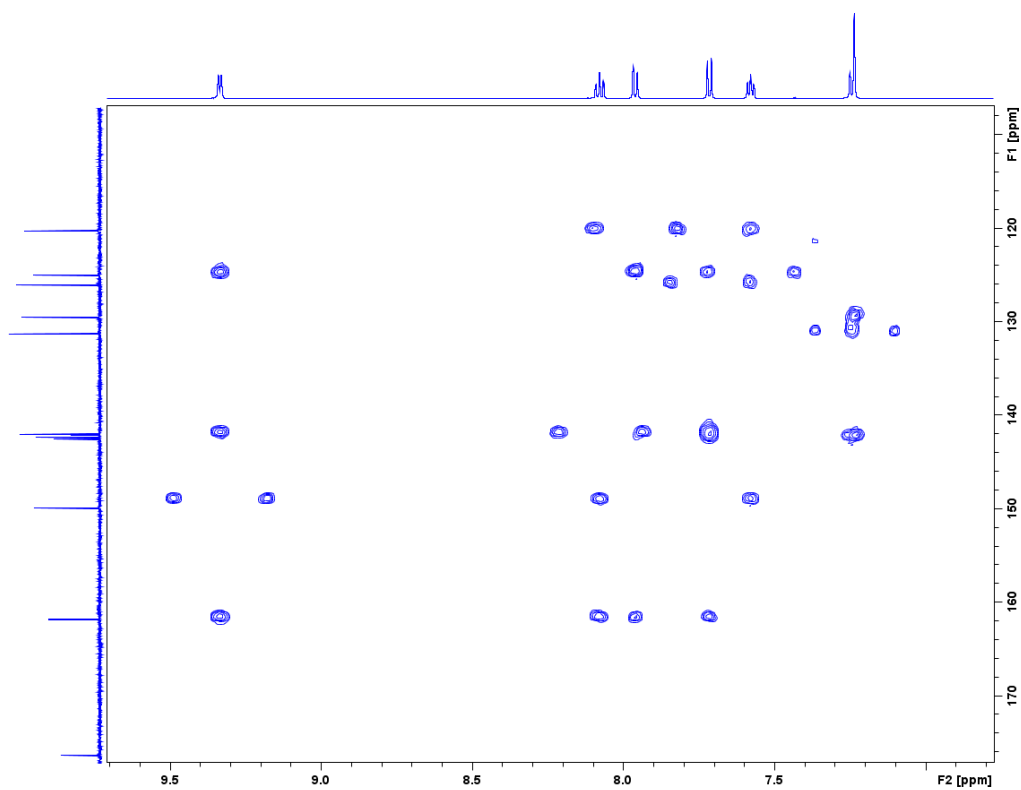
Figure S9. HMBC (600 MHz, CD$_2$Cl$_2$, no decoupling) of Au(III) complex **3**. Close-up of the aromatic region.
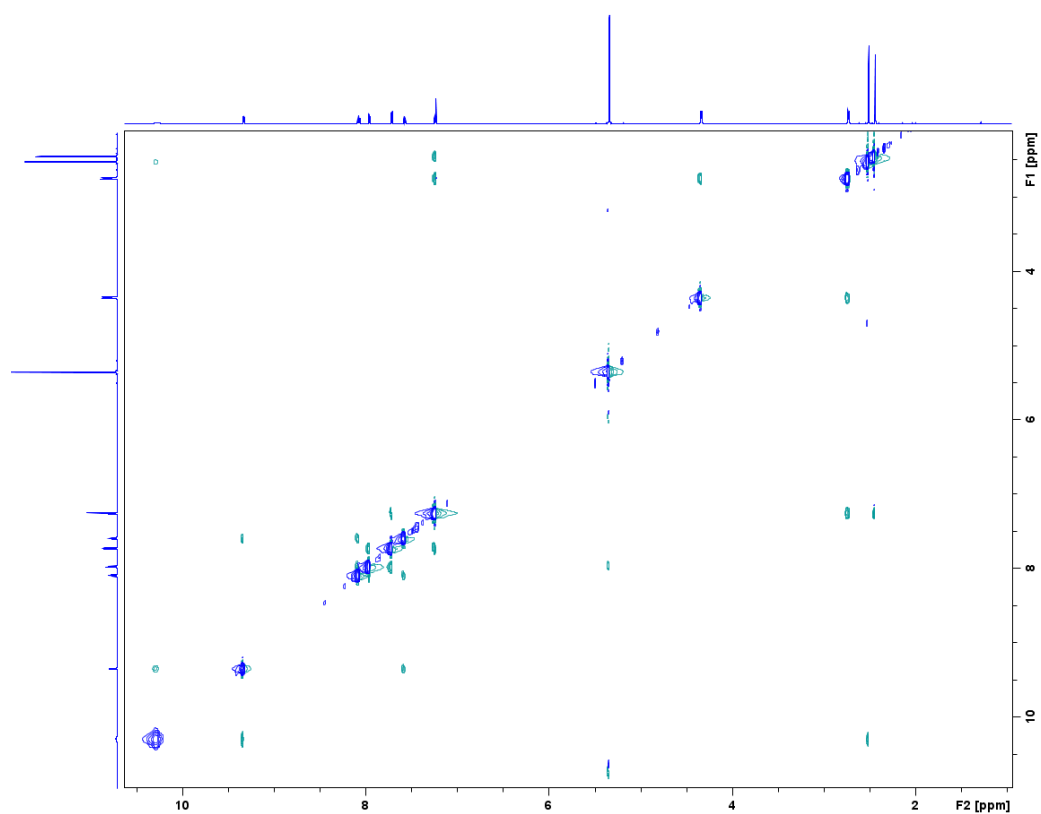
Figure S10. NOESY (600 MHz, CD$_2$Cl$_2$, mixing time = 1 s) of Au(III) complex **3**.
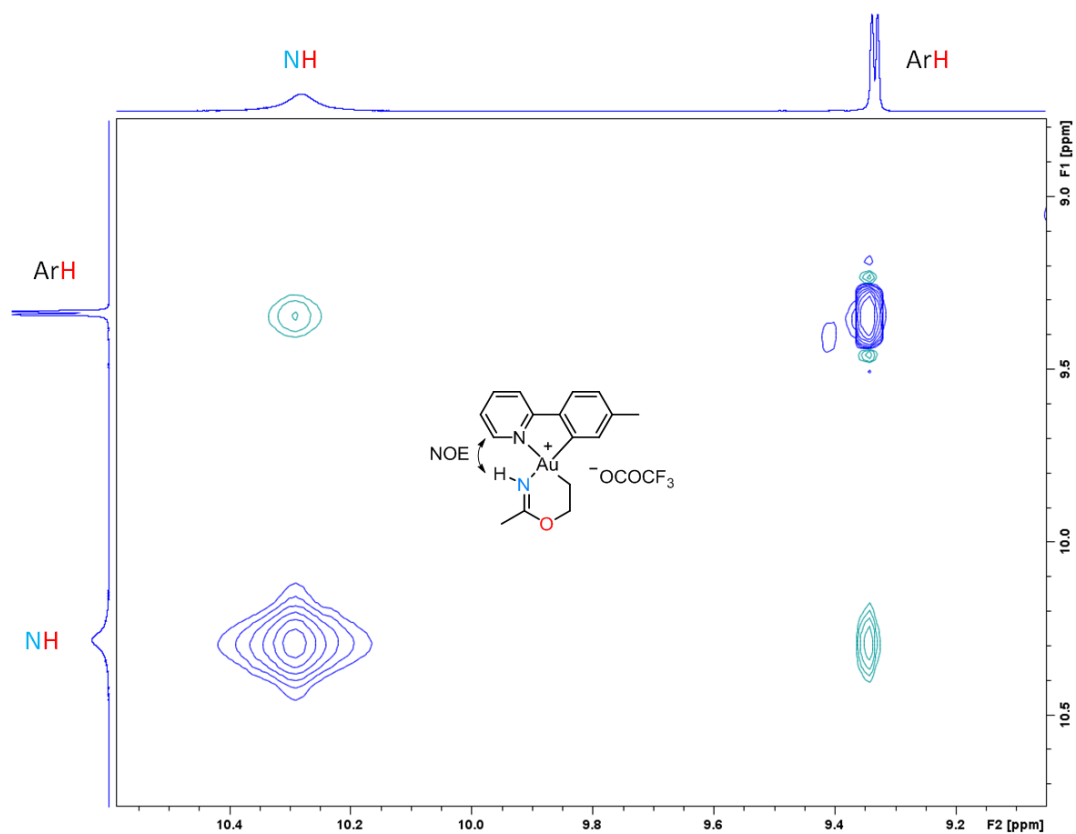
Figure S11. NOESY (600 MHz, CD$_2$Cl$_2$, mixing time = 1 s) of Au(III) complex **3**. Close-up of the NOE correlation between NH and tpy.
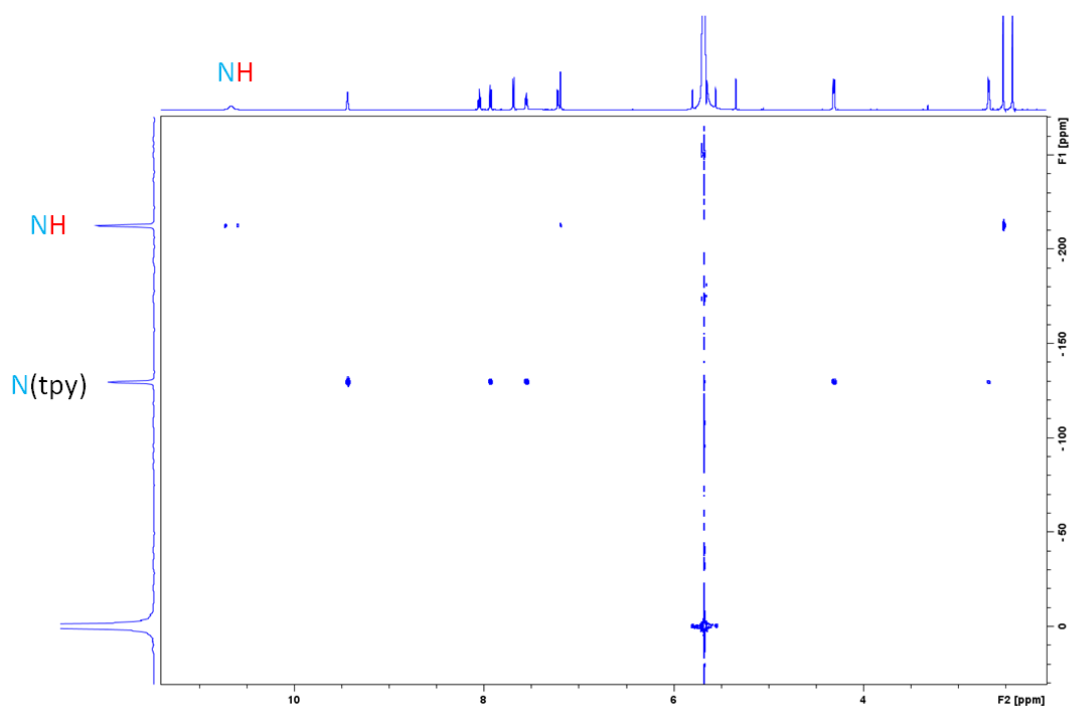
Figure S12. ^{1}H-^{15}N HMBC (600 MHz, CD$_2$Cl$_2$, no decoupling) of Au(III) complex **3**. The ^{15}N chemical shifts have been calibrated using MeNO$_2$ as an external standard at 0 ppm.
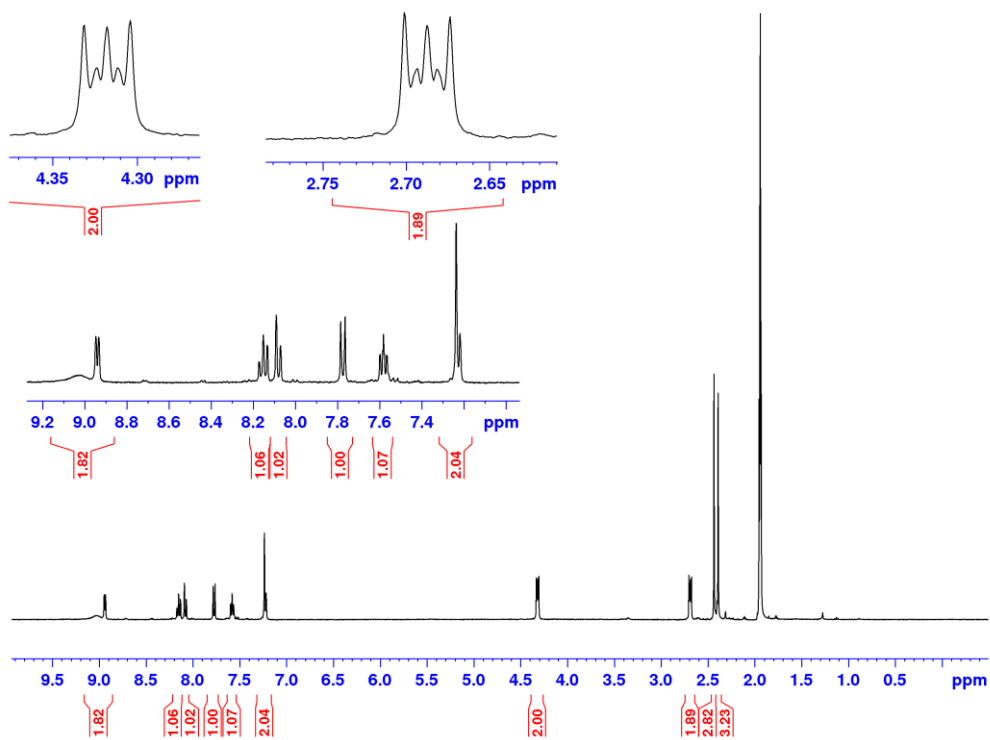
Figure S13: ^{1}H NMR (400 MHz, CD$_3$CN) of Au(III) complex **3**.
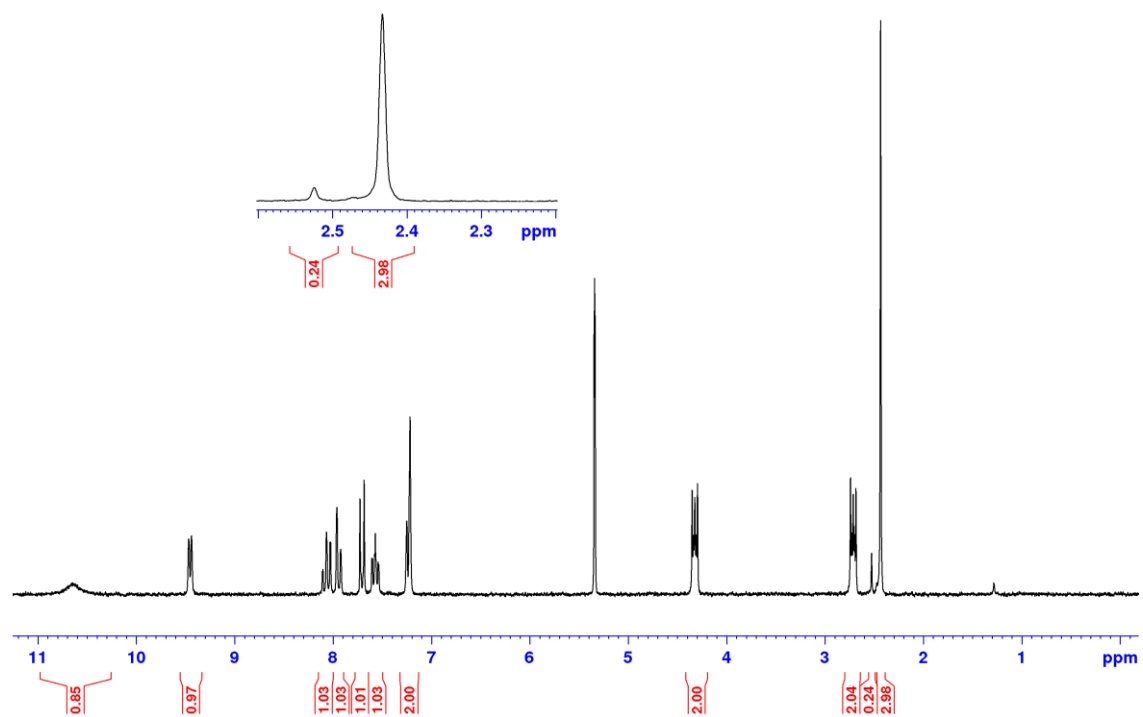
Figure S14: ^{1}H NMR (200 MHz, CD_2Cl_2) of Au(III) complex **3-d_3**. Small amounts of **3** (ca 8% by integration) can also be observed.

Complex **9**
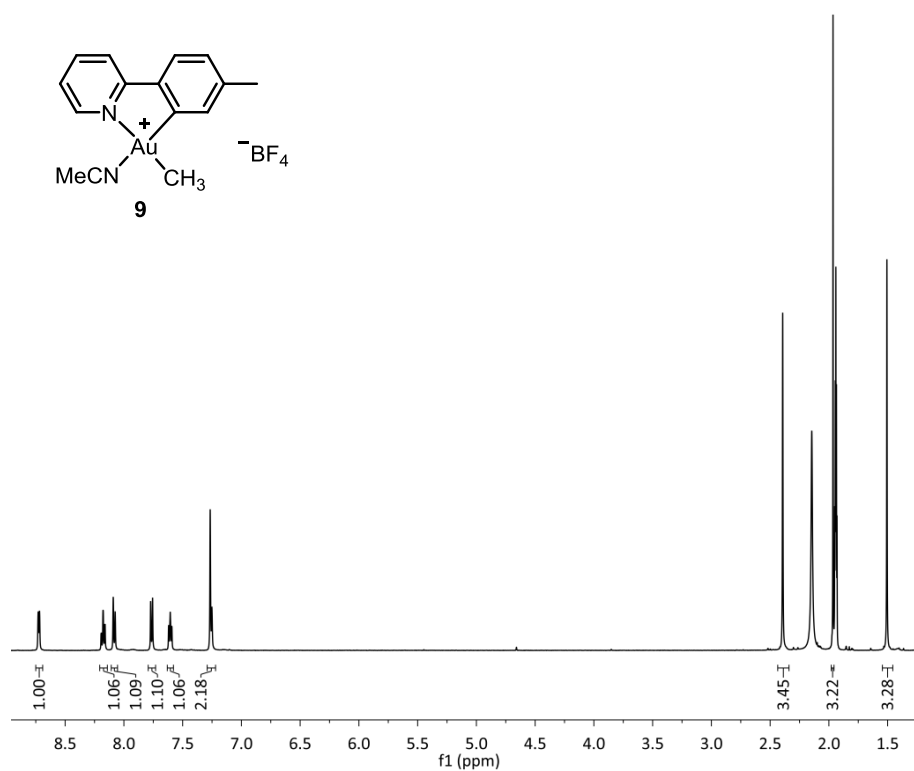
Figure S15. ^{1}H NMR (500 MHz, CD$_3$CN) of **9**.
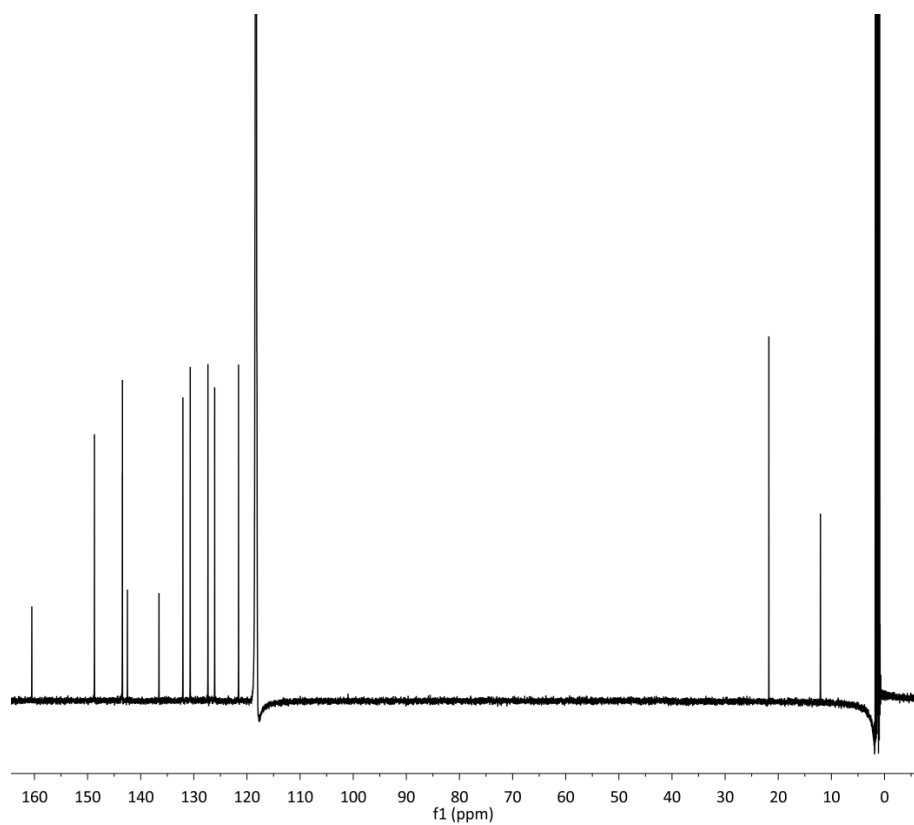
Figure S16. ^{13}C NMR (150 MHz, CD$_3$CN) of **9**.
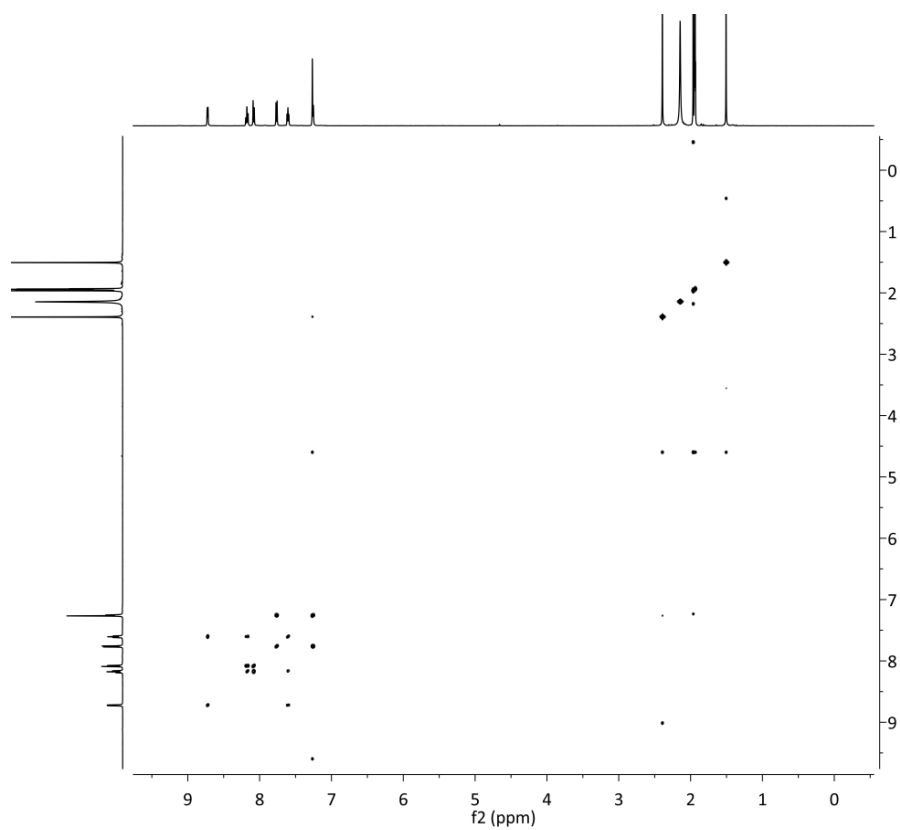
Figure S17. COSY (500 MHz, CD$_3$CN) of **9**.
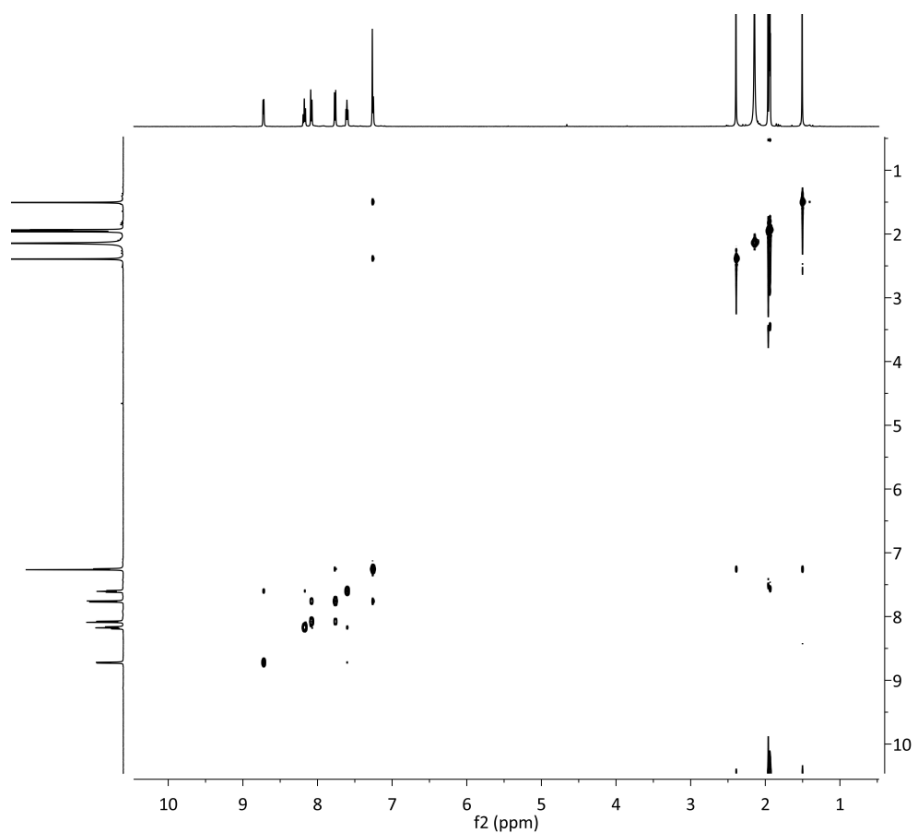
Figure S18. NOESY (500 MHz, CD$_3$CN) of **9**.
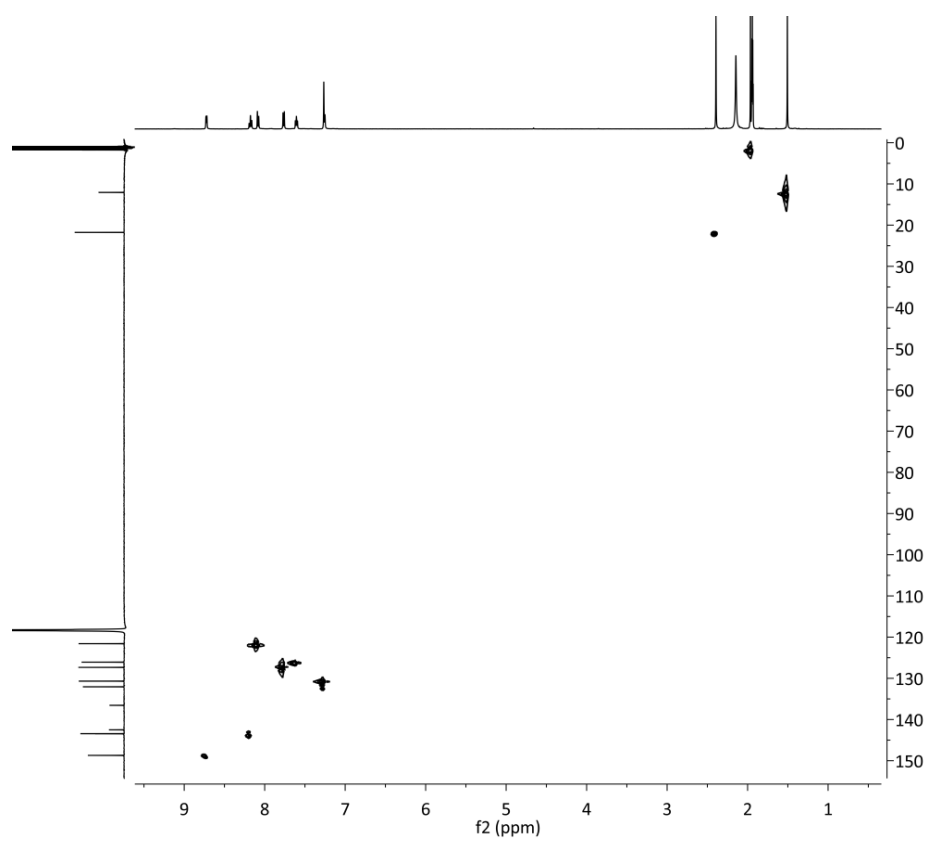
Figure S19. HSQC (600 MHz, CD$_3$CN) of **9**.
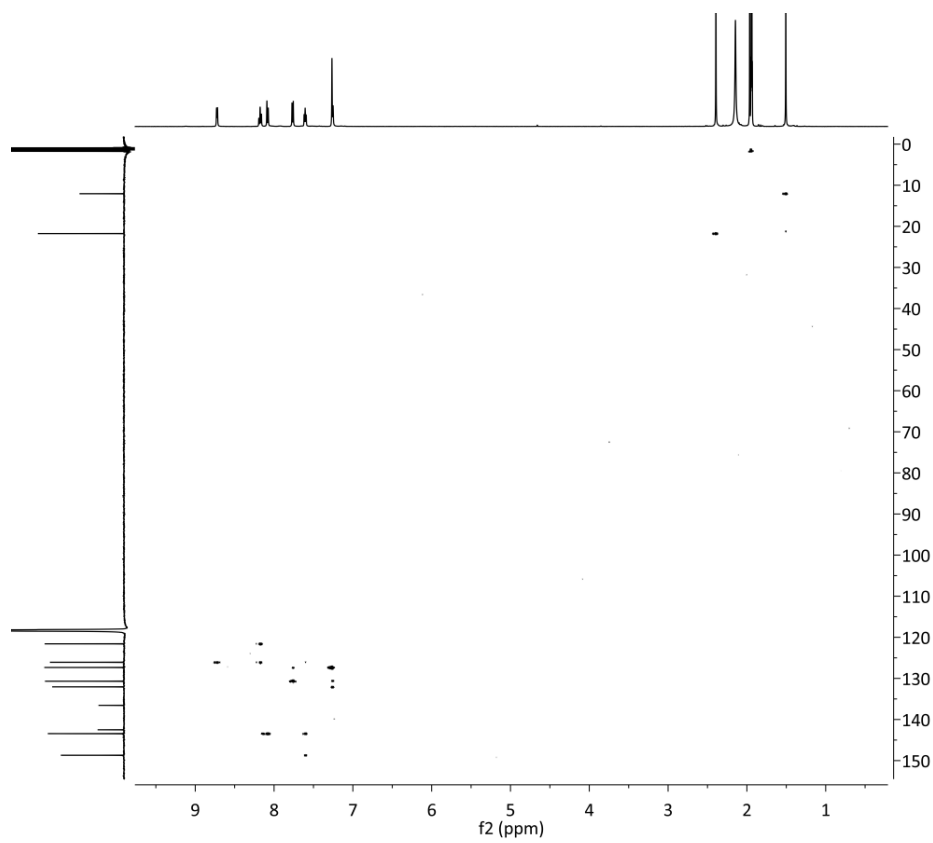
Figure S20. H2BC (500 MHz, CD$_3$CN) of **9**.

Crystallographic methods

Crystals of **3** were grown by the vapor diffusion technique. A small vial with a reaction mixture containing **2** dissolved in acetonitrile was placed in a larger vial containing pentane slowly affording crystals of **3**. Crystals of **9** were grown by slow diffusion of ether layered on top of a concentrated solution of **9** in acetonitrile.

The data were acquired using a Bruker D8 Venture diffractometer with the APEX2 suite, integrated with SAINT V8.32B, solved with SHELXT[11] in the OLEX2 GUI[12], and refined with SHELXL[13]. The cif files were edited with enCIFer v1.4[14], and molecular graphics were produced with Diamond v4.1.2.[15]

All metric data are contained in the respective cif files, available as ESI and from https://www.ccdc.cam.ac.uk/ (CCDC numbers 1443528 for **3;** 1443527 for **9**).

[11] G. Sheldrick, *Acta Crystallogr., Sect. A,* 2015, **71**, 3-8.
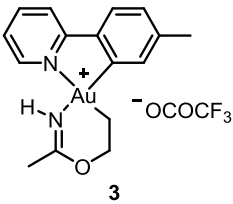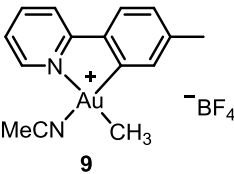
[12] O. V. Dolomanov, L. J. Bourhis, R. J Gildea, J. A. K. Howard and H. Puschmann, *J. Appl. Crystallogr*. 2009, **42**, 339-341.

[13] G. Sheldrick, *Acta Crystallogr., Sect. C,* 2015, **71**, 3-8.

[14] F. H. Allen, O. Johnson, G. P. Shields, B. R. Smith and M. Towler, *J. Appl. Crystallogr.* 2004, **37**, 335-338.

[15] H. Putz, K. Brandenburg, *Diamond - Crystal and Molecular Structure Visualization*, 4.1.2; Crystal Impact: Kreuzherrenstr. 102, 53227 Bonn, Germany, 1997.

Table S1. Crystal and structure refinement data for **3** and **9**.

Compound		
	3	**9**
CCDC no	1443528	1443527
Identification code	msh-246-mp_sx	EAT-156-P1_b
Empirical formula	$C_{18}H_{18}AuF_3N_2O_3$	$C_{15}H_{16}AuBF_4N_2$
Formula weight	564.31	508.07
Temperature/K	100	100
Crystal system	monoclinic	monoclinic
Space group	$P112_1/n$	$P2_1/m$
a/Å	7.1906(6)	10.2527(5)
b/Å	12.6491(10)	6.6903(3)
c/Å	19.3960(16)	12.3307(6)
α/°	90	90
β/°	89.9973(16)	109.737(2)
γ/°	90	90
Volume/Å^3	1764.2(2)	796.12(7)
Z	4	4
ρ_{calc}g/cm^3	2.125	2.119
μ/mm^{-1}	8.391	9.279
F(000)	1080	960
Crystal size/mm^3	0.472 × 0.123 × 0.077	0.2 × 0.15 × 0.08
Radiation	MoKα (λ = 0.71073)	MoKα (λ = 0.71073)
2Θ range for data collection/°	5.292 to 63.234	4.22 to 52.896
Index ranges	-10 ≤ h ≤ 10, -18 ≤ k ≤ 18, -28 ≤ l ≤ 28	-12 ≤ h ≤ 12, -8 ≤ k ≤ 8, -15 ≤ l ≤ 15
Reflections collected	28613	12713
Independent reflections	5951 [R_{int} = 0.0480, R_{sigma} = 0.0353]	1786 [R_{int} = 0.0380, R_{sigma} = 0.0222]
Data/restraints/parameters	5951/0/247	1786/0/142
Goodness-of-fit on F^2	1.05	1.016
Final R indexes [I>=2σ (I)]	R_1 = 0.0187, wR_2 = 0.0415	R_1 = 0.0221, wR_2 = 0.0504
Final R indexes [all data]	R_1 = 0.0214, wR_2 = 0.0424	R_1 = 0.0229, wR_2 = 0.0507
Largest diff. peak/hole / e Å^{-3}	0.79/-1.51	1.13/-0.73
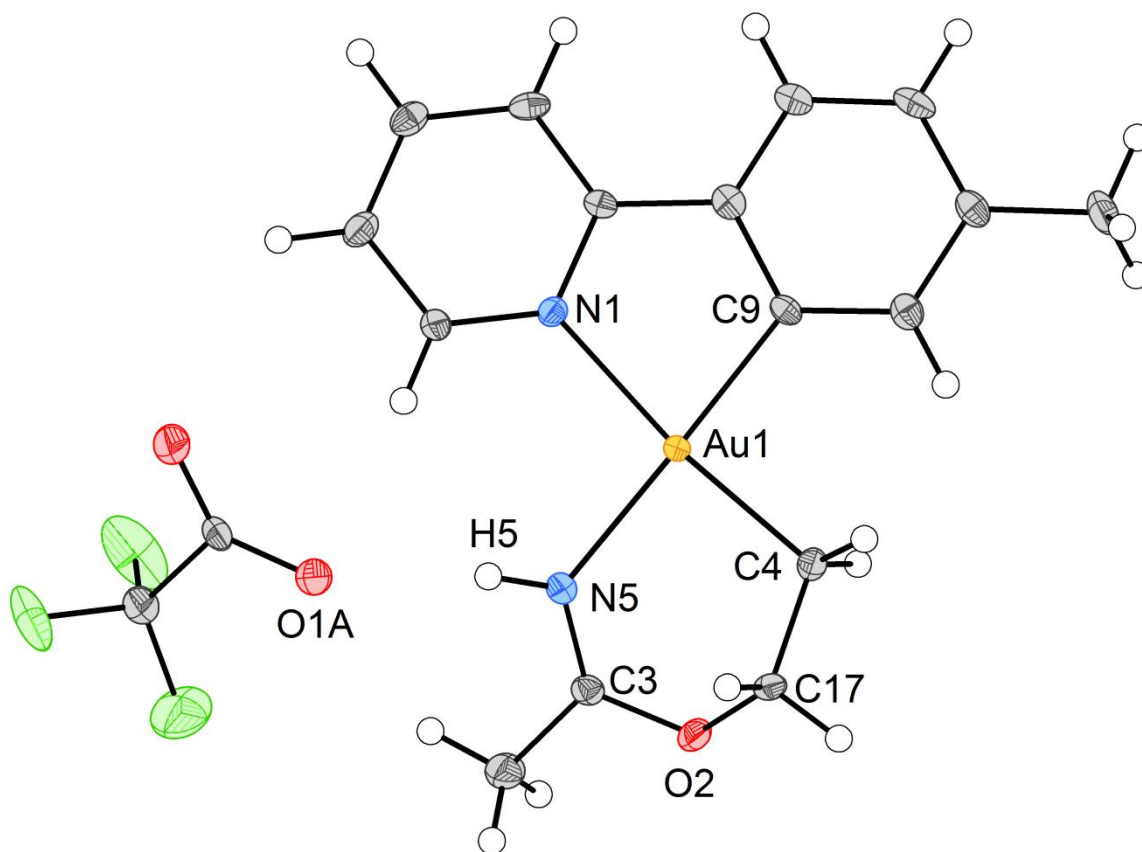
Figure S21. ORTEP plot of **3** with 50% ellipsoids. Selected bond distances and angles: Au1-C4, 2.042(3); Au1-C9, 2.019(3); Au1-N1, 2.126(2); Au1-N5, 2.092(3); C3-N5, 1.284(4); C3-O2, 1.332(3); C17-O2, 1.449(4); C4-C17, 1.510(4); O1A···N5, 2.8708(2); C4-Au1-C9, 92.39(12); C4-Au1-N5, 89.54(11); C9-Au1-N1, 80.60(10); N1-Au1-N5, 97.43(9); C4-Au1-N1, 172.99(11); C9-Au1-N5, 174.24(12); C3-O2-C17-C4, -70.8(4); Au1-C4-C17-O2, 60.2(3); Au1-N5-C3-O2, 26.5(5); C17-O2-C3-N5, 21.8(5).
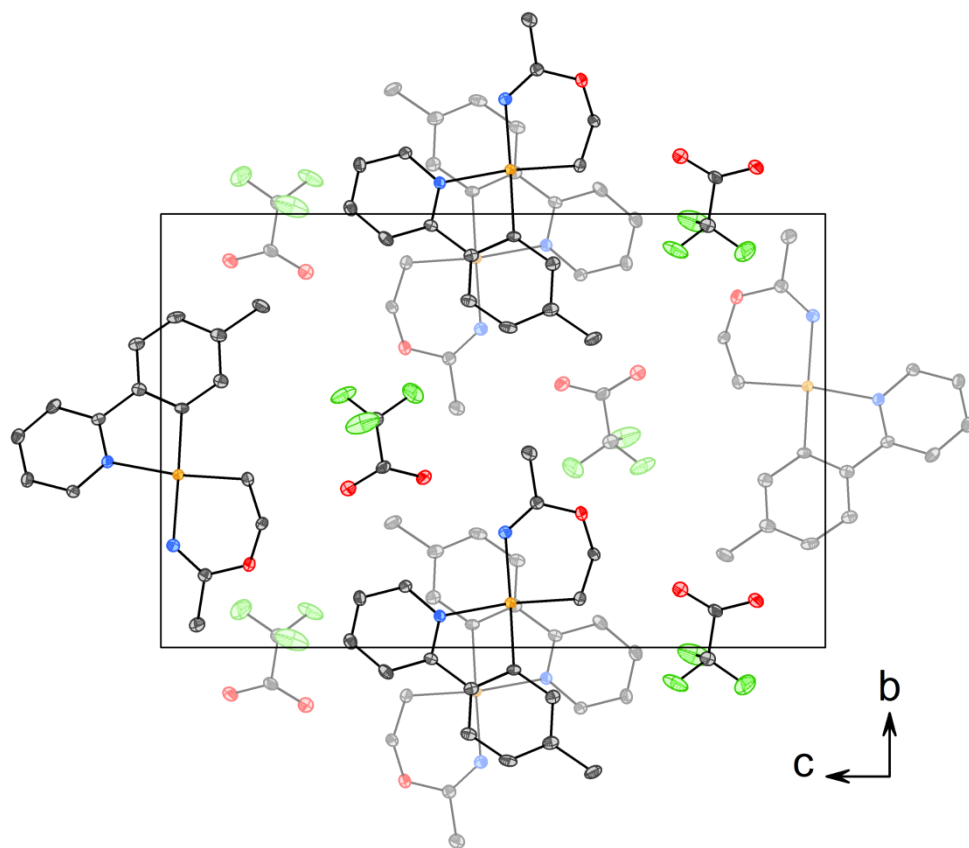
Figure S 22. Packing diagram of **1** viewed along the *a* axis showing stacking between the tpy ligands. The thermal ellipsoids are displayed at 50 % probability, and H atoms are omitted for clarity.
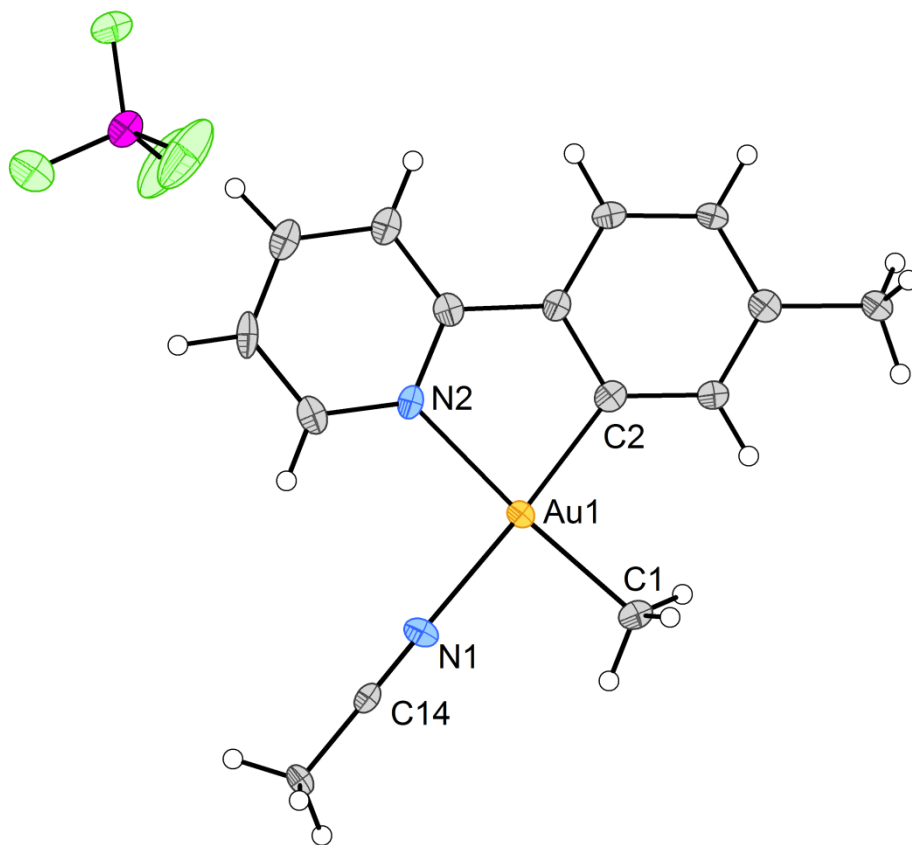
Figure S23. ORTEP plot of **9** with 50% ellipsoids. Selected bond distances and angles: Au1-C1, 2.049(6); Au1-C2, 2.002(6); Au1-N1, 2.088(5); Au1-N2, 2.113(5); C14-N1, 1.144(8); C1-Au1-C2, 93.6(2); C1-Au1-N1, 89.3(2); C2-Au1-N2, 82.2(2); N1-Au1-N2, 94.87(19); C1-Au1-N2, 175.8(2); C2-Au1-N1, 177.0 (2); Au1-N1-C14, 179.0(5).
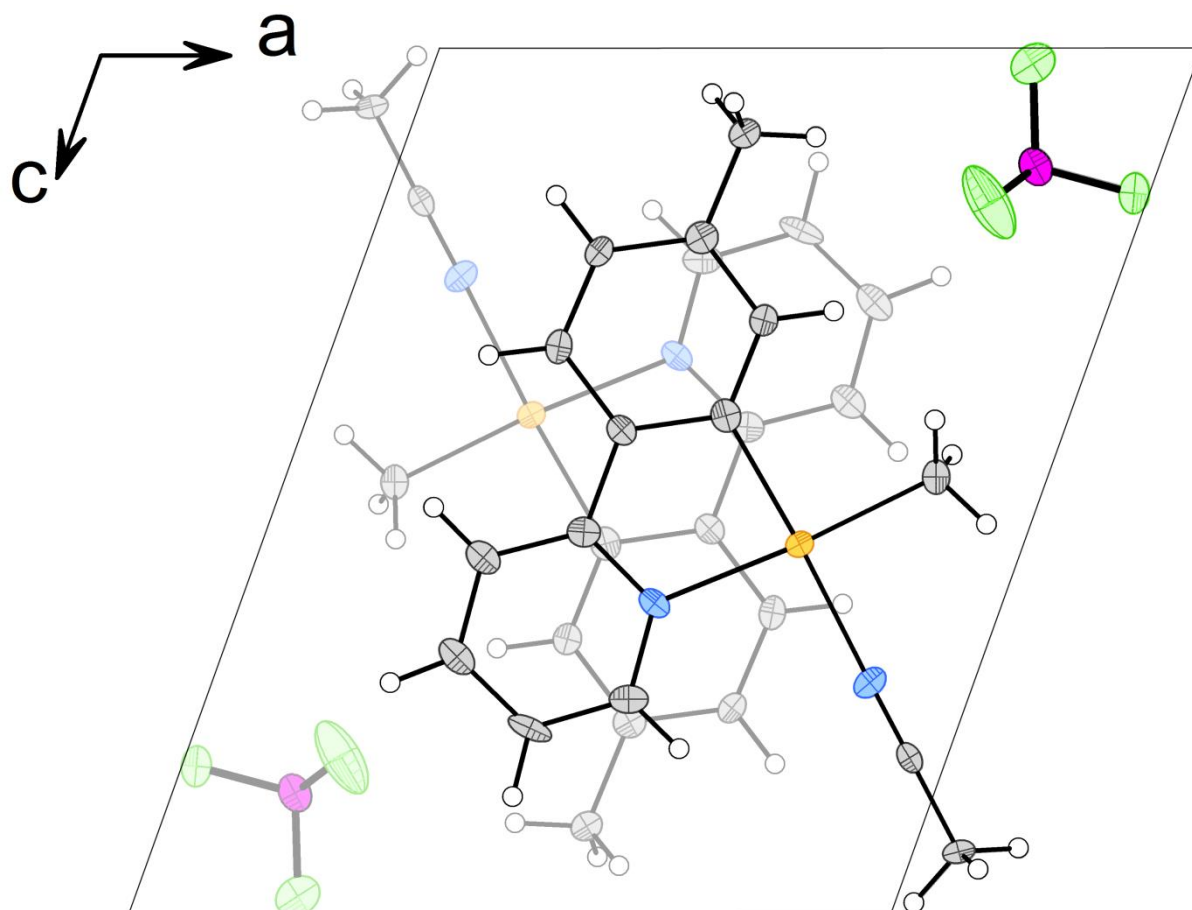
Figure S 24. Packing diagram of **9** viewed along the *b* axis showing stacking between the tpy ligands. The thermal ellipsoids are displayed at 50 % probability. All non-H atoms in **9** are confined to the mirror plane b=0.25. The structure displays parallel displaced $\pi - \pi$ −stacking along the *b* axis, with an interplanar distance of 3.345(3) Å. This packing is rather close due to the perfect planarity of the molecule.

Computational Details

Calculations were carried out at the DFT level as implemented in the Gaussian09 software package.[16] The hybrid PBE0+GD3 functional[17,18] including Grimme's model for dispersion forces was used to optimize all geometries. This methodology was selected because previous studies have proven its solid performance in the modeling of Au(III) alkene complexes.[19] C, H, N and O were described with the all-electron triple-ζ 6-311+G** basis set,[20] whereas Au was described with the Stuttgart–Köln basis set including a small-core quasi-relativistic pseudopotential.[21] Geometries were fully optimized without any constraint. Vibrational frequencies were computed analytically to verify that the stationary points found were energy minima or transition states. All optimizations needed for the mechanism proposal were carried out in solvent (acetonitrile) using the SMD solvation model.[22] Complexes **3**, **4** and **5** were optimized in gas phase with the aim of comparing their geometries with an X-Ray crystal structure. Gibbs energies were obtained for T = 298.15 K and p = 1 atm. In the bimolecular steps, these energies were corrected for the 1M standard state (T = 298.15 K and p = 24.465 atm).

[16] Gaussian 09, Revision D.01, M. J. Frisch, G. W. Trucks, H. B. Schlegel, G. E. Scuseria, M. A. Robb, J. R. Cheeseman, G. Scalmani, V. Barone, B. Mennucci, G. A. Petersson, H. Nakatsuji, M. Caricato, X. Li, H. P. Hratchian, A. F. Izmaylov, J. Bloino, G. Zheng, J. L. Sonnenberg, M. Hada, M. Ehara, K. Toyota, R. Fukuda, J. Hasegawa, M. Ishida, T. Nakajima, Y. Honda, O. Kitao, H. Nakai, T. Vreven, J. A. Montgomery, Jr., J. E. Peralta, F. Ogliaro, M. Bearpark, J. J. Heyd, E. Brothers, K. N. Kudin, V. N. Staroverov, R. Kobayashi, J. Normand, K. Raghavachari, A. Rendell, J. C. Burant, S. S. Iyengar, J. Tomasi, M. Cossi, N. Rega, J. M. Millam, M. Klene, J. E. Knox, J. B. Cross, V. Bakken, C. Adamo, J. Jaramillo, R. Gomperts, R. E. Stratmann, O. Yazyev, A. J. Austin, R. Cammi, C. Pomelli, J. W. Ochterski, R. L. Martin, K. Morokuma, V. G. Zakrzewski, G. A. Voth, P. Salvador, J. J. Dannenberg, S. Dapprich, A. D. Daniels, Ö. Farkas, J. B. Foresman, J. V. Ortiz, J. Cioslowski, and D. J. Fox, Gaussian, Inc., Wallingford CT, 2009.

[17] C. Adamo and V. J. Barone, *J. Chem. Phys.,* 1999, **110**, 6158-6170.

[18] S. Grimme, J. Antony, S. Ehrlich and H. Krieg, *J. Chem. Phys.,* 2010, **132**, 154104/1-19.

[19] a) E. Langseth, M. L. Scheuermann, D. Balcells, W. Kaminsky, K. I. Goldberg, O. Eisenstein, R. H. Heyn and M. Tilset, *Angew. Chem., Int. Ed.* 2013, **52**, 1660-1663. b) E. Langseth, A. Nova, E. A. Tråseth, F. Rise, S. Øien, R. H. Heyn and M. Tilset, J. Am. Chem. Soc., 2014, **136**, 10104–10115. c) D. Balcells, O. Eisenstein, M. Tilset and A. Nova, *Dalton Trans.*, 2016, **45**, 5504-5513.

[20] (a) R. Krishnan, J. S. Binkley, R. Seeger and J. A. Pople, *J. Chem. Phys,.* 1980, **72**, 650-654. (b) A. D. McLean and G. S. Chandler, *J. Chem. Phys.* 1980, **72**, 5639-5648.

[21] (a) D. Figgen, G. Rauhut, M. Dolg and H. Stoll, *Chem. Phys.*, 2005, **311**, 227-244. (b) D. Figgen, K. A. Peterson, M. Dolg and H. Stoll, H. *J. Chem. Phys.,* 2009, **130**, 164108/1-12.

[22] A. V. Marenich, C. J Cramer and D. G. Truhlar, *J. Phys. Chem. B*, 2009, **113**, 6378-6396.

Comparison of the X-Ray geometry with the optimized 3, 4 and 5 geometries.

The fully DFT-optimized geometries of **3**, **4** and **5** were compared to the X-Ray crystal structure (Table S1). The selected bond distances, including all involved in covalent bonds to the metal center, yield the lowest RMSD value for complex **3**.

Table S 2: Bond distances (d) and root-mean-square deviations (RMSD), in Å.

d	X-Ray	DFT **3**	DFT **4**	DFT **5**
Au-C	2.042	2.040	2.038	2.037
C-C	1.509	1.504	1.517	1.508
C-X[a]	1.449	1.443	1.460	1.451
X-C	1.333	1.306	1.325	1.303
C-CH$_3$	1.504	1.488	1.492	1.485
C-Y[a]	1.284	1.292	1.256	1.239
Y-Au	2.093	2.118	2.143	2.166
Au-C'	2.019	2.010	1.999	1.997
Au-N	2.127	2.136	2.114	2.113
RMSD		0.015	0.022	0.032

[a]X = N and Y = O in **3**; X = O and Y = N in **4**; X = Y = O in **5**.

Optimized coordinates and energies

See **Scheme 5** for the labels used for all intermediates and TS.

1
E : -1705.0796184
G : -1704.896934

Au	-0.192386	-0.248599	-0.008542
N	-1.051644	-2.052941	-0.223527
C	-0.347201	-3.172845	-0.423614
H	0.729864	-3.069569	-0.458297
C	-0.981462	-4.388541	-0.584548
H	-0.388528	-5.280080	-0.744746
C	-2.370518	-4.428807	-0.537986
H	-2.895106	-5.369586	-0.663399
C	-3.087317	-3.261243	-0.332356
H	-4.169395	-3.272430	-0.294205
C	-2.409618	-2.059527	-0.173441
C	-2.997697	-0.749649	0.050337
C	-4.361215	-0.481425	0.149366
H	-5.086715	-1.282718	0.053657
C	-4.795804	0.818964	0.370204
H	-5.860072	1.019347	0.442850
C	-3.892912	1.874941	0.502064
C	-2.518630	1.606444	0.400478
H	-1.808828	2.420057	0.504405
C	-2.091523	0.316128	0.176311
C	-4.362005	3.274006	0.751605
H	-5.451821	3.335368	0.730178
H	-3.959952	3.961446	0.000908
H	-4.017824	3.629020	1.728860
O	0.557508	1.605833	0.295331
C	0.861031	2.301347	-0.744428
O	0.718661	2.042403	-1.914795
C	1.481319	3.651681	-0.307105
F	0.605610	4.367325	0.413525
F	2.568774	3.462175	0.451202
F	1.839894	4.386539	-1.356762
O	1.798168	-0.917625	-0.319035
C	2.534535	-1.095912	0.709218
O	2.252917	-1.030555	1.887359
C	3.984003	-1.449953	0.289796
F	4.526446	-0.469263	-0.448075
F	4.777753	-1.644926	1.342833
F	4.012680	-2.570187	-0.450162

2
E: -1783.625807
G : -1783.38686

Au	-0.779820	-0.114270	-0.287779

NMR spectra of unpublished compounds

NMR spectra of Au(OCOCH₃)₂(tpy)
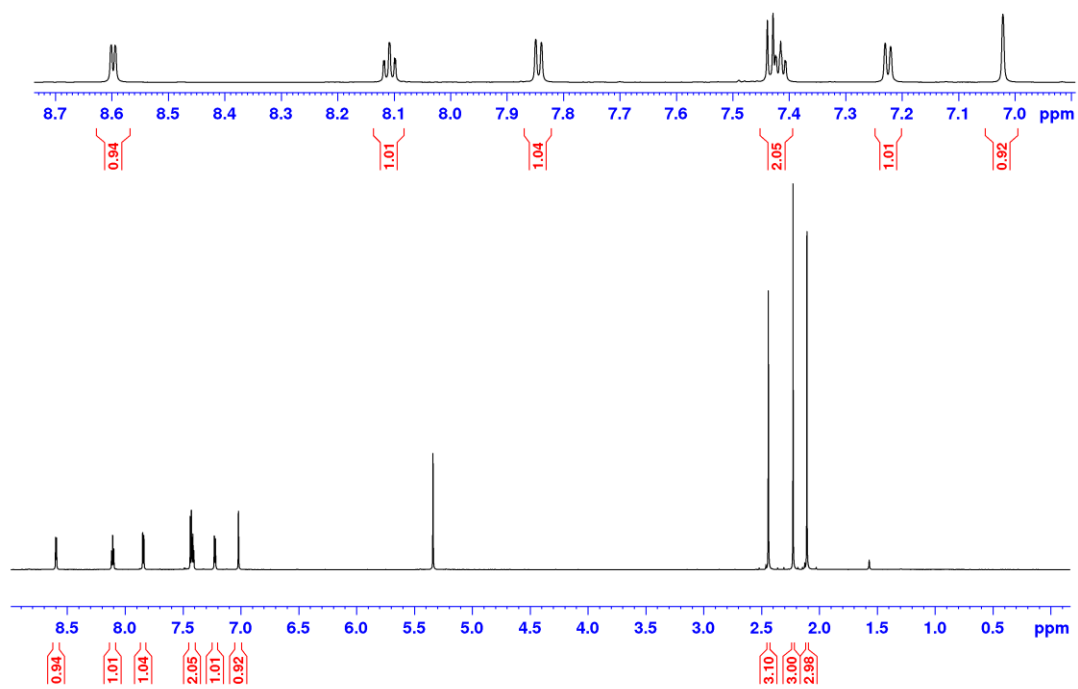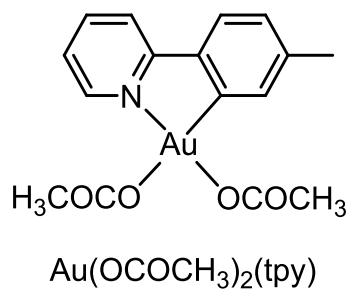
Figure A1. ¹H NMR (800 MHz, CD₂Cl₂) spectrum of Au(OCOCH₃)₂(tpy).
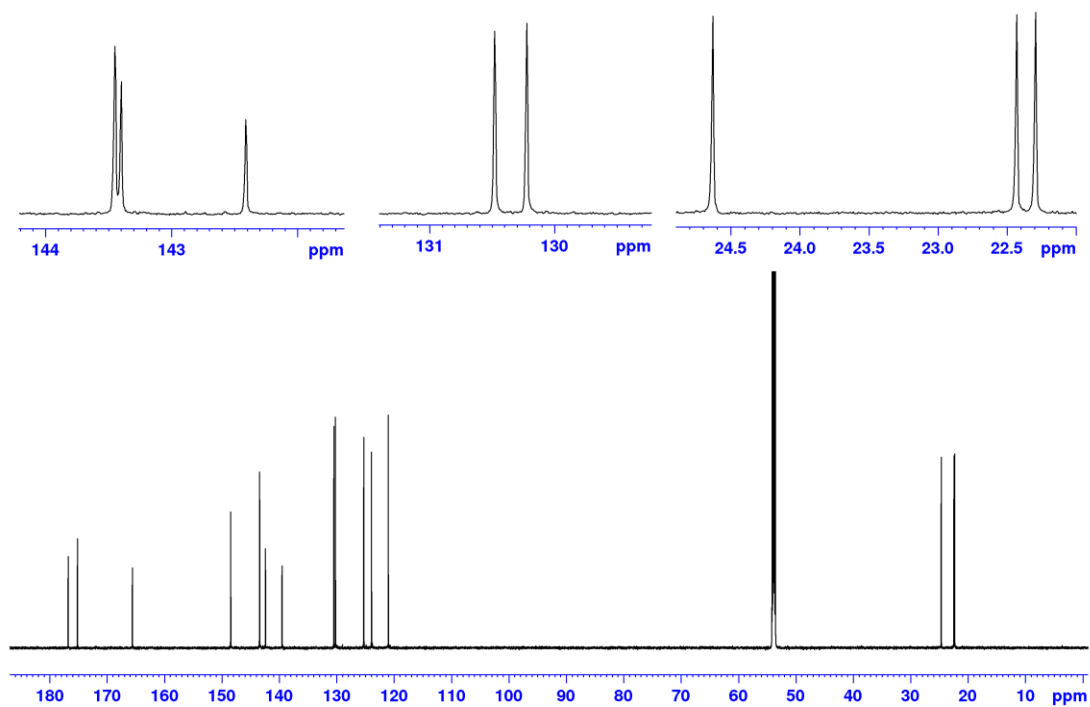
Figure A2. ^{13}C NMR (201 MHz, CD_2Cl_2, ns = 6144, d1 = 6 s) spectrum of $Au(OCOCH_3)_2(tpy)$.
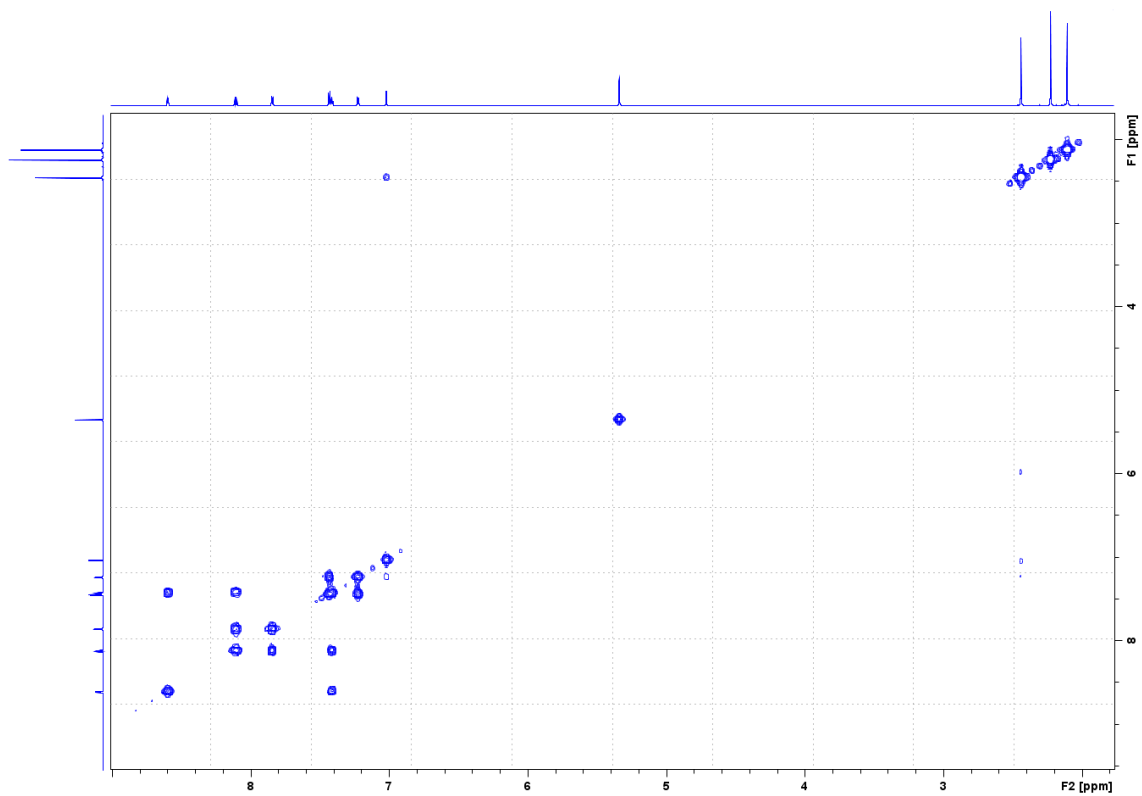
Figure A3. COSY (800 MHz, CD_2Cl_2) spectrum of $Au(OCOCH_3)_2(tpy)$.
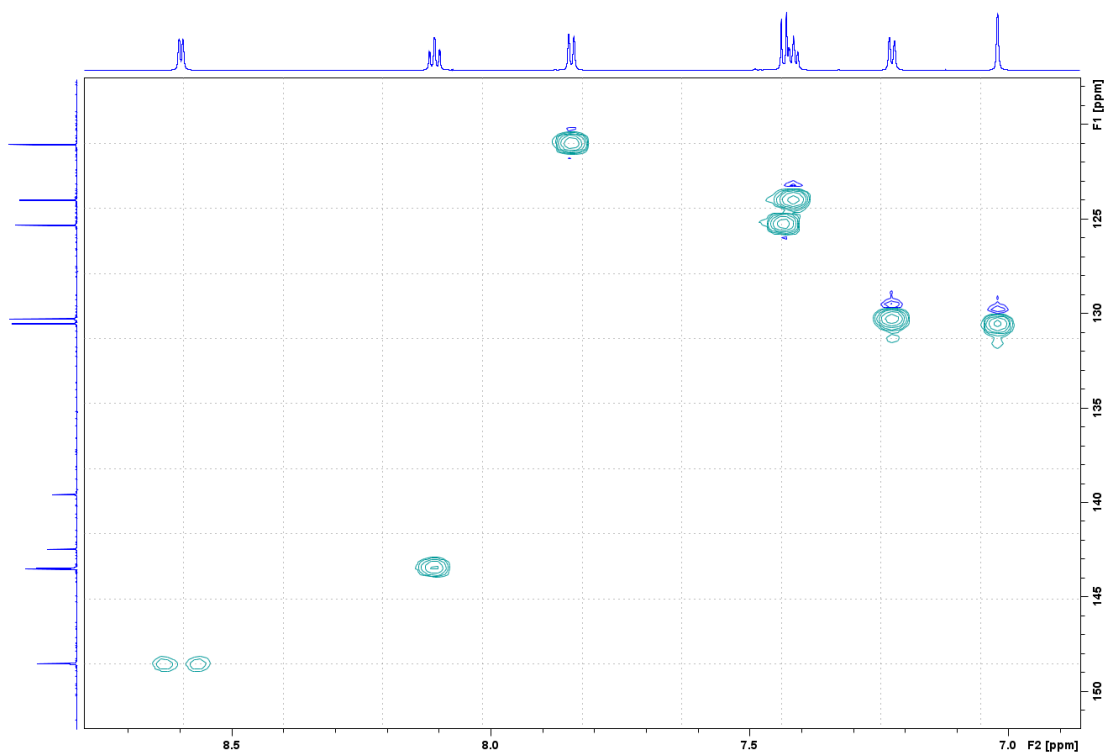
Figure A4. HSQC (800 MHz, CD_2Cl_2) spectrum of $Au(OCOCH_3)_2(tpy)$. Close up view on the aromatic region.
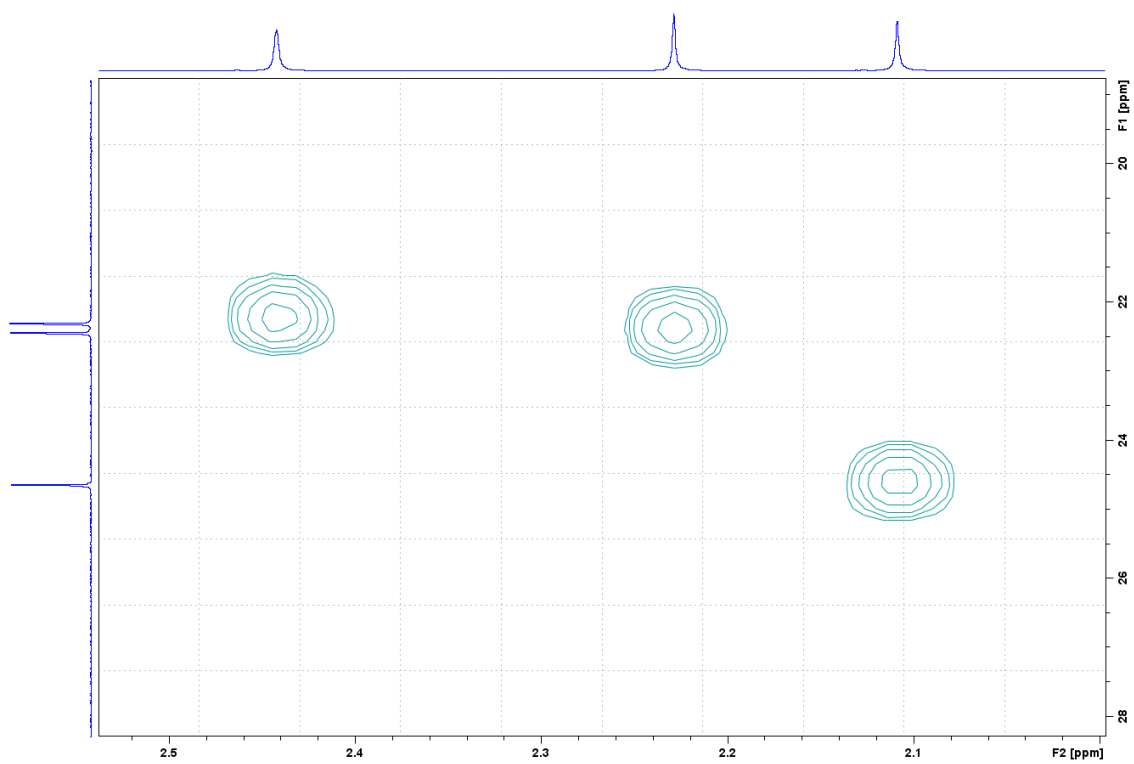
Figure A5. HSQC (800 MHz, CD_2Cl_2) spectrum of $Au(OCOCH_3)_2(tpy)$. Close up view on the aliphatic region.
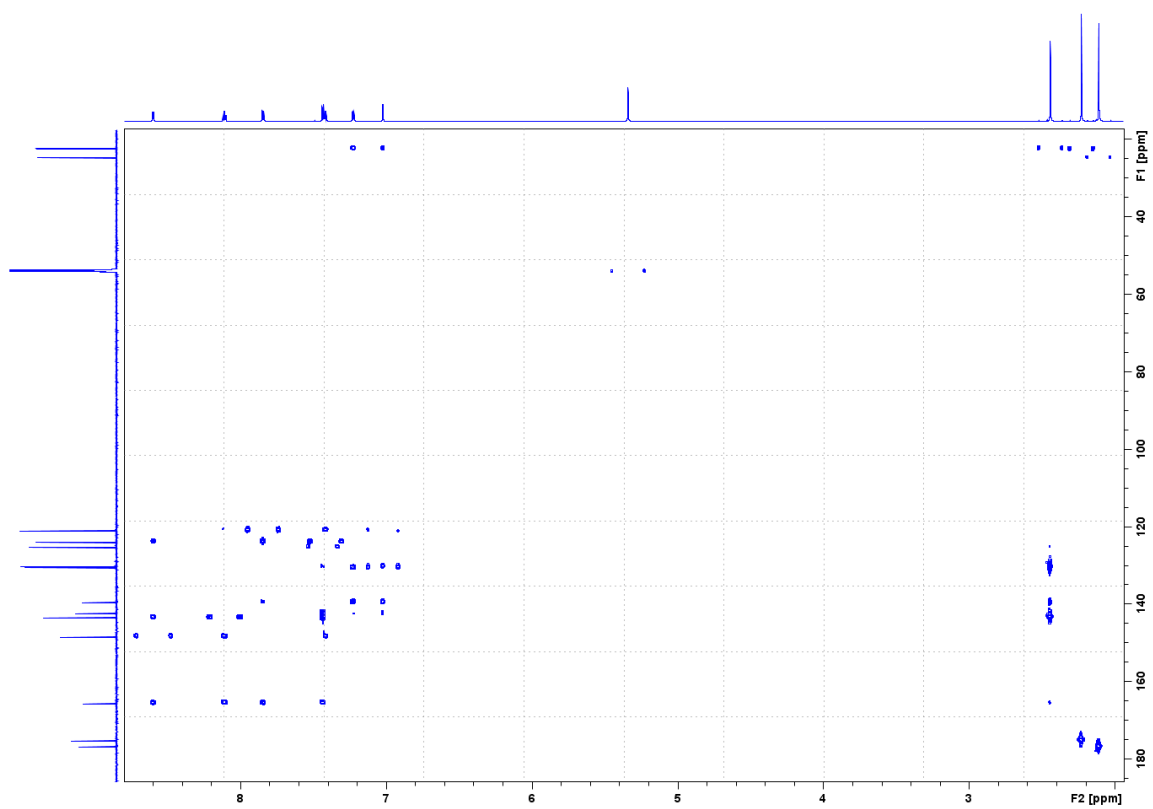
Figure A6. HMBC (800 MHz, CD$_2$Cl$_2$) spectrum of Au(OCOCH$_3$)$_2$(tpy).
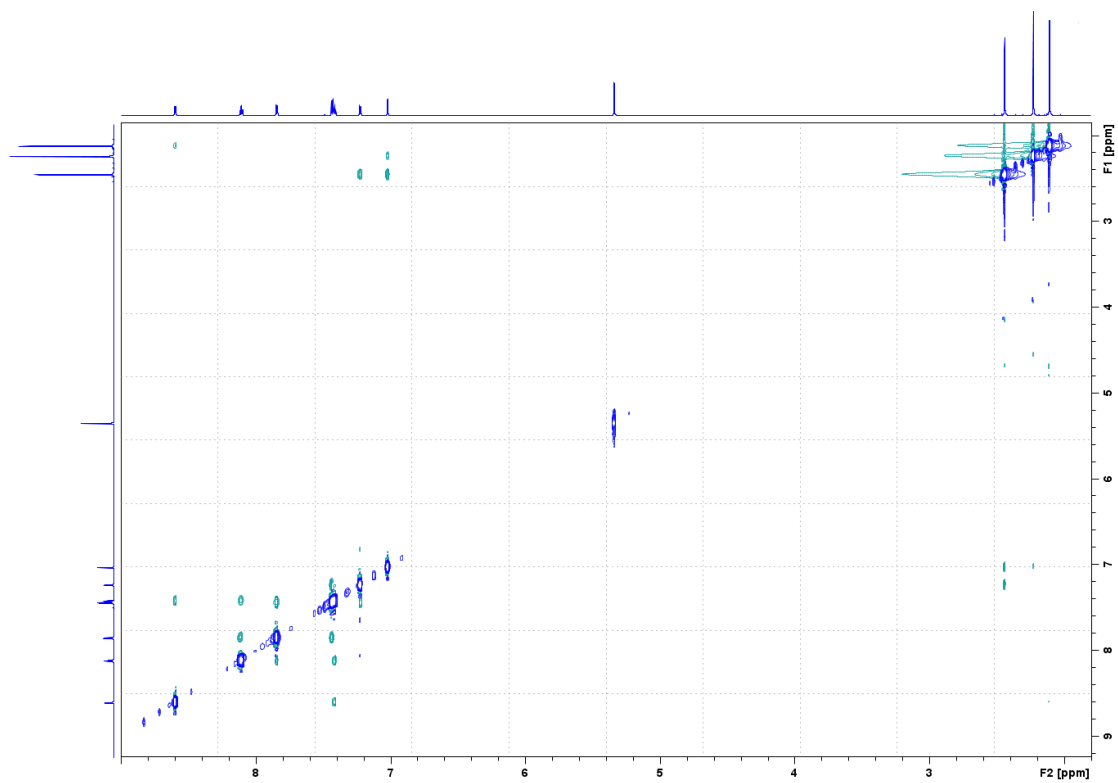
Figure A7. NOESY (800 MHz, CD$_2$Cl$_2$, mixing time = 1 s) spectrum of Au(OCOCH$_3$)$_2$(tpy).

NMR spectra of [Au(tpy)₂]⁺[OCOCF₃]⁻
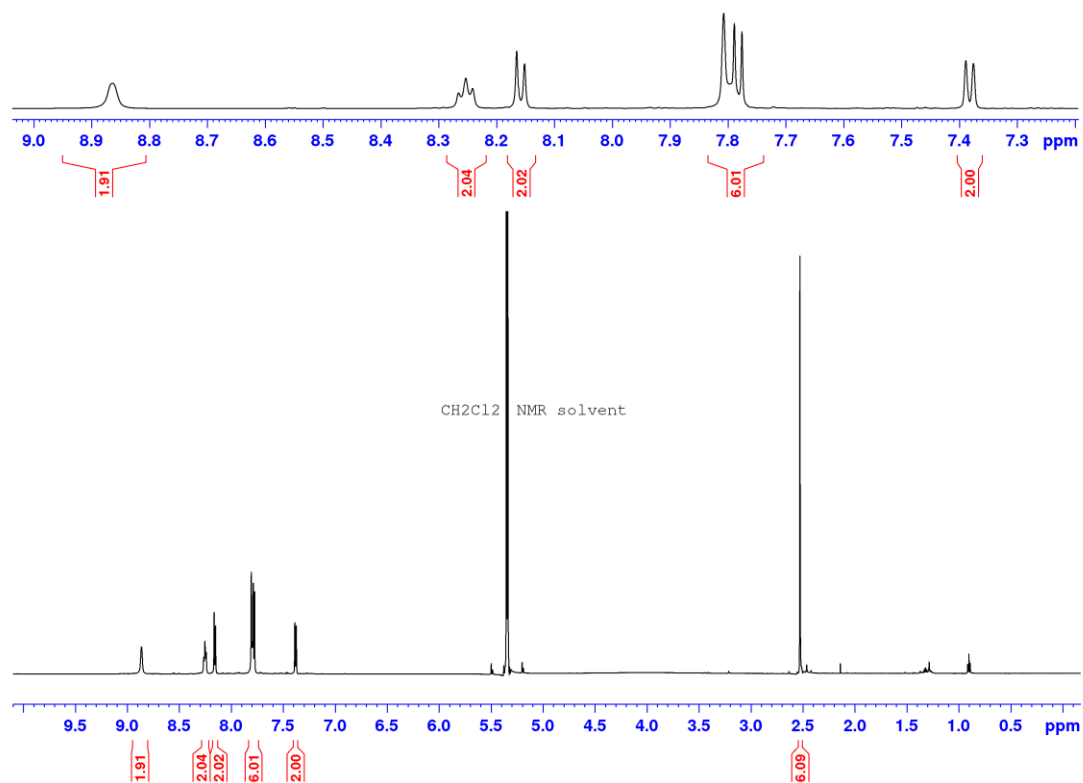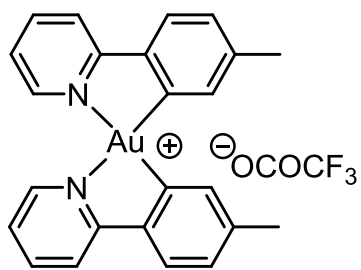
[Au(tpy)₂]⁺[OCOCF₃]⁻

Figure A8. ¹H NMR (600 MHz, CD₂Cl₂) spectrum of [Au(tpy)₂]⁺[OCOCF₃]⁻. NB: the sample contains small amounts of CH₂Cl₂.
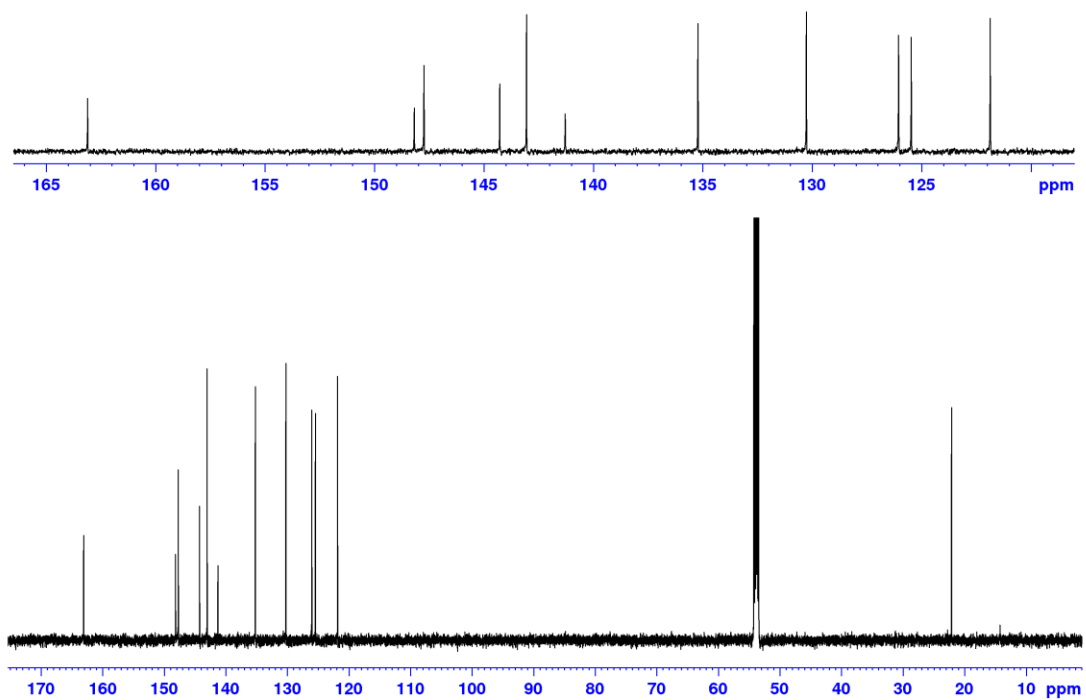
Figure A9. ^{13}C NMR (151 MHz, CD$_2$Cl$_2$, ns = 4096, d1 = 4 s) spectrum of [Au(tpy)$_2$]$^+$[OCOCF$_3$]$^-$.
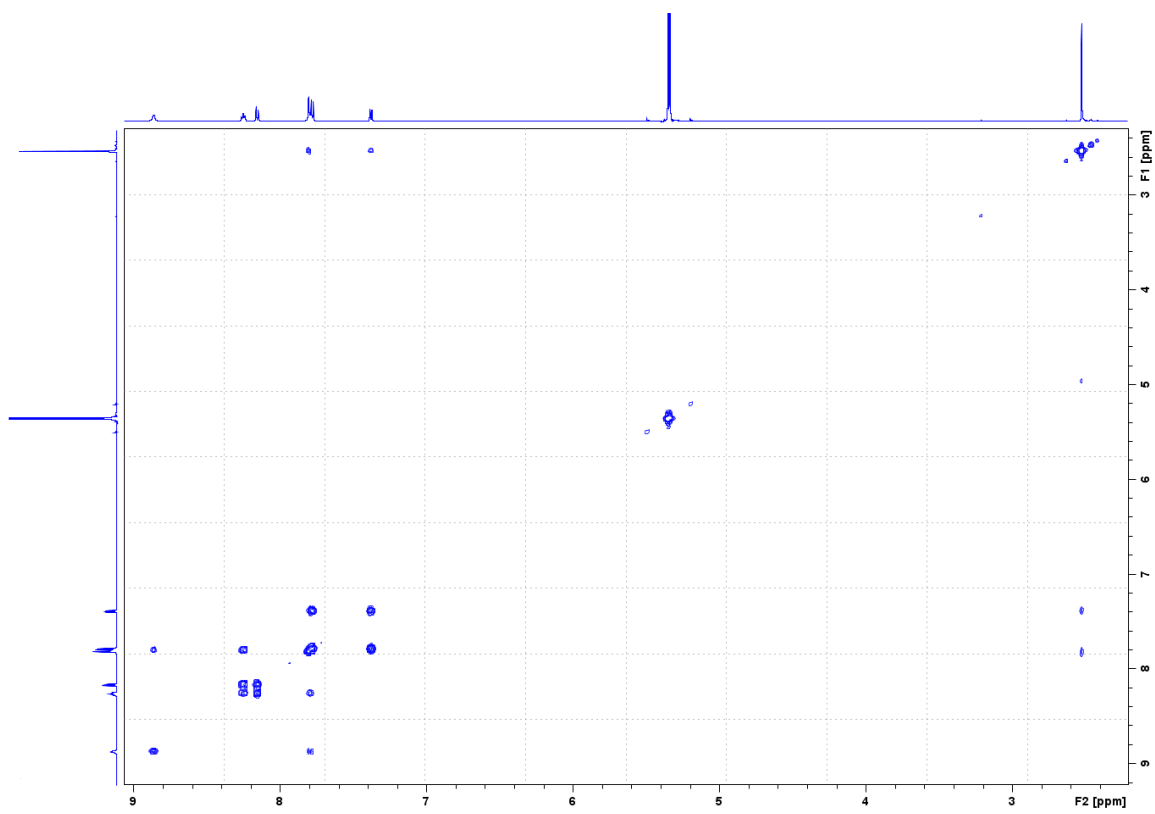
Figure A10. COSY (600 MHz, CD$_2$Cl$_2$) spectrum of [Au(tpy)$_2$]$^+$[OCOCF$_3$]$^-$.
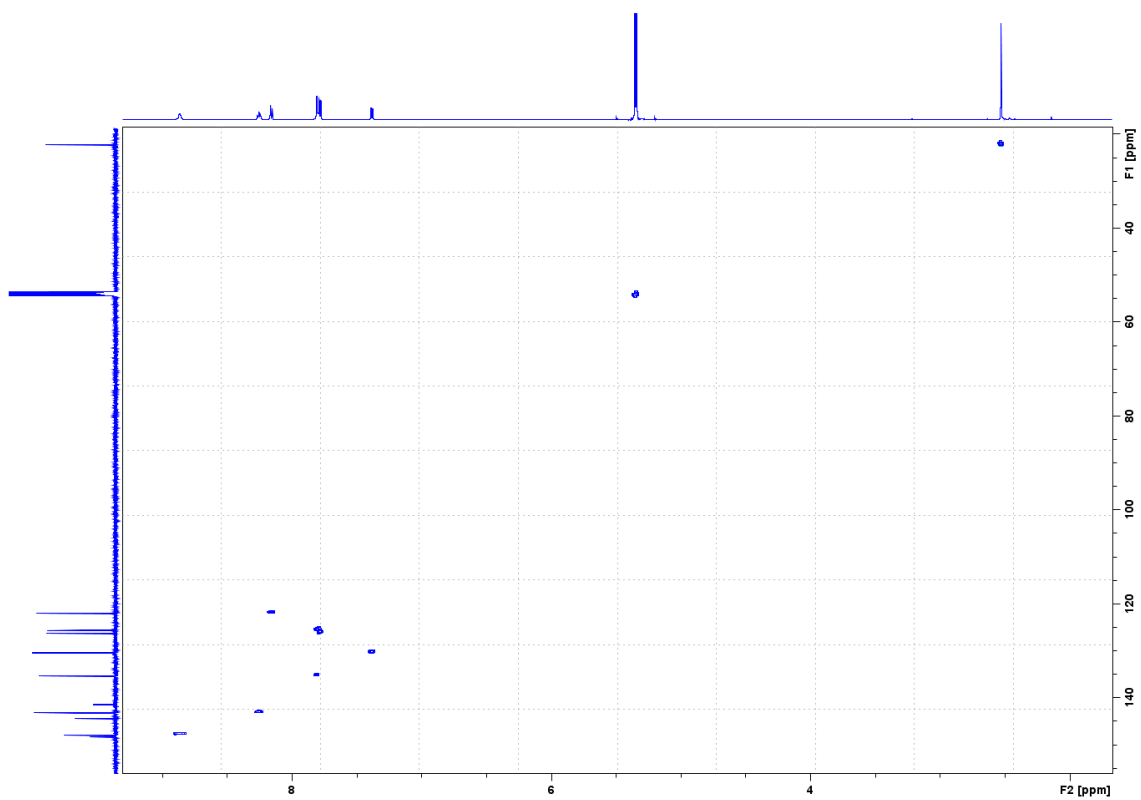
Figure A11. HSQC (600 MHz, CD$_2$Cl$_2$) spectrum of [Au(tpy)$_2$]$^+$[OCOCF$_3$]$^-$.
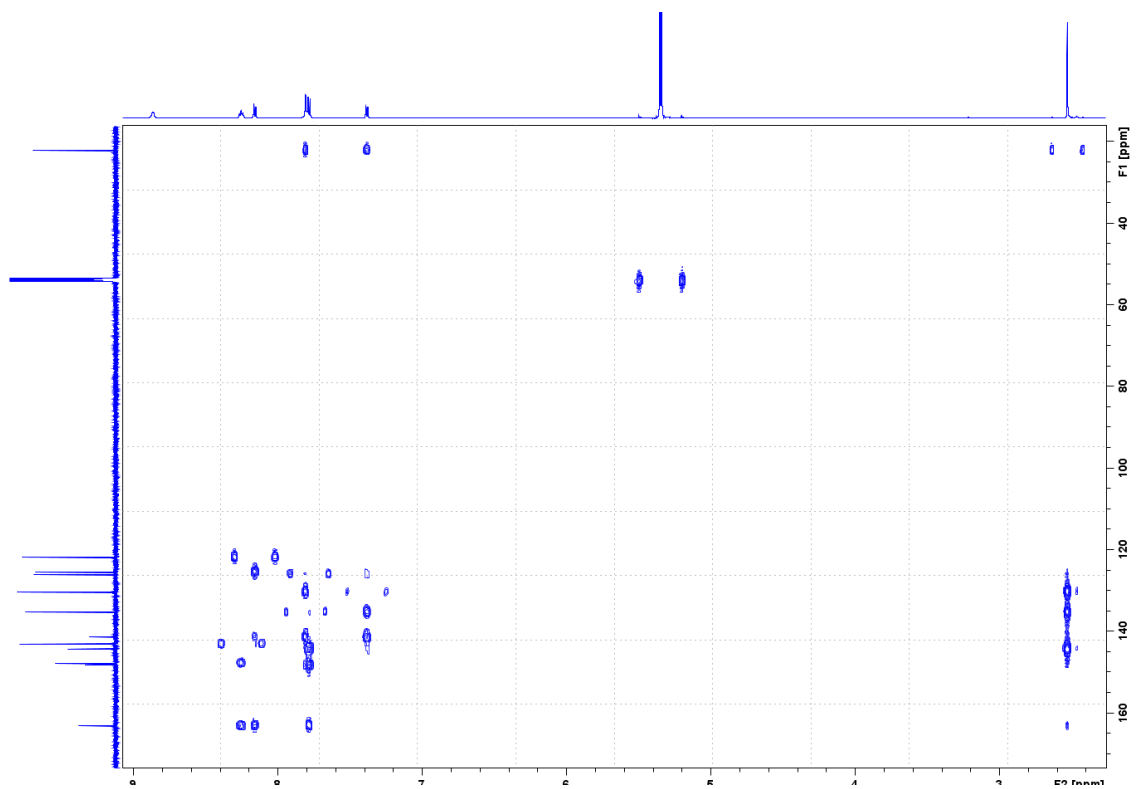
Figure A12. HMBC (600 MHz, CD$_2$Cl$_2$) spectrum of [Au(tpy)$_2$]$^+$[OCOCF$_3$]$^-$.
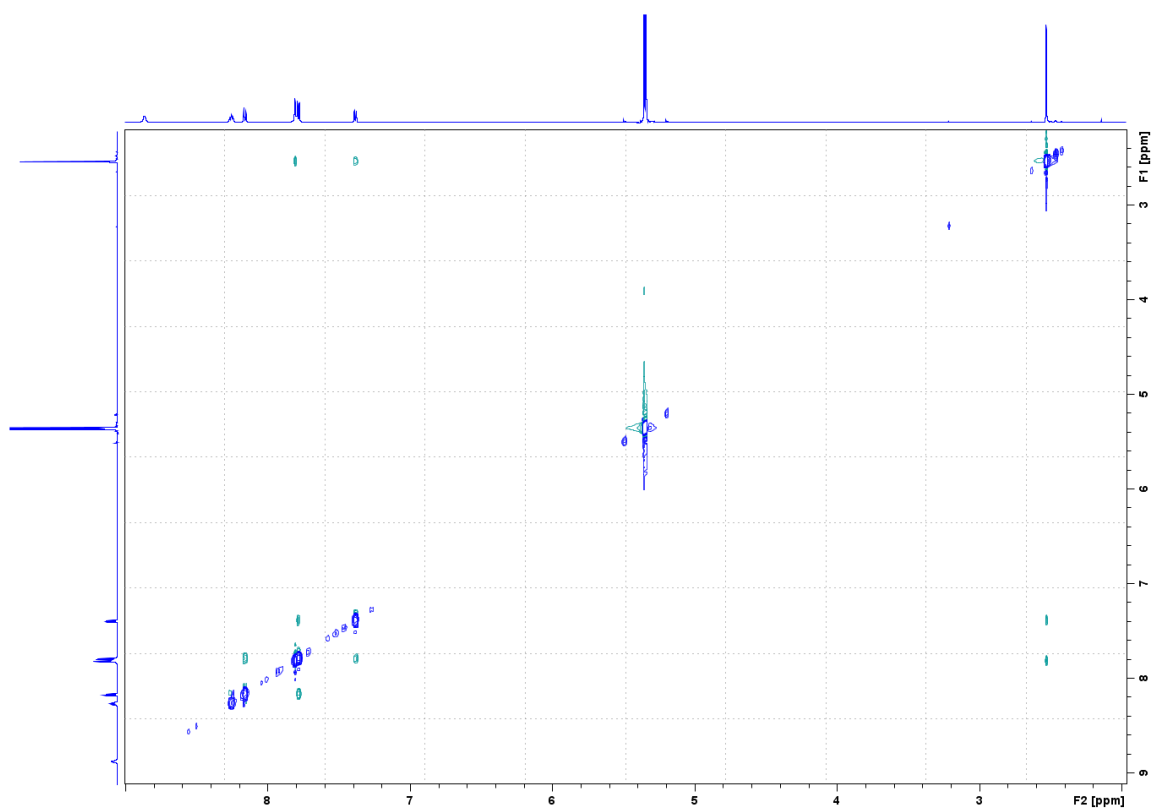
Figure A13. NOESY (600 MHz, CD_2Cl_2, mixing time = 1 s) spectrum of $[Au(tpy)_2]^+[OCOCF_3]^-$.

NMR spectra of complex 16
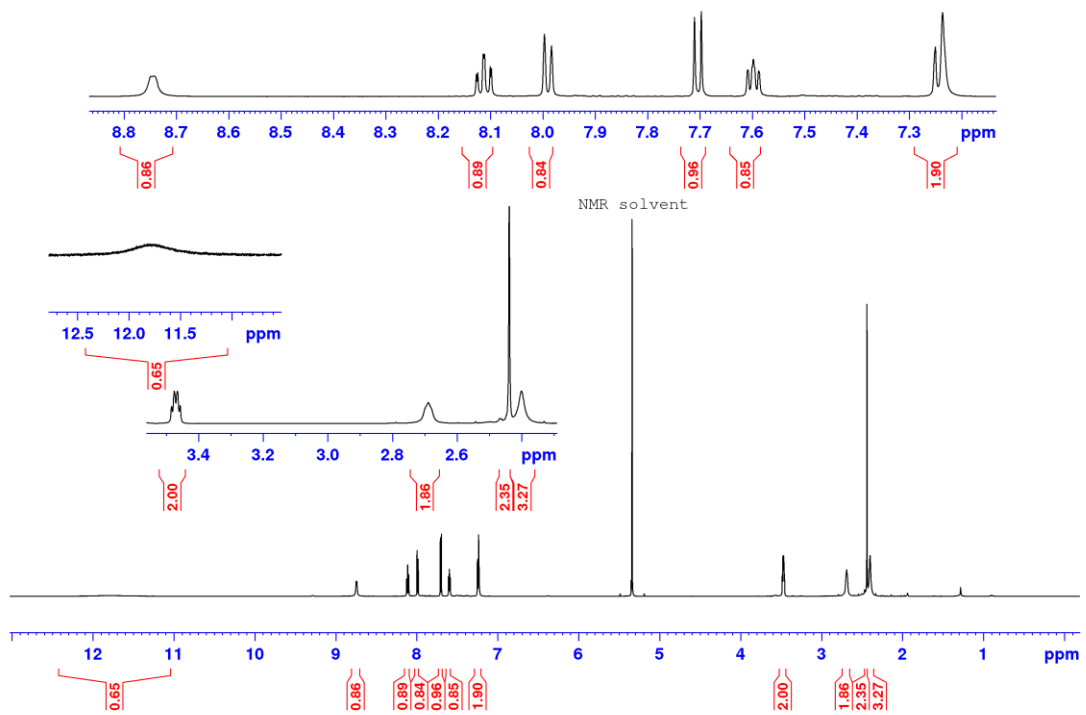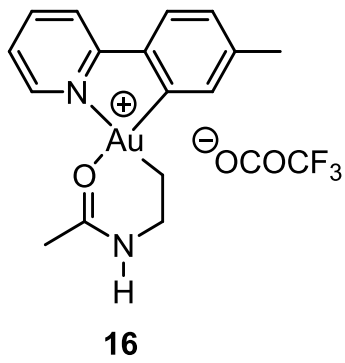
Figure A14. ^{1}H NMR (600 MHz, CD$_2$Cl$_2$) spectrum of complex **16**. Several of the resonances are broadened.
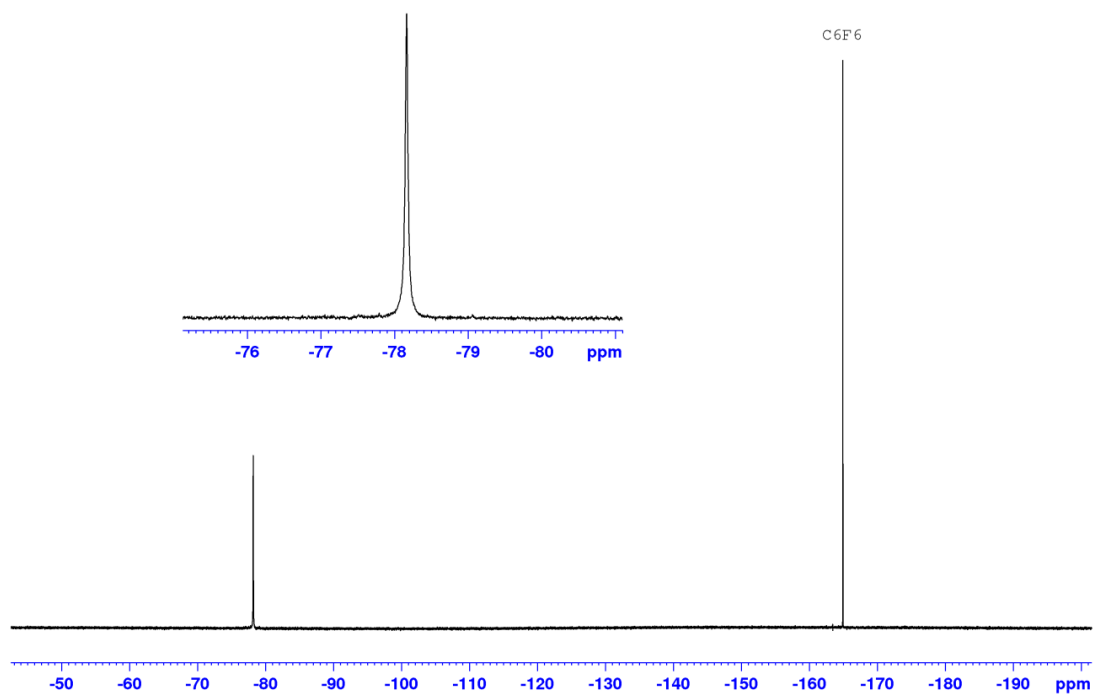
Figure A15. ^{19}F NMR (188 MHz, CD$_2$Cl$_2$) spectrum of complex **16**.
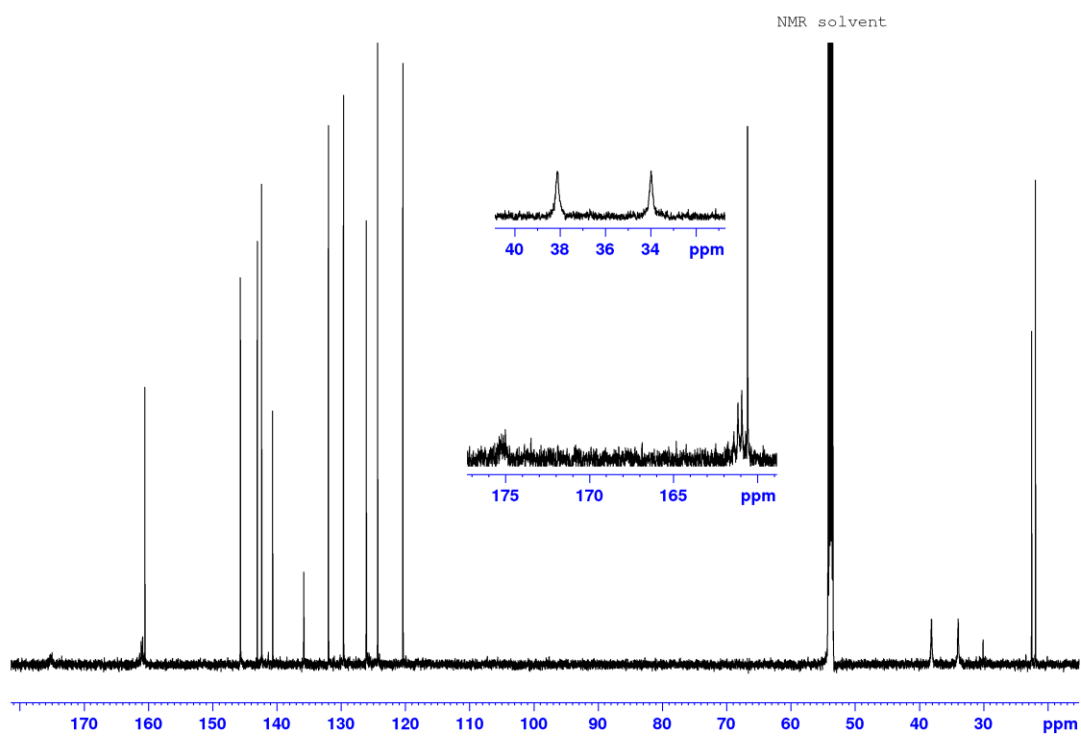
Figure A16. ^{13}C NMR (151 MHz, CD$_2$Cl$_2$, ns = 5120, d1 = 6 s) spectrum of complex **16**. Several of the resonances are broadened, especially those of OCCH$_3$ (δ 175), OCOCF$_3$ (δ 161.0), HNCH$_2$ (δ 38.1), and AuCH$_2$ (δ 34.0, see insets).
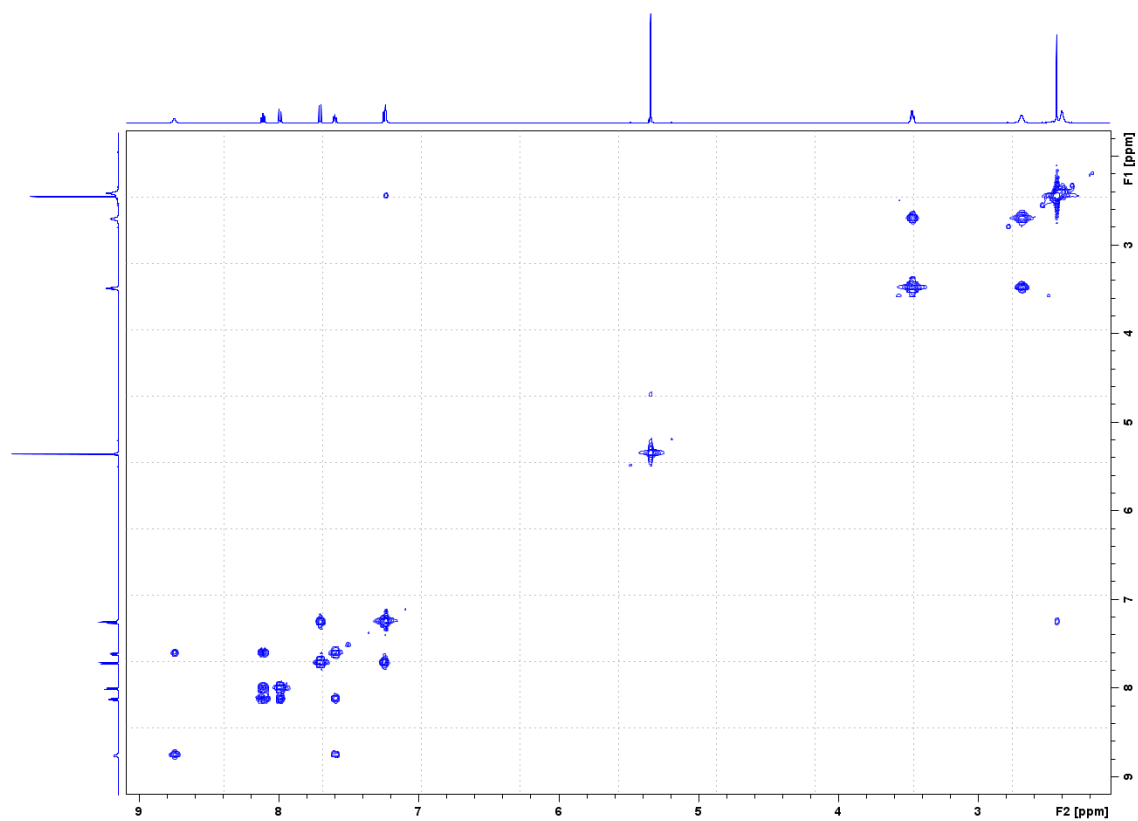
Figure A17. COSY (600 MHz, CD$_2$Cl$_2$) spectrum of complex **16**.
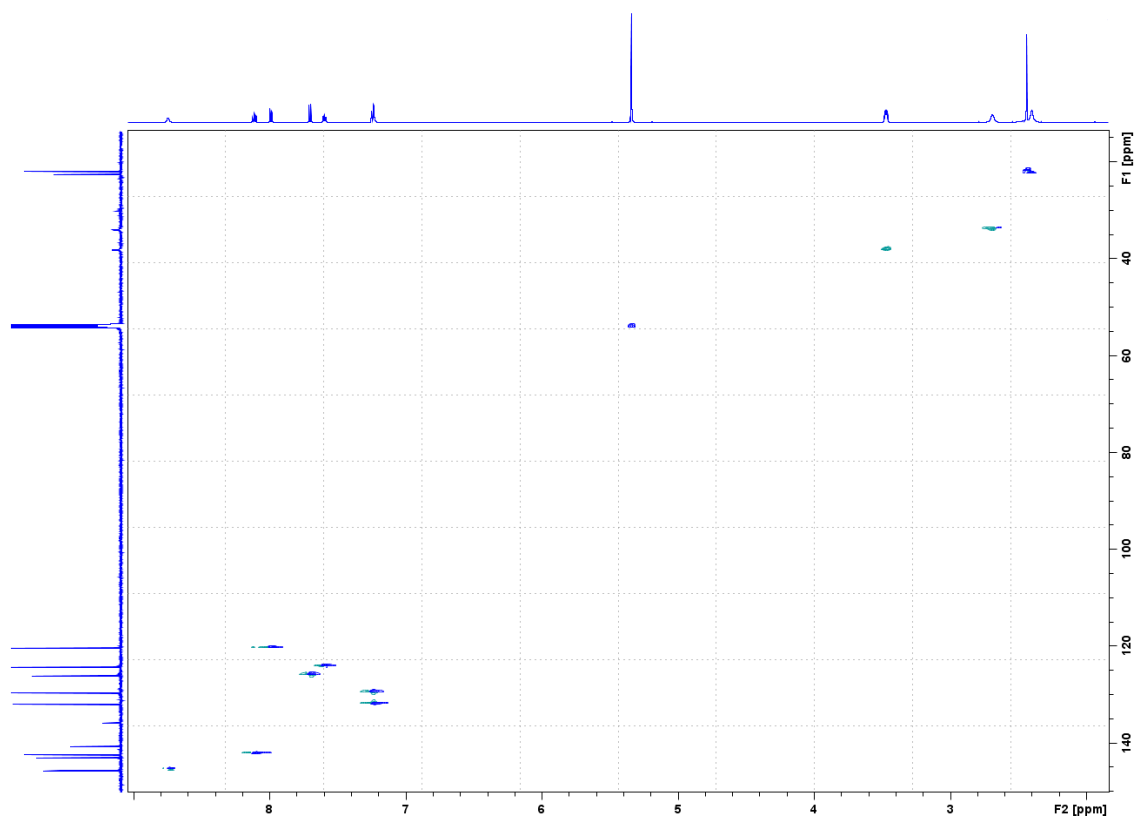
Figure A18. HSQC (600 MHz, CD$_2$Cl$_2$) spectrum of complex **16**.
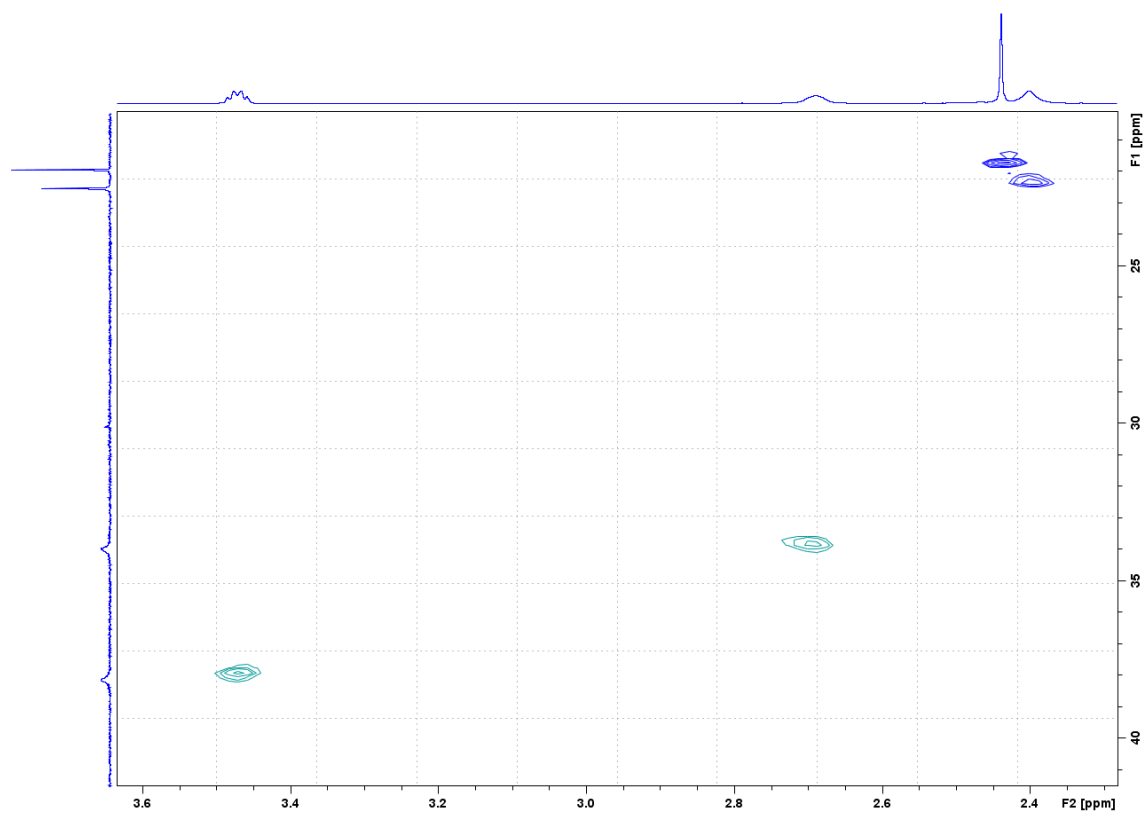
Figure A19. HSQC (600 MHz, CD$_2$Cl$_2$) spectrum of complex **16**. Close up view on the aliphatic region.
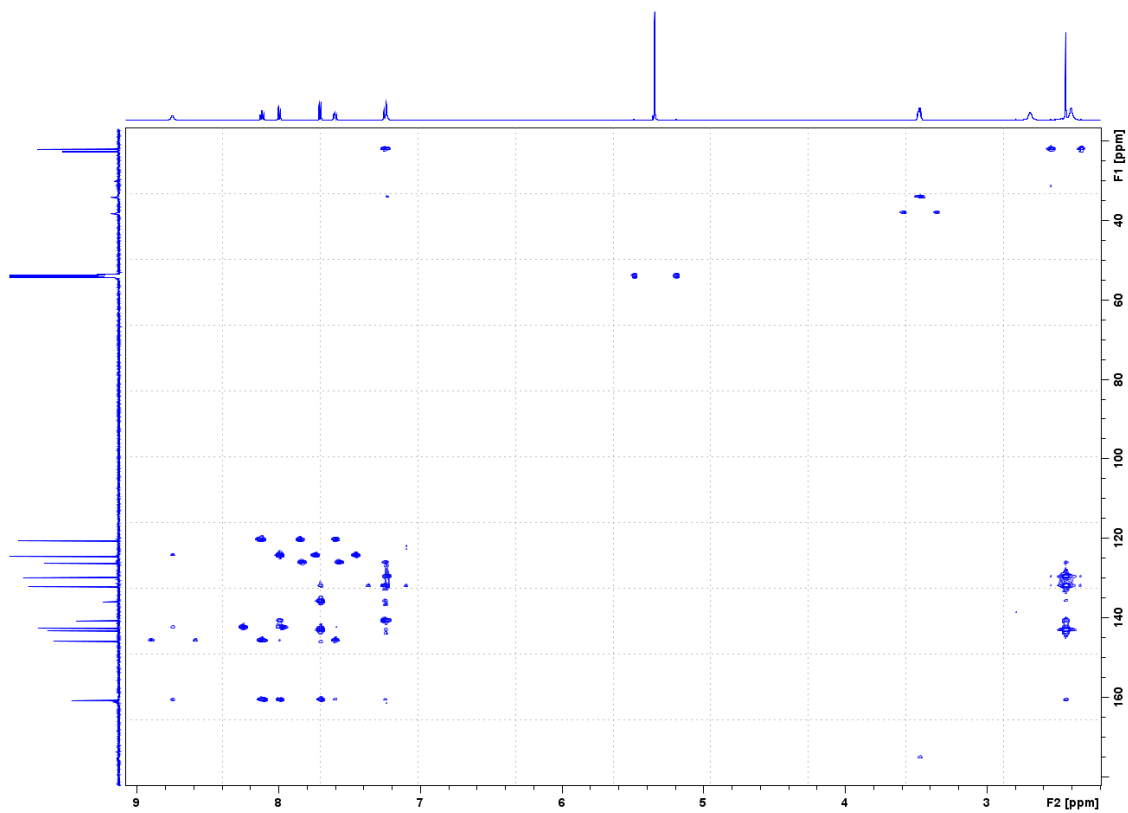
Figure A20. HMBC (600 MHz, CD$_2$Cl$_2$) spectrum of complex **16**.

Figure A21. NOESY (600 MHz, CD$_2$Cl$_2$, mixing time = 1 s) spectrum of Au(III) complex **1**. Peaks due to what is probably chemical exchange are observed.
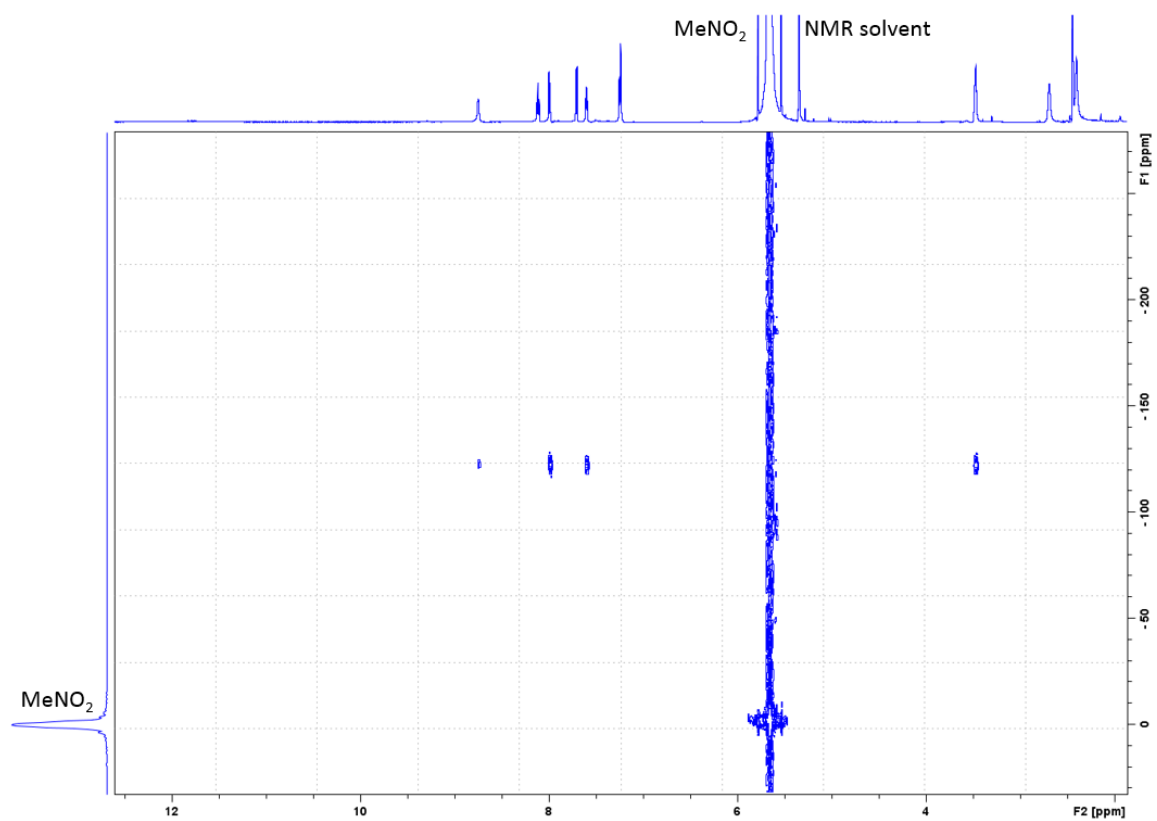
Figure A22. ^{1}H-^{15}N HMBC (600 MHz, CD$_2$Cl$_2$) spectrum of **16**. The resonance of the metallacycle-*NH* is not observed.
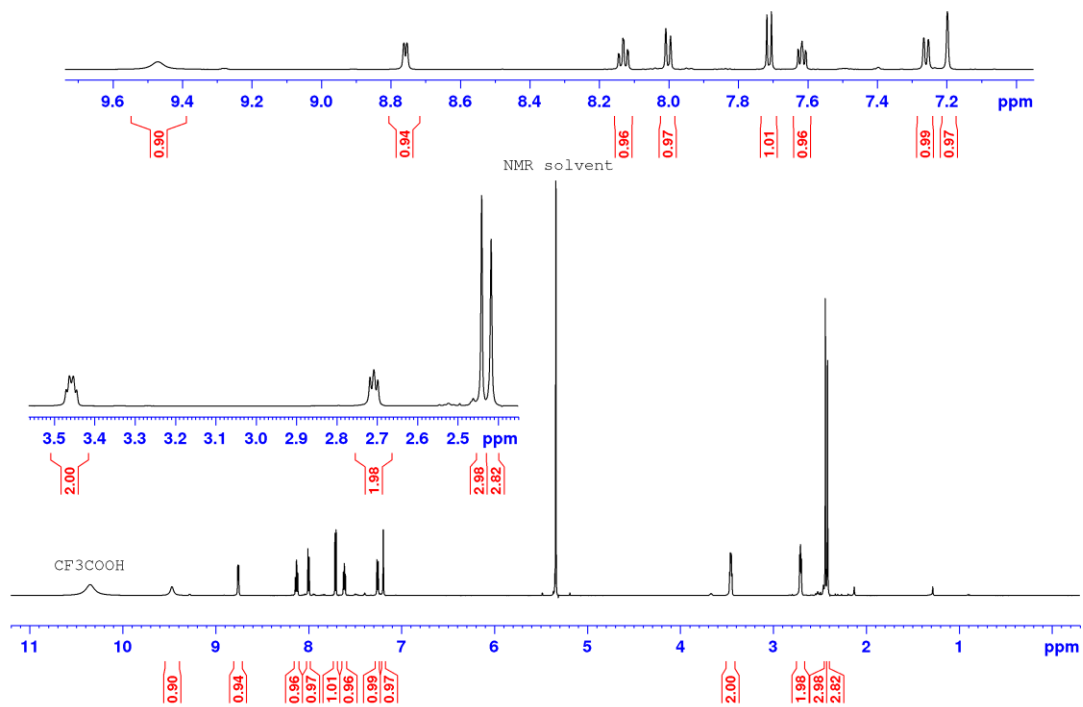
Figure A23. ^{1}H NMR (600 MHz, CD$_2$Cl$_2$) spectrum of complex **16** with *ca.* 0.7 equiv of CF$_3$COOH added.
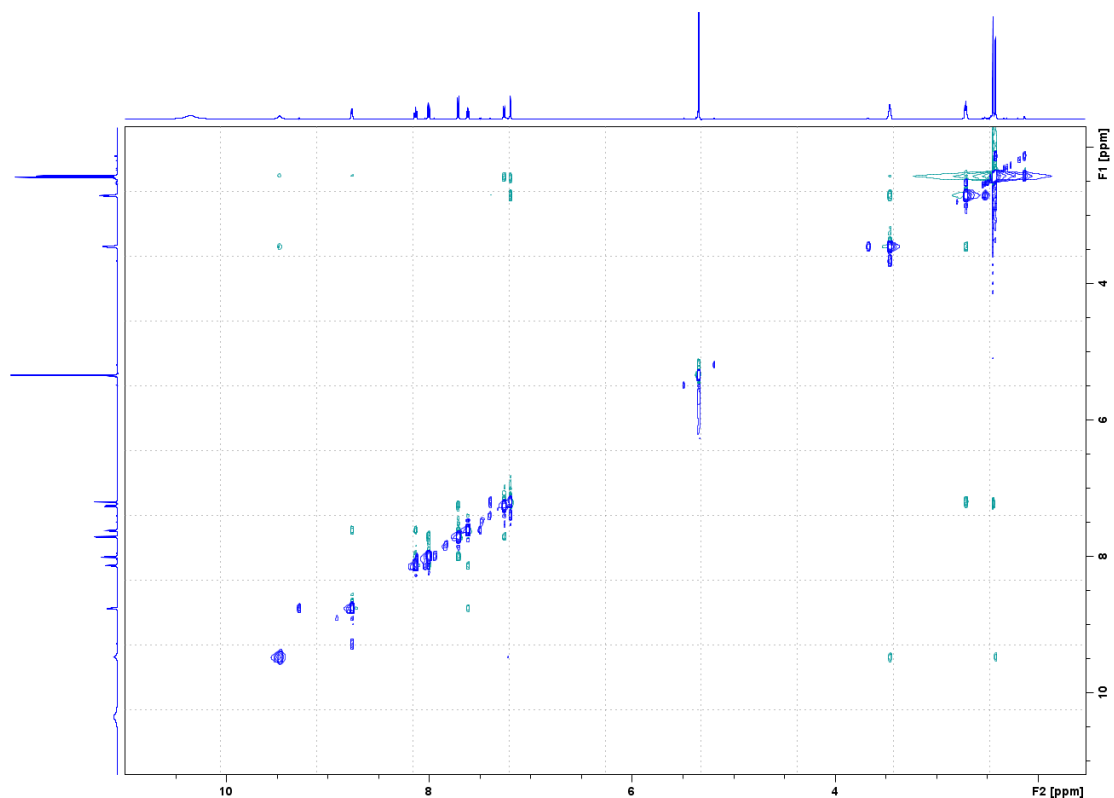
Figure A24. NOESY (600 MHz, CD$_2$Cl$_2$, mixing time = 1 s) spectrum of complex **16** with *ca.* 0.7 equiv CF$_3$COOH added. The peak at *ca.* δ 10.4 is due to excess CF$_3$COOH. Peaks due to what is probably chemical exchange are observed.
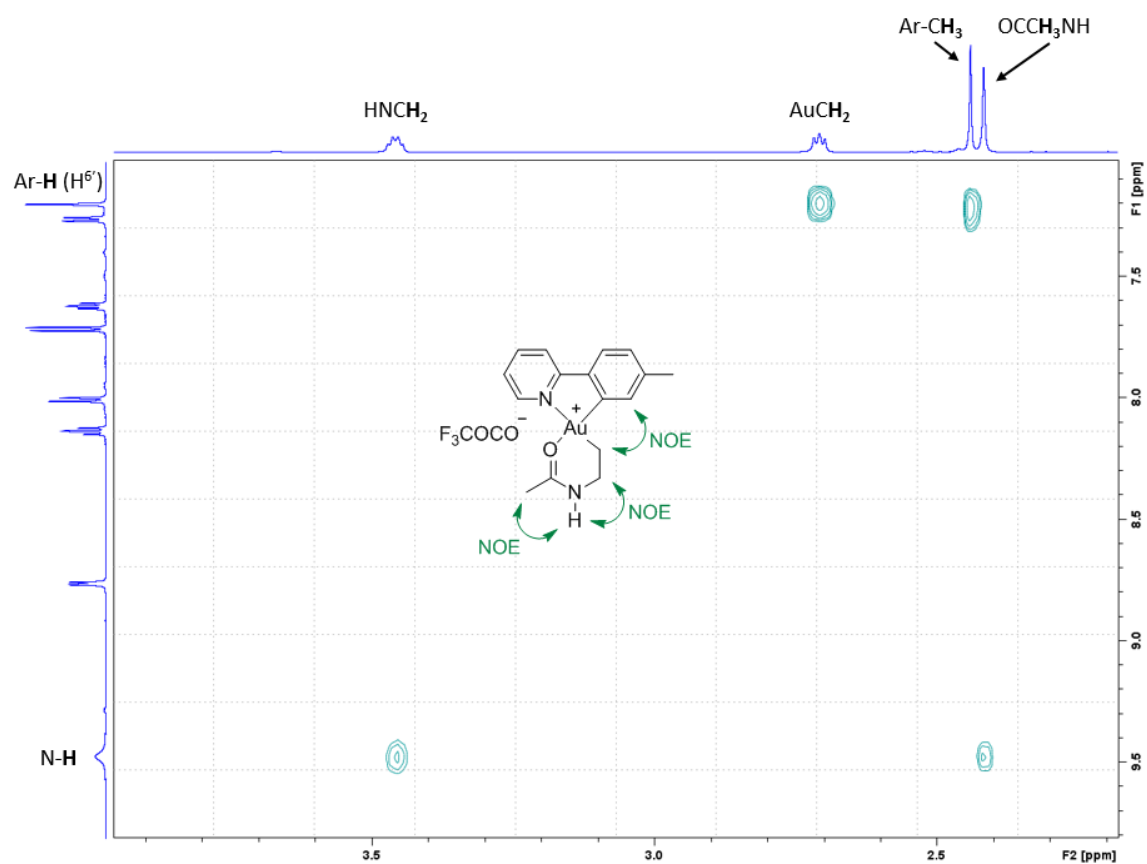
Figure A25. NOESY (600 MHz, CD$_2$Cl$_2$, mixing time = 1 s) spectrum of **16** with *ca*. 0.7 equiv CF$_3$COOH added. Close up view on the NOE between AuC**H$_2$** and H$^{6'}$, N**H** and NHC**H$_2$**, and N**H** and OCC**H$_3$**NH.
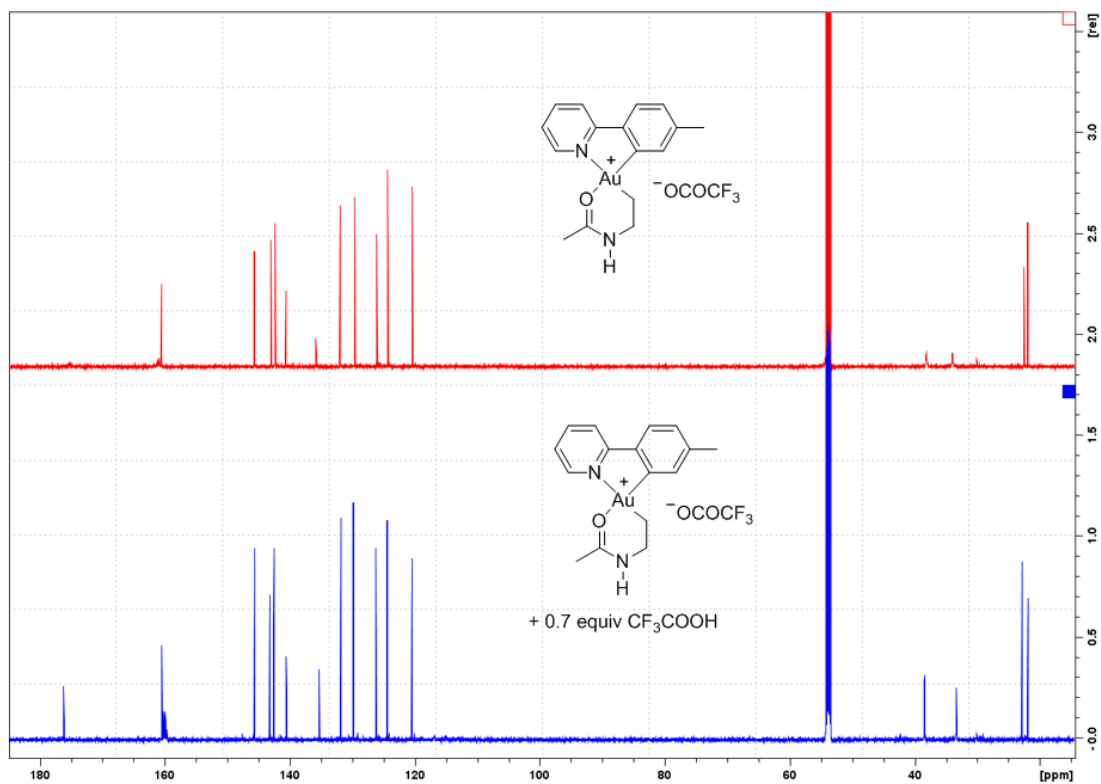
Figure A26. Stacked ^{13}C NMR (600 MHz, CD$_2$Cl$_2$) spectra of complex **16**. Top: ^{13}C NMR spectrum of dry **16**. Bottom: ^{13}C NMR spectrum of **16** with *ca*. 0.7 equiv CF$_3$COOH added, leading to less broadened resonances.
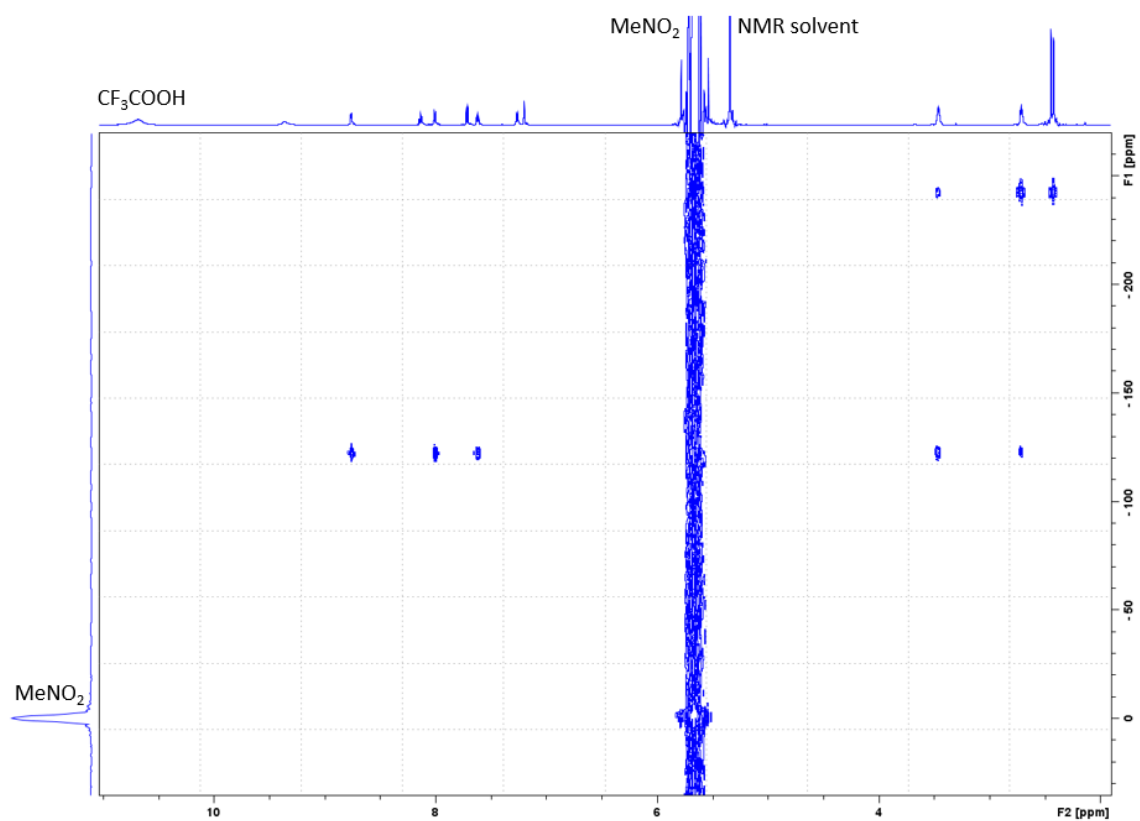
Figure A27. ^{1}H-^{15}N HMBC (600 MHz, CD$_2$Cl$_2$) spectrum of complex **16** with *ca.* 0.7 equiv CF$_3$COOH added.
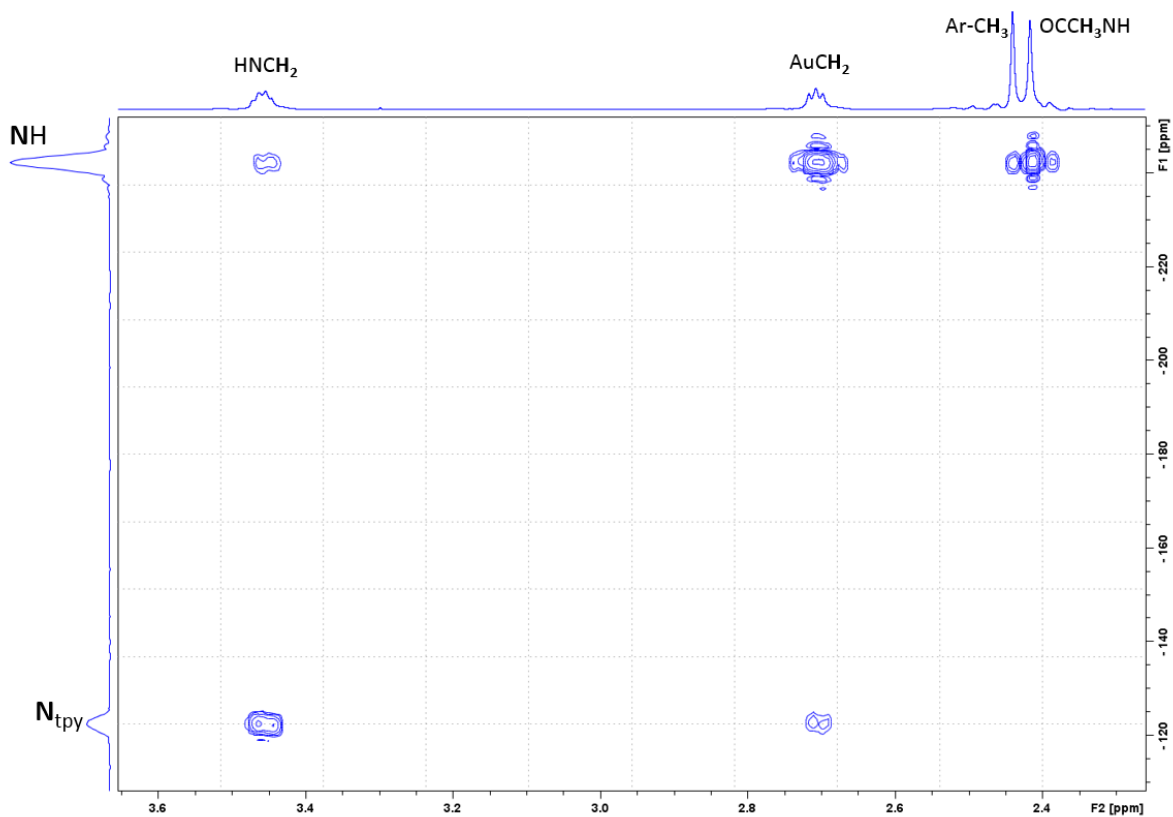
Figure A28. ^{1}H-^{15}N HMBC (600 MHz, CD$_2$Cl$_2$) spectrum of complex **16** with *ca.* 0.7 equiv CF$_3$COOH added. Close up view of the correlations of the nitrogens with the protons in the aliphatic region.

NMR spectra of complex 31b
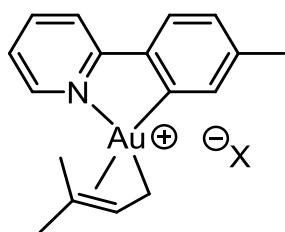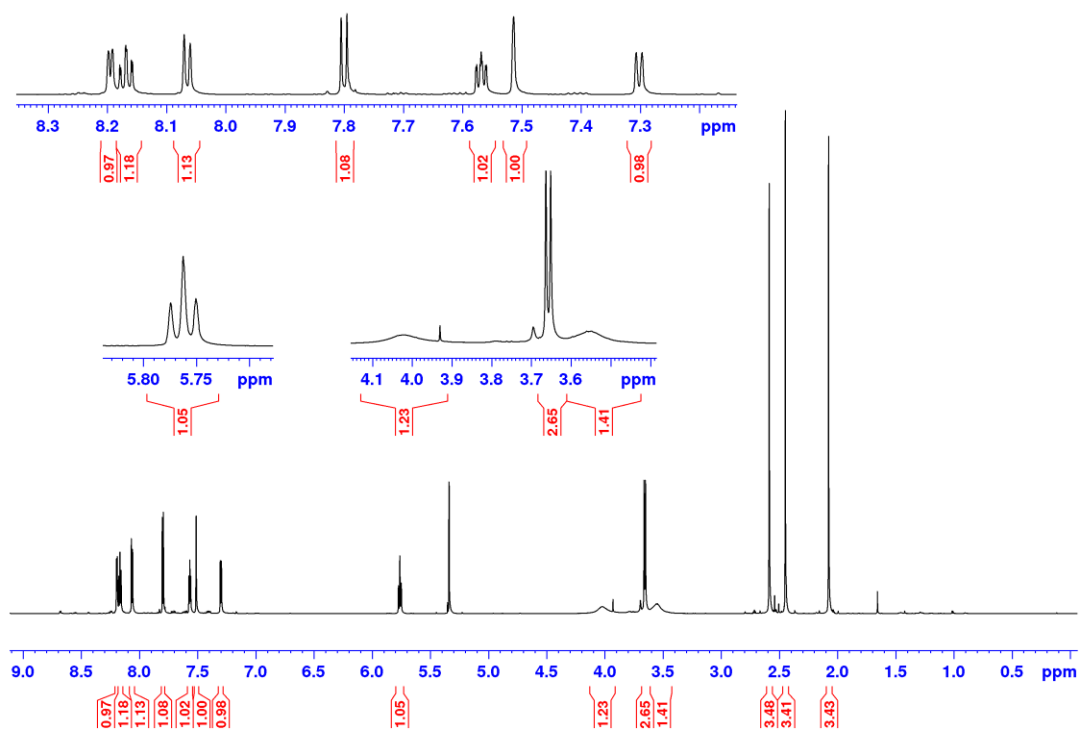
Figure A29. ^{1}H NMR (800 MHz, CD$_2$Cl$_2$) spectrum of complex **31b**. The two broad resonances at δ 4.02 and δ 3.55 are of unknown origin.
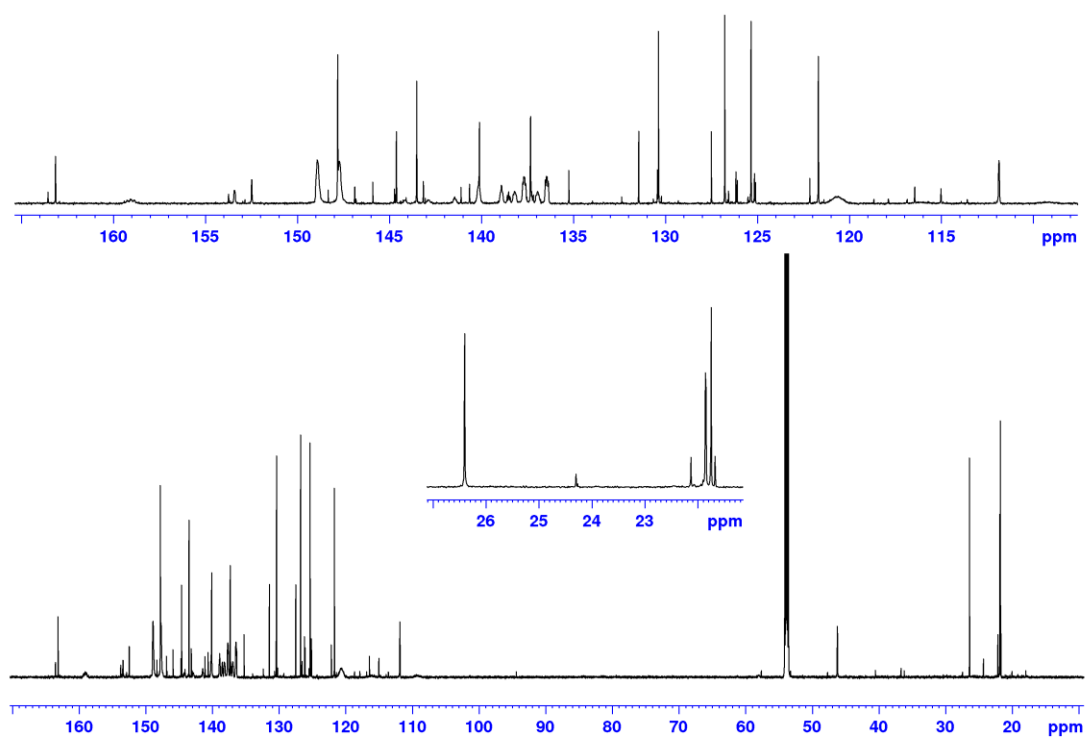
Figure A30. ^{13}C NMR (201 MHz, CD$_2$Cl$_2$, ns = 7168, d1 = 6 s) spectrum of complex **31b**. Several resonances due to decomposition are observed.
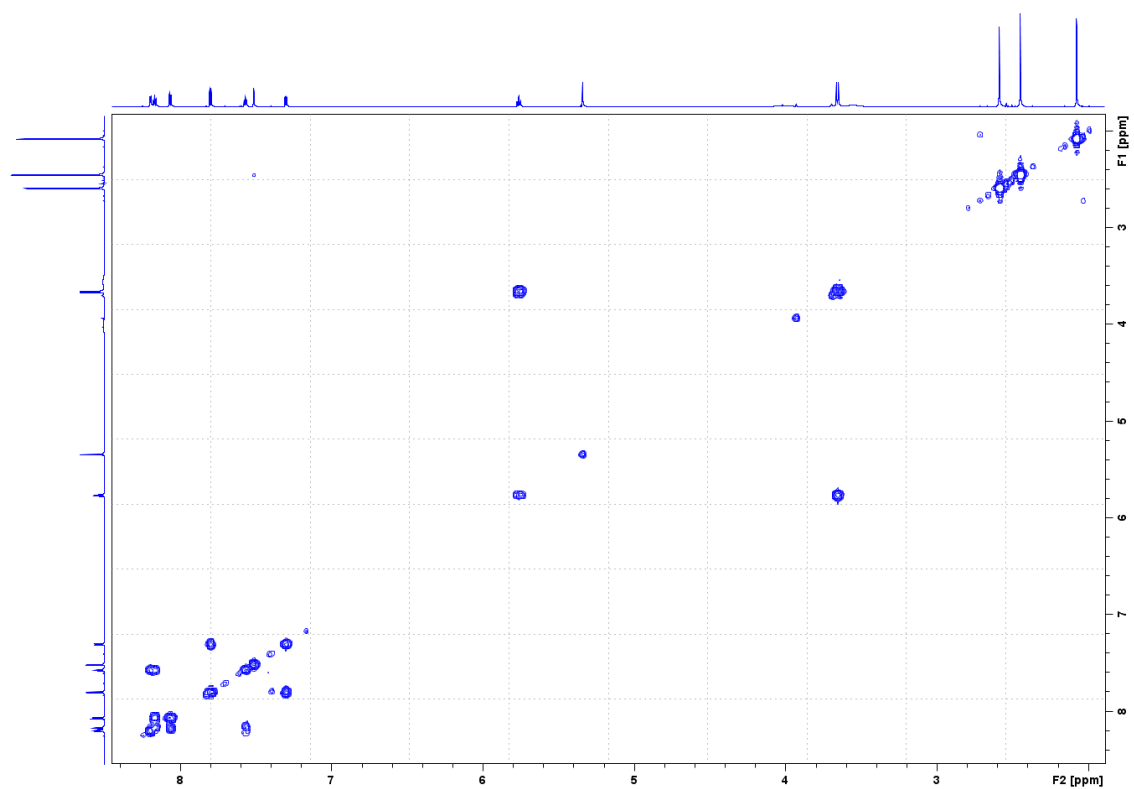
Figure A31. COSY (800 MHz, CD$_2$Cl$_2$) spectrum of complex **31b**.
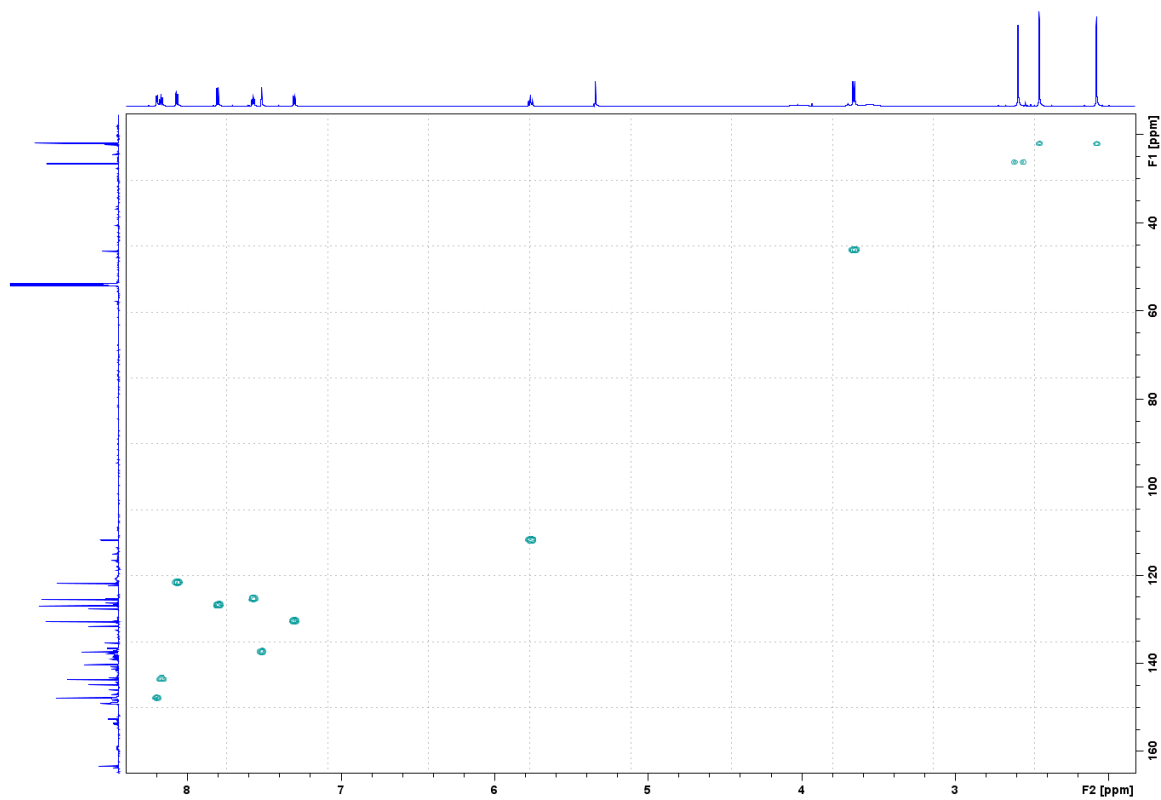
Figure A32. HSQC (800 MHz, CD$_2$Cl$_2$) spectrum of complex **31b**.
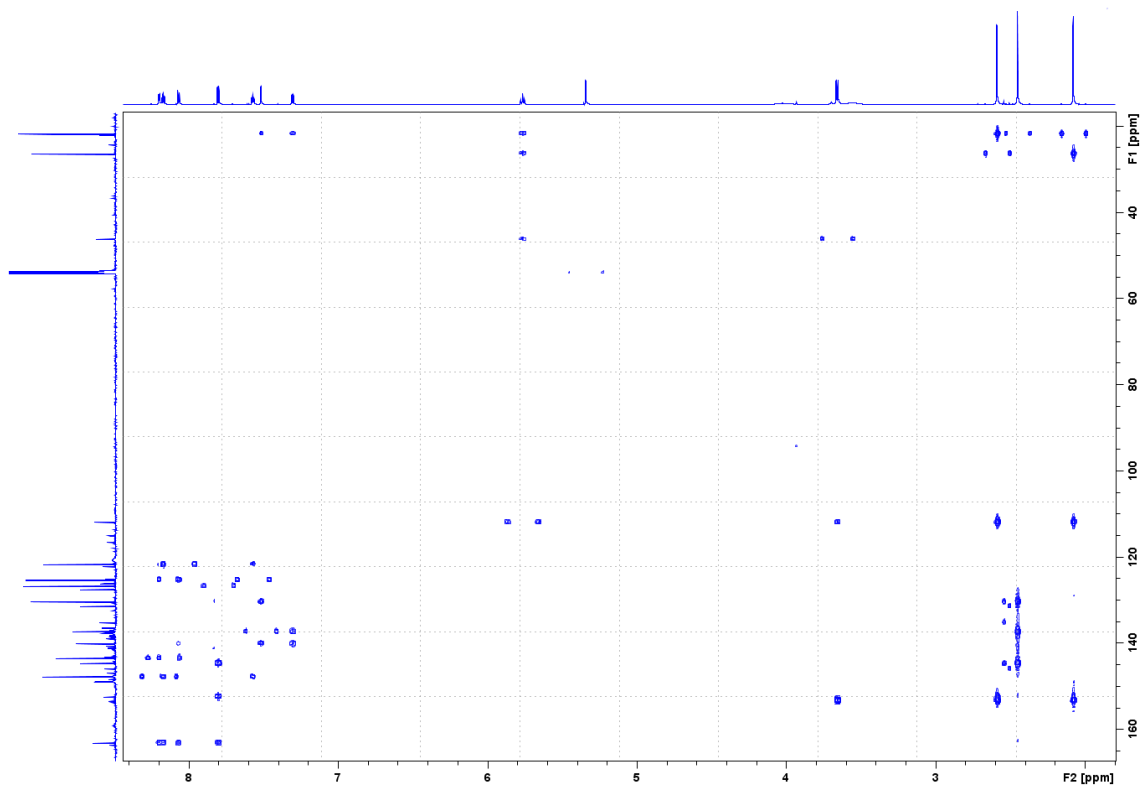
Figure A33. HMBC (800 MHz, CD$_2$Cl$_2$) spectrum of complex **31b**.
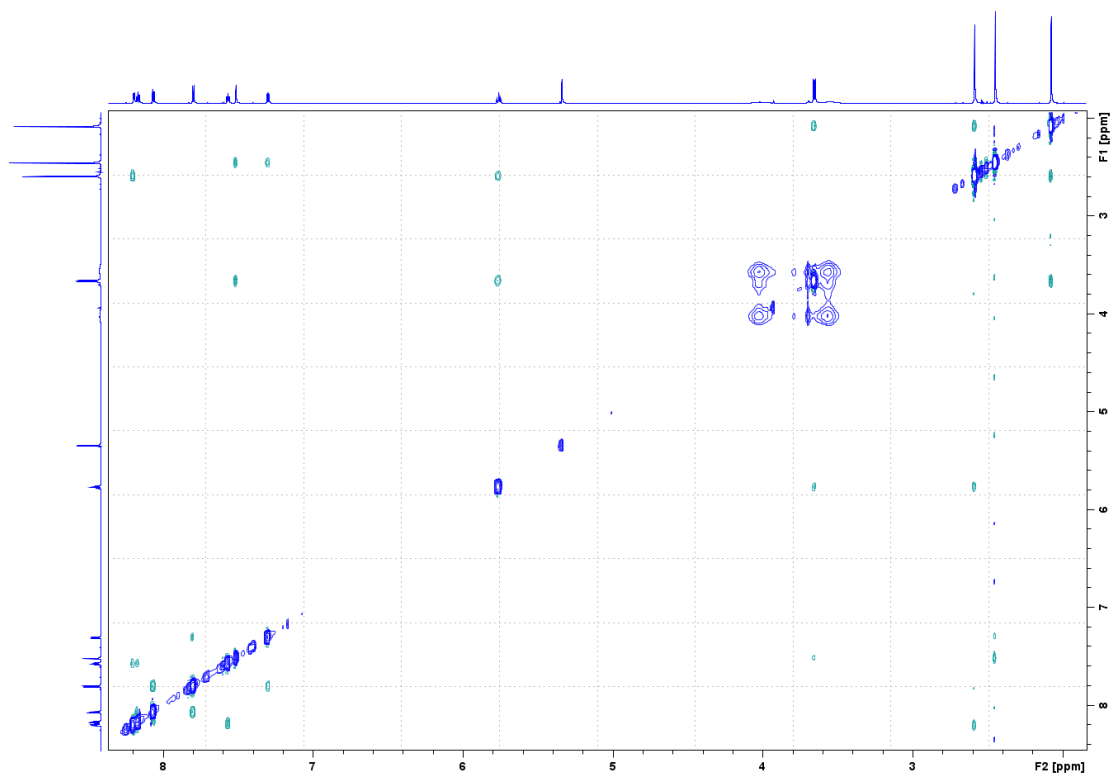
Figure A34. NOESY (800 MHz, CD_2Cl_2, mixing time = 1 s) spectrum of complex **31b**.

NMR spectra of complex 32
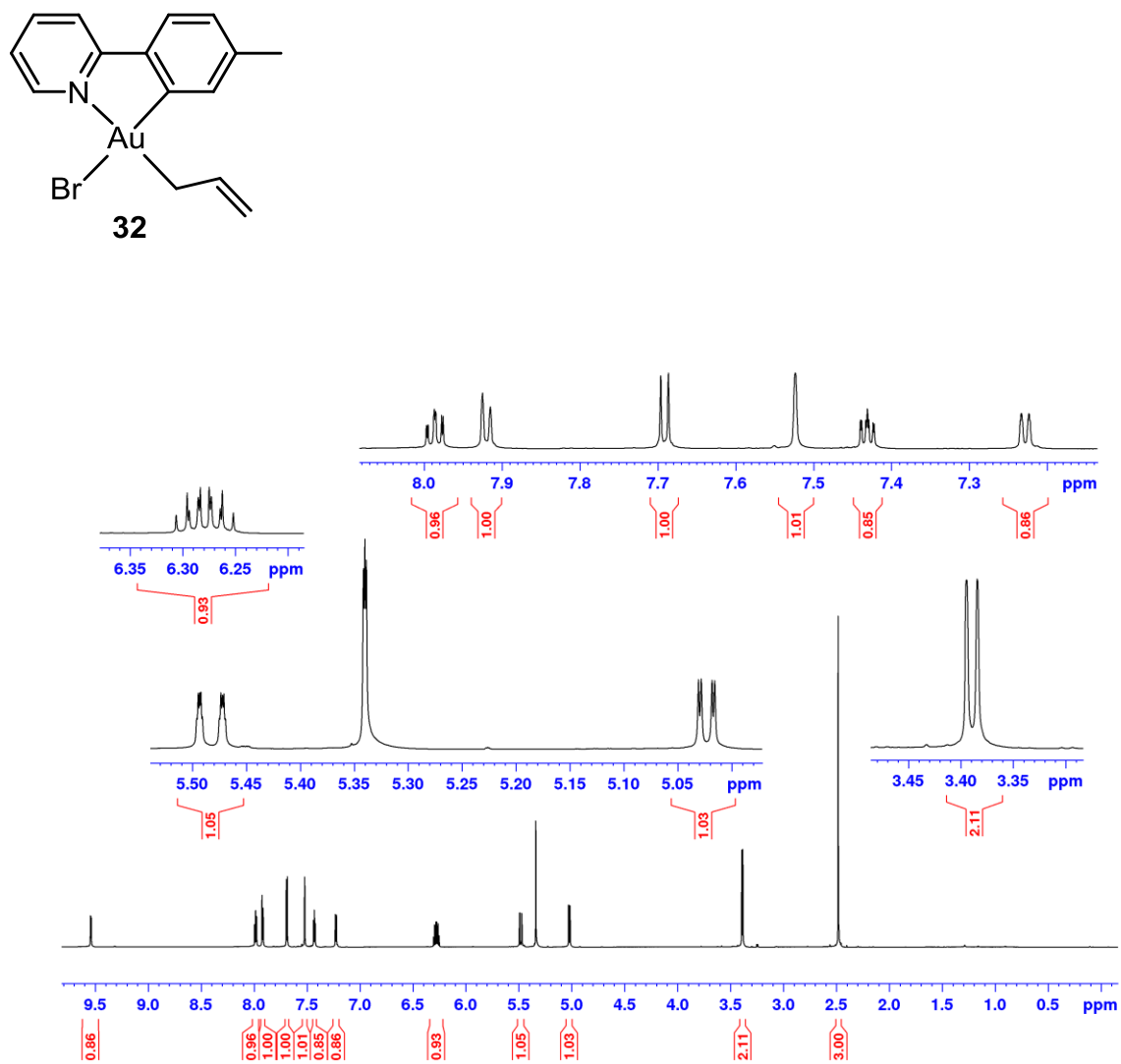
Figure A35. ^{1}H NMR (800 MHz, CD$_2$Cl$_2$) spectrum of complex **32**.
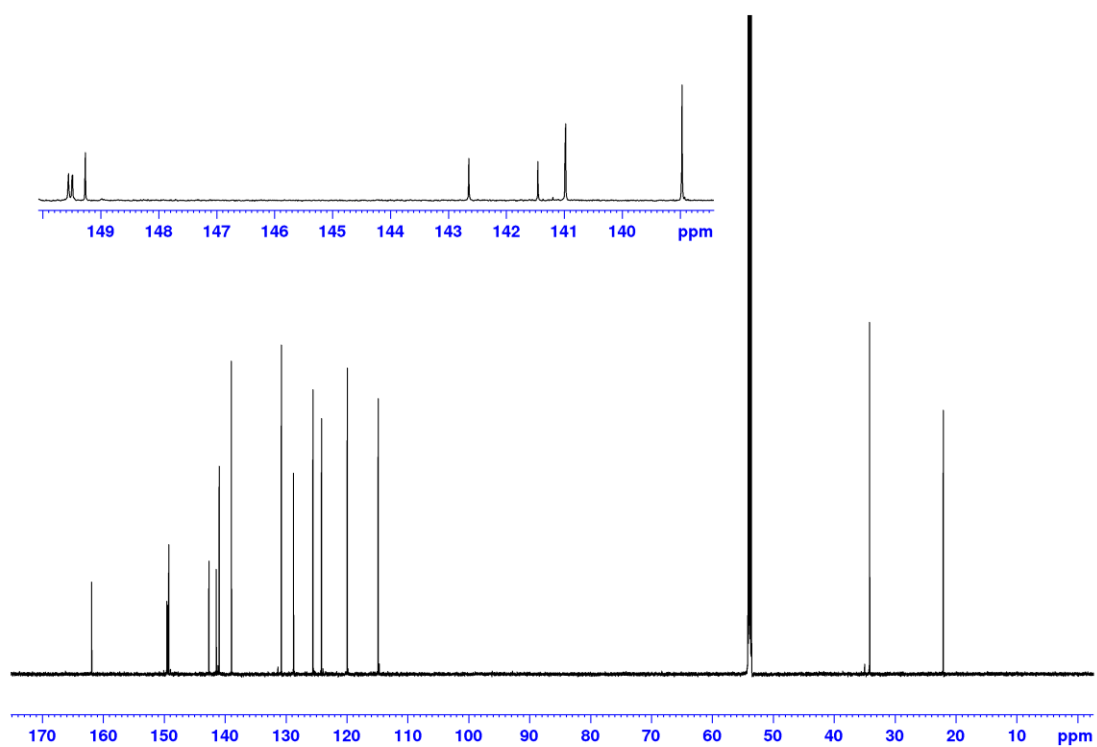
Figure A36. ^{13}C NMR (201 MHz, CD_2Cl_2, ns = 4096, d1 = 3 s) spectrum of complex **32**. The resonance at δ 149.5 appears as a doublet due to insufficient ^1H decoupling.
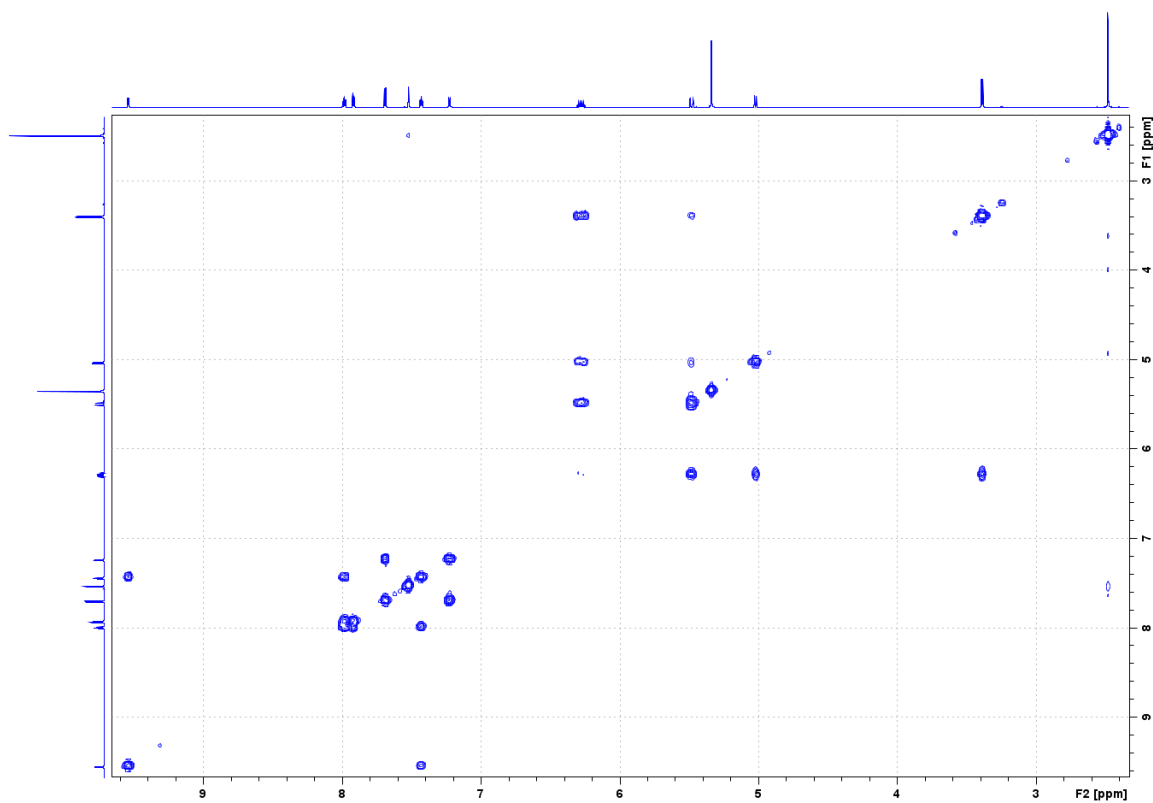
Figure A37. COSY (800 MHz, CD_2Cl_2) spectrum of complex **32**.
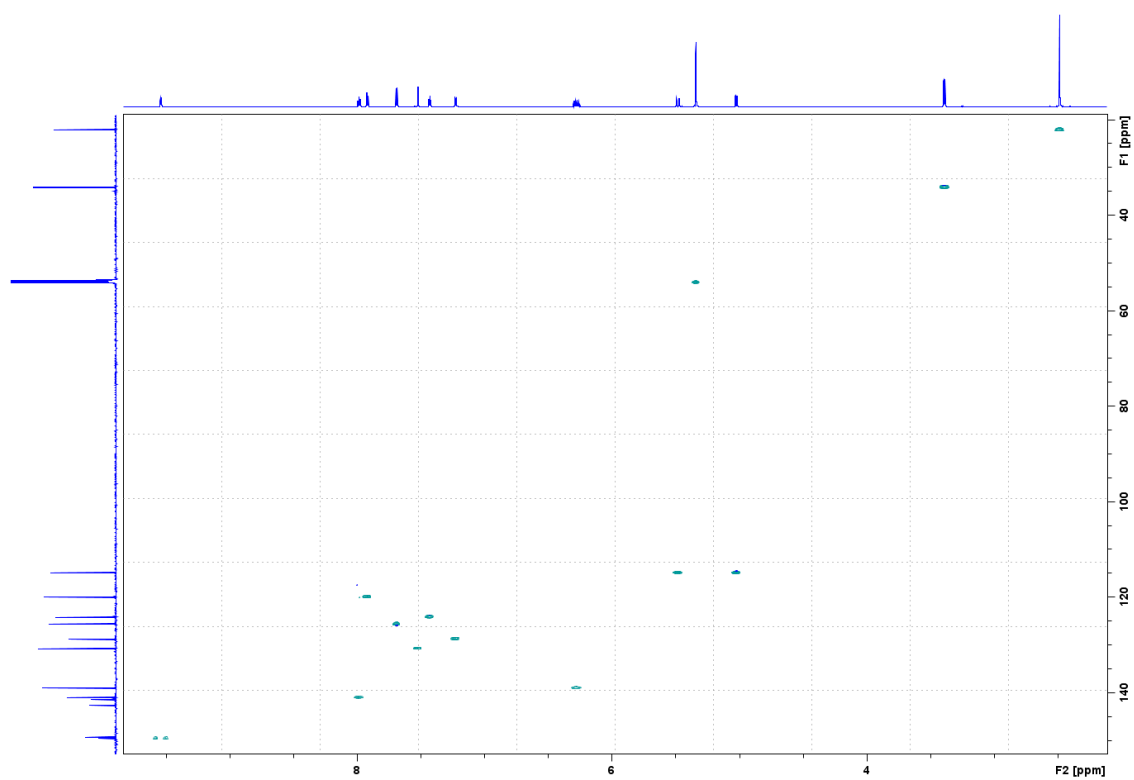
Figure A38. HSQC (800 MHz, CD_2Cl_2) spectrum of complex **32**.
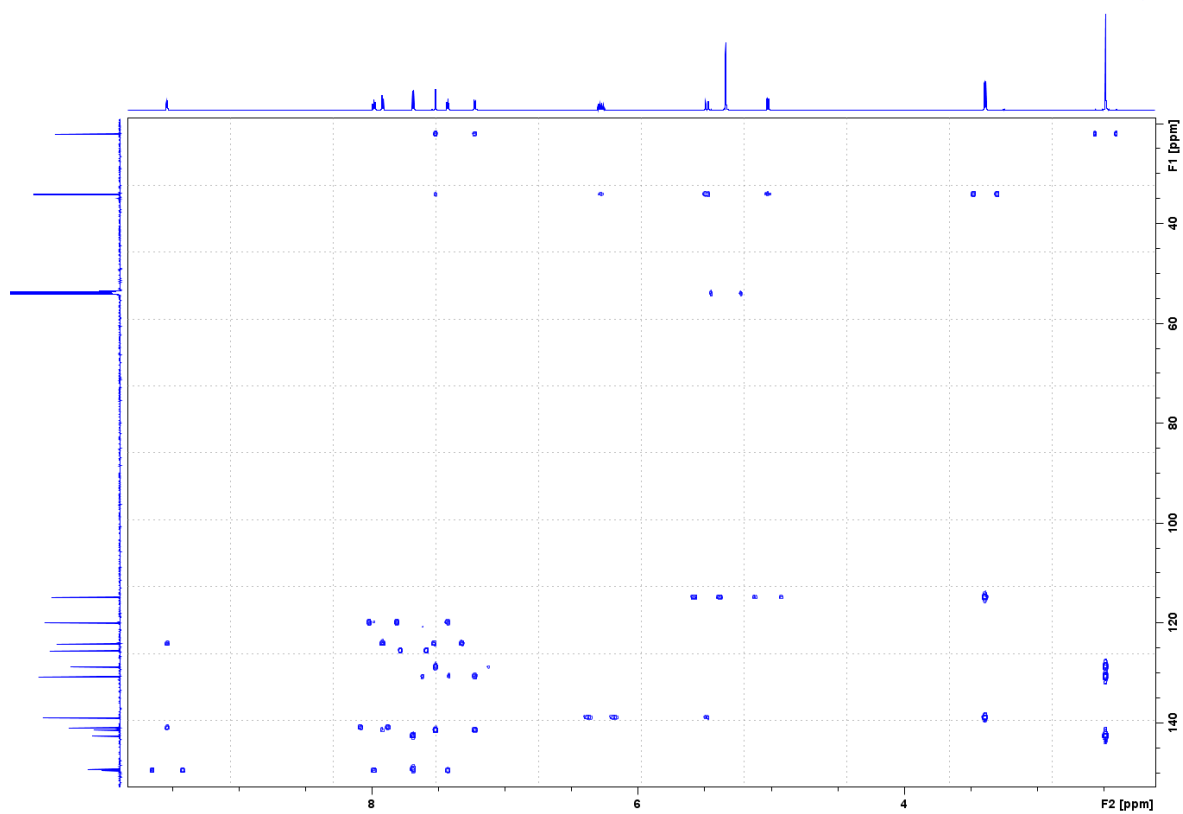
Figure A39. HMBC (800 MHz, CD_2Cl_2) spectrum of complex **32**.
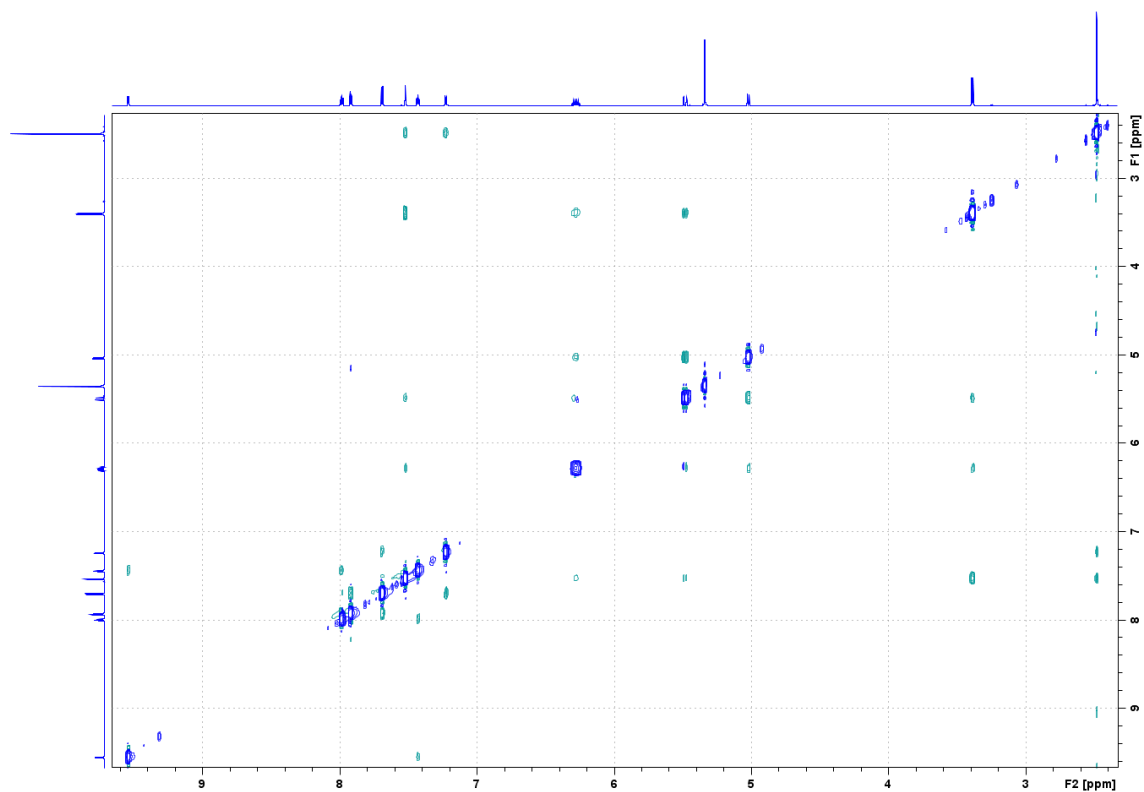
Figure A40. NOESY (800 MHz, CD$_2$Cl$_2$, mixing time = 1 s) spectrum of complex **32**.
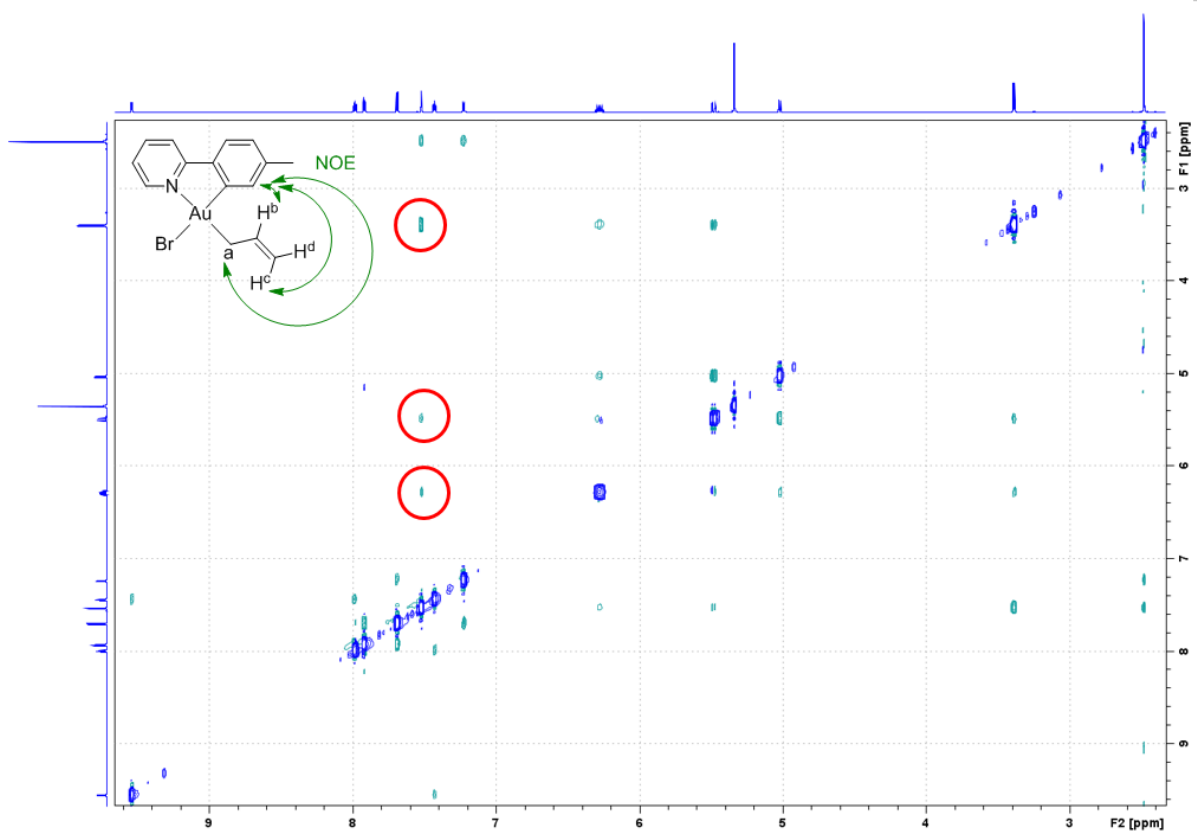
Figure A41. NOESY (800 MHz, CD$_2$Cl$_2$, mixing time = 1 s) spectrum of complex **32**. Close up view on NOE between H^a and H$^{6'}$, H^b and H$^{6'}$, and H^c and H$^{6'}$, showing that the allyl group is located *trans* to tpy-*N*.

NMR spectra of complex 33
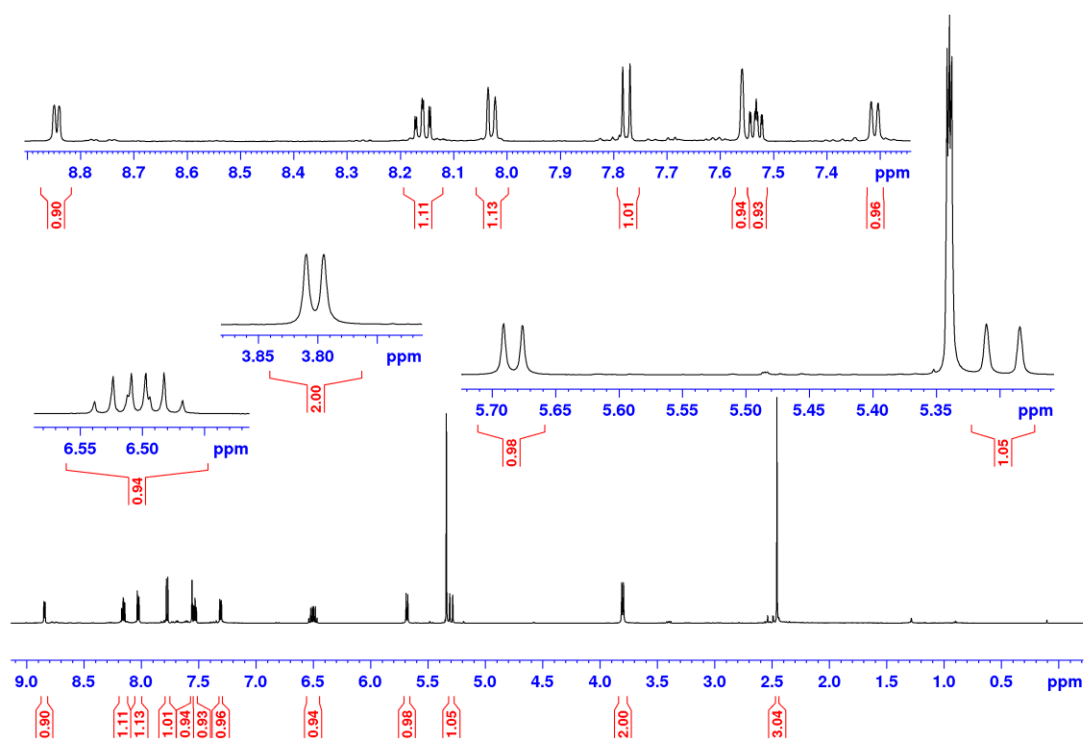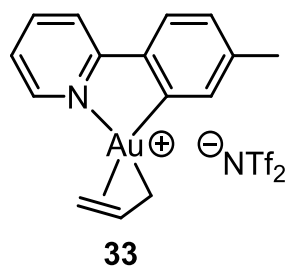
Figure A42. ^{1}H NMR (600 MHz, CD$_2$Cl$_2$, 27 ^{o}C) spectrum of complex **33**.
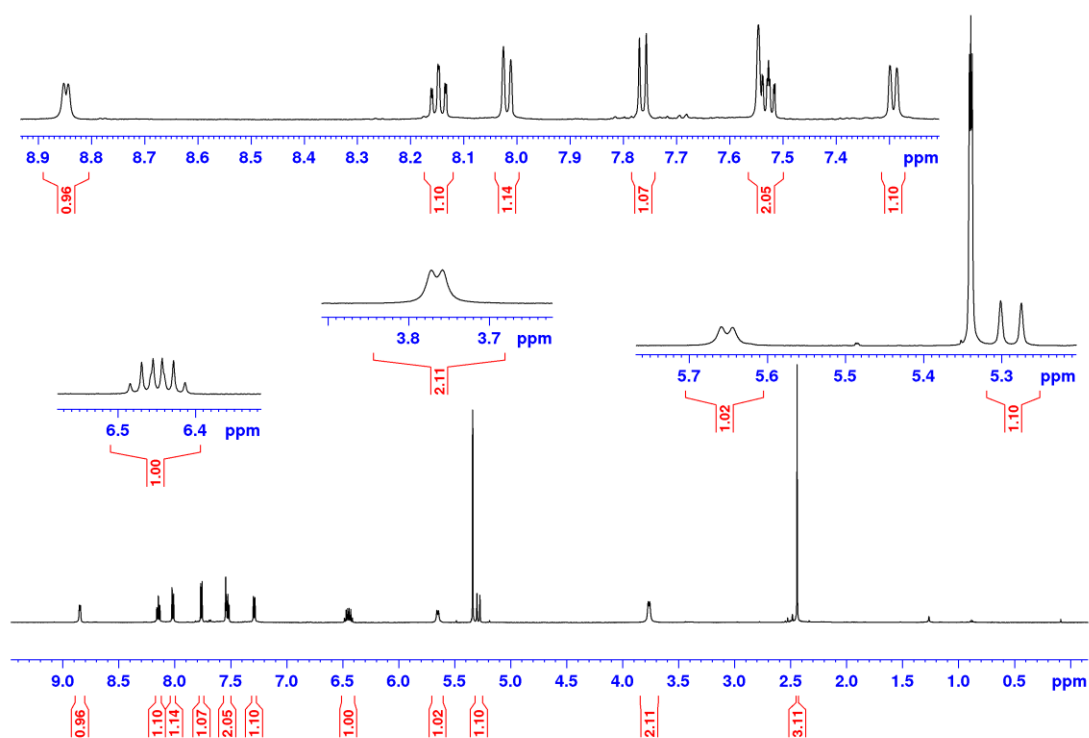
Figure A43. ^{1}H NMR (600 MHz, CD$_2$Cl$_2$, 7 °C) spectrum of complex **33**.
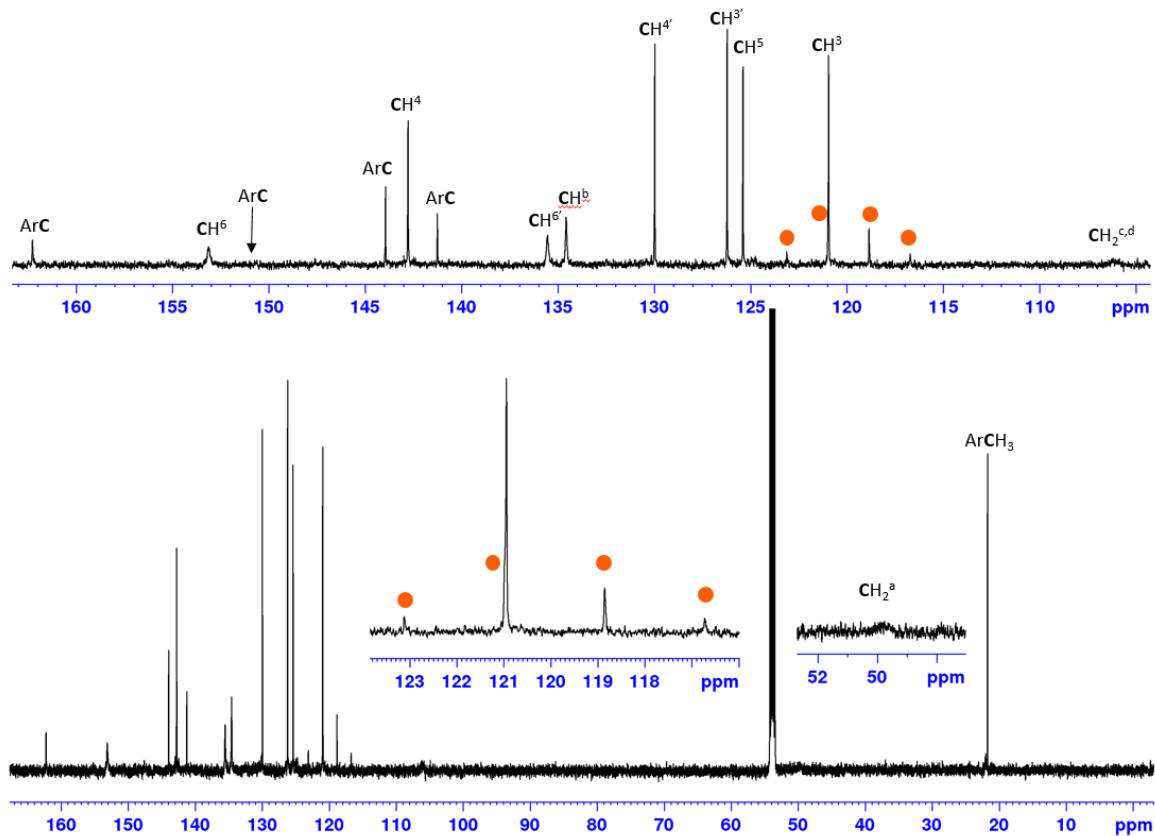
Figure A44. ^{13}C NMR (151 MHz, CD$_2$Cl$_2$, ns = 3072, d1 = 4 s, 7 °C) spectrum of complex **33**. Several resonances are broadened (see insets). The quartet of CF$_3$, arising from coupling to ^{19}F, is marked with four orange circles.
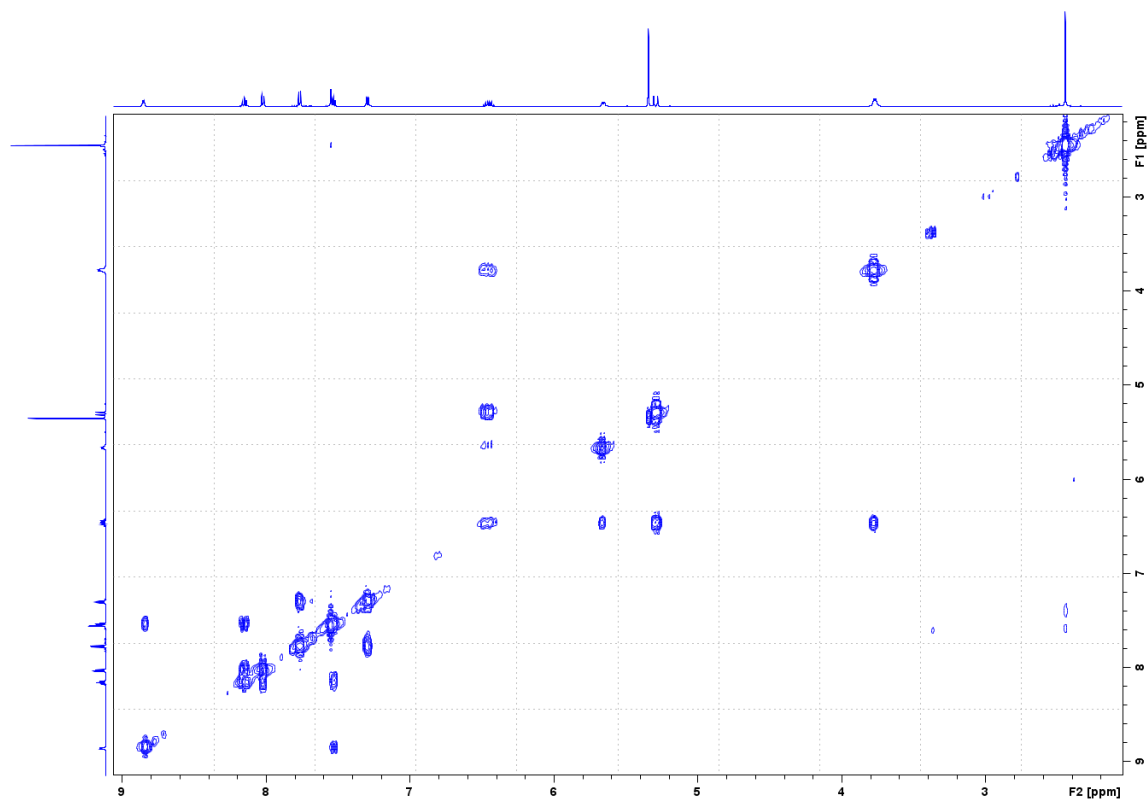
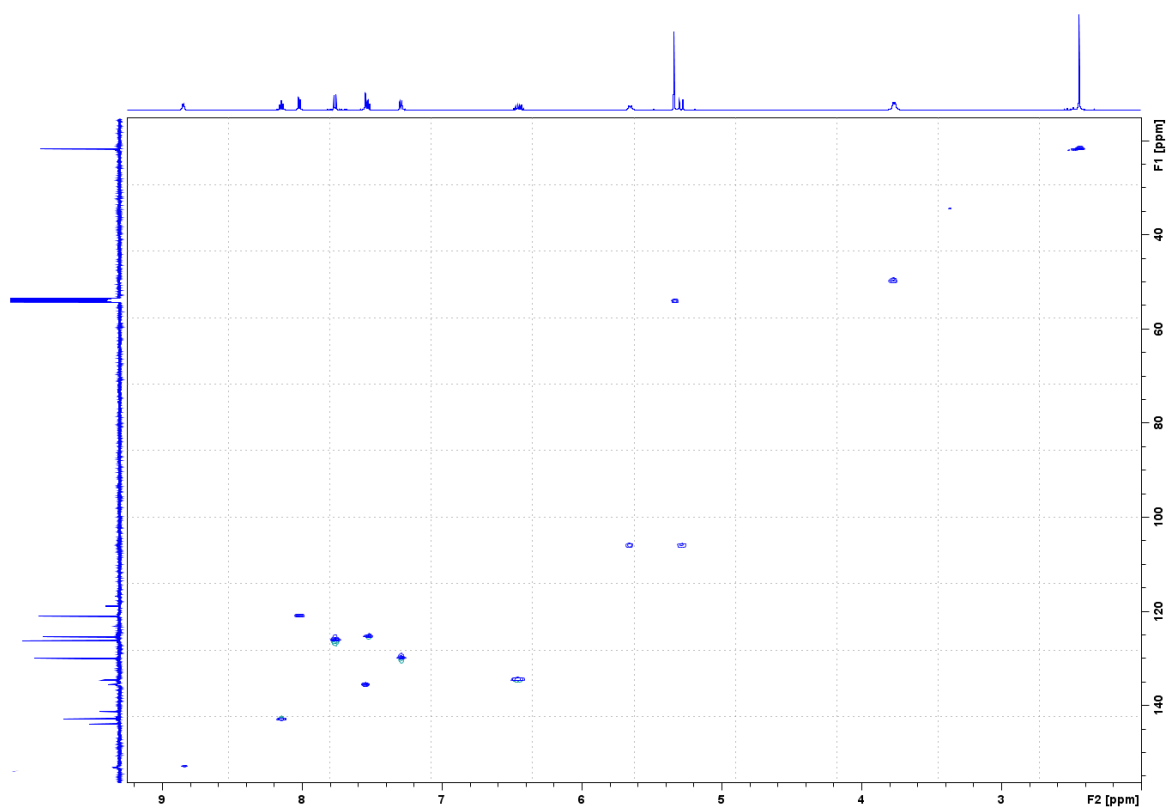**Figure A45.** COSY (600 MHz, CD$_2$Cl$_2$, 7 °C) spectrum of complex **33**.

Figure A46. HSQC (600 MHz, CD$_2$Cl$_2$, 7 °C) spectrum of complex **33**.

Figure A47. HMBC (600 MHz, CD$_2$Cl$_2$, 7 °C) spectrum of complex **33**.
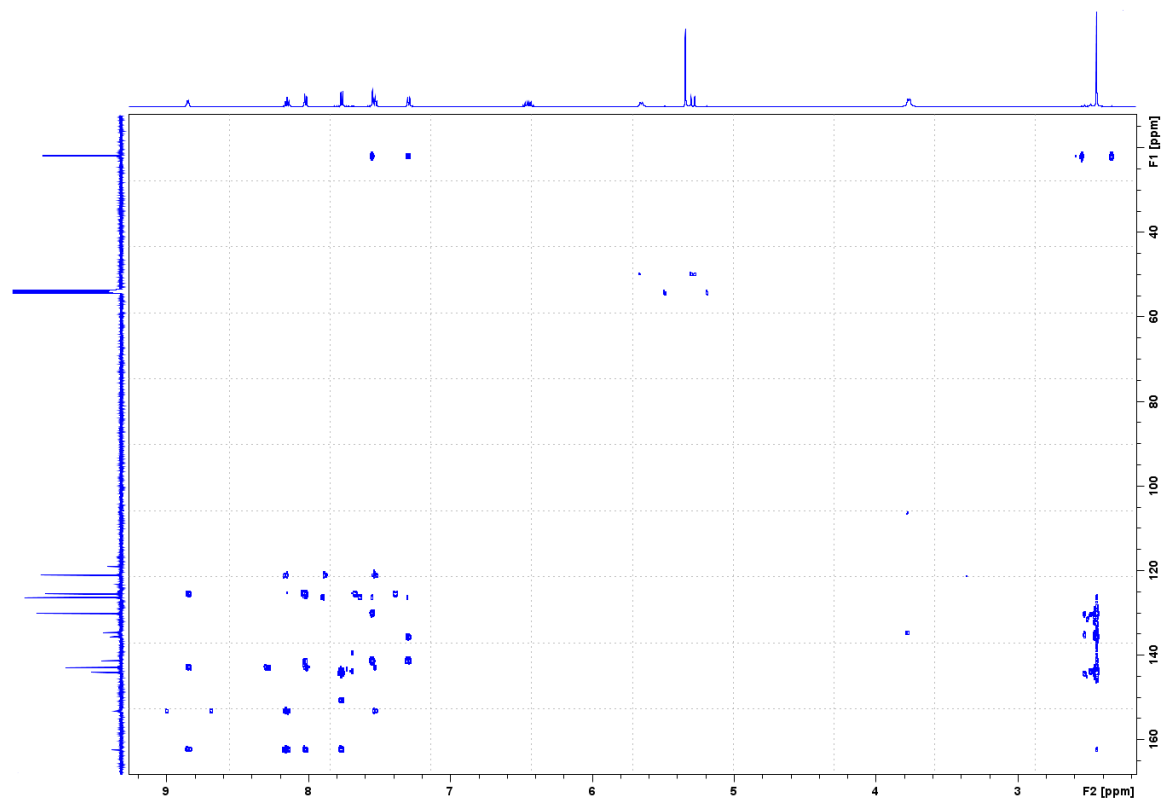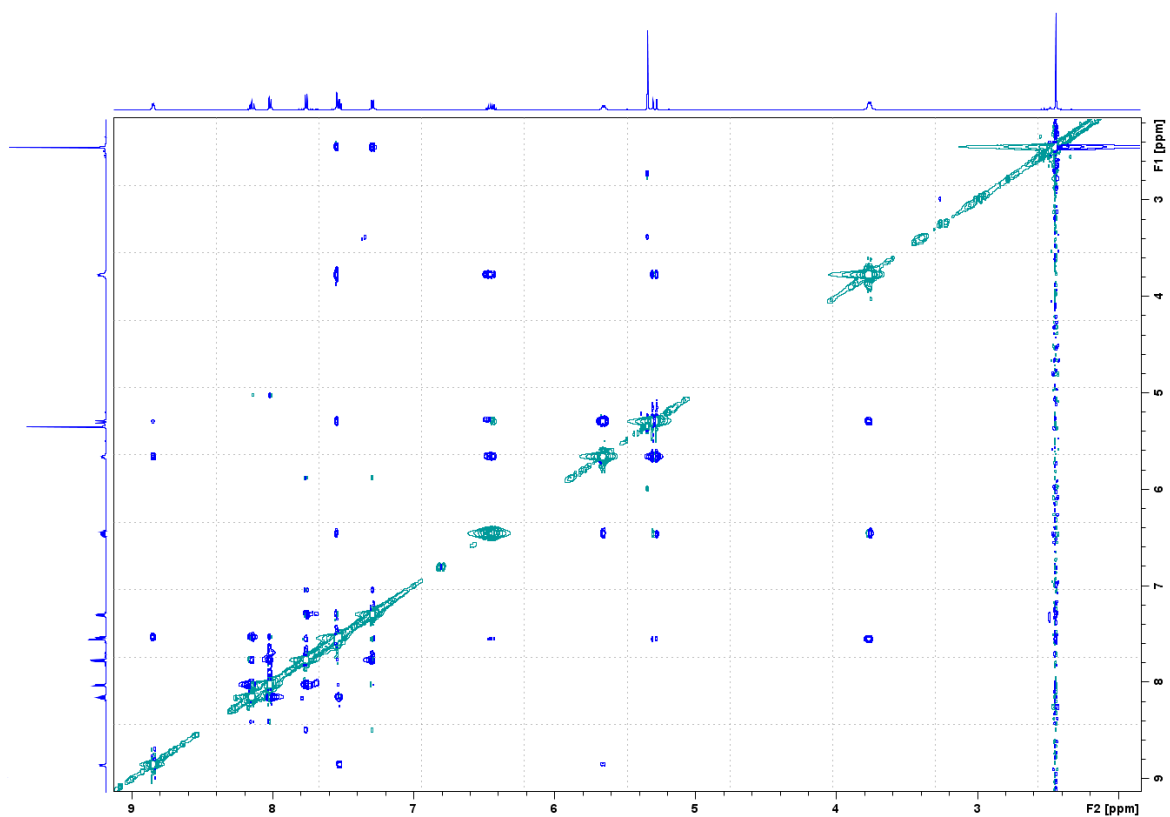

Figure A48. NOESY (600 MHz, CD$_2$Cl$_2$, mixing time = 1 s, 7 °C) spectrum of complex **33**.